DEGRADATION OF SOLID PHARMACEUTICAL WASTE USING SUPEROXIDE RADICAL ION GENERATED IN IONIC LIQUID/APROTIC SOLVENT MIXTURE SYSTEMS

SABA HUMAYUN

FACULTY OF SCIENCE
UNIVERSITI MALAYA
KUALA LUMPUR

2024

DEGRADATION OF SOLID PHARMACEUTICAL WASTE USING SUPEROXIDE RADICAL ION GENERATED IN IONIC LIQUID/APROTIC SOLVENT MIXTURE SYSTEMS

SABA HUMAYUN

THESIS SUBMITTED IN FULFILMENT OF THE REQUIREMENTS FOR THE DEGREE OF DOCTOR OF PHILOSOPHY

**FACULTY OF SCIENCE
UNIVERSITI MALAYA
KUALA LUMPUR**

2024

UNIVERSITI MALAYA

ORIGINAL LITERARY WORK DECLARATION

Name of Candidate: **SABA HUMAYUN**
Matric No: **SVA180028**
Name of Degree: **DOCTOR OF PHILOSOPHY**

Title of Project Paper/Research Report/Dissertation/Thesis ("this Work"):
DEGRADATION OF SOLID PHARMACEUTICAL WASTE USING SUPEROXIDE RADICAL ION GENERATED IN IONIC LIQUID/APROTIC SOLVENT MIXTURE SYSTEMS
Field of Study: **ORGANIC CHEMISTRY**

 I do solemnly and sincerely declare that:

(1) I am the sole author/writer of this Work.
(2) This Work is original.
(3) Any use of any work in which copyright exists was done by way of fair dealing and for permitted purposes and any excerpt or extract from, or reference to or reproduction of any copyright work has been disclosed expressly and sufficiently and the title of the Work and its authorship have been acknowledged in this Work.
(4) I do not have any actual knowledge, nor do I reasonably ought to know that the making of this work constitutes an infringement of any copyright work.
(5) I hereby assign all and every right in the copyright to this Work to the University of Malaya ("UM"), who henceforth shall be owner of the copyright in this Work and that any reproduction or use in any form or by any means whatsoever is prohibited without the written consent of UM having been first had and obtained.
(6) I am fully aware that if in the course of making this Work I have infringed any copyright whether intentionally or otherwise, I may be subject to legal action or any other action as may be determined by UM.

    Candidate's Signature   Date: **March 18, 2024**

Subscribed and solemnly declared before,

            Date: **March 18, 2024**

Designation:

DEGRADATION OF SOLID P HARMACEUTICAL WASTE USING SUPEROXIDE RADICAL ION GENERATED IN IONIC LIQUID/APROTIC SOLVENT MIXTURE SYSTEMS

ABSTRACT

Environmental contamination by pharmaceuticals is on the rise, ensuing levels which are imminent globally. While the alleged harmful effects of drug waste are being rapidly substantiated at present, the development of effective and 'greener' techniques to degrade pharmaceuticals is a new challenge. This study explores a method using superoxide ion ($O_2^{\bullet-}$) as the reactive oxygen species (ROS) for the degradation of APIs. Owing to the simplicity of its chemical structure and extensive research on the degradation of acetaminophen via various ROS, it was chosen for investigation as a model drug pollutant to thoroughly explore the advanced oxidation method. With an aim to further explore the universality of the oxidation process under investigation, the degradation of some other representative drug compounds was also examined; carbamazepine (CBM) and riluzole (RLZ) were additionally selected as target contaminants. The applicability of this oxidative degradation method on various pharmaceutical substances was validated using binary mixture systems consisting of butyltriethylammonium [BTEAmm$^+$], triethylpentylammonium [PTEAmm$^+$] and octyltriethylammonium [OTEAmm$^+$] cations with bis(trifluoromethylsulfonyl)imide [TFSI$^-$] anion-based hydrophobic ionic liquids (ILs) and acetonitrile (AcN) as an aprotic solvent (ApS). The ILs and AcN were used in varied combinations to generate $O_2^{\bullet-}$ for subsequent in-situ degradation of APIs. The $O_2^{\bullet-}$ was chemically generated by the dissolution of potassium superoxide (KO$_2$) in [BTEAmm+][TFSI$^-$]/AcN, [PTEAmm$^+$][TFSI$^-$]/AcN, [OTEAmm$^+$] [TFSI$^-$]/AcN and [EMIm$^+$][TFSI$^-$]/AcN systems to achieve complete degradation of the drugs. The novelty of

this work lies in the demonstration of using IL/ApS binary mixtures which allow API removal of up to 98.9% within 210 mins of reaction. The extent of degradation of APIs was analyzed via the HPLC (high-performance liquid chromatography) technique by investigating the influence of different parameters and operating conditions, such as the amount of oxidant, nature of cations in ILs, length of cationic alkyl chain, ratio of IL:AcN (constituency of binary mixture), reaction time and reaction temperature. The most efficient degradation of ACTM was observed to occur utilizing 10% [OTEAmm$^+$]/AcN as the reaction medium with a KO_2/ACTM molar ratio of 50 at RT. A characteristic peak at the wavelength of 258 nm in UV-visible spectrophotometry was indicative of the stable generation of $O_2^{\bullet-}$ species, which confirms its presence in certain reaction media used. Cyclic voltammetry (CV) was used in order to further validate $O_2^{\bullet-}$ as a major reactive oxygen species generated in selected aprotic media, as evidently indicated by the oxygen reduction peak in the cyclic voltammograms. The ILs were recycled and found to be reusable for up to five replica cycles without significant changes in the degradation efficiencies, depicting the high efficacy of the environmentally benign regenerated media. Moreover, the evaluation of TOC decay determined that complete mineralization of APIs was achieved under optimum conditions. Degradation mechanism pathways for the pharmaceutical compounds were proposed based on LCMS analysis for the identification of intermediate transformation products resulting from drug oxidation. This work will serve to instigate further progression in the direct use of $O_2^{\bullet-}$ as a suitable alternative approach for environmental remediation pertaining to pharmaceutical contaminants.

Keywords: Pharmaceutical contaminants, oxidative degradation, superoxide radical ions, reactive oxygen species, binary mixture system, regenerated media.

DEGRADATION OF SOLID PHARMACEUTICAL WASTE USING SUPEROXIDE RADICAL ION GENERATED IN IONIC LIQUID/APROTIC SOLVENT MIXTURE SYSTEMS

ABSTRAK

Pencemaran alam sekitar oleh bidang farmaseutikal terus meningkat, seterusnya ke tahap yang akan berlaku di seluruh dunia. Walaupun kesan bahaya yang didakwa daripada sisa ubat sedang dibuktikan dengan pantas pada masa kini, pembangunan teknik yang berkesan dan lebih mesra alam untuk merendahkan farmaseutikal adalah satu cabaran baharu. Kajian ini meneroka kaedah menggunakan ion superoksida ($O_2^{\bullet-}$) sebagai spesies oksigen reaktif (ROS) untuk degradasi API. Disebabkan oleh struktur kimia yang mudah dan penyelidikan yang meluas mengenai degradasi asetaminofen melalui pelbagai ROS, ia dipilih untuk penyiasatan sebagai bahan model pencemar dadah untuk meneroka kaedah pengoksidaan lanjutan secara menyeluruh. Dengan tujuan untuk meneroka lebih lanjut kesejagatan proses pengoksidaan yang sedang disiasat, degradasi beberapa sebatian ubat juga telah diperiksa; carbamazepine (CBM) dan riluzole (RLZ) juga dipilih sebagai bahan cemar sasaran. Kebolehgunaan kaedah degradasi oksidatif ini pada pelbagai bahan farmaseutikal telah disahkan menggunakan sistem campuran binari yang terdiri daripada butiltrietilammonium [BTEAmm$^+$], trietilpentylammonium [PTEAmm$^+$] dan octyltrietilammonium [OTEAmm$^+$] kation dengan kation bis(trifuoromethyl anbicionic-hidrofonik imfonik berasaskan bis(trifuorometil anbicionic TFSI) (ILs) dan asetonitril (AcN) sebagai pelarut aprotik (ApS). IL dan AcN digunakan dalam kombinasi yang berbeza-beza untuk menjana $O_2^{\bullet-}$ untuk kemerosotan *in-situ* seterusnya bagi API. $O_2^{\bullet-}$ dijana secara kimia melalui pembubaran kalium superoksida (KO$_2$) dalam [BTEAmm$^+$][TFSI$^-$]/AcN, [PTEAmm$^+$][TFSI$^-$]/AcN, [OTEAmm$^+$][TFSI$^-$]/AcN dan [EMIm$^+$][Sistem TFSI$^-$]/AcN untuk mencapai degradasi

.

lengkap ubat. Kebaharuan penyelidikan ini terletak pada demonstrasi penggunaan campuran binari IL/ApS yang membenarkan penyingkiran API sehingga 98.9% dalam masa 210 minit. Tahap degradasi API telah dianalisis melalui teknik HPLC (kromatografi cecair berprestasi tinggi) dengan menyiasat pengaruh parameter dan keadaan operasi yang berbeza, seperti jumlah oksidan, sifat kation dalam IL, panjang rantai alkil kationik, nisbah IL : AcN (konstituensi campuran binari), masa tindak balas dan suhu tindak balas. Degradasi ACTM yang paling cekap diperhatikan berlaku menggunakan 10% [OTEAmm$^+$]/AcN sebagai medium tindak balas dengan nisbah molar KO$_2$/ACTM 50 pada RT. Nilai puncak pada panjang gelombang 258 nm dalam spektrofotometri UV-visible menunjukkan penjanaan stabil spesies O$_2^{\bullet-}$, yang mengesahkan kehadirannya dalam media tindak balas tertentu yang digunakan. Voltammetri kitaran (CV) digunakan untuk mengesahkan lagi O$_2^{\bullet-}$ sebagai spesies oksigen reaktif utama yang dijana dalam media aprotik terpilih, seperti yang ditunjukkan oleh puncak pengurangan oksigen dalam voltammogram kitaran. IL telah dikitar semula dan didapati boleh diguna semula sehingga lima kitaran replika tanpa perubahan ketara dalam kecekapan degradasi, menggambarkan keberkesanan tinggi media jana semula jinak alam sekitar. Selain itu, penilaian pereputan TOC menentukan bahawa pemineralan API yang lengkap telah dicapai dalam keadaan optimum. Laluan mekanisme degradasi untuk sebatian farmaseutikal telah dicadangkan berdasarkan analisis LCMS untuk mengenal pasti produk transformasi perantaraan yang terhasil daripada pengoksidaan ubat. Penyelidikan ini berfungsi untuk mencetuskan perkembangan selanjutnya dalam penggunaan langsung O$_2^{\bullet-}$ sebagai pendekatan alternatif yang sesuai untuk pemulihan alam sekitar yang berkaitan dengan bahan cemar farmaseutikal.

Kata kunci: Bahan cemar farmaseutikal, degradasi oksidatif, ion superoksida, spesies oksigen reaktif, sistem campuran binari, media yang dijana semula

ACKNOWLEDGEMENTS

I would deeply thank all the participants in my study for their time and willingness to share their experiences. This work would not have been possible or reached timely completion without their contribution.

TABLE OF CONTENTS

LIST OF SCHEMES

LIST OF FIGURES

LIST OF TABLES

LIST OF SYMBOLS AND ABBREVIATIONS

Σ	:	electrical conductivity
Γ	:	gamma
H	:	viscosity
$)))$	:	ultrasound irradiation
ΔEp	:	peak potential separation
µL	:	microlitre
2-MTH	:	2-methylthiophene
AcN	:	acetonitrile
ACTM	:	acetaminophen (also Paracetamol)
AgCl	:	silver chloride
AILs	:	aprotic ionic liquids
$AlCl_4^-$	:	tetrachloroaluminate anion
AMR	:	antimicrobial resistance
AMX	:	amoxicillin
AOPs	:	advanced oxidation processes
APIs	:	active pharmaceutical ingredients
ApS	:	aprotic solvent
ARB	:	antibiotic-resistant bacteria
ARGs	:	antibiotic-resistant genes
ATR	:	attenuated total reflection
B^-	:	base
BDD	:	boron-doped diamond
$[BF_4]^-$	:	tetrafluoroborate anion

[bmim][HFP]	:	1-methyl-3-n-butylimidazolium hexafluorophospate
[bpy]$^+$	:	*N*-butylpyridinium cation
BT	:	benzothiophene
[BTEAmm][TFSI]	:	butyltriethylammonium bis(trifluoromethylsulfonyl)imide
Ca(O$_2$)$_2$	:	calcium superoxide
CCl$_4$	:	carbon tetrachloride
CD$_3$OD	:	deuterated methanol
CdS	:	cadmium sulfide
CFCs	:	chlorofluorocarbons
CF$_3$SO^{3-}	:	trifluoromethanesulfonate anion
CHBr$_3$	:	bromoform
CHCl$_3$	:	chloroform
CH$_3$CN	:	acetonitrile
CH$_3$COO$^-$	:	acetate anion
Cl$^\bullet$	:	chlorine radical
Cl$^-$	:	chloride ion
Cl$_2$	:	chlorine gas
Cl$_2^{\bullet-}$	:	chloride radical
ClO$^-$	:	hypochlorite anion
[C$_4$mim]$^+$	:	1-butyl-3-methylimidazolium cation
[C$_4$mpyr]$^+$	:	*N*-butyl-N-methylpyrrolidinium cation
[C$_4$NMe$_3$]$^+$	:	*N*-butyl-*N*,*N*,*N*-trimethylammonium cation
CNS	:	central nervous system
CO$_2$	:	carbon dioxide

$CO_3^{\bullet-}$	:	carbonate radical anion
COD	:	chemical oxygen demand
cP	:	centipoise
CV	:	cyclic voltammetry
Cyphos IL 104	:	trihexyl(tetradecyl)phosphonium bis(2,4,4-trimethylpentyl) phosphinate
D	:	self-diffusion
DBT	:	dibenzothiophene
[DCA]	:	dicyanamide
DCF	:	diclofenac
DFT	:	density functional theory
[dmbim][HFP]	:	1,2-dimethyl-3-n-butylimidazolium hexafluorophospate
DMF	:	dimethylformamide
DMSO	:	dimethylsulfoxide
DOC	:	dissolved organic carbon
e^-	:	electron
e_{aq}^-	:	hydrated electron
EB	:	electron beam
e^-_{CB}	:	conduction band electrons
ECs	:	emerging contaminants
ECWAO	:	electro-assisted catalytic wet air oxidation
EDCs	:	endocrine-disrupting compounds
[EDMPAmm][TFSI]	:	ethyldimethyl-propylammonium bis(trifluoromethylsulfonyl)imide

E/E°	:	standard cell potential/formal potential
EH&S	:	environmental health and safety
[EMIm][TFSI]	:	1-ethyl-3-methylimidazolium bis(trifluoromethylsulfonyl)imide
EPA	:	environmental protection agency
ESR	:	electron spin resonance
Fe^0	:	zero-valent iron
Fe^{2+}	:	ferrous ions
Fe^{3+}	:	ferric ions
Fe_2O_3	:	iron (III) oxide/ferric oxide
FIL	:	fresh ionic liquid
FTIR	:	fourier transform infrared
GC	:	glassy carbon
$g\text{-}C_3N_4$	:	graphitic carbon nitride
Gy	:	gray
$^\bullet H$	:	hydrogen radical
H^+	:	hydrogen ion
HClO	:	hypochlorous acid
HCO^{3-}	:	bicarbonate ion
HDME	:	hanging drop mercury electrode
HHC	:	halogenated hydrocarbons
^1H NMR	:	proton nuclear magnetic resonance
HO^-	:	hydroxide ion
HO^{2-}	:	hydroperoxide anion

$HO_2^{\bullet}$	:	hydroperoxyl radical
H_2O	:	water
H_2O_2	:	hydrogen peroxide
H_3O^+	:	hydroxonium ion
HPLC	:	high-performance liquid chromatography
HPO_4^{2-}	:	phosphate ion
$h\nu$	:	photon (sunlight) [Plank's constant (h), frequency (ν)]
h^+ / h_{VB}^+	:	valence band holes
I^-	:	iodide ion
IL	:	ionic liquid
K	:	kelvin
k^1	:	rate constant of pseudo-first order
KAERI	:	Korean atomic energy research institute
kGy	:	kiloGray
KO_2	:	potassium superoxide
$K_2S_2O_8$	:	potassium persulfate
LC/MS-QToF	:	liquid chromatography/mass spectrometry-quadrupole time-of-flight
log K	:	stability constant
M	:	molar concentration
mg/L	:	milligrams per litre
MHz	:	megahertz
mM	:	millimolar
mmol/L	:	millimoles per litre

MOFs	:	metal organic frameworks
MPa	:	megapascal
m.S	:	millisiemens
[MS]	:	methylsulfate
mV	:	millivolt
m/z	:	mass-to-charge ratio
N_2	:	nitrogen gas
Na_2O	:	sodium oxide
Na_2O_2	:	sodium peroxide
NaCl	:	sodium chloride
NaO_2	:	sodium superoxide
NaOH	:	sodium hydroxide
NH_4^+	:	ammonium cation
nm	:	nanometer
NO_3^-	:	nitrate ion
NOM	:	natural organic matter
$[N_{2112}O_1][TFSI]$	:	N-ethyl-N,N-dimethyl-2-methoxyethylammonium bis(trifluoromethyl sulfonyl)imide
NSAIDs	:	non-steroidal anti-inflammatory drugs
$[NTF_2]^-$	:	bis(trifluoromethylsulfonyl)imide anion
nZVI	:	nano zero-valent iron (nano-Fe^0)
O_2	:	molecular oxygen/dioxygen/oxygen gas
$O_2^{\bullet-}$	:	superoxide radical anion
O_3	:	ozone

$^1O_2$	:	singlet oxygen
$^\bullet OH$	:	hydroxyl radicals
[OTEAmm][TFSI]	:	octyltriethylammonium bis(trifluoromethylsulfonyl)imide
$[OTF]^-$	:	trifluoromethanesulfonate anion
PAA	:	peracetic acid
PAHs	:	polycyclic aromatic hydrocarbons
PCBs	:	polychlorinated biphenyls
PCDDs	:	polychlorinated dibenzodioxins
PCDFs	:	polychlorinated dibenzofurans
PDS	:	peroxydisulfate
$[PF_6]^-$	:	hexafluorophosphate anion
PILs	:	protic ionic liquids
pKa	:	negative log of the acid dissociation constant (K_a value)
PMS	:	peroxymonosulfate
PO_4^{3-}	:	phosphate anion
ppb	:	parts per billion
PPE	:	personal protective equipment
PS	:	persulfate
[PTEAmm][TFSI]	:	triethylpentylammonium bis(trifluoromethylsulfonyl)imide
PTFE	:	polytetrafluoroethylene
Py	:	pyridine
REM	:	reactive electrochemical membrane
rGO	:	reduced graphene oxide
RIL	:	recycled ionic liquid

ROS	:	reactive oxygen species
(R)/(S) enantiomers	:	R: "Rectus" (Latin) = right / S: "Sinister" (Latin) = left enantiomers
RSM	:	response surface methodology
RT	:	room temperature
RTIL	:	room-temperature ionic liquid
SAA	:	satellite accumulation area
SCE	:	saturated calomel electrode
SCWO	:	supercritical water oxidation
SDS	:	safety data sheet
SHE	:	standard hydrogen electrode
SMM	:	sulfamonomethoxine
SMX	:	sulfamethoxazole
$SO_4^{\bullet-}$	:	sulfate radical
$S_2O_8^{2-}$	:	peroxydisulfate ion
SOD	:	superoxide dismutase
TAP	:	thermally activated persulfate
TBA	:	*tert*-butyl alcohol
TC	:	tetracycline
TEAP	:	tetraethylammonium perchlorate
[TFA]	:	trifluoroacetate
[TfO]	:	trifluoromethanesulfonate
$[TFSI]^-$	:	bis(trifluoromethylsulfonyl)imide anion
$[TFSI]^-$	:	bis(trifluoromethane)sulfonimide

TH	:	thiophene
TiO_2	:	titanium dioxide
Tm	:	melting point
TMS	:	tetramethylsilane
TOC	:	total organic carbon
TPs	:	transformation products
US	:	ultrasound
UV	:	ultraviolet irradiation
UV/H_2O_2	:	ultraviolet peroxide
UV-LED	:	ultraviolet light emitting diode
UV-Vis	:	ultraviolet-visible spectrophotometry
VDW	:	van der Waals interactions
VOCs	:	volatile organic compounds
WAO	:	wet air oxidation
WO_3	:	tungsten (VI) oxide/tungsten trioxide
WO_3^-	:	tungsten (VI) oxide anion
WWTPs	:	wastewater treatment plants
ZnO	:	zinc oxide
ZVI	:	zero-valent iron

LIST OF APPENDICES

CHAPTER 1: INTRODUCTION

1.1 Overview

Active pharmaceutical ingredients (APIs) can be precisely defined as compounds which have a direct effect on the treatment, prevention, mitigation, or diagnosis of a disease, resulting in restoration, improvement, or alteration of physiological functions in an organism. All APIs used in pharmaceutical products are intended to provide pharmacological activity. The wide range of different pharmaceuticals does not essentially possess analogous chemical, structural, physical, or biological properties, unlike other classified groups of homogenous compounds (Taylor & Senac, 2014), for example, polychlorinated biphenyls (PCBs), chlorofluorocarbons (CFCs), polycyclic aromatic hydrocarbons (PAHs), etc.

The few characteristics most pharmaceuticals share are their typically polar nature, possess multiple ionization sites, have complex molecular structures, and exhibit polymorphism (Fatta-Kassinos et al., 2011). Several pharmaceutical substances are known to be lipophilic, while some may have a moderate level of water solubility (Rivera-Utrilla, Sanchez-Polo, et al., 2013). Although pharmaceuticals tend to undergo metabolism while their adsorption and distribution in an organism leads to modification of chemical structures, these also generally have the ability to remain physiologically active, hence, an accumulation in life forms results in a persisting nature of these compounds. Many drugs, for instance, sulfamethoxazole, erythromycin and naproxen may persist for about one year, while clofibric acid is known to remain unaffected for several years (Kummerer, 2009a, 2009b; Rivera-Utrilla, Gómez-Pacheco, et al., 2013; Rivera-Utrilla, Sanchez-Polo, et al., 2013). Certain drug substances have particular enantiomers which demonstrate desired pharmaceutical activity, and therefore the interaction in the living system takes place enantioselectively

(Sanganyado et al., 2017). Consequently, the ratios of (R)/(S) enantiomers tend to alter in the environment as they persevere over time.

The persistence of pharmaceuticals or drug substances in the environment has posed a latent threat to the health of various organisms (Archer et al., 2017). Previously these chemicals were not regulated by the U.S. EPA (Environmental Protection Agency), as the occurrence was presumed harmless owing to the minute quantities. However, recent research has led us to infer that exposure to a number of pharmaceuticals, for example, endocrine-disrupting compounds (EDCs) can cause hormonal disorders both in aquatic life and humans, particularly in the male reproductive system. Therefore, drugs or pharmaceutics as waste in our surroundings also fall under the category of emerging contaminants (ECs). This new family of municipal-derived chemicals known as ECs (Emerging Contaminants) has posed excessive concern as environmental pollutants. Conventionally, chemicals from agriculture or industrial origin become a source of a variety of organic and inorganic contaminants in surface waters which are controlled by regulatory laws (Commission, 2008). More recently, ECs which include pharmaceuticals such as diclofenac and estradiol have gained priority among the list of hazardous substances and thus need to be controlled through legislation (Commission, 2012). Another incipient concern involves the propagation of antibiotic-resistant bacteria in the environment as a consequence of increased consumption of antibacterial medicines (Marti et al., 2014). Substantial amounts (generally in nanograms to micrograms per litre) of non-regulated pharmaceutical contaminants have been detected in surface waters (Ashton et al., 2004; Gracia-Lor et al., 2011).

Advanced oxidation processes (AOPs) can be comprehended as modern alternatives to the conventional incineration of hazardous organic wastes. Although incineration is usually assumed as a viable substitute for landfills, in practice, incineration invites serious and

2

detrimental problems as it becomes a source of toxic substances such as polychlorinated dibenzofurans (PCDFs) and polychlorinated dibenzodioxins (PCDDs) released into the environment, either via fly ash or off-gas emissions from the incinerator. Adsorption is a non-destructive process and requires dealing with the resultant saturated adsorbent.

AOPs have been extensively explored for their feasibility and prospective applications in post-tertiary treatment of sewage in view of the highly efficient degradation of organics, convenient operative measures, the ability to inactivate pathogens, and the lesser formation of by-products resulting from disinfection. Advanced oxidation involves a set of comparable, yet diverse processes aimed at combating water, air and soil pollution. According to Glaze et al. (Glaze et al., 1987), AOPs are the 'near ambient temperature and pressure water treatment processes which involve the generation of hydroxyl radicals in an amount sufficient to achieve water purification'.

AOPs can be predominantly defined as methods involving oxidation, the mechanism of which is characterized by the intermediacy of highly reactive radical species, particularly reactive oxygen species (ROS) resulting in the destruction of the target pollutant. The conventional AOPs mainly include peroxide-based oxidation, ozonation, Fenton's reagent, wet air oxidation, ultrasound, electrochemical oxidation, and photocatalysis based upon either solar visible or near ultraviolet irradiation. While some are less investigated, advancing processes concern the oxidation via pulsed plasma, microwaves, and ionizing radiation. The vast research and development pertaining to AOPs in the last three decades have been primarily in the wake of immensely diversified technologies and various potential areas of applications involved, especially as supplemental techniques to conventional physicochemical, chemical, and biological methods for waste remediation and treatment of waters for municipal and industrial usage. A major limitation related to such processes is the

high expense owing to the consumption of an excessive amount of energy required for the complete mineralization of the substance (Monteil et al., 2019).

The superoxide radical is a reactive anion of oxygen with the chemical formula $O_2^{\bullet-}$ (Hayyan et al., 2016). This ionic moiety with a negative charge (-1) owing to an unpaired electron, is produced as a result of the addition of an electron to molecular oxygen (or dioxygen), O_2. Hence the systematic name of $O_2^{\bullet-}$ is dioxide. The reaction chemistry and biochemistry of $O_2^{\bullet-}$ are critically significant in processes like ageing, oxygen toxicity, and carcinogenesis, since about 1 to 15% of respiratory oxygen goes through the oxidation state of $O_2^{\bullet-}$ (Sawyer, 2020).

The name "superoxide" has although incorrectly incited many to suppose that the species possess an exceedingly high degree of reactivity, this prefix was in fact proposed to indicate the stoichiometry of the salts. The newly synthesized potassium salt - KO_2 - was given the name superoxide in 1934, in order to distinguish its stoichiometry of two oxygen atoms per metal atom from the majority of other metal-oxygen compounds having fewer oxygen atoms per metal, such as Fe_2O_3, Na_2O_2, Na_2O and $NaOH$, etc.

The commonly used methods for the generation of $O_2^{\bullet-}$ involve either direct dissolution of KO_2 in aprotic solvents or reduction of dioxygen on the cathode (E= -1.0V vs SCE) electrochemically. The electrochemical reduction of O_2 dissolved in aprotic solvents to produce $O_2^{\bullet-}$ is a pioneering work initiated by Sawyer and fellow workers (Merritt & Sawyer, 1970; Sawyer, 1992a; Sugimoto et al., 1988). The reaction is depicted in Eq. 1.1 (Fridovich & Handler, 1961).

$$O_2 + e^- \leftrightarrows O_2^{\bullet-} \tag{1.1}$$

As a strong nucleophile, the $O_2{}^{\bullet-}$ undergoes a disproportionation reaction in water, resulting in the formation of oxygen, hydroxyl ion (HO^-) and hydroperoxide ion ($HO_2{}^-$) (Eq. 1.2) (Ballou et al., 1969). Acetonitrile (AcN), dimethyl formamide (DMF) and dimethyl sulfoxide (DMSO) are examples of some generally used aprotic solvents that can be used to generate $O_2{}^{\bullet-}$ in order to avoid the disproportionation reaction.

$$2O_2{}^{\bullet-} + H_2O \rightarrow O_2 + HOO^- + HO^- \tag{1.2}$$

Environmental chemistry additionally pertains to the procedures and practices which implicate cleaner solvents to minimize the reliance on volatile organic compounds (VOCs). In that regard, the use of ionic liquids (ILs) as solvents in chemical reactions has intrigued chemists to much extent as these compounds have proved to be greatly beneficial as alternative reaction media (Huddleston et al., 1998; Welton, 1999). Owing to the ease with which these can be recycled, ILs have been introduced as green solvents for organic synthesis, which also offer plentiful electrochemical uses. Virtually, ILs can be tailored for a particular application by altering the physical and chemical properties of these organic salts as a result of variations in their anions and cations. The properties which make ILs a fascinating choice for electrochemists include high conductivity, low dielectric constant, wide electrochemical window, etc. One of the most significant features of these compounds is the negligible vapor pressure at room temperature resulting in a non-volatile nature, thus facilitating the safety of the processes in which ILs are employed (Carlin et al., 1992). Markedly, ILs are thermally and electrically stable and are also resistant to oxidation. Since an extensive and wide-ranging diversity of ILs is available, and it is possible to tune their properties, therefore, this enables a chemist to design an IL solvent system augmented for a specific process.

IL binary mixtures with other solvents can enhance the selectivity of chemical reactions due to the unique properties of ILs, such as:

1. Low volatility: ILs have low vapor pressures, which can prevent the loss of reactive intermediates and increase reaction selectivity.
2. High conductivity: ILs have high ionic conductivity, which can facilitate ion transport and enhance the rate of certain chemical reactions.
3. Chemical stability: ILs are often highly chemically stable, which can prevent unwanted side reactions and increase the selectivity of the desired reaction.

Therefore, the properties of both components can be exploited to enhance the selectivity of chemical reactions by combining ILs with other solvents, leading to improved yields and reaction outcomes.

In this study, an efficient, cost-effective, and environmentally friendly method for the degradation of pharmaceutical waste involving $O_2^{\bullet-}$ generated in an IL/aprotic solvent mixture system has been devised. In that perspective, the occurrence and stability of $O_2^{\bullet-}$ in the proposed IL/aprotic solvent media and the kinetics of such reactions have been established via chemical and electrochemical generation techniques. Finally, the transformation products formed as a result of the oxidation of pharmaceutical compounds under analysis were identified so as to propose a mechanistic pathway for oxidative degradation.

1.2   Motivation

Multiple studies have shown that pharmaceuticals are occurring ubiquitously in the environment of industrialized, developing, and emerging countries. The waterways,

including drinking water sources are polluted when drugs are trashed or flushed. As reported by EPA ((PSI), 2023), as much as 2,300 tons of hazardous waste are produced annually just by flushed medications, polluting drinking water and harming aquatic species.

More than 1016 publications (plus 139 review articles) have reported MECs (measured environmental concentrations) of pharmaceuticals in various countries (aus der Beek et al., 2016), as more and more pharmaceuticals and their metabolites are recognized as environmental pollutants. Even the trace amounts (µg/l and ng/l) of occurring pharmaceuticals are likely to have an impact on the non-target organisms, especially aquatic invertebrates, since these substances are particularly designed to be (i) suffice at low concentration levels and (ii) resistant against degradation.

Ample investigations have been conducted to establish the various hazardous effects posed potentially on human health and on the ecosystem by pharmaceutical contamination in the environment. Some of the noteworthy concerns include bioaccumulation and ecotoxicity, developmental issues, reproductive impairments, antibiotic resistance and resistant microbes in the environment, disruption of microbial communities, phytotoxicity, and impact on human health, such as endocrine disruption, depending on the nature and concentration of the specific substance, type of ecosystem and the duration of exposure. Hence as research in this area continues, it becomes crucial to adopt sustainable practices in the use and disposal of pharmaceuticals, as well as to improvise the treatment processes to increasingly combat the impact of these micropollutants.

1.3   Problem Statement

Pharmaceutical wastes which primarily comprise APIs have unfavorably turned out to cause environmental havoc. This has been evident in the last few decades with the reported

studies on their fatal effects on aquatic organisms, antibiotic-resistant bacteria (ARB) and antibiotic-resistant genes (ARGs), reducing the diversity of microbial communities in several environmental compartments, inhibition of microbial growth leads to a reduced rate of nutrient cycle, interference in biodegradation of organic matter, hormonal disarray in exposed organisms, etc. In the bargain, the potential for bioaccumulation and the persistent nature of these compounds results in a longer life cycle and activity in the ecological niches.

The removal of pharmaceutical waste has been a progressive area of research, for when compared to ordinary waste, complex chemicals such as drugs require treatment plants to have special techniques and distinctive designs for complete elimination. Several proficient technologies in waste processing have been developed lately, especially for removing pharmaceuticals but the methods being used are complicated involving sophisticated systems (Jallouli et al., 2017). Comprised of specific experimental conditions and unique materials, these groups of processes are merely efficient as a combination of different treatments rather than one exclusive method when it comes to removing different types of pharmaceutical ingredients. Moreover, high expenses and energy constraints are major drawbacks associated with such techniques (Monteil et al., 2019). Thus, there exists an ample requirement for the formulation of a simple, economical, and ecologically friendly method for the degradation of hazardous chemicals which emanate from medicinal products.

The primary challenge in coping with the employment of $O_2^{\bullet-}$ for oxidation is the stability of this radical anion, as it is readily converted to oxygen and other byproducts while undergoing disproportionation reactions in the presence of water (Ballou et al., 1969). In an attempt to contribute to resolving the aforementioned concerns, this research project involves the generation of stable $O_2^{\bullet-}$ in a non-aqueous IL/aprotic solvent mixture system, which would be utilized for the purpose of pharmaceutical waste degradation. ILs are depicted by

their unique properties such as low volatility and slight vapor pressure, which also sort these chemicals as greener, environmentally friendly alternative solvents for various chemical reactions. Hence the proposed method has many advantages over the previously developed processes, as it is lucrative, sustainable, and does not require complex conditions like high pressure or temperature for drug degradation.

1.4   Significance and Scope

The proposed investigation focuses on the chemical generation of $O_2^{\bullet-}$ in various types of IL and aprotic solvent mixture systems. In an effort to obtain a medium which provides a stable $O_2^{\bullet-}$ generation, the volume ratios of the IL and aprotic solvent involved are altered. The stability of $O_2^{\bullet-}$ depends on the chemical structure of cations in the ILs used, as well as on the amount (ratio) of the ILs being employed as a medium. Henceforth, the medium producing the most stable of $O_2^{\bullet-}$ is used for the in-situ degradation of several pharmaceutical substances belonging to different genres which define the application of the project. In order to achieve the maximum percentage of degradation, several parameters, for example, the amount of oxidant (KO_2) used, the nature of IL, amount of IL ratio, reaction temperature, etc. are optimized. Eventually, the degradation products are identified so as to possibly propose a mechanistic pathway for the reaction.

The study has great significance pertaining to the welfare of the environment and subsequently people's health. The expected interpretations, when executed, might very well aid society by contributing to the techniques used for the removal of hazardous pharmaceutical waste which we encounter in everyday life as a contaminant. With an increasing environmental impact on various organisms in the food web, these wastes are particularly detrimental to human health as well, since long-term exposure might pose the

possibility of various serious conditions (for example, hormonal disorders). Furthermore, antimicrobial resistance (AMR) as a result of the misuse and overuse of antibiotics in human and veterinary medicine is well-recognized as a phenomenon giving rise to severe risks concerning global health and livelihoods.

1.5   Applications

Although a large body of literature is directed toward the studies investigating the remediation or degradation of APIs persistent in natural waters, many pharmaceuticals are lipophilic in nature (such as fluoxetine and simvastatin (Zhi et al., 2003)) and thus have the potential to accumulate in sediments, as they are scarcely soluble in water (Nentwig, 2008). Moreover, remobilization of these substances can also arise when the sediment is churned up (Kram et al., 1989). The implications of several environmental compartments such as the sediment phase have been recognized especially using the mesocosm structure of long-term tests and the sediment-dwelling test organisms, which can provide new insights into the modes of action of pharmaceuticals in the environment. This infers that the sediments can also be a reservoir for potentially harmful xenobiotics (Nentwig, 2008).

Therefore, the application of the treatment method developed and optimized in this work implicates the residual pharmaceuticals in the natural sediments, apart from the pharmaceuticals which are released into the environment through improper disposal of expired or unused medications. Provided the lesser number of studies in this domain compared to the oxidative degradation processes for water treatment, this technique for oxidation of solid pharmaceutical waste would notably contribute to the continually evolving field of environmental remediation through sustainable processes.

1.6   Objectives

The major objectives of this study aim to achieve the following:

1. To examine the superoxide radical ion ($O_2{}^{\bullet-}$) in the presence of ILs as reaction media and analyze its stability via kinetic studies.

2. To investigate the in-situ oxidative degradation of active pharmaceutical ingredients (APIs) using $O_2{}^{\bullet-}$ generated in the selected IL/aprotic solvent binary mixtures, and to optimize various operating conditions.

3. To identify the degradation products of APIs formed after oxidation, and to propose possible pathways for the reactions.

1.7   Research Methodology

The specific stages involved in the research methodology are listed as follows:

1. Identification of the superoxide radical ion ($O_2{}^{\bullet-}$) as the potential reactive oxygen species (ROS) in the reaction mixtures contributing toward the degradation.

    (a) Determination of the long-term stability of $O_2{}^{\bullet-}$ (reaction kinetics and percentage consumption rate) via UV-visible spectrophotometry.

    (b) Detection of $O_2{}^{\bullet-}$ as a major ROS using cyclic voltammetry (CV) as an electrochemical proof of its stable generation.

2. Investigation of the in-situ oxidative degradation of APIs using $O_2{}^{\bullet-}$ generated in the selected IL/aprotic solvent binary mixtures.

    (a) Degradation of API in the selected binary mixture (IL/ApS) using a certain ratio while analyzing the extent of degradation as a function of time (using HPLC), along with optimization of various other parameters mentioned as follows:

i. Nature of the IL cation (aromatic/aliphatic)

ii. Alkyl chain length of IL cation

iii. IL/ApS ratio

iv. Oxidant dose

v. Initial concentration of API

vi. Temperature of the media

(b) TOC removal analysis to evaluate the total mineralization of the APIs.

(c) Recycling of ILs and reusing for degradation of APIs while analyzing the purity and potential of ILs in subsequent cycles.

3. Identification of transformation/oxidation products of the API after degradation via LC/MS-QToF, and proposition of the possible reaction pathways for degradation of pharmaceutical compound(s).

1.8   Thesis framework

An abridged outline of the thesis comprising five chapters is mentioned as follows:

1. Chapter 1 (Introduction) acquaints with the fundamentals of the subject matter; pharmaceuticals in the environment, and the superoxide ion radical ($O_2^{\bullet-}$). Subsequently, it indicates the problem statement, the significance, the objectives, and the key stages in research methodology of the study.

2. Chapter 2 (Literature Review) provides an exhaustive account of the numerous methods recently utilized for the oxidative degradation of pharmaceutical waste. A comprehensive background of several different aspects of ionic liquids (ILs) is reflected, along with the listing of ILs employed for the generation of

$O_2^{\bullet-}$. The studies on $O_2^{\bullet-}$ generated in ILs used for degradation of hazardous waste are also cited.

3. Chapter 3 (Research methodology) describes extensively the materials and equipment used, and the experimentation and analysis undertaken to carry out the original work.

4. Chapter 4 (Results and Discussion) thoroughly furnishes attained data as outcomes, followed by discussions and comparisons with the literature.

5. Chapter 5 (Conclusions) delivers the gist of the study and provides recommendations for future studies.

CHAPTER 2: LITERATURE REVIEW

2.1   Oxidative Degradation of Pharmaceutical Waste

Oxidation reactions represent a significant method for the degradation of pharmaceuticals and organic materials in general.

2.1.1   Advanced Oxidation Processes for degradation of pharmaceutical waste

Advanced Oxidation Processes (AOPs) can be predominantly defined as methods involving oxidation, the mechanism of which is characterized by the intermediacy of highly reactive radical species, resulting in destruction of the target pollutant (Wang & Zhuan, 2020). The conventional AOPs mainly include ozonation, Fenton's reagent, electrolysis, wet air oxidation (WAO), ultrasound (US), and photocatalysis based upon either solar visible or near ultraviolet (UV) irradiation. Some less investigated but advancing processes concern the ferrate reagent, pulsed plasma, microwaves, and ionizing radiation. Figure 2.1 illustrates various AOPs utilized for the oxidative degradation of pharmaceuticals and the possible reactive oxygen species (ROS) these processes can produce.

The AOPs may proceed along one of the two routes: (i) oxidation with molecular oxygen (O_2) in an intermediary temperature range (200-300 °C) i.e., between ambient conditions and those used in incinerators Wet Air Oxidation (WAO) processes (1-20 MPa), and (ii) utilization of high energy oxidants such as H_2O_2, ozone and/or photons capable of generating highly reactive intermediate radicals in situ. AOPs can be comprehended as modern alternatives to the conventional incineration of hazardous organic wastes. Although incineration is usually assumed to be a viable substitute for landfill, in practice, incineration invites serious and detrimental problems as it becomes a source of toxic substances such as

polychlorinated dibenzofurans (PCDFs) and polychlorinated dibenzodioxins (PCDDs) released into the environment, either via fly ash or off-gas emissions from the incinerator. Adsorption is a non-destructive process that requires dealing with the resultant saturated adsorbent.
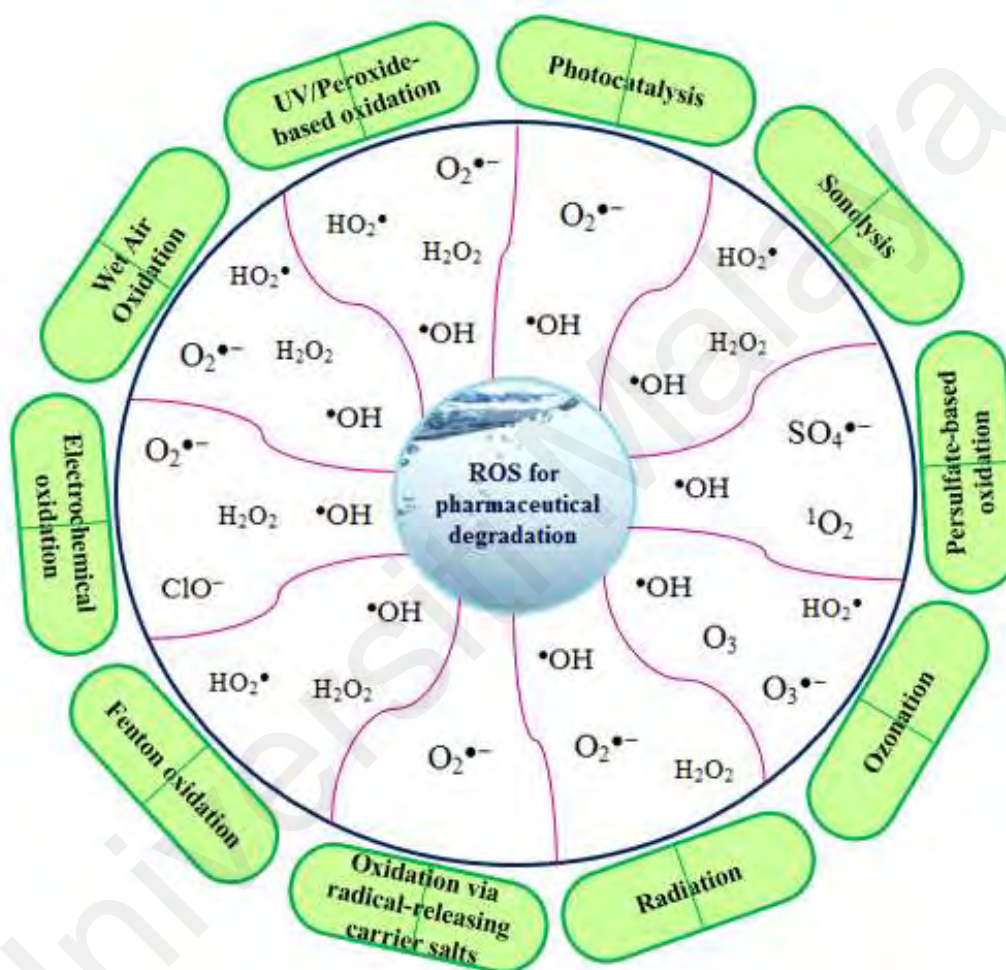
Figure 2.1: Various AOPs utilized for the oxidative degradation of pharmaceuticals.

A tabulated summary of the most recent reports with various types of AOPs being currently utilized for the degradation of pharmaceuticals specifying the target pollutant, the

treatment conditions used, the contribution of the generated ROS, and the outcomes of the

process in the form of removal efficiency are listed in Table 2.1.

Table 2.1: Overview of the most recent publications for degradation of pharmaceutical substances by various AOPs specifying the contributive ROS.

Target drug pollutant/ Initial concentration	System / Experimental conditions	Contributive ROS	Degradation efficiency	Ref.
Tetracycline (40 mg/L) and Ciprofloxacin (50 mg/L)	Sonoplasma treatment with CeO_2 nanocatalysts, Medium: Municipal water, Frequency range: 0.3 to 60 kHz	$^{\bullet}OH$ (primary ROS) and H_2O_2	67% for tetracycline and 55% for ciprofloxacin, after three treatment cycles (5 msec each)	(Abramov et al., 2022)
Ranitidine (5 mg/L)	Co_3O_4 nanosheet (Co_3O_4 NS) membrane/ PMS system Medium: Milli-Q water [Co_3O_4 NS] = 0.7 mg/cm^2, [PMS] = 0.16 mM initial pH = 4.0, T = 298 K	$SO_4^{\bullet-}$ (primary ROS) and $^{\bullet}OH$	>90% for 13 h of continuous-flow operation at a high flux of 176 L m^{-2} h^{-1} bar^{-1}. 100% removal efficiency with calcination performed at 500 °C under air atmosphere	(Wang et al., 2022)
Sulfamethazine (10 mg/L)	Expanded perlite (Ep) supported oxygen vacancies-$CuFe_2O_4$ (OVs-CFEp) photocatalyst/ visible light/ PMS system Medium: Deionized water [PMS] = 0.1 g/L, [catalyst] = 1 g/L, initial pH = 7.0, T = 25 °C	$SO_4^{\bullet-}$, $^{\bullet}OH$, $O_2^{\bullet-}$ and $^1O_2$	Degradation rate up to 95% within 90 min	(Sun et al., 2022)
Ciprofloxacin (10 mg/L)	$Co^0/CoO/Co_3O_4$ @ K, N, O-doped carbons (Co-K-N-O-C) for PMS activation Medium: Deionized water PMS concentration = 2 mM, catalyst dosage = 0.1 g/L, T = 25 °C	$^{\bullet}OH$ (~64.8 ± 1.2%), $SO_4^{\bullet-}$ (~34.2 ± 1.1%) and $^1O_2$ (< 2.0%)	Total removal achieved within 40 min, mineralization efficiency of 84.3% attained within 120 min	(Liang et al., 2022)

Target drug pollutant/ Initial concentration	System / Experimental conditions	Contributive ROS	Degradation efficiency	Ref.
Carbamazepine, sulfamethoxazole, 4-acetamidophenol, ciprofloxacin (10 mg/L each)	CuO/MXene nanocomposites for PMS activation Medium: Ultrapure water [PMS] = 2 mM, [CuO] = [ex-MXene] = 0.3 g/L, T = 293 K, initial solution pH 7.0	$^1O_2$ (primary ROS, contributing by 80.87%), $^\bullet OH$ and $SO_4^{\bullet-}$	Degradation efficiencies attained for SMX, CBZ, APAP and CIP were 100%, 95.88%, 90.07% and 87.02% respectively, within 20 min.	(Yang et al., 2022)
Sulfamethoxazole, trimethoprim, sulfadimethoxine, ibuprofen, carbamazepine and atrazine (10.0 μM each)	PDS activation by visible light (PDS/visible light system) Medium: Deionized water [PDS] = 5.0 mM, [Na2HPO4] = 10.0 mM, pH = 7.0, T = 25 °C	$SO_4^{\bullet-}$ (primary ROS), $O_2^{\bullet-}$ and $^1O_2$	Complete degradation of atrazine achieved by PDS/light system in 30 min	(Wen et al., 2022)
Norfloxacin (10 mg/L)	Magnetic Fe/N/C nanocomposites (FeNGO) catalysts for PMS activation (FeNGO/PMS system). Medium: Ultrapure water [PMS] = 1 mM, [FeNGO] = 50 mg/L, pH = 4.66	$O_2^{\bullet-}$ and $^1O_2$	The FeNGO catalyst/PMS achieved 97.7% removal of norfloxacin after 30 min	(Wang et al., 2022)
Sulfamethoxazole, carbamazepine, naproxen (10 μM each)	Activation of peracetic acid (PAA) by FeS system, Medium: Ultrapure water, tap water and lake water, Oxidants: PAA and H_2O_2, PDS [FeS] = 25 mg/L, [PAA] = 100 μM, [PMS] = 100 μM, [PDS] = 100 μM, [H_2O_2] = 100 μM, initial pH 7 ± 0.2, except for H_2O_2/FeS system (initial pH = 3)	$^\bullet OH$ (primary ROS) and $R\text{-}O^\bullet$	Overall removal rate: 80~100% within 5 min. In the FeS/PAA system, 80.32 ± 0.76% of sulfamethoxazole was degraded within 3 min.	(Yang et al., 2022)

Table 2.1, Continued.

Target drug pollutant/ Initial concentration	System / Experimental conditions	Contributive ROS	Degradation efficiency	Ref.
Sulfamethoxazole, carbamazepine, diclofenac (5 µM each)	Activation of Cr(VI) by UVA-LED (UVA-LED/ Cr(VI) system) Medium: Deionized water $[Cr(VI)]$ = 0.5 mM, pH = 6.0, UVA-LED λ = 365 nm	$^\bullet OH$ (primary ROS)	Degradation efficiency of SMX was 97.5 % at 0.7 mM of Cr(VI) dosage within 30 min. An overall efficient removal with pseudo-first-order rate constants of 0.0610–0.159 min-1 was achieved.	(Huang et al., 2023)
Cefadroxil, tetracycline, levofloxacin (30 mg/L each)	Electrochemical activation of PMS at $Ti/La_2O_3\text{-}PbO_2$ anode (($Ti/La_2O_3\text{-}PbO_2$)EA-PMS system) Medium: Deionized water $[PMS]$ = 5 mM, 0.1 M Na_2SO_4, pH = 3, current density = 30 mA·cm^{-2}	Free $^\bullet OH$, adsorbed $^\bullet OH$ ($PbO_2(^\bullet OH)$) and $SO_4^{\bullet-}$	Removal efficiency of 98.07% for cefadroxil in 60 min. Overall degradation rate was greater than ~95%.	(Yu et al., 2022)
Cyclophosphamide (10 ppm)	Catalytic ozonation by $Mg(OH)_2$ ($Mg(OH)_2/O_3$ system) Medium: Synthetic effluent $Mg(OH)_2$ dosage = 100 mg , pH = 10	$^\bullet OH$ (primary ROS)	93% degradation achieved after 30 min	(Prasanna & Avisar, 2022)
Sulfamethoxazole (10 mg/L)	Heterogeneous photo-Fenton catalysis using Fe-O clusters incorporated in multivariate (MTV) MOF (MIL-100) catalysts (visible-light/ MIL-100 (Sc, Fe)/ Fe-O system) Medium: Ultrapure water MOFs = 0.25 g/L, $[H_2O_2]$ = 19.4 mM, pH = 6.8	$^\bullet OH$, $^1O_2$ and $O_2^{\bullet-}$	Degradation rate of SMX was improved by 11.85 times during the photo-Fenton process in 100 min.	(Li et al., 2022)

Target drug pollutant/ Initial concentration	System / Experimental conditions	Contributive ROS	Degradation efficiency	Ref.
Sulfamethoxazole, sulfachloropyridazine (10 mg/L)	Catalytic PMS activation by ultrathin NiAl-layered double hydroxides (U–NiAl-LDH/PMS system) Medium: Deionized water [PMS] = 0.15 g/L, T = 298 K and [Total metal content of catalyst] = 0.10 g/L	$^\bullet OH$ and $SO_4^{\bullet-}$	Degradation rates of 95.7% and 98.8% obtained in 2.5 and 5 min respectively, using U–NiAl-LDH for PMS activation.	(Wang et al., 2022)
Carbamazepine (CBZ:2 mg/L), thiamphenicol (TAP:5 mg/L), florfenicol (FF:5 mg/L)), phenobarbital (PBB:5 mg/L) and primidone (PMD:2 mg/L)	In-situ chemical oxidation process using CaO_2 as solid oxidant (CaO_2 hydrolysis) Medium: Pure water and surface water CaO_2 dosage = 0.1 g/L (1.0 mM) pH = no adjustment T = 20 °C	H_2O_2, OH^-, $^\bullet OH$ and $O_2^{\bullet-}$	In surface water, removal of FF, TAP, CBZ, and PMD by 0.1 mM of CaO_2 was ~100%, 63%, 60% and 21%, respectively, at a pH < 8.2, in 2 days. Notably, CaO_2 has little effect on TOC and TN removal.	(Zheng et al., 2022)
Tetracycline (20 mg/L)	PMS activation by Fe/Fe₃C embedded in N-dope carbon nanofiber (Fe/Fe₃C@NCNF) Medium: Ultrapure water, reverse osmosis water and tap water PMS = 1.0 mM, Fe/Fe₃C@NCNF = 0.3 g/L, T = 25 °C	$O_2^{\bullet-}$ and $^1O_2$ (primary ROS), $^\bullet OH$ and $SO_4^{\bullet-}$ (minor contribution)	Degradation rate of 90.8% achieved in 30 min. Degradation efficiency in all water quality maintained over 84%.	(Zhu et al., 2022)
Carbamazepine, acyclovir, dexamethasone, ibuprofen (0.5 mg/L each) (+126 pharmaceutical compounds identified in real wastewater)	Electro-peroxone process (with graphite felt as ozone diffusion electrode (ODE)) Medium: Ultrapure water and real hospital wastewater Ozone flow rate = 0.6 L/min, applied current = 0.7 A, Na_2SO_4 = 0.05 mol/L, reaction time = 60 min	H_2O_2 and $^\bullet OH$	Complete degradation for selected pharmaceuticals in mixed synthetic solutions observed in 210 s. 110 pharmaceutical compounds	(Yu et al., 2022)

Table 2.1, Continued.

Target drug pollutant/ Initial concentration	System / Experimental conditions	Contributive ROS	Degradation efficiency	Ref.
			(about 87% of pollutants) achieved higher than 86.0 % removal rates.	
Acetaminophen (10 mg/L)	Electrocatalytic oxidation via Ni–metal–organic framework/ reduced graphene oxide (Ni-MOF/rGO) heterostructure (Ni$_3$HITP$_2$@rGO) Electrolyte solution: 1 g/L NaCl, Applied current (I) = 20 mA, pH = 6.55, T = 25 °C	$^\bullet$OH, O$_2$$^{\bullet-}$, ^{1}O$_2$ and active chlorine (HClO)	100% removal efficiency achieved with 20 mA applied current in 60 min.	(Yang et al., 2023)
Acetaminophen (5 mg/L)	Photo-Fenton oxidation via CuS/MIL-Fe heterojunction catalyst Medium: Deionized water [catalyst] = 200 mg/L, [30% H$_2$O$_2$] = 15 mM, initial pH = 5 ± 0.2, T = 25 °C solar irradiation: 300 W Xenon lamp	$^\bullet$OH and ^{1}O$_2$	Removal efficiency of 99.8% was obtained under optimum conditions after 30 min. TOC removal rate of 60.12 % achieved within 120 min.	(Fang et al., 2023)
Carbamazepine (10 μM)	Solar/sulfite autoxidation (solar/sulfite process) Light source: Xenon lamp (250 W) Medium: Real waters (lake water, river water) [Sulfite] = 1.0 mM, pH = 7.0 ± 0.2, initial DO of 8.0 ± 0.2 mg/L, [T] = 25± 1 °C	SO$_4$$^{\bullet-}$ (74.4%) and $^\bullet$OH (25.6%)	Degradation efficiency was 78.8 % after 30 min, with a corresponding pseudo-first-order rate constant of 0.0454 min^{-1}.	(Chen et al., 2023)
Sulfamethoxazole (20 mg/L)	Photo-Fenton-like oxidation by graphitic carbon nitride engineered α-Fe$_2$O$_3$/rGO photocatalyst (g-C$_3$N$_4$/Fe$_2$O$_3$/rGO) Medium: Deionized water, visible light irradiation, [Catalyst] = 25 mg/L, [H$_2$O$_2$] = 6 mM and T = 25 °C	$^\bullet$OH, O$_2$$^{\bullet-}$ and ^{1}O$_2$	Degradation efficiency of 99.9 % achieved in 45 mins. High mineralization ability of about 73 % was observed via TOC analysis.	(Asif et al., 2023)

Target drug pollutant/ Initial concentration	System / Experimental conditions	Contributive ROS	Degradation efficiency	Ref.
Sulfamethoxazole (50 μM)	PMS activation via MOF (ZIF-67)-based Co_3O_4 NPs@N-doped porous carbon polyhedral nanocomposites (Co_3O_4 NPs@N-PC catalyst/PMS system) Medium: Deionized water Catalyst dosage = 10 mg, PMS dosage = 250 μM, pH = 3.9, T = 25 °C	$SO_4^{\bullet-} > {}^{\bullet}OH > {}^1O_2$	Complete degradation was achieved within 15 mins. The degradation rate attained was 0.21 min^{-1} with the mineralization of 36.8%.	(Mohtasham et al., 2023)
Sulfamethoxazole (5 mg/L)	PMS activation by Mg-introduced Fe-N carbon nanotube catalysts (FeMg@NCNTs/PMS system) Medium: Tap water, river water and lake water Catalyst = 0.1 g/L, PMS = 1.0 mM, pH = 6.4, T = 25 °C	${}^1O_2$ (primary ROS)	The removal rates of SMX in tap water, river water and lake water were 100%, 96.6% and 93.1% after 40 min, respectively.	(Zheng et al., 2023)
Sulfamethoxazole (10 mg/L)	Photocatalytic oxidation by anatase/rutile TiO_2 heterojunction with function-specified micro-zones Medium: Ultra-pure water Light source: Xenon lamp (300 W) Catalyst = 0.01 g	${}^{\bullet}OH$, h^+ (primary ROS) and $O_2^{\bullet-}$	Degradation efficiency of the optimized catalyst reached 99.3 % within 60 min, with degradation constant of 0.07 min^{-1}. The COD removal rate was 84.8 % at 480 min and the TOC removal rate was 49.2 % at 60 min.	(Zhang et al., 2023)
Sulfamethoxazole (12 mg/L)	PMS catalytic activation via bowl-like $FeCuS@Cu_2S@Fe^0$ nanohybrid catalyst (B-$FeCuS@Cu_2S@Fe^0$/PMS system) Medium: Double-distilled water. PMS = 0.2 g/L, Catalyst = 0.15 g/L, initial pH = 6.0, T = 25 °C	${}^{\bullet}OH$ (primary ROS), $SO_4^{\bullet-}$, $O_2^{\bullet-}$ and ${}^1O_2$	Complete degradation achieved within 5 mins under optimum conditions, with a rate constant k of 0.89 min^{-1}	(Wang et al., 2023)
Sulfamethoxazole (20 mg/L)	PMS activation using ternary MOFs-derived MnCoFeO (MnCoFeO-2/PMS system) Medium: Ultrapure water, [catalyst] = 30 mg/L, [PMS] = 0.2 mM, initial pH = 7.0, T = 25 °C	$SO_4^{\bullet-}$ and ${}^1O_2$ (primary ROS)	The MnCoFeO-2/PMS system exhibited highest degradation efficacy with 100% removal within 5 min. The removal efficiency of SMX in river water reached almost 100% within 15 min.	(Chen et al., 2023)

2.2 Oxidative Degradation via Radical-releasing Carrier Salts

2.2.1 The Superoxide Ion ($O_2^{\bullet-}$)

The superoxide is a reactive anion of oxygen with the chemical formula $O_2^{\bullet-}$ (Hayyan et al., 2016). This ionic moiety with a negative charge (-1) owing to an unpaired electron, is produced as a result of the addition of an electron to molecular oxygen (or dioxygen), O_2. Hence the systematic name of superoxide anion ($O_2^{\bullet-}$) is dioxide. The anionic radical behaves either as an electron donor, an oxidant, an electron-reducing agent, a base, or a nucleophile (Frimer, 1983; Gülçin et al., 2010; Sawyer & Roberts, 1988). The reaction chemistry and biochemistry of $O_2^{\bullet-}$ are critically significant in processes like ageing, oxygen toxicity, and carcinogenesis, since about 1 to 15% of respiratory oxygen goes through the oxidation state of $O_2^{\bullet-}$ (Sawyer, 2020).

Early interest in $O_2^{\bullet-}$ was found to have originated when the breathing device was invented using KO_2 combined with catalysts generating O_2 from CO_2. Nevertheless, $O_2^{\bullet-}$ has been recognized as far back as 1934 by researchers proposing that the species is produced during H_2O_2 degradation and in the oxidation of ferrous ions by O_2 in an aqueous solution. In 1969, the detection of $O_2^{\bullet-}$ via electron spin resonance (ESR) in an enzymatic reaction involving O_2 (Knowles et al., 1969) and metalloproteins catalyzing disproportionation of $O_2^{\bullet-}$, i.e. superoxide dismutases (SODs) (McCord & Fridovich, 1969) spurred great curiosity. Many studies on $O_2^{\bullet-}$ reactivity followed the finding that $O_2^{\bullet-}$ was a significant intermediate in aerobic organisms. The research on this species did not flourish until 1970-75 when the techniques for investigating $O_2^{\bullet-}$ were developed. This includes aqueous solution pulse radiolysis, flash photolysis, electrochemical reduction of O_2, and the use of aprotic media for KO_2-crown ether solutions (Daniels, 2002).

The commonly used methods for the generation of $O_2^{\bullet-}$ involve either direct dissolution of KO_2 in aprotic solvents or reduction of dioxygen on the cathode ($E = -1.0V$ vs SCE) electrochemically. The electrochemical reduction of oxygen gas (O_2) dissolved in aprotic solvents to produce $O_2^{\bullet-}$ is a pioneering work initiated by Sawyer and fellow workers (Merritt & Sawyer, 1970; Sawyer, 1992a; Sugimoto et al., 1988). The reaction is depicted in Eq. (2.1) (Fridovich & Handler, 1961).

$$O_2 + e^- \leftrightarrows O_2^{\bullet-} \tag{2.1}$$

As a strong nucleophile, the $O_2^{\bullet-}$ undergoes a disproportionation reaction in water resulting in the formation of oxygen, hydroxyl ion (HO^-) and hydroperoxide ion (HO_2^-) (Eq. 2.2) (Ballou et al., 1969). Acetonitrile, dimethyl formamide (DMF) and dimethyl sulfoxide (DMSO) are examples of some generally used aprotic solvents, which can be used to generate $O_2^{\bullet-}$ in order to avoid the disproportionation reaction.

$$2O_2^{\bullet-} + H_2O \rightarrow O_2 + HOO^- + HO^- \tag{2.2}$$

2.2.1.1   Superoxide salts

The name "superoxide" has incorrectly incited many to suppose that the species possesses an exceedingly high degree of reactivity, this prefix was in fact proposed to indicate the stoichiometry of the salts. The newly synthesized potassium salt - KO_2 - was given the name superoxide in 1934, in order to distinguish its stoichiometry of two oxygen atoms per metal atom from the majority of other metal-oxygen compounds having fewer oxygen atoms per metal, such as Fe_2O_3, Na_2O_2, Na_2O, $NaOH$, etc.

Sources of solid superoxide include metal superoxide salts or organic compounds like tetraalkylammonium superoxides (Bovard, 1960). However, increasing the atomic weight of the metal generally tends to reduce the ease of formation of the superoxide salt (Bovard, 1960; White & Paris, 1982). The most commonly used superoxide salt is potassium superoxide (KO_2), which is manufactured by atomizing molten potassium in dry air (Bovard, 1960). A fluffy yellow solid is formed, later crushed or compacted to the desired particle size (White & Paris, 1982). KO_2 is well-characterized and cheaper, often making it the best choice among other salts for many applications (Krawietz et al., 1998). Sodium superoxide (NaO_2), for example, costs about ten times as much as KO_2. Mixtures of peroxide and superoxide phases are frequently produced by the oxidation of potassium, although the formation of oxide has also been documented (White & Paris, 1982).

Calcium superoxide ($Ca(O_2)_2$) can also be formed from the group II metals, nonetheless, it has limited application because high-purity salt is rarely attained owing to its instability. The maximum purity possibly obtained for $Ca(O_2)_2$ by the equimolar disproportionation reaction is 58.4% by weight. Attempts to scale up the process to produce commercial amounts of this superoxide salt were restricted by lower product purity (Bovard, 1960).

The most common usage of superoxide salts is in oxygen regeneration apparatus for firefighters, mining procedures and space travel. The operation involves exhalation into a mouthpiece by the user. The exhaled CO_2 and H_2O vapors travel via a duct and enter the KO_2 container where they are absorbed and replaced with O_2 which is released (Huang et al., 2009a).

More contemporary work on the degradation of organic contaminants utilizes carrier salts for releasing ROS as potential oxidizing agents. This mainly involves the dissolution of

potassium superoxide (KO_2) to release superoxide radical anion ($O_2^{\bullet-}$) for the purpose of in situ oxidative degradation. KO_2 is an intricate and widely used source of $O_2^{\bullet-}$ in diverse chemical and biochemical studies. As recently quantified by Tsaplev and Trofimov (Tsaplev & Trofimov, 2021), pure KO_2 generates up to 1.7 mM of $O_2^{\bullet-}$ in saturated DMSO solutions. These salts can significantly reduce the reactor volume and weight of the required oxidant dose, along with facilitating the storage and shipping requirements as compared to those necessary against H_2O_2 (Chan et al., 2008).

2.2.1.2   Generation of $O_2^{\bullet-}$ in Aprotic solvents

The generation of $O_2^{\bullet-}$, an oxygen-centered radical is a consequence of the reduction of molecular oxygen (Hayyan et al., 2016). The electroreduction of O_2 is a significant reaction in numerous applications, including metal-air batteries, fuel cells and the electrosynthesis of ROS (Evans et al., 2004b). The electrochemical behavior of O_2 in conventional organic and aqueous solvents has been well investigated in studies indicating that its reduction is a complex process.

In an aqueous medium, $O_2^{\bullet-}$ is in a pH-dependent equilibrium with its conjugate acid, $HO_2^{\bullet}$. The pK_a of $HO_2^{\bullet}$ is however 4.88 (Behar et al., 1970), which suggests that at a neutral pH all but 0.3% of superoxide exists as an anion (negatively charged species). Moreover, subject to the pH and the substrate under investigation, $O_2^{\bullet-}/HO_2^{\bullet}$ may react either through oxidation or reduction. Nolte and Peijnenburg (Nolte & Peijnenburg, 2018) while predicting the aqueous-phase rate constant for the reaction between $O_2^{\bullet-}$ and various organic compounds determined that the average experimental pH (although highly variable) for all data was ~7, inferring that the anionic form of superoxide ($O_2^{\bullet-}$) is prevalent which increases the prospect of a reductive pathway.

As a nucleophilic species and a strong Bronsted base, $O_2^{\bullet-}$ is extremely reactive in protic solvents resulting in its spontaneous disproportionation (Huang et al., 2009a) taking place in the two steps represented in Eqs. (2.3) and (2.4) (Rogers et al., 2009):

$$O_2^{\bullet-} + H^+ \leftrightarrows HO_2^{\bullet} \qquad \log K = -4.88 \tag{2.3}$$

$$2HO_2^{\bullet} \rightarrow H_2O_2 + O_2 \tag{2.4}$$

The proclivity of $O_2^{\bullet-}$ reacting with water (Eq. 2.5) was the underlying basis for its generation in non-aqueous media, such as aprotic solvents for e.g., acetonitrile (AcN), dimethyl sulfoxide (DMSO), pyridine and acetone (Barnes et al., 2008a; Buzzeo, Klymenko, et al., 2004; Sawyer, 1995; Hayyan et al., 2012a; Pozo-Gonzalo et al., 2013; Sawyer & Valentine, 1981).

$$2O_2^{\bullet-} + H_2O \rightarrow O_2 + HOO^- + HO^- \tag{2.5}$$

While using aprotic solvents when it is not exposed to a proton source, the $O_2^{\bullet-}$ does not react. Reversible voltammetry O_2 electroreduction has been attained in many commonly used aprotic solvents such as DMSO, AcN, and DMF, as well as in less frequently used ones, e.g., acetone and propylene carbonate (Huang et al., 2009a). In aprotic media, the reversible, one-electron reduction of O_2 producing $O_2^{\bullet-}$ (Eq. 2.45) (Barnes et al., 2008a; Evans et al., 2004b; Huang et al., 2009a) usually takes place at a potential of -1.0 V vs SCE.

The dissolution of superoxide salts such as KO_2 directly in the aprotic solvents also results in the formation of $O_2^{\bullet-}$. However, these solvents rendered limited applications for $O_2^{\bullet-}$ generation owing to their high volatility, imparting unfavorable ecological effects (Hayyan et al., 2011a).

2.2.1.3 Generation of $O_2^{\bullet-}$ in Ionic Liquids (ILs)

Other non-aqueous media include ionic liquids (ILs) largely considered as 'green' solvents in view of their unique properties compared to conventional solvents, such as non-volatility, non-flammability, high ionic conductivity, and thermal stability. In addition to having tuneable physicochemical properties by varying the cation or anion, ILs also hold potential as a recyclable alternative to the classical organic solvents making them exceedingly pertinent to numerous industrial applications (Hayyan, Mjalli, Hashim, & AlNashef, 2010; Wang et al., 2005). Subsequent to the first evidence on the generation of stable $O_2^{\bullet-}$ in an IL by AlNashef et al (AlNashef et al., 2001a; AlNashef et al., 2002a), a number of studies (Barnes et al., 2008a; Buzzeo et al., 2003a; Hayyan et al., 2011a; Huang et al., 2009a; Islam & Ohsaka, 2008b; Katayama et al., 2004a; Rene et al., 2009; Rogers et al., 2009) investigating the stability of $O_2^{\bullet-}$ in many ILs (as listed in Table 2.2) based on various cations and anions have been executed.

Table 2.2: Summary of ILs investigated for $O_2^{\bullet-}$ generation.

IL	Reference
Ammonium-based ionic liquids	
Methyltrioctylammonium bis(trifluoromethylsulfonyl)imide	(Al-Saleem et al., 2019)
Octyltriethylammonium bis(trifluoromethylsulfonyl)imide	(Al-Saleem et al., 2019)
Tributylmethylammonium bis(trifluoromethylsulfonyl)imide	(Al-Saleem et al., 2019)
Butyltriethylammonium bis(trifluoromethylsulfonyl)imide	(AlSaleem et al., 2019; Humayun et al., 2021)
Butyltrimethylammonium bis(trifluoromethylsulfonyl)imide	(AlSaleem et al., 2019; Halilu et al., 2021; Martiz et al., 2004)
Triethylbutylammonium bis(trifluoromethylsulfonyl)imide	(Ghilane et al., 2007; Zigah et al., 2009)
N-Hexyltriethylammonium bis(trifluoromethylsulfonyl)imide	(Buzzeo et al., 2003a; Buzzeo et al., 2004; Evans et al., 2004a; Huang et al., 2009b; Rogers et al., 2009)
Trimethyl-*N*-hexylammonium bis(trifluoromethylsulfonyl)imide	(Katayama et al., 2004b)
Ethyl-dimethyl-propylammonium bis(trifluoromethylsulfonyl)imide	(Halilu et al., 2019; Hayyan et al., 2017)
N,*N*-Diethyl-*N*-methyl-*N*-(2-methoxyethyl)ammonium bis(trifluoromethylsulfonyl)imide	(AlSaleem et al., 2019)
N-Ethyl-*N*,*N*-dimethyl-2-methoxyethylammonium bis(trifluoromethylsulfonyl)imide	(Hayyan et al., 2015; Hayyan et al., 2017; Hayyan et al., 2012)
N-Ethyl-*N*,*N*-dimethyl-2-methoxyethylammonium tris(pentafluoroethyl)trifluorophosphate	(AlSaleem et al., 2019)
Tetrabutylammonium hexafluorophosphate (TBAHFP)/AcN	(Laoire et al., 2009)
Lithium hexafluorophosphate (LiHFP)/AcN	(Laoire et al., 2009)
Potassium hexafluorophosphate (KHFP)/AcN	(Laoire et al., 2009)
Sodium hexafluorophosphate (NaHFP)/AcN	(Laoire et al., 2009)
Tetrabutylammonium perchlorate (TBAClO$_4$)/AcN	(Laoire et al., 2009)
Morpholinium-based ionic liquids	
N-Methoxyethyl-*N*-methylmorpholinium bis(trifluoromethylsulfonyl)imide	(Halilu et al., 2019; Hayyan et al., 2015; Hayyan et al., 2015a; Hayyan et al., 2012)
N-Methoxyethyl-*N*-methylmorpholinium tris(pentafluoroethyl)trifluorophosphate	(Hayyan et al., 2015a)
4-(2-Methoxyethyl)-4-methylmorpholinium tris(pentafluoroethyl)trifluorophosphate	(Hayyan et al., 2015)
Pyrrolidinium-based ionic liquids	
1-Hexyl-1-methyl-pyrrolidinium bis(trifluoromethylsulfonyl)imide	(Ahmed et al., 2015; Al-Saleem et al., 2019; Hayyan et al., 2012; Hayyan et al., 2011b)

IL	Reference
1-Butyl-1-methylpyrrolidinium bis(trifluoromethanesulfonyl)imide	(Ahmed et al., 2015; Al-Saleem et al., 2019; Evans et al., 2004a; Hayyan et al., 2015a; Hayyan, Ibrahim, et al., 2015; Hayyan et al., 2012b; Huang et al., 2009b; Jusys et al., 2019; Katayama et al., 2004b; Katayama et al., 2005; Khan & Zhao, 2014, 2016; Lee et al., 2013; Monaco et al., 2012; Neale et al., 2016; Randström et al., 2007b; Villagrán et al., 2006; Xiao & Zeng, 2013; Yuan et al., 2014)
1-Octyl-1-Methylpyrrolidinium bis(trifluoromethylsulfonyl)imide	(AlSaleem et al., 2019)
1-Propyl-1-Methylpyrrolidinium bis(trifluoromethylsulfonyl)imide	(AlSaleem et al., 2019)
1-(2-Methoxyethyl)-1-methylpyrrolidinium bis(trifluoromethylsulfonyl)imide	(Neale et al., 2016)
1-(2-Methoxyethyl)-1-methylpyrrolidinium tris(pentafluoroethyl)trifluorophosphate	(Halilu et al., 2021)
1-Butyl-1-methylpyrrolidinium dicyanamide	(Hayyan et al., 2015a)
1-Butyl-1-methylpyrrolidinium bromide	(Neale et al., 2016)
1-Butyl-1-methylpyrrolidinium trifluoroacetate	(Hayyan et al., 2015a; Hayyan et al., 2012a)
1-Butyl-1-methylpyrrolidinium trifluoromethanesulfonate	(Hayyan et al., 2015a; Hayyan, Mjalli et al., 2012e)
1-(2-Methoxyethyl)-1-methylpyrrolidinium methylsulfate	(Neale et al., 2016)
Piperidinium-based ionic liquids	
1-(3-Methoxypropyl)-1-methylpiperidinium bis(trifluoromethylsulfonyl)imide	(Hayyan, Ibrahim, et al., 2017; Hayyan, Mjalli, Hashim, & AlNashef, 2011b; Hayyan et al., 2012; Hayyan et al., 2011b)
1-Propyl-1-methylpiperidinium bis(trifluoromethylsulfonyl)imide	(AlSaleem et al., 2019)
1-Butyl-1-methylpiperidinium bis(trifluoromethylsulfonyl)imide	(Al-Saleem et al., 2019; Neale et al., 2016)
1-(2-Methoxyethyl)-1-methylpiperidinium bis(trifluoromethylsulfonyl)imide	(Neale et al., 2016)
1-(2-Methoxyethyl)-1-methylpiperidinium Tris(pentafluoroethyl)trifluorophosphate	(Hayyan et al., 2015a; Hayyan et al., 2017; Hayyan et al., 2015)
1-Butyl-1-methylpiperidinium bromide	(Neale et al., 2016)
1-(2-Methoxyethyl)-1-methylpiperidinium methylsulfate	(Neale et al., 2016)
Azepinium-based ionic liquids	
1-Butyl-1-methylazepinium bis(trifluoromethylsulfonyl)imide	(Neale et al., 2016)
1-Butyl-1-methylazepinium iodide	(Neale et al., 2016)
Phosphonium-based ionic liquids	
Tris(n-hexyl)tetradecylphosphonium bis(trifluoromethylsulfonyl)imide	(Baltes et al., 2013; Evans et al., 2004a; Hayyan et al., 2012; Hayyan et al., 2010; Lee et al., 2013; Pozo-Gonzalo et al., 2014)
Trihexyl(tetradecyl)phosphonium tris(pentafluoroethyl)trifluorophosphate	(Hayyan et al., 2015a; Hayyan et al., 2012c; Lee et al., 2013)

IL	Reference
Tris(n-hexyl)tetradecylphosphonium trifluorotris(pentafluoroethyl)phosphate	(Evans et al., 2004a; Huang et al., 2010)
Trihexyl(tetradecyl)phosphonium bis(2,4,4-trimethylpentyl)phosphinate	(Ahmed et al., 2015)
Triisobutyl(methyl)phosphonium bis(2,4,4-trimethylpentyl)phosphinate	(Ahmed et al., 2015)
Trihexyl(tetradecyl)phosphonium bromide	(Ahmed et al., 2015)
Triisobutyl(methyl)phosphonium bromide	(Ahmed et al., 2015)
Trihexyl(tetradecyl)phosphonium chloride	(Ahmed et al., 2015; Pozo-Gonzalo et al., 2014; Pozo-Gonzalo et al., 2013)
Triisobutyl(methyl)phosphonium chloride	(Ahmed et al., 2015)
Trihexyl(tetradecyl)phosphonium tosylate	(Ahmed et al., 2015)
Triisobutyl(methyl)phosphonium tosylate	(Ahmed et al., 2015)
Trihexyl(tetradecyl)phosphonium dicyanamide	(Ahmed et al., 2015; Pozo-Gonzalo et al., 2014)
Triisobutyl(methyl)phosphonium dicyanamide	(Ahmed et al., 2015)
Imidazolium-based ionic liquids	
1-Methyl-3-octylimidazolium bis(trifluoromethylsulfonyl)imide	(Baltes et al., 2013)
1,2-Dimethyl-3-propylimidazolium bis(trifluoromethylsulfonyl)imide	(Katayama et al., 2004b)
1-Ethyl-3-methylimidazolium bis(trifluoromethylsulfonyl)imide	(Al-Nashef et al., 2010a; Baltes et al., 2013; Buzzeo et al., 2003a; Buzzeo, Klymenko, et al., 2004; Halilu et al., 2021; Hayyan et al., 2015a; Humayun et al., 2021; Katayama et al., 2004b; Lee et al., 2013; Villagrán et al., 2006)
1-Butyl-3-methylimidazolium bis(trifluoromethylsulfonyl)imide	(AlNashef et al., 2010a; Ghilane et al., 2007; Huang et al., 2009b; Khan & Zhao, 2016; Lee et al., 2013; Rene et al., 2009; Xiao & Zeng, 2013)
1-Butyl-2,3-methylimidazolium bis(trifluoromethanesulfonyl)imide	(Barnes et al., 2008a; Huang et al., 2009b; Rogers et al., 2009; Silvester, Rogers, et al., 2008; Xiao & Zeng, 2013)
1-Hexyl-3-methylimidazolium bis(trifluoromethylsulfonyl)imide	(Baltes et al., 2013)
1-Hexyl-3-methylimidazolium trifluorotris(pentafluoroethyl)phosphate	(Baltes et al., 2013; Lee et al., 2013)
1,3-Dimethylimidazolium trifluoromethanesulfonate	(AlNashef et al., 2010a)
1-Butyl-2,3-dimethylimidazolium trifluoromethanesulfonate	(Hayyan, Hashim, et al., 2015; Hayyan, Mjalli, AlNashef, et al., 2012e)
1-Ethyl-3-methylimidazolium tetrafluoroborate	(Ding, 2009; Islam, Ferdousi, et al., 2005; Islam & Ohsaka, 2008a; Zhang et al., 2004)
1-n-Propyl-3-methylimidazolium tetrafluoroborate	(Ding, 2009; Zhang et al., 2004)
1-Butyl-3-methylimidazolium tetrafluoroborate	(Khan & Zhao, 2016; Lee et al., 2013)
1-n-Butyl-3-methylimidazolium tetrafluoroborate	(Ding, 2009; Huang et al., 2009b; Islam, Ferdousi, et al., 2005; Tang et al., 2005; Zhang et al., 2004; Zhao et al., 2010)
1,2-Dimethyl-3-n-butylimidazolium hexafluorophosphate	(AlNashef & Hayyan, 2012; AlNashef et al., 2001b)

IL	Reference
1-Butyl-3-methylimidazoliumhexafluoro phosphate	(AlNashef et al., 2010a; AlNashef et al., 2001b; AlNashef et al., 2002b; Huang et al., 2009b; Khan & Zhao, 2016; Lee et al., 2013; Silvester, Rogers, et al., 2008)
1-Ethyl-3-methylimidazolium tetracyanoborate	(Baltes et al., 2013)
1-Butyl-3-methylimidazolium tetracyanoborate	(Baltes et al., 2013)
1-Hexyl-3-methylimidazolium tetracyanoborate	(Baltes et al., 2013)
1-Ethyl-3-methylimidazolium chloride mixed with AlCl₃	(Carter et al., 1991b)
1-Hexyl-3-methylimidazolium chloride	(Al-Nashef et al., 2010a)
1-Octyl-3-methylimidazolium chloride	(Al-Nashef et al., 2010a)
1,3-Dimethylimidazolium methylsulfate	(Hayyan, Hashim, et al., 2015)
1-Ethyl-3-methylimidazolium methylsulfate	(Hayyan, Hashim, et al., 2015)
1-Ethyl-3-methylimidazolium ethylsulfate	(Al-Nashef et al., 2010a)
1,3-Dimethylimidazolium diphosphate	(Al-Nashef et al., 2010a)
Pyridinium-based ionic liquids	
1-Butyl-3-methylpyridinium bis(trifluoromethylsulfonyl)imide	(Khan & Zhao, 2016)
1-Propyl-3-methylimidazolium bis(trifluoromethylsulfonyl)imide	(Halilu et al., 2019)
n-(3-Hydroxypropyl)pyridinium bis(trifluoromethylsulfonyl)imide	(Hayyan et al., 2011b)
n-Hexylpyridinium bis(trifluoromethylsulfonyl)imide	(Hayyan et al., 2012)
1-(2-Methoxyethyl)-1-methylpyridinium tris(pentafluoroethyl)trifluorophosphate	(Hayyan et al., 2012c)
Sulfonium-based ionic liquids	
Triethylsulfonium bis(trifluoromethylsulfonyl)imide	(Hayyan et al., 2015a; Hayyan et al., 2012)

(a) *Electrochemical generation of $O_2^{\bullet-}$ in ILs*

On account of their remarkably discriminating properties such as low volatility, high thermal stability, high conductivity and wide electrochemical potential windows, ILs have been investigated at length as potent media to carry out electrochemical analyses (Carter et al., 1991a; Huang et al., 2009a). They have also intrigued considerable attention as electrolytes in gas sensors, thus many groups seem to focus on studies related to the reduction of O_2 in ILs (Buzzeo, Hardacre, et al., 2004; Huang et al., 2010; O'Mahony et al., 2008).

Cyclic voltammetry (CV) is a robust and prevalent electrochemical technique frequently employed to investigate the reduction and oxidation processes of molecular species. CV is also invaluable for electron transfer-initiated chemical reactions, including catalysis. The electrochemical reduction of oxygen in aprotic solvents typically occurs at E = + (−1.0) V vs. the saturated calomel electrode (SCE) in the absence of protonic species or water (Costentin et al., 2010; Sawyer, 1992a), according to the reaction shown in Eq. (2.1).

The CV of an electrochemically active species provides information on the redox behavior of the species and the kinetics of reactions at the electrode surface. Moreover, insight into the reaction products and intermediates can also be attained via this technique (Henze, 2001). Numerous studies on CV as a well-established and standard method, for electrochemical generation and simultaneous identification of $O_2^{\bullet-}$ have been reported in the literature (Alnashef et al., 2001a; Al-Nashef et al., 2002a; Barnes et al., 2008b; Buzzeo et al., 2003b; Hayyan et al., 2012d; Islam et al., 2009b; Vasudevan & Wendt, 1995; Wang et al., 2018).

Many studies used the electroreduction of pure oxygen for electrochemical generation of $O_2^{\bullet-}$ (Al-Nashef et al., 2001b; Evans et al., 2004b; Pozo-Gonzalo et al., 2013). It was also reported that $O_2^{\bullet-}$ generated by reducing air at 20 °C resulted in a reduction peak of about one-tenth of that obtained by reducing pure oxygen at 25 °C (Randström et al., 2007b). The observed ratio was also consequent while considering the lower concentration of oxygen in air compared to pure oxygen, besides the lower experimental temperature which also leads to a lower diffusion coefficient. The mechanism in most of these CV analyses with oxygen has been examined using experimental data and fitted with simulation models.

Carter et al published one of the first reports investigating the reduction of O_2 in IL, mainly involving the voltammetry of O_2 gas in 1-ethyl-3-methylimidazolium chloride/aluminum

chloride using a 3 mm diameter glassy carbon (GC) electrode (Carter et al., 1991a; Evans et al., 2004b). No oxidation peak was observed and a single reduction peak was indicated, interpreting the reduction of O_2 to $O_2^{\bullet-}$ which readily and irreversibly reacts with protic moieties found in IL as impurities (Eq. 2.6) (Al-Nashef et al., 2001b).

$$O_2 + 2e^- + 2H^+ \rightarrow H_2O_2 \tag{2.6}$$

The electroreduction of O_2 dissolved in two ILs individually, i.e., 1,2-dimethyl-3-n-butylimidazolium and 1-methyl-3-n-butylimidazolium cations with [PF$_6$] anion was investigated using a GC macro-electrode (Al-Nashef et al., 2001b). A reduction peak was observed with no reverse oxidation peak in the case of 1,2-dimethyl-3-n-butylimidazolium hexafluorophosphate [dmbim][HFP]. This was reported to be caused by the reaction of $O_2^{\bullet-}$ with intrinsic impurities found in the IL. Conversely, in 1-methyl-3-n-butylimidazolium hexafluorophosphate [bmim][HFP], the electrogenerated $O_2^{\bullet-}$ oxidation peak was detected by CV indicating its stability in the IL (Figure 2.2). This was successively followed by O_2 reduction in several ILs comprising ammonium, morpholinium, pyrrolidinium, sulfonium, imidazolium, pyridinium and phosphonium-based cations by a number of research groups (Evans et al., 2004b; Hayyan et al., 2011a; Katayama et al., 2005; Pozo-Gonzalo et al., 2013; Zigah et al., 2009).
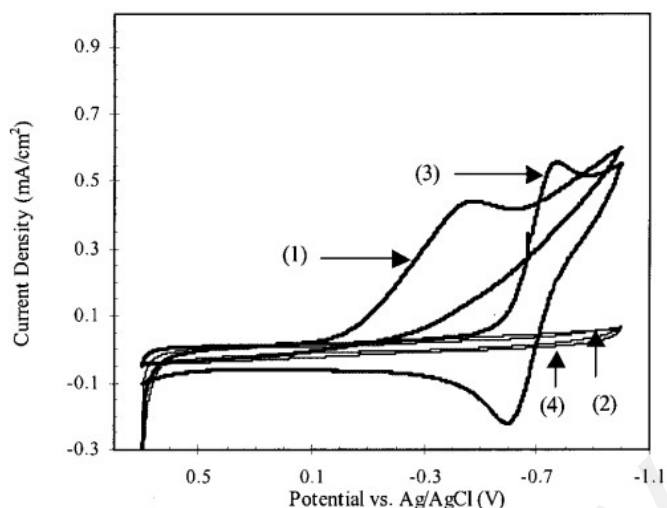
Figure 2.2: The first report of stable $O_2^{\bullet-}$ generated in an IL. CVs at 37 °C at 100 mV/s scan rate in (1) [dmbim][HFP] with O_2, (2) [dmbim][HFP] with N_2, (3) [bmim][HFP] with O_2, and (4) [bmim][HFP] with N_2. The working electrode was glassy carbon and the reference electrode was Ag/AgCl (Al-Nashef et al., 2001b).

A significant influencing factor in the cyclic voltammetric analysis of O_2 is the type of working electrode used. The effect of the working electrode on the potential of the $O_2/O_2^{\bullet-}$ redox couple in different aprotic solvents is presented in Table 2.3. Several working electrodes such as GC, Au, Pt and HDME have been used in the CV of O_2 reduction utilizing ILs. The separation between the oxidative and reductive peaks (ΔE_p) is highly dependent on the material of the working electrode, for e.g., a broader CV curve was observed while using a Pt electrode in comparison with a GC and Au electrode (specifically in the order GC < Au < Pt). This variance has been ascribed to the likely product adsorption or coupled chemical reaction taking place on the Pt electrode (Rogers et al., 2009; Zhang et al., 2004).

Table 2.3: O₂/O₂•⁻ potentials for different electrode materials (Song & Zhang, 2008).

Solvent	Potentials at electrodes (V) vs. NHE			
	C	Pt	Au	Hg
AcN	− 0.63	− 0.65	− 0.65	0.63
Py	− 0.64	− 0.65	− 0.63	-
DMF	− 0.62	− 0.62	− 0.64	-
DMSO	− 0.54	− 0.78	− 0.55	-

In addition, with an increase in solvation energy, this potential value tends to become more positive (Song & Zhang, 2008). The degree of solvation of negatively charged $O_2^{•-}$ increases with the acceptor number of the solvent. Hence, the $O_2/O_2^{•-}$ redox potential further becomes positive as the solvent acceptor number increases. The acceptor numbers of H_2O, DMF, DMSO and AcN are 54.8, 16.0, 19.3 and 19.3 respectively (Staemmler, 1979). The $O_2/O_2^{•-}$ redox potential, oxygen diffusion coefficient (D_{oxygen}), concentration of oxygen (C_{oxygen}), and formal potential (E^0) at a scan rate of 0.1 V/s in a number of solvents are enlisted in Table 2.4.

Table 2.4: O₂/O₂•⁻ redox potential in selected solvents (1 atm O₂) (Song & Zhang, 2008).

Solvent	C_{oxygen} (mM)	$D_{oxygen} \times 10^5$ (cm² s⁻¹)	E^0 (V) vs. NHE
H_2O	1.00	2.10	− 0.16
DMSO	2.10	2.10	− 0.54
DMF	4.80	5.00	− 0.62
Py	4.90	5.70	− 0.62
MeCN	8.10	7.20	− 0.63
Quinoline	1.50	1.80	− 0.63
EMIBF₄	1.10	1.70	− 0.61
PMIBF₄	1.00	1.30	− 0.58
BMIBF₄	1.10	1.20	− 0.62
[BMIM][PF₆]	3.60	0.22	− 0.64

Temperature is another substantial factor affecting the voltammetric analysis. The influence of temperature on the voltammetry of ILs was investigated by Huang et al (Huang et al., 2009a). It was revealed that at higher temperatures, the ΔE_p in all the studied ILs was reduced which is suggestive of more rapid kinetics.

The nature of the cation has also been found to have a principal effect on the voltammetric behavior of O_2 reduction in ILs. This has been demonstrated by examining the CVs for the reduction of O_2 (Au vs Ag) using ILs with varying cations while having a common anion ([TFSI]$^-$) (Huang et al., 2009a). It was observed that the limiting currents were different in the four ILs comprising 1-methyl-3-n-butylimidazolium [BMIm]$^+$, *N*-butyl-*N*-methylpyrrolidinium, 1-butyl-2,3-methylimidazolium and n-hexyltriethylammonium cations. On the contrary, upon variation of the anion with a fixed cation ([BMIm]$^+$), slight variation in limiting currents was detected utilizing [TFSI]$^-$, [PF$_6$]$^-$ and [BF$_4$]$^-$ anions. This inferred that the cationic species in ILs have a notable impact on the voltammetry, while the nature of anion has been observed to have a very meek influence.

Many studies have established the finding that neutral O_2 undergoes diffusion in an IL at a faster rate which leads to a more steady state-like behavior, however, the charged radical anion $O_2^{\bullet-}$ goes through a relatively slow diffusion, resulting in a more transient reverse peak (Buzzeo et al., 2003b; Evans et al., 2004b; Huang et al., 2009a). Most likely, the diffusion of $O_2^{\bullet-}$ is influenced by Coulombic interaction with the organic cations in ILs (Katayama et al., 2005). This strong interaction between $O_2^{\bullet-}$ and the IL cation could obstruct the species more than the neutral O_2 is capable of. These interactions might also alter the diffusion coefficient and the mass transfer of $O_2^{\bullet-}$. The diffusion coefficient of $O_2^{\bullet-}$ in ILs is generally 1/30 to 1/50 times smaller than the diffusion coefficient of O_2 (Pozo-Gonzalo et al., 2013; Silvester,

Rogers, et al., 2008), which is in contrast only 3 in aprotic solvent acetonitrile (Silvester, Rogers, et al., 2008).

(b)   Chemical generation of $O_2^{\bullet-}$ in ILs

While a large body of studies conducted on ILs accompanying the generation of $O_2^{\bullet-}$ have widely used cyclic voltammetry. Given that the analysis most often lasts less than a minute (a few seconds), it is deliberated as a test capable of estimating stability over a short span (thus also referred to as a "short-term stability" test). Therefore, in order to gather more insight into the stability of generated $O_2^{\bullet-}$ over a longer period of time, other techniques have been successfully utilized such as UV-visible spectrophotometry. This assessment over a longer time span (a few hours) is imperative to estimate the applicability of ILs as media for the generation of $O_2^{\bullet-}$ (Islam et al., 2009b). The long-term stability of $O_2^{\bullet-}$ in imidazolium-based ILs has been investigated using UV-visible spectrophotometry (Al-Nashef et al., 2010a; Islam et al., 2009b), reporting the absorbance of the peak as directly proportional to its concentration. Similarly, the chemical generation and stability determination of $O_2^{\bullet-}$ in various phosphonium-based ILs were explored over a longer time period (130 min) by Ahmed et al (Ahmed et al., 2015) (Figure 2.3).
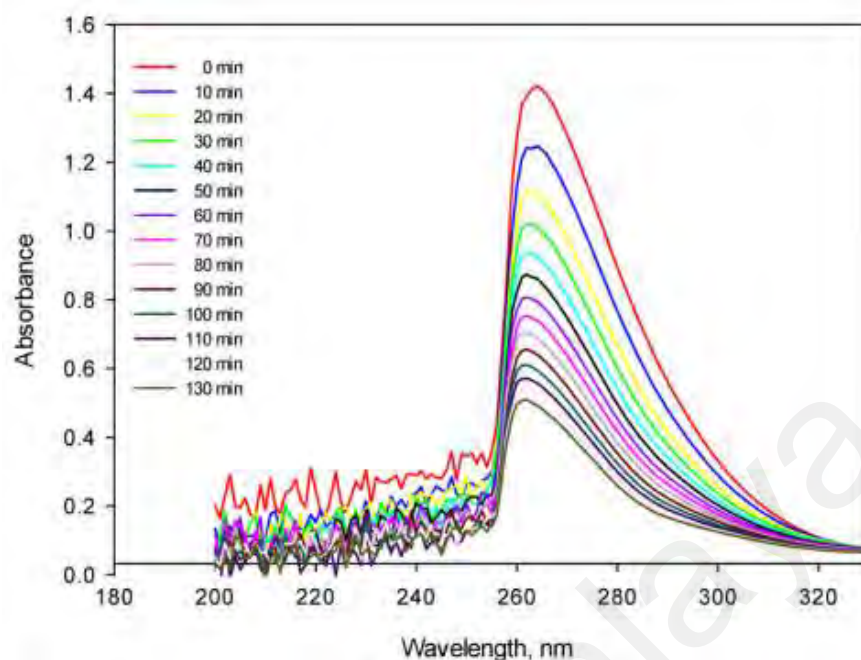
Figure 2.3: UV-visible spectra (long-term stability; 130 min) of $O_2^{\bullet-}$ demonstrating the consumption of the generated ion in the presence of trihexyl(tetradecyl)phosphonium chloride (Cyphos IL 101) as a function of time (Ahmed et al., 2015).

These works were followed by further exploration of $O_2^{\bullet-}$ stability in numerous ILs by Hayyan and co-workers, making use of both CV and UV-visible spectrophotometric techniques (Hayyan et al., 2012; Hayyan et al., 2012). The studied ILs used as media comprised imidazolium, piperidinium, pyridinium, pyrrolidinium, phosphonium, sulfonium, morpholinium, and ammonium-based cations paired with several anions such as bis(trifluoromethylsulfonyl)imide [TFSI], tris(pentafluoroethyl)trifluorophosphate [TPTP], trifluoroacetate [TFA], trifluoromethanesulfonate [TfO], dicyanamide [DCA], and methylsulfate [MS] (Hayyan et al., 2015). Conducive to efficiently implementing the $O_2^{\bullet-}$ in different industrial applications, it is crucial to embark on in-depth studies for the $O_2^{\bullet-}$ stability and kinetics over a certain time period (Hayyan et al., 2012).

2.3   Ionic Liquids (ILs)

Ionic liquids (ILs) can be described as a subset of molten salts with melting points (T_m) below 373 K (Hayes et al., 2015). Walden's original work has designated these materials as "water-free salts… which melt at relatively low temperatures, about up to 100 °C" (Reichardt, 2007); this was also a definition later endorsed and codified in 2000 in a NATO workshop in Crete (Rogers et al., 2012). ILs may as well be adequately discernible as semi-organic fluid salts exclusively comprising bulky asymmetric organic cations and organic or inorganic anions, either near or at room temperature. There exists significant unanimity for a qualified IL to essentially have a melting point below 100 °C. ILs are hence salts which exist in the liquid phase at and/or around 298 K. However, some authors also discriminate between ILs ($T_m < 373$ K) and room-temperature ionic liquids (RTILs) ($T_m < 298$ K).

A series of low-melting ILs is typically composed of a bulky organic cation (such as alkylimidazolium, *N,N*-dialkylimidazolium, *N*-alkylpyridinium, alkylammonium, and alkylphosphonium) weakly coordinated to an organic or inorganic anion (for example, $CF_3SO_3^-$, $[(CF_3SO_2)_2N^-]$, CH_3COO^-, $AlCl_4^-$, NO_3^-, PF_6^-, BF_4^-, I^-, Cl^-, etc.), as presented in Scheme 2.1.

ILs as solvent media have gained much consideration as they revel in a plethora of applications due to their supple properties which are task-specific, because they can be tailored by tuning the structure of the ionic species involved (Hajipour & Rafiee, 2009). Some common properties include a wide liquid phase range with lower melting points, stability in air and moisture, insignificant vapor pressure and high degrees of solubility, even in polymeric materials (Yavari & Kowsari, 2007). ILs, when used as reaction media, are not merely greener, but also resolve issues like solvent emission and recycling of catalysts (Gong

et al., 2008). Various organic chemical reactions can be carried out in ionic liquids; esterification reaction (Fang et al., 2006; Fraga-Dubreuil et al., 2002), aldol condensation (Zhu et al., 2005), Koch carbonylation (Qiao & Chiaki, 2006), polymerization (Ogoshi et al., 2008), hydrogenation, regioselective alkylation and Friedal-Crafts reaction (Cui et al., 2006; Lin et al., 2009), DielsAlder reaction (Fischer et al., 1999; Janus et al., 2006), Mannich reaction (Sahoo et al., 2006; Zhao et al., 2004), oxidation (Chaskar et al., 2009; Hajipour et al., 2006; Hajipour et al., 2007), Heck reaction (Li et al., 2006), Knoevenagel reaction (Hu et al., 2005; Zhang et al., 2006), Henry reactions (Jiang et al., 2004), heterocyclic synthesis (Bao et al., 2008; Siddiqui et al., 2005; Wang et al., 2008) and some enzyme reactions are to name a few.
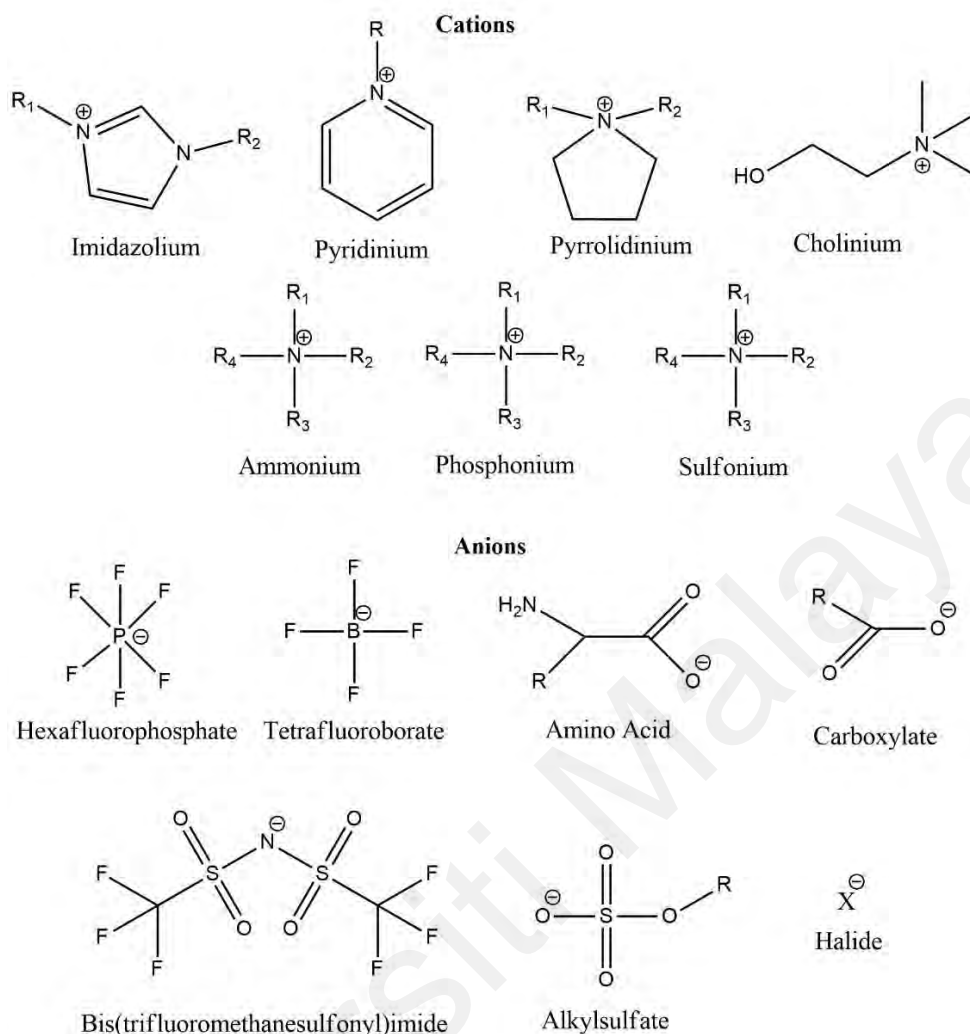
Scheme 2.1: Typical ions in ionic liquids (ILs).

Moreover, ILs are being explored as promising electrolytes in numerous modern applications, e.g., fuel and solar cells, gas sensing (Buzzeo et al., 2004; Silvester et al., 2008), electrochemical devices, capacitors, lubricants, liquid crystals, in production of high-conductivity materials (Hayyan et al., 2011a), organometallic synthesis, synthesis templates for nanomaterials, materials for tissue preservation, biphasic catalysis and in the preparation of polymer-gel catalytic membranes, enzyme immobilization supports, in separation technologies (Chen & Hussey, 2005; Cocalia et al., 2006; Vayssière et al., 2005; Visser et

al., 2000; Visser et al., 2002) such as chromatographic stationary phases and in matrices for mass spectrometry.

The past three decades have been particularly marked by an exponential growth in publications involving liquid salts or "ionic liquids", with findings straddling various areas of chemistry (Rogers, 2007; Rogers & Seddon, 2003), in a way that the subject has extensively outgrown its stirps in electrochemistry (Mamantov, 1994; Wilkes, 2002) and organic synthesis (Welton, 1999). Currently, this interdisciplinary area has been incited even more by the evolution of green chemistry (Anastas, 1998). In addition, the relative ease with which ILs can be integrated into existing systems as solvents is remarkable, considering the solubility of materials in ILs, known since the 1950s to dissolve both polar and nonpolar compounds. Therefore, the key to the advent and impact of ILs is their distinct solvent structure or nanostructure which has been the driving interest in their research even before the wide appreciation of ILs.

2.3.1 Structure of ILs

At ambient temperatures, ILs tend to exist as liquids by virtue of their chemical structure. More often than not, the cation/anion pairing is a penchant for the precise destabilization of solid-phase crystals. Hence, this is predominantly achievable within a fairly large window of ion structures by balancing ion-ion interactions (adjusting distance between charges via carbon chain length) and by fine-tuning the symmetry of cations (Hayes et al., 2015), however, there are no set rules to making an IL. The cation alkyl chain, for example, must be long enough so as to diminish the Coulombic forces resulting in disruption of lattice packing. On the other hand, despite the enhanced symmetry, the melting point of salt may increase if the chain length is excessively long ($\sim$ n < 12). This implies that regarding linear alkanes, cohesive interactions presumably increase with the length of non-polar groups. Davis et al.

conversely indicated that low-melting salts can be produced from rather long chain ($> C_{16}$) cations by insertion of a cis double bond (kink) on the alkyl group (Murray et al., 2010), akin to homeoviscous adaptation in cellular membranes (Sinensky, 1974). This draws attention to the complex array of chemical factors and packing dynamics that govern the melting point of an IL.

2.3.1.1 Classification by structure

Similar to conventional solvents, ILs in general are also characteristically classified on the basis of their chemical structure. Nevertheless, the structural features of ILs are implicative of molten salts, ionic crystals (Hamaguchi & Ozawa, 2005), ionic surfactants, and molecular liquids. Moreover, potential neat ILs outnumber other solvents (Earle & Seddon, 2000), making their classification relatively perplexing since more than a few labels can suggestively be apt for a particular IL. This may be determined by whether cogent significance is held by the cation, anion, or other functional group(s). On the basis of proton-donating (protic) and non-proton-donating (aprotic) molecular solvents (Parker, 1962), the two most well-recognized types of ILs are "protic" (Greaves & Drummond, 2008) and "aprotic" (Angell et al., 2007) ILs. Even though this categorization does not appear to be much of a hardline from the time when Davis et al described dicationic ILs as being able to retain one protic and one aprotic charge center, thus pronouncing both functionalities simultaneously (Mirjafari et al., 2013).

(a)   Protic ILs

The transfer of a proton from an equimolar combination of a Bronsted acid and a Bronsted base generates protic ILs (PILs) (Greaves & Drummond, 2008). As there are no byproducts produced in the process, this refers to PILs as being more economical and simpler to synthesize compared to other classes of ILs (Scheme 2.2). Proton transfer is pervasive in

nature; intriguingly, the characterization of a naturally occurring PIL has been reported in the recent past (Chen et al., 2014). PILs may behave as pure mixtures of ions despite the proton transfer, which is a chemical equilibrium occasionally leading to the propagation of neutral species. This is owing to the fact that the ionic behavior of PILs is much more comparable to ideal aqueous KCl solutions (Xu & Angell, 2003).
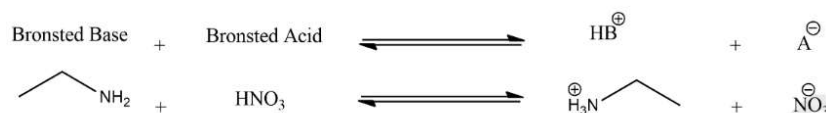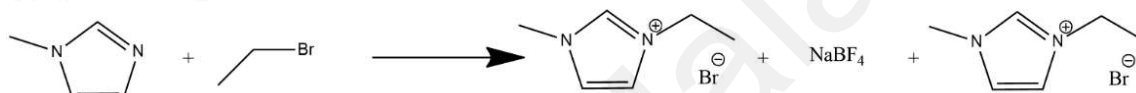
Scheme 2.2: Typical synthetic routes of (A) ethylammonium nitrate (PIL) and (B) 1-ethyl-3-methylimidazolium tetrafluoroborate (AIL).

PILs are capable of hydrogen bonding since H-bond donor and acceptor sites are formed on the ions as a result of proton transfer. Thus far, the vague proton transfer mechanism in PILs resembles the Grotthuss-like behavior in molecular protic solvents with labile protons "hopping" between ions alongside H-bonds (Miran et al., 2014; Noda et al., 2003). This proton transfer has implications in various properties, such as conductivity (Belieres & Angell, 2007), catalytic activity (Greaves & Drummond, 2008), protein stabilization (Mann et al., 2009), vapor pressure (Belieres & Angell, 2007) and thermal stability (Yoshizawa et al., 2003). Therefore, insight into the PIL solvent behavior can be achieved via familiarity with their H-bonding structures.

(b)   Aprotic ILs

Aprotic ILs (AILs) can possess a vast array of chemical structures both in cations and anions. Several of these can form hydrogen bonds while others cannot, and hence the structural features of AILs differ from PILs. Many initial studies on AILs were delimited to halo-metallate ions (Estager et al., 2014), however, this has now stretched out to include an enormous series of chemical structures.

In general, the synthesis of AILs often involves multi-step reactions (Beyersdorff et al., 2008; Wasserscheid & Welton, 2008) (Scheme 2.2), which makes the preparation process more complex and costly when compared to PILs. In the case of AILs ions are formed by the formation of a covalent bond between two functional groups. This in most instances leads to a more electrochemically and thermally stable solvent. Against the corresponding PIL, "good" ionic behavior is usually indicated for AILs in Walden plots.

(c)   Other IL Subclasses

A number of further subclasses of ILs are stated in the literature, subject to specific structural features, such as a divalent ion (divalent ILs), a polymeric or polymerizable ion (polymeric ILs (Mecerreyes, 2011)), a paramagnetic atom or group (magnetic ILs) (Santos et al., 2014), a chiral center (chiral ILs) (Ding & Armstrong, 2005), a coordinated ion (solvate ILs (Zech et al., 2009)), or a fluorocarbon moiety (fluorous ILs (Shen et al., 2012)). Moreover, some reports also exist on aryl and alkyl ILs (Ahrens et al., 2009) and amino acid ILs (Ohno & Fukumoto, 2007) which are named after certain functional groups present in the ions. More particularly, the magnetic, polymeric and fluorous ILs have a solvent type associated with ferrofluids (Holm & Weis, 2005; Jain et al., 2010), polymer melts (Kremer & Grest, 1990; Münstedt, 2011), or fluorous solvents (Gladysz et al., 2006) respectively. This

attribution also facilitates the reciprocation of discrete chemistries while steering future research into these types of ILs.

2.3.2   Toxicity of ILs and impact on the environment

The toxicological effects of ILs on the environment have been receiving increased consideration, since the permeating use of ILs owing to their vast and varied applications, including the food, pharmaceutical and chemical industries. Designer solvents have gained such colossal interest and are affirmed as environmentally friendly compounds because of their exceptionally distinctive and favorable properties, e.g., high thermal stability and negligible vapor pressure, therefore preventing the direct release of ILs into the atmosphere. Hence, these can serve as 'better' alternatives to hazardous organic chemicals, suiting many industrial precincts such as biomaterial pretreatment and production of energy storage materials.

The flip side of this account, however, despite all the acclaimed eminence ILs celebrate, is that the prerogative of ILs as being 'green' solvents might be revisited from an environmental perspective. By virtue of the range of applications ILs offer in numerous evolving fields, a looming hazard of contamination of the aquatic and terrestrial environments by these substances arises. Moreover, leakage into the environment due to spillage for instance, by human or technical errors might also cause adverse effects. As much as the likelihood of the release of ILs into the environment increases systematically, there is urgent coercion to analyze their toxic and antimicrobial impact. In order to evaluate the potential risks of ILs manifesting in various environmental segments, many studies on the assessment of their toxicity towards several organisms from different trophic levels were carried out.

One of the very first presumptions regarding the ecotoxicity of ILs emerged at the beginning of the 21st century. Based on the structure-activity relationships, several theoretical simulations have been validated by experimental estimations (Jastorff et al., 2003; Ranke et al., 2004; Składanowski et al., 2005; Stock et al., 2004), including the cytotoxicity evaluations by the use of human cell lines (Stepnowski et al., 2004). Appallingly, a significant structural resemblance exists between particular cations of ILs and biologically active plant growth regulators or cationic surfactants which are identified to have a negative impact on the environment.

It was revealed by Gathergood and Scammells in 2002 that the imidazolium-based ILs experience a very slight level of biodegradation (Gathergood & Scammells, 2002). It was further asserted by Stepnowski (Stepnowski & Zaleska, 2005), specifying that ILs with imidazolium cations are resistant to photodegradation. Hence, the poor biodegradability of these persisting ILs may affect the aquatic ecosystems. This impelled the United States National Toxicology (NTP) to carry out extended toxicological analyses of imidazolium, pyridinium and pyrrolidinium ILs. Numerous reports have been documenting the systematic toxicity referable to ILs (Bernot et al., 2005; Cho et al., 2008; Peric et al., 2013; Ventura et al., 2012; Yu et al., 2020; Zhang, Zhang, et al., 2017). These comprise the impact on aquatic biomes via shifts in demographic rates, mortality of organisms, modifications in interaction between species, bioaccumulation ascending at several trophic levels, and changes in biogeochemical processes.

An estimation of the environmental risks ought to encompass the recognition of the outcomes detected as an effect of interactions between the chemical and numerous organisms as well as the calculation of the PNEC (predicted no-effect concentration). Furthermore, other coefficients such as median effective concentration (EC_{50}) and median lethal

concentration (LC_{50}) might be applicable. Many biological tests are employed to evaluate the ecotoxicity of ILs utilizing species living in aquatic habitats such as invertebrates, fish, phytoplankton (Maciorowski et al., 1981), marine bacteria *Vibrio fischeri* (Ranke et al., 2004), and their effect on enzyme activities (Stock et al., 2004).

In addition to reports substantiating the relation between structures and toxicity for ILs, several bioassays gauging the biodegradability of ILs have also been mostly questioning their features as 'clean technology'. Therefore, it is vital to direct the studies more towards designing and utilizing safer and 'greener' ILs synthesized from renewable sources for improved biodegradability.

2.3.3 Impurities

The chemical, physical and spectroscopic characteristics are noticeably influenced by the impurities present in ILs, which mainly include halide ions, unreacted VOCs, residual solvents, acids and water. These impurities primarily arise during the process of synthesis of ILs, since preserving the purity of the product in IL synthesis is one of the key challenges. Generally, the reaction outcomes are prone to have a marked effect even with low levels of impurities ("Ionic Liquids-Properties & Preparation," 2005), for e.g., halide or water. In theory, ILs should be clear, odorless, and in certain cases also colorless (if there are no functional groups attached). Although colorless ILs are not always considered pure, some colorless contaminants such as halides can still be found. For example, hydrophilic ILs with $[BF_4]^-$ or $[OTF]^-$ anions are likely to contain residual halide impurities. In the case of hydrophobic ILs these halide contaminants can be conveniently extracted, however, ILs comprising $[PF_6]^-$ and, to a lesser extent $[BF_4]^-$ anions tend to form hydrogen fluoride on contact with water (Wasserscheid & Welton, 2008). Water as an impurity can be almost always found in ILs unless handled using drying techniques and in a moisture-free

environment. Approximately 1.4 mass% H_2O at saturation can be absorbed even by a hydrophobic IL such as 1-butyl-3-methylimidazolium bis(trifluoromethylsulfonyl)imide, which is significant in terms of molar amount. In IL applications, the presence of H_2O might be critical in some reactions, while it is more negligible in others. In addition, H_2O content can have a prominent impact on the physicochemical properties of ILs and may also affect the IL-soluble catalysts (Wasserscheid & Welton, 2008).

2.4 Degradation of Hazardous Materials using IL-generated $O_2^{\bullet-}$

The ILs have been used as reaction media to release $O_2^{\bullet-}$ by direct dissolution of KO_2 salt, demonstrating that the reactive species generated is stable enough for implications in the degradation of organic contaminants, such as halogenated hydrocarbons and sulfur compounds.

2.4.1 Degradation of halogenated hydrocarbons using $O_2^{\bullet-}$

Several organic contaminants including halogenated hydrocarbons (AlSaleem et al., 2019; Hayyan et al., 2012a), e.g., chloroethanes, chlorophenols, chloroform, bromoform, and carbon tetrachloride have been successfully degraded using IL-generated $O_2^{\bullet-}$. Hayyan et al. chemically generated this reactive species by dissolving KO_2 in various ILs for the oxidative degradation of dichlorophenol (Hayyan et al., 2012), chlorobenzenes (Hayyan et al., 2012a) and hexachloroethane (Hayyan et al., 2012). These experiments have been reported to achieve a degradation rate of more than 90% and were conducted at room temperature and under atmospheric pressure. The efficient oxidation was ascribed to the nucleophilic substitution of $O_2^{\bullet-}$ with chlorine atoms. The destruction of carbon tetrachloride (CCl_4), chloroform ($CHCl_3$) and bromoform ($CHBr_3$) was investigated in 13 different hydrophobic ILs based on ammonium, pyrrolidinium and piperidinium cations (Al-Saleem et al., 2019).

1-Propyl-1-methylpiperidinium, 1-octyl-1-methylpyrrolidinium and octyltriethylammonium paired with bis(trifluoromethylsulfonyl)imide anion contributed to accomplish the best (95%) destruction efficiency for the halogenated hydrocarbons. Table 2.5 summarizes the halogenated hydrocarbons which underwent degradation, and the ILs utilized in the process to generate stable $O_2{}^{\bullet-}$.

Table 2.5: Destruction of halogenated hydrocarbons using $O_2{}^{\bullet-}$ generated in IL media.

HHC	IL	Ref.
2,4-Dichlorophenol (DCP)	N-Methoxyethyl-N-methylmorpholinium bis(trifluoromethylsulfonyl)imide [MOEMMor][TFSI]	(Hayyan et al., 2012)
1,2-Dichlorobenzene (DCB)	1-(3-Methoxypropyl)-1-methylpiperidinium bis(trifluoromethylsulfonyl)imide [MOPMPip][TFSI]	(Hayyan et al., 2012)
1,2-Dichlorobenzene (DCB)	1-Hexyl-1-methyl-pyrrolidinium bis(trifluoromethylsulfonyl)imide [HMPyrr][TFSI]	(Hayyan et al., 2012)
1,2-Dichlorobenzene (DCB), 1,3-Dichlorobenzene (1,3-DCB), 1,3,5-Trichlorobenzene (TCB), Pentachlorobenzene (PCB), and Hexachlorobenzene (HCB)	1-(3-Methoxypropyl)-1-methylpiperidinium bis(trifluoromethylsulfonyl)imide [MOPMPip][TFSI] and 1-hexyl-1-methyl-pyrrolidinium bis(trifluoromethylsulfonyl)imide [HMPyrr][TFSI]	(Hayyan et al., 2012a)
Hexachloroethane	1-Butyl-1-methylpyrrolidinium trifluoroacetate [BMPyrr][TFA]	(Hayyan et al., 2012a)
Carbon tetrachloride (CCl_4), chloroform ($CHCl_3$) and bromoform ($CHBr_3$)	1-Propyl-1-methylpiperidinium bis(trifluoromethylsulfonyl)imide [C_3mPip][TFSI], 1-octyl-1-methylpyrrolidinium bis(trifluoromethylsulfonyl)imide [C_8mPyrr][TFSI] and octyltriethylammonium bis(trifluoromethylsulfonyl)imide [N_{8222}][TFSI]	(AlSaleem et al., 2019)

2.4.2 Desulfurization of sulfur compounds using $O_2^{\bullet-}$

Considering oxidative desulfurization, the $O_2^{\bullet-}$ has not been much investigated as an oxidant. However, the reported reactions of sulfur compounds with $O_2^{\bullet-}$ (Chan, 2010; Oae et al., 1981) reveal that disulfide, sodium sulfonate, thiolsulfinate, thiol, sodium thiolate and thiolsulfonate were readily oxidized to sulfonic and sulfinic acids. The dissolution of KO_2 in solvent using 18-crown-6-ether generated $O_2^{\bullet-}$ under mild conditions (Chan, 2010; Oae et al., 1981). It was found that the reactivity increased in the following order: disulphide $\simeq$ sodium thiolate $\simeq$ sodium sulfonate < thiolsulfonate < thiolsulfinate. More polar solvents such as acetonitrile and pyridine demonstrated better outcomes compared to reactions carried out in benzene. Furthermore, larger amounts of crown ether increased the rate of reaction. The reaction could be accredited to the nucleophilic attack of $O_2^{\bullet-}$ and subsequent electron transfer (Oae et al., 1981). It is possible to oxidize some more complex sulfur compounds like thioureas, thioamides and thiouracils with $O_2^{\bullet-}$ into amides or other corresponding hydrocarbons , as well as to inorganic sulfate or elemental sulfur (Chan, 2010).

Chan et al. (Chan et al., 2008) have also documented the use of $O_2^{\bullet-}$ generated in ILs for oxidative desulfurization, by solubilizing KO_2 in [BMIm][PF_6] for the purpose of its reaction with sulfur compounds. It was later established in further studies, however, that $O_2^{\bullet-}$ reacts with imidazolium-based cations of the ILs to produce 2-imidazolones (Al-Nashef et al., 2010a; Hayyan et al., 2013).

In addition, prior to the dissolution of the salt if there is no drying of ILs as a precautionary step during $O_2^{\bullet-}$ generation, there is a high likelihood that a reaction occurs between H_2O and $O_2^{\bullet-}$ to form H_2O_2. Hence, the desulfurization reaction reported could probably be a result of oxidation via H_2O_2 rather than $O_2^{\bullet-}$. Ahmed et al (Ahmed et al., 2015) reported the use of KO_2 as an oxidant for the desulfurization of dibenzothiophene (DBT) and thiophene

(TH) in ILs. While TH showed up to a 15% conversion after 2 h, DBT seemed to be unreactive towards $O_2^{\bullet-}$. This difference in reactivity has been described to be due to the changes in electron densities of the S atoms in the two compounds, which affect the nucleophilicity of $O_2^{\bullet-}$.

The conversion of TH after oxidative desulfurization was found to be influenced by the alkyl chain length of the IL cation. The longer alkyl chain of ILs led to higher TH conversion, in the following order (Ahmed et al., 2015): trihexyl(tetradecyl)phosphonium bis(2,4,4-trimethylpentyl)phosphinate (Cyphos IL 104), 15% conversion > 1-hexyl-1-methylpyrrolidinium bis(trifluoromethylsulfonyl)imide [HMPyrr][TFSI], 8% conversion > 1-butyl-1-methylpyrrolidinium bis(trifluoromethylsulfonyl)imide [BMPyrr][TFSI], 7% conversion.

The desulfurization reactions using $O_2^{\bullet-}$ as an oxidant have also been reported by Hayyan et al for oxidative conversions of thiophene (TH) (Hayyan et al., 2017) and 2-methylthiophene (2-MTH) (Hayyan et al., 2015), as well as for benzothiophene (BT) and dibenzothiophene (DBT) (Hayyan et al., 2017) in different ILs employed as reaction media. Some sulfur compounds reported for conversion studies along with the ILs utilized for stable generation of $O_2^{\bullet-}$ are listed in Table 2.6. Owing to the nucleophilic characteristic of $O_2^{\bullet-}$ and the greater electron density on the sulfur atom in DBT as compared to that in BT, the BT molecule experienced conversion more easily than DBT (Hayyan et al., 2017).

Furthermore, the ILs had a certain influence on the oxidative desulfurization reaction. This can be depicted as a higher conversion percentage, which is obtainable by $O_2^{\bullet-}$ using [MOEMMor][TFSI] than in [BMPyrr][TFSI].

Table 2.6: Desulfurization of sulfur-containing compounds using O₂•⁻ generated in IL media.

Sulfur compound	IL	Ref.
Thiophene (TH) and 2-methylthiophene (2-MTH)	1-Butyl-1-methylpyrrolidinium bis(trifluoromethylsulfonyl)imide [BMPyrr][TFSI], *N*-Methoxyethyl-*N*-methylmorpholinium bis(trifluoromethylsulfonyl)imide [MOEMMor][TFSI], 1-(2-methoxyethyl)-1-methylpiperidinium tris(pentafluoroethyl)trifluorophosphate [MOEMPip][TPTP] and 4-(2-methoxyethyl)-4-methylmorpholilnium tris(pentafluoroethyl)trifluorophosphate [MOEMMor][TPTP]	(Hayyan et al., 2015)
Benzothiophene (BT) and dibenzothiophene (DBT)	1-Butyl-1-methylpyrrolidinium bis(trifluoromethylsulfonyl)imide [BMPyrr][TFSI] and *N*-Methoxyethyl-*N*-methylmorpholinium bis(trifluoromethylsulfonyl)imide [MOEMMor][TFSI]	(Hayyan et al., 2017)
Thiophene (TH)	Ethyldimethyl-propylammonium bis(trifluoromethylsulfonyl)imide [EDMPAmm][TFSI]	(Hayyan et al., 2017a)

2.5 Recent studies on degradation of APIs investigated in this study

2.5.1 Acetaminophen

The word "acetaminophen" is a condensed form of *N*-acetyl aminophenol, and its alternative name "paracetamol" is a reduced form of para-acetyl-amino-phenol. Acetaminophen, chemically *N*-(4-hydroxyphenyl) ethanamide, has two vulnerable positions in its structure; an acetamido group (–NH–CO–CH₃) and an aromatic ring. Such susceptible sites in a molecule can be readily attacked by ROS.

Acetaminophen is considered a polar compound. This polarity also arises from the presence of functional groups in its structure, such as the hydroxyl group (–OH) and the amide group (–CONH₂). Since these functional groups contain electronegative atoms (nitrogen and oxygen), partial positive and partial negative charges are created within the

molecule. As a result, acetaminophen exhibits some degree of solubility in water and interacts with other polar molecules and solvents.

Owing to the simplicity in chemical structure and extensive research on degradation of acetaminophen via various ROS, it was chosen for investigation as a model drug pollutant to thoroughly explore the oxidation process under study. With the purpose of further exploring the universality of the oxidation process under investigation, the degradation of some other representative drug compounds was also studied; carbamazepine and riluzole were selected as target contaminants.

2.5.1.1 Recent studies on degradation of Acetaminophen

Acetaminophen (also known as paracetamol) belongs to a class of pharmaceuticals called analgesics (pain relievers) and antipyretics (fever reducers). Since the drug can relieve mild to moderate pain, the wide usage of acetaminophen as an analgesic ranges from treating migraines (Haag et al., 2011), muscle aches, colds and sore throats, toothaches, back aches, COVID-19 infection (Tan et al., 2020), reactions to vaccination, to relieving the pain caused by osteoarthritis (Hochberg et al., 2012). It mainly works by altering the way the body senses pain and by cooling down the body temperature. Paracetamol is also often used by patients with low tolerance for NSAIDs like ibuprofen (Conaghan et al., 2019; Moore & Moore, 2016). This makes paracetamol one of the most commonly used medications for relief of such symptoms as pain and fever (Perrott et al., 2004).

Paracetamol is listed on the World Health Organization's List of Essential Medicines (World Health Organization, 2019), and is a drug ingredient in more than 600 brand names which include both prescription and over-the-counter medicines. Classified amongst the top 200 preparations in the US, it is enumerated as one of the three most frequently prescribed

drugs (Sole et al., 2010; Wu et al., 2012; Zhang et al., 2008), with more than 5 million prescriptions in the year 2020 (S.P., 2023). As recent as in 2017, reports have signaled a concentration of 0.01 mg/L acetaminophen present in sewage effluent (CheeMei et al., 2017).

Currently, there have been numerous reports on investigative AOPs for degradation of acetaminophen. A tabulated summary of the most recent reports with various types of AOPs being currently utilized for the degradation of acetaminophen the treatment conditions used, the generated ROS, and the outcomes of process in the form of removal efficiency is listed in Table 2.7.

Table 2.7: Overview of the most recent publications for degradation of Acetaminophen by various AOPs.

System / Experimental conditions	Contributive ROS	Degradation efficiency	Ref.
Photo-electrocatalytic process via BiVO$_4$/BiOI heterojunction photoanode, at 1V vs Ag/AgCl under simulated sunlight Medium: Demineralized water [ACT] = 40µg/L	O$_2^{\bullet-}$ (main ROS) and $^{\bullet}$OH	87% removal efficiency within the first 120 min	(Ali et al., 2023)
Photocatalytic oxidation by multi-anion (P, S)-doped g-C$_3$N$_4$/ 2D TiO$_2$ (5%) composite, under simulated solar light irradiation [ACT] = 20 mg/dm^3, photocatalyst loading = 1 g/dm^3, T = 20°C, pH = neutral	O$_2^{\bullet-}$ and $^{\bullet}$OH	Complete removal in 60 min; TOC removal was 40%	(Cako et al., 2023)
Photocatalytic oxidation via TiO$_2$/Ti$_3$C$_2$ composite fabricated with MXene under simulated solar light irradiation Medium: Deionized water [ACT] = 20 mg/dm^3, photocatalyst loading = 2 g/dm^3	O$_2^{\bullet-}$ and $^{\bullet}$OH	92% removal within 1 h, 3-hydroxyacetaminophen detected as the first main intermediate of ACT decomposition	(Grzegórska et al., 2023)
Photocatalysis using CTAB*-capped and PVP*-capped V$_2$O$_5$ nanocrystals, under simulated solar light radiation. Medium: triple distilled water [ACT] = 10 mg/dm^3, catalyst loading = 0.006 g, pH = 6	-	65% (CTAB-capped V$_2$O$_5$) and 71% (PVP-capped V$_2$O$_5$) degradation after 270 min, COD reduced by 40% and 44% by CTAB-capped and PVP-capped V$_2$O$_5$, respectively	(Borah et al., 2023)
Photodegradation using TiO$_2$/RGO catalyst blends, under UV light irradiation. Medium: mineral spring water	-	Approximately 95.18% removal after 100 min	(Daescu et al., 2023)

System / Experimental conditions	Contributive ROS	Degradation efficiency	Ref.
[ACT] = 0.2 mM, 0.2 mg/mL TiO_2/RGO blends, [RGO] = 5 wt. %			
Photodegradation by integrated PES-ZnO* photocatalyst sheets under UV light irradiation, Medium: Distilled water [ACT] = 10 mg/L, PZ-15 (sheet containing 15 wt% of ZnO), Number of sheets = 4, pH = 7.8	$^{\bullet}OH$	91.5 % degradation efficiency after 420 min	(Chijioke-Okere et al., 2023)
Fenton-like catalytic degradation by SACu-hsCN*/H_2O_2 system [ACT] = 20 mg/L, 5.5SACu-hsCN [Catalyst] = 0.2 g/L, [H_2O_2] = 1000 ppm, T = 40 °C	$^1O_2$ (dominant role) and $^{\bullet}OH$	94.8% removal after 180 min	(Tian et al., 2023)
Fe(III)/H_2O_2 Fenton-like degradation via WS_2 as a co-catalyst (H_2O_2/Fe^{3+}/WS_2 system), Medium: Deionized water [ACT] = 5 mg/L, [H_2O_2] = 1.5 mM, [Fe^{3+}] = 0.15 mM, [WS_2] = 0.3 g/L, pH = 3.0	$^{\bullet}OH$ and $O_2^{\bullet-}$	99.6% degradation in 2.5 min	(He et al., 2023)
Cu^0*/H_2O_2 (Fe^{3+}/Cl^-/Cu^0 /H_2O_2) system Medium: Ultrapure water [ACT] = 5 μM, [Fe^{3+}] = 40 μM, [Cu^0] = 0.1 g/L, [Cl^-] = 2 mM, [H_2O_2] = 0.1 mM, pH = 4 ± 0.1, RT	$^{\bullet}OH$ (62.6%), $Fe^{IV}O^{2+}$(14.1%) and reactive Cl species (RCS) (21.7%)	91.1% degradation and 14.3% TOC removal in 10 min	(Liu, Xu, et al., 2023)
Photocatalytic process coupling a metal-free carbon/g-C_3N_4 (CNC) catalyst with persulfate (PDS); CNC-PDS system, under simulated sunlight [ACT] =10 mg/L, Catalyst dose = 0.5 g/L, [PDS] = 0.5 mM	$O_2^{\bullet-} > {}^1O_2 > h^+$	Complete degradation after 40 min	(Shen et al., 2023)
PMS activation using natural pyrite (FeS_2)/PMS system, Medium: Purified water [ACT] = 20μM, [PMS]$_0$ = 0.15 mM, [pyrite] = 1.0 g/L, pH = 3	$SO_4^{\bullet-}$ (88.8%) and $^1O_2$ (11.2%)	99.2% degradation efficiency after 15 min	(Wang & Dong, 2023)

Nomenclature and description:

CTAB*-capped: Cetyl trimethyl ammonium bromide
PVP*-capped: Polyvinylpyrrolidone
SACu-hsCN*: Single atom Cu-N_3 sites anchored on hsCN (hollow spherical graphitic carbon nitride)
Cu^0*/H_2O_2: Zero-valent copper-triggered hydrogen peroxide process
PES-ZnO*: Polyethersulphone-Zinc oxide (PZ) photocatalyst sheets

2.5.2 Carbamazepine

Carbamazepine is a potentially toxic compound (Sisodiya & Goldstein, 2007; Staines et al., 2004). It is structurally a dibenzoazepine, i.e., 5*H*-dibenzoazepine bearing a carbamoyl substituent at the azepine nitrogen, used frequently as an anticonvulsant. Compounds with two benzene rings linked with an azepine ring are known as dibenzazepines. Azepine is an unsaturated 7-membered heterocycle with one carbon atom replaced by a nitrogen atom. Carbamazepine is essentially neutral or very weakly basic in nature. It is also studied as a moderately polar molecule, as it comprises polar functional groups, such as a carbonyl group (C=O) and various nitrogen atoms in its chemical structure, contributing to its overall polarity. However, compared to highly polar compounds, carbamazepine is not considered as polar. The presence of both polar and non-polar regions in its structure gives it a moderate degree of water solubility and allows it to interact with both polar and nonpolar solvents.

Since the micropollutants consisting of electron-donating groups and unsaturated bonds are easily degradable, carbamazepine was also used as a model contaminant to assess the efficiency of the system.

2.5.2.1 Recent studies on degradation of Carbamazepine

Carbamazepine is an anticonvulsant and analgesic medication specified primarily for the treatment of several forms of epileptic seizures and neuropathic pain associated with trigeminal neuralgia (TN) (Al-Quliti, 2015). TN is a condition involving an intense, debilitating, electric shock-like pain caused by irritation of the trigeminal nerve, usually limited to one side of the face. Moreover, mixed manic-depressive episodes caused by bipolar disorder are also known to be dealt with this anticonvulsant (Weisler, 2006). Accessible as a generic medication (Chin et al., 2008), carbamazepine has been included in the WHO's List

of Essential Medicines (World Health Organization, 2019). With more than 2 million prescriptions in 2020 (August 5, 2023), carbamazepine was the 185th most frequently prescribed medication in the US.

The drug compound along with its biotransformation products have been frequently identified in wastewater treatment plant effluent (Prosser & Sibley, 2015), as well as in streams collecting the treated wastewater (Posselt et al., 2018). The recurring occurrence of this antiepileptic in aquatic compartments has caused alarming apprehensions concerning its potential impacts. Studies on the effects of carbamazepine on zebrafish embryos revealed disrupted growth and development of exposed larvae, i.e., upon exposure to 1 µg/L of carbamazepine, the body length, yolk sac absorption rate, hatching rate, etc. were observed to increase notably.

Moreover, enhanced sensitivity to stimuli (touch and light), behavior impairment, and patterns of neural-related gene expression in zebrafish embryos and larvae were also reported (Qiang et al., 2016). Such impacts on fish population structure can certainly have impending environmental repercussions. Table 2.8 summarizes some recent reports on investigative AOPs for degradation of carbamazepine through various methods.

Table 2.8: Overview of the most recent publications for degradation of Carbamazepine by various AOPs.

System / Experimental conditions	Contributive ROS	Degradation efficiency	Ref.
Photocatalytic oxidation by multi-anion (P, S)-doped g-C_3N_4/ 2D TiO_2 (5%) composite, under simulated solar light irradiation [CBZ] = 14 mg/dm^3, photocatalyst loading = 1 g/dm^3, T = 20°C, pH = neutral	$O_2^{\bullet-}$ and $^{\bullet}OH$	100% degradation achieved in less than 30 min; TOC removal was 76%	(Cako et al., 2023)
Photocatalysis using TiO_2 in ceramic form (PSF-01 solid flake) under simulated sunlight (total energy of 150.92 kJ used in 6 h of irradiation) Medium: Ultrapure, tap, mineral, sea, and river water [CBZ] = 5 mg/L, TiO_2 = 40 g, pH = 2, T = 25 °C	h^+ (95.0%) and $^{\bullet}OH$ (3.2%)	>99% removal efficiency after 120 min; mineralization efficiency was 31.7–71.3% after 6 h	(Nghia et al., 2023)
Photoelectrochemical degradation by MOF*/Bi4O$_7$ S-scheme heterojunction (MIL-68(In)-NH$_2$/Bi4O$_7$ S-scheme system) under visible light [CBZ] = 50 mg/L, photocatalyst dosage: 1.0 g/L	$^{\bullet}OH$, $O_2^{\bullet-}$ and h^+	92.7 % degradation at 120 min	(Zhao et al., 2023)
PMS activation via Co_2P catalyst with surface-active center (Co_2P/PMS system) [CBZ] = 0.010 g/L, [Co_2P] = 0.050 g/L, [PMS] = 0.50 g/L, pH = 5.0, T = 25 °C	$SO_4^{\bullet-}$ and $^{\bullet}OH$	Removal ratio of 98% achieved in 10 min and removal ratio of TOC reached 60% in 60 min	(Chen et al., 2023)
PMS activation using Fe^{3+} doped 1T/2H hybrid MoS_2 (molybdenum disulfide) (Fe^{3+}/N–MoS_2 + PMS system) Medium: Saline wastewaters (0–200 mM) [CBZ] =10 mg/L, catalyst dosage = 75 mg/L, PMS dosage = 50 mg/L, pH = 3	$SO_4^{\bullet-}$	More than 90% degradation in 10 min	(Ye et al., 2023)
Degradation by activation of potassium pyrosulfite (PPS) (S(IV)) using iron (Fe^{3+}/PPS system) [CBZ] = 2 mg/L, [PPS] = [Na_2SO_3] = [$NaHSO_3$] = 0.1 mM, [Fe^{3+}] = 0.06 mM, T = 25 ℃, initial pH = 2.0	$SO_4^{\bullet-}$ (64%) and $^{\bullet}OH$ (35%)	More than 90% degradation in 5 min	(Liu et al., 2022)
Photo-Fenton oxidation by recycled magnetite nanoparticles (Fe(III)-citrate complex) under UV radiation Medium: Ultrapure water [CBZ] = 5 µM, [magnetite] = 0.1 g/L, [H_2O_2] = 3 mM, [citrate] = 1 mM, pH = 7.5 ± 0.2	$^{\bullet}OH$	About 99 % degradation efficiency after 2 h	(Gabet et al., 2023)

Table 2.8, Continued.

System / Experimental conditions	Contributive ROS	Degradation efficiency	Ref.
Photochemical degradation via.: (a) Direct photolysis using accelerated UV treatment under 222 nm irradiation (KrCl* excimer lamp), (b) UV/H$_2$O$_2$-driven AOP ([H$_2$O$_2$] = 10 mg/L) Medium: Laboratory grade water (LGW) and treated secondary effluent (SE) [CBZ] = 1 mg/L	$^\bullet$OH	Fluence-based degradation rate constants for 222 nm direct photolysis was $(9.49 \pm 0.23) \times 10^{-4}$ cm^2/mJ and for UV/AOP it was $(2.58 \pm 0.08) \times 10^{-2}$ m^2/mJ	(Liu, Mullen, et al., 2023)
Electrochemical process combined with UV-LED (UV/EC/Cl$^-$ process) Medium: Wastewater containing Cl$^-$ [CBZ] = 5 µM, [NaCl] = 7 mM, [Borate] = 4 mM, [Na$_2$SO$_4$] = 4 mM, T = 25 °C, pH = 8, I = 800 mA, UV-LED lamp (265 nm) current = 0.75 A	$^\bullet$OH (26%), Cl$^\bullet$ (17%), other reactive species (28%), direct e$^-$ transfer (28%)	Degradation efficiency of 99.8 % after 15 min treatment	(Hu et al., 2023)

Nomenclature and description:
MOF*: Metal-organic framework
KrCl*: Krypton chloride

2.5.3 Riluzole

Belonging to the benzothiazole class, riluzole is chemically 2-amino-6-(trifluoromethoxy) benzothiazole. The benzothiazole moiety, being the key structural feature of riluzole, is a type of heterocyclic compound consisting of a fused ring system involving a benzene ring and a thiazole ring (a 5-membered ring containing a sulfur and a nitrogen atom). This bicyclic ring system is the core structural feature of riluzole molecule, along with an amine group (–NH$_2$) attached to one of its carbon atoms which can likely participate in various interactions.

Riluzole is a moderately polar compound, since it consists of both polar and nonpolar functional groups within its chemical structure. The presence of polar groups such as amine (–NH$_2$) and trifluoromethoxy (–OCF$_3$) groups contribute to its overall polarity. However,

compared to highly polar molecules, riluzole is considered relatively less polar. This moderate polarity of riluzole influences its solubility in water as well as its interactions with other polar and nonpolar substances.

2.5.3.1   Recent studies on degradation of Riluzole

Riluzole is a neuroprotective agent with anticonvulsant properties and is known to treat motor neuron diseases, including neurodegenerative diseases (Nagoshi et al., 2015). At present, riluzole is the only available FDA-approved disease-modifying treatment for amyotrophic lateral sclerosis (ALS) patients (Cheah et al., 2010), a unanimously fatal neurodegenerative disease resulting in progressive loss of motor neurons controlling the voluntary muscles.

There have been very scarce, in fact, deficient studies on the exploration of methods or AOPs for the degradation of riluzole in the recent past. Currently, Bensalah and co-workers (Bensalah et al., 2023) report the heterogenous Fenton-oxidation process utilizing natural iron catalysts for the mineralization of riluzole. The Fenton (H_2O_2/Fe^{2+}) system has been widely used for the treatment of persistent organic pollutants in soil and water. The study investigates the use of a natural iron-based catalyst (comprising a significant amount of hematite (Fe_2O_3) and magnetite (Fe_3O_4)) to decompose H_2O_2 into ROS, such as $^\bullet OH$ and $HO_2^\bullet$ (hydroperoxyl radicals).

The degradation of riluzole in synthetic medium using deionized water employed the Fe-based catalyst/H_2O_2 system. The photo-assisted Fenton process was found to be optimal under UV irradiation (200–600 nm), for 23.4 mg/L initial concentration of riluzole, using 1000 mg/L of H_2O_2, 200 mg/L of Fe-based catalyst (particle size < 200 μm), 140 mg/L of Fe^{2+}, at 23 – 25 °C and pH value of 3. Complete removal of riluzole was attained after 300

min of reaction, while the TOC removal was demonstrated as 88.4% and 92.3% for Fe-based catalyst/H_2O_2/UV and Fe^{2+}/H_2O_2/UV respectively, after 360 min of treatment. Chromatographic analysis revealed that riluzole degradation initiated with the triazole ring-opening, and eventually released sulfate, nitrate, and fluoride ions.

CHAPTER 3: EXPERIMENTAL

In order to develop a perspective of the steps involved in this study in the big picture, the key stages comprising experimental methodology crafted to achieve research objectives are illustrated in the form of a schematic flow diagram in Figure 3.1.
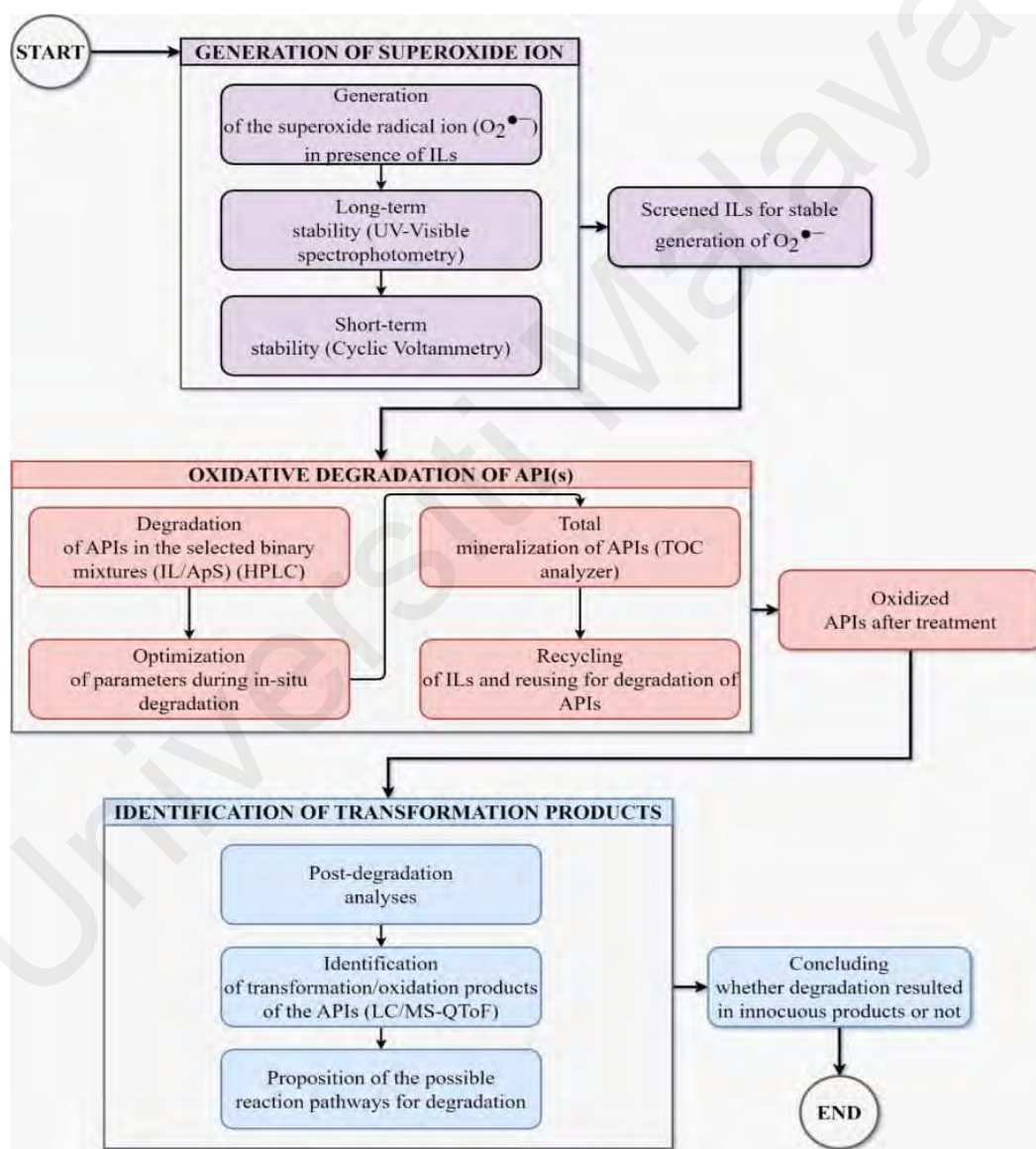
Figure 3.1: Schematic flow chart summarizing key stages comprising the research methodology.

3.1 Chemicals, Reagents and Equipment

The chemicals, reagents and equipment used in the experimental procedures are listed as follows along with the source of procurement:

3.1.1 Analytical Instruments

1. High Performance Liquid Chromatography (HPLC) (Shimadzu)

2. Quadrupole Time of Flight - Liquid Chromatography Mass Spectrometer (QToF-LC/MS) (Agilent)

3. Liquid Chromatography Tandem Mass Spectrometry (LC-MS/MS) (Agilent)

4. UV-Visible spectrophotometer (PerkinElmer-Lambda 35)

5. Potentiostat/Galvanostat (PAR Model 263A)

6. Total Organic Carbon Analyzer (TOC) (Shimadzu)

7. Proton Nuclear Magnetic Resonance spectrometer (^{1}H NMR) (AVN Bruker 400)

8. Fourier Transform Infrared spectrometer (FTIR) (PerkinElmer)

9. Conductivity meter (JENCO VisionPlus EC3175)

10. pH meter (Trans Instruments BP 3001)

3.1.2 Apparatus and Equipment

1. Digital balance (Mettler Toledo AG204)

2. Glove box (Pure Lab^{HE} GP-1)

3. Vacuum oven (Memmert VO500)

4. Centrifuge

5. Ultrasonic cleaner (SASTEC)

6. Hotplates (Fisher Scientific / SASTEC and WiseStire)

7. Teflon-coated magnetic stirrers

8. Refrigerator (Toshiba GR-R72MD)

9. Water circulator (Protech Model 631D)

10. EPA vials fitted with polytetrafluoroethylene (PTFE) lined caps (25 mL, 50 mL)

11. Autosampler screw-top vials (2 mL) and screw caps (Agilent)

12. Syringe filters (PTFE) 0.22 µm (Agilent)

3.1.3   Accessories

3.1.3.1   Electrodes

1.   Glassy carbon macro-electrode (BASi, 3mm)

2.   Platinum macro-electrode (BASi, 3 mm)

3.   Ag/AgCl reference electrode (BASi, 5.7 mm)

3.1.3.2   Polishing kit (BASi PK-4)

1.   Polishing suspension: 0.05 µm alumina polish

2.   Base plates: Heavy glass plates

3.   Substrates: Alumina pad/brown texmet

3.1.4   Gases

1. Ultra-high pure O_2 (99.99%) (Gaslink Sdn, Malaysia)

2. Ultra-high pure N_2 (99.99%) (Gaslink Sdn, Malaysia)

3. Helium / Argon (Gaslink Sdn, Malaysia)

3.1.5   Chemicals and reagents

1.   Potassium superoxide (KO_2) (Sigma Aldrich, 99.9%)

2.   Dimethyl sulfoxide (DMSO) (Fisher Scientific, 99.98%)

3.   Acetonitrile (AcN) (UNICHROM/Merck, HPLC grade 99.9%)

4.   Isopropanol (R&M Chemicals, GC Assay 99.7%)

5.   Deionized water (Milli-Q water system)

6. Ultrapure water (HPLC grade)

7. Deuterated methanol (Methanol-d4, CD$_3$OD) (Sigma Aldrich)

8. Distilled water

3.1.5.1 Pharmaceutical standards

The pharmaceutical standards for the study were purchased from Fisher Scientific. The structures and therapeutic classes are listed in Table 3.1. The specifications and physicochemical properties of the model drug compounds are included in Table 3.2. All chemical reagents and drug standards were used as received without further purification unless stated otherwise.

Table 3.1: Pharmaceutical standards (APIs) investigated in the study, their structure and therapeutic class.
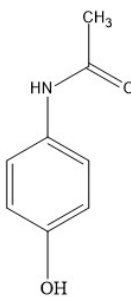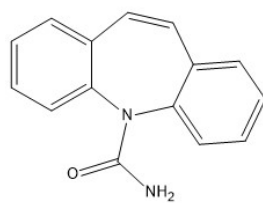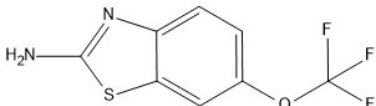
Sr. #	APIs	Structure	Therapeutic class
1	Acetaminophen		Analgesic/antipyretic
2	Carbamazepine		Anticonvulsant
3	Riluzole		CNS (Amyotrophic Lateral Sclerosis) Agent

Table 3.2: Specifications and physicochemical properties of the model drug compounds investigated in the study.

Specifications and physicochemical properties	Pharmaceutical standards (APIs)		
	Acetaminophen	**Carbamazepine**	**Riluzole**
Molecular formula	$C_8H_9NO_2$	$C_{15}H_{12}N_2O$	$C_8H_5F_3N_2O$
Molar masses	151.16 g/mol	236.28 g/mol	234.14 g/mol
Physical appearance	White crystalline powder	White crystalline powder	White to pale yellow powder
Solubility in water	Moderately soluble	Sparingly soluble	Slightly soluble
Melting point	169-170 °C	189-193 °C	194-195 °C
pKa value	~ 9.5 (weak acid)	~ 12.1 (weak base)	~ 4.75 (weak acid)
Partition Coefficient (octanol/water Log^P)	~ 0.35 (moderately lipophilic)	~ 2.58 (moderately lipophilic)	~ 1.53 (moderately lipophilic)
Stability	Stable under normal conditions	Stable under normal conditions	Stable under normal conditions
Polarity	Polar	Moderately polar	Moderately polar

3.1.5.2 Ionic Liquids

The ionic liquids (ILs) investigated in this work were of high-quality synthesis grade (98%) and a part of those, including butyltriethylammonium bis (trifluoromethylsulfonyl) imide, triethylpentylammonium bis(trifluoromethylsulfonyl) imide and octyltriethyl ammonium bis(trifluoromethylsulfonyl)imide were procured from Iolitec. Additional ILs enlisted in Table 3.3 were supplied by Merck. Table 3.3 further provides the abbreviations for all ILs used in this study, their molecular formula, molecular weight, physical state at room temperature, and moisture levels. Schemes 3.1 and 3.2 illustrate the structures of the cations and anions constituting these ILs.

Table 3.3: Specifications of ILs.

IL	Abbreviation	Formula	Mw (g/mol)	Physical form at RT	Moisture level [a] (ppm)
1-Butyl-3-methylimidazolium chloride	[BMIm][Cl]	$C_8H_{15}ClN_2$	174.67	solid	< 100
1-Butyl-3-methylimidazolium dicyanamide	[BMIm][DCA]	$C_1H_{15}N_5$	205.26	liquid	< 100
1-Butyl-3-methylimidazolium trifluoromethanesulfonate	[BMIm][TfO]	$C_9H_{15}F_3N_2O_3S$	288.29	liquid	< 100
1-Butyl-3-methylimidazolium bis (trifluoromethylsulfonyl)imide	[BMIm][TFSI]	$C_{10}H_{15}F_6N_3O_4S_2$	419.36	liquid	< 100
1-Butyl-2,3-dimethyl imidazolium chloride	[BMMIm][Cl]	$C_9H_{17}ClN_2$	188.70	solid (crystals)	< 100
1-Butyl-2,3-dimethylimidazolium iodide	[C4DMIm][I]	$C_9H_{17}IN_2$	280.15	solid	< 100
1,3-Dimethylimidazolium dimethyl phosphate	[MMIm][DMP]	$C_7H_{15}N_2O_4P$	222.18	liquid	< 100
1,2,3-Trimethylimidazolium iodide	[MMMIm][I]	$C_6H_{11}IN_2$	238.07	solid	< 100
1-Ethyl-3-methylimidazolium bis (trifluoromethyl sulfonyl)imide	[EMIm][TFSI]	$C_8H_{11}F_6N_3O_4S_2$	391.31	liquid	< 100
1-Ethyl-3-methylimidazolium ethylsulfate	[EMIm][EtSO4]	$C_8H_{16}N_2O_4S$	236.29	liquid	< 500
1-Ethyl-3-methylimidazolium thiocyanate	[EMIm][SCN]	$C_7H_{11}N_3S$	169.25	liquid	< 100
1-Propyl-3-methylimidazolium bis (trifluoromethylsulfonyl)imide	[PMIm][TFSI]	$C_9H_{13}F_6N_3O_4S_2$	405.34	liquid	< 100
Butyl triethylammonium bis (trifluoromethylsulfonyl)imide	[BTEAmm][TFSI]	$C_9H_{18}F_6N_2O_4S_2$	396.37	liquid	< 100
Ethyldimethyl-(2-methoxyethyl)ammonium tris(pentafluoroethyl)trifluoro phosphate	[N211,mom][E3FAP]	$C_{13}H_{18}F_{18}NOP$	577.23	liquid	< 100
Ethyl-dimethyl-propylammonium bis (trifluoromethylsulfonyl)imide	[EDMPAmm][TFSI]	$C_9H_{18}F_6N_2O_4S_2$	396.37	liquid	< 100
Octyltriethylammonium bis (trifluoromethylsulfonyl)imide	[OTEAmm][TFSI]	$C_{16}H_{32}F_6N_2O_4S_2$	494.56	liquid	< 100
Tetrabutylammonium bis (trifluoromethylsulfonyl)imide	[TBAmm][TFSI]	$C_{18}H_{36}F_6N_2O_4S_2$	522.61	solid	< 500

IL	Abbreviation	Formula	Mw (g/mol)	Physical form at RT	Moisture level [a] (ppm)
Triethylpentylammonium bis (trifluoromethylsulfonyl)imide	[PTEAmm] [TFSI]	$C_{13}H_{26}F_6N_2O_4S_2$	452.48	liquid	< 100
1-Butyl-1-methylpyrrolidinium chloride	[BMPyrr][Cl]	$C_9H_{20}ClN$	177.71	solid	< 100
1-Butyl-1-methylpyrrolidinium tetracyanoborate	[BMPyrr][TCB]	$C_{13}H_{20}BN_5$	257.15	liquid	< 100
1-(2-Methoxyethyl)-1-methylpyrrolidinium bis (trifluoromethylsulfonyl)imide	[MOPyrr][TFSI]	$C_{10}H_{18}F_6N_2O_5S_2$	424.38	liquid	< 100
1-(2-Methoxyethyl)-1-methylpyrrolidinium tris(pentafluoroethyl)trifluorophosphate	[MOPyrr] [E₃FAP]	$C_{14}H_{18}F_{18}NOP$	589.24	liquid	< 100
Guanidinium trifluoromethane sulfonate	[gua][TfO]	$C_2H_6F_3N_3O_3S$	209.15	solid	< 100
N-Methoxyethyl-N-methylmorpholinium bis (trifluoromethylsulfonyl)imide	[MOEMMo] [TFSI]	$C_{10}H_{18}F_6N_2O_6S_2$	440.4	liquid	< 100
Triethylsulfonium bis (trifluoromethylsulfonyl)imide	[SEt₃][TFSI]	$C_8H_{15}F_6NO_4S_3$	399.39	liquid	< 200

[a] Determined by Karl Fisher titration.
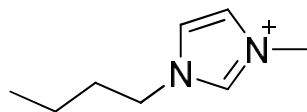
1-Butyl-3-methylimidazolium [BMIm]
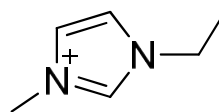
1-Ethyl-3-methylimidazolium [EMIm]
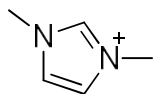
1,3-Dimethylimidazolium [MMIm]
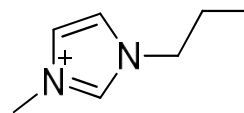
1-Propyl-3-methylimidazolium [PMIm]
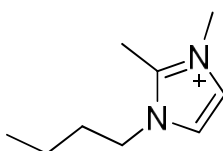
1-Butyl-2,3-dimethylimidazolium [BMMIm]
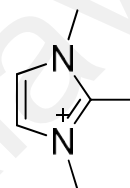
1,2,3-Trimethylimidazolium [MMMIm]
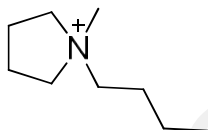
1-Butyl-1-methylpyrrolidinium [BMPyrr]
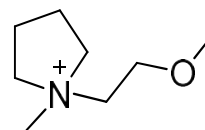
1-(2-Methoxyethyl)-1-methylpyrrolidinium
[MOPyrr]
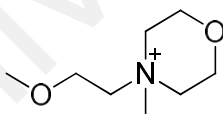
N-Methoxyethyl-*N*-methylmorpholinium
[MOEMMo]
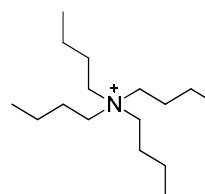
Tetrabutylammonium [TBAmm]

Scheme 3.1: Chemical structures of cations constituting the ILs.
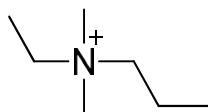
Ethyldimethylpropylammonium [EDMPAmm]
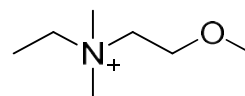
Ethyldimethyl-(2-methoxyethyl)ammonium [N$_{211}$,mom]
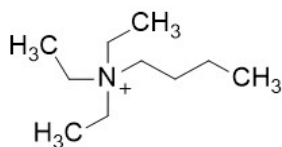
Butyltriethylammonium [BTEAmm]
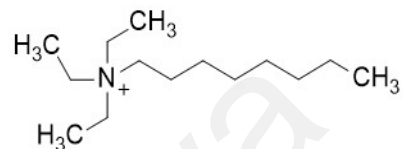
Octyltriethylammonium [OTEAmm]
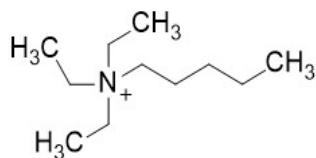
Triethylpentylammonium [PTEAmm]
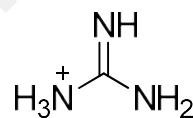
Guanidinium [gua]
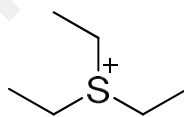
Triethylsulfonium [SEt$_3$]

Scheme 3.1, Continued.

Bis(trifluoromethylsulfonyl)imide [TFSI]

Trifluoromethanesulfonate [TfO]

Chloride [Cl]

Thiocyanate [SCN]

Iodide [I]

Dicyanamide [DCA]

Tricyanomethane [TCM]

Dimethyl phosphate [DMP]

Tri(pentafluoroethyl)trifluorophosphate [E₃FAP]

Tetracyanoborate [TCB]

Ethylsulfate [EtSO₄]
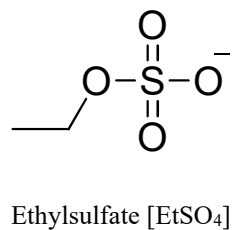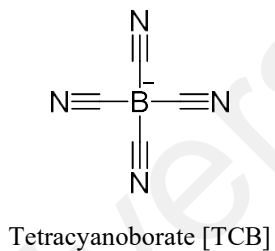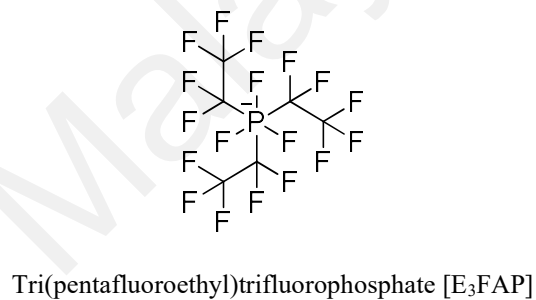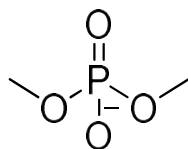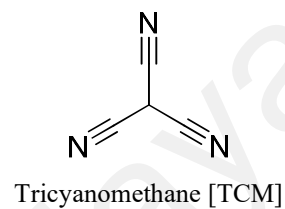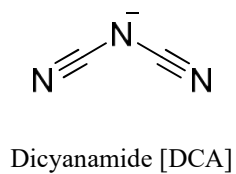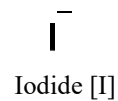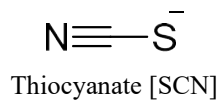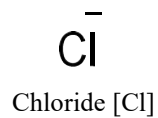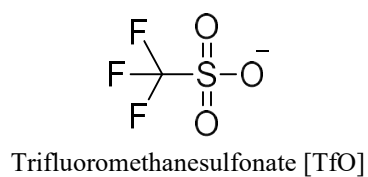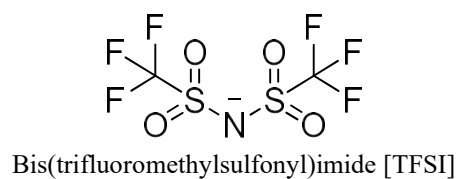
Scheme 3.2: Chemical structures of anions constituting the ILs.

3.2   Experimental Procedures

3.2.1   Preliminary preparation

A sealed vessel with molecular sieves was used to contain KO_2 to prevent contamination via atmospheric moisture. Most of the handling, such as the weighing and dissolution of KO_2, was carried out in a glove box to avoid any possible moisture contamination.

3.2.1.1   Drying of ILs and ApS

The ILs were vacuum dried at 60 °C for 5−6 h prior to all experiments, in order to remove moisture and volatile impurities, since these undesirably affect the generation of $O_2^{\bullet-}$. This was necessary to ensure that the results obtained were precise and consistent with the objective. It has also been extensively reported that it is critical to eliminate such electrochemically active molecules preceding the voltammetric measurements (O'Mahony et al., 2008; Ohno, 2005; Zhao et al., 2010). The moisture content of all ILs used for stability experiments was determined by Karl-Fischer titration with a Mettler Toledo Karl Fischer titrator, and each IL had a moisture level of less than 1.0% after drying. The DMSO was also vacuum dried at 50 °C for ca. 6 h.

3.2.1.2   Acidity of ILs

The pH of all ILs was initially measured using Merck pH strips. In the event that an IL was found to be acidic, a very minute quantity of KO_2 (0.0005−0.001 g) was added to approximately 5 g of IL until the pH reached 7. This small quantity of KO_2 is used to neutralize IL (acidic) without having an influence on the electrochemical behavior of IL.

3.2.2 Chemical generation of $O_2^{\bullet-}$

3.2.2.1 Calibration of $O_2^{\bullet-}$ in DMSO using UV-visible spectrophotometry

Various concentrations of KO_2 prepared in dried DMSO were analyzed using a UV-visible spectrophotometer, and the corresponding height of the absorbance peak corresponding to $O_2^{\bullet-}$ was determined. Pure DMSO was used as a blank reference for analysis. It was noted that the absorbance decreased with the decreasing concentration. Figure 3.2 displays that a KO_2 concentration of 2.397 mmol/L, 2.115 mmol/L and 1.833 mmol/L produced an absorbance peak nearly at 3, 2 and 1 respectively against the same wavelength, representing that an increased concentration of the generated $O_2^{\bullet-}$ results in greater absorbance in the range of 250–270 nm.
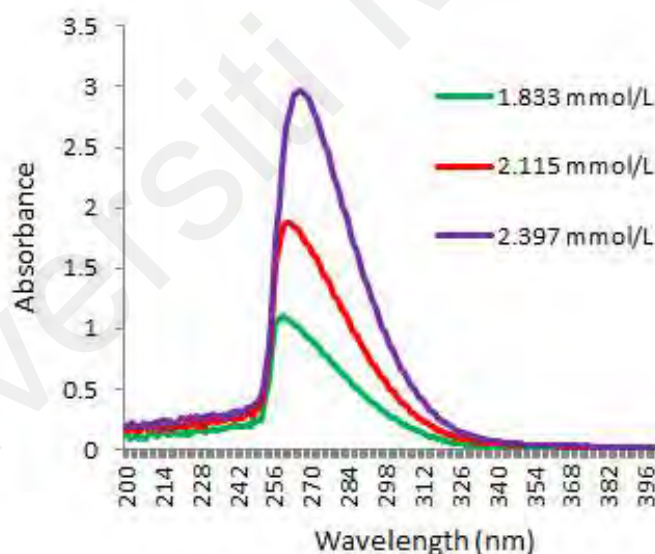
Figure 3.2: KO₂ concentration of 2.397 mmol/L, 2.115 mmol/L and 1.833 mmol/L produced an absorbance peak nearly at 3, 2 and 1 respectively.

3.2.2.2   Generation of $O_2^{\bullet-}$ in IL/aprotic solvent binary system

The DMSO was dried in a vacuum oven overnight at 50 °C prior to the stability test. A sealed vessel containing molecular sieves was used to store KO_2 to prevent atmospheric moisture contamination. To chemically generate the $O_2^{\bullet-}$, a calculated amount of KO_2 was weighed and solubilized in a known quantity of dried DMSO. Complete dissolution of KO_2 was followed by addition of an appropriate volume/amount of the selected IL, and long-term stability of the generated $O_2^{\bullet-}$ was evaluated over time by monitoring its absorption spectrum using a UV-visible spectrophotometer (PerkinElmer-Lambda 35) with a time interval of 10 min for the duration of 120 min. Pure DMSO or the appropriate DMSO/IL mixture was used as the reference for spectral measurements.

3.2.3   Electrochemical generation of $O_2^{\bullet-}$

3.2.3.1   Cleaning of the electrochemical cell

The electrochemical cell and its lid were cleaned and rinsed using isopropanol and subsequently air-dried. The connection clips to the electrodes were scrubbed to remove the corroded layer on the connecting part to prevent potential and current overload during experimentation.

3.2.3.2   Polishing of electrodes

The working electrode and the counter electrode were polished using alumina solution (BASi). Prior to use this was followed by sonication in distilled water for 10 min. Polishing helps remove impurities on the electrode surface emerging from earlier experimental procedures. The content of the reference electrode was separated using a filtering material made of glass frit, in order to avoid contamination of the IL under investigation (Ohno, 2005).

3.2.3.3 Electrochemical procedure (Cyclic Voltammetry)

All chemicals were stored in a drying cabinet and manipulated in a glove box. A single-compartment, air-tight, glass electrochemical cell (50 mL) was used for cyclic voltammetry (CV). High-purity dry O_2 and N_2 were routed and introduced into the cell during the experimental procedure. A glassy carbon (GC) macro-disk electrode (BASi, 3 mm diameter) was used as a working electrode with Ag/AgCl (6 mm) reference electrode, and Pt (5.7 cm, BASi Inc.) as a counter electrode. The CV experiments were carried out on an Autolab potentiostat, (Model PGSTAT302N) with a potential range of -10 to 10 V, and a high-speed Nova 2.1 data acquisition system controlled by a computer.

The CV analysis was performed on the aprotic system comprising a known optimal ratio (90% v/v) of ILs in AcN and in neat $[BTEAmm^+][TFSI^-]$ and $[EMIm^+][TFSI^-]$. The ILs were dried under vacuum at 50 °C for ca. 6 h prior to preparing binary mixtures and conducting experimentation. Preceding the tests, an inert atmosphere was attained by filling the interior of the dry glove box with helium. The electrochemical cell placed therein, containing the test sample and the three-electrode system clasped with an activated potentiostat, was sparged with N_2 to exude any traces of species which might result in an electrochemical activity causing likely interference with the $O_2^{\bullet-}$ generation. A background voltammogram was obtained after the N_2 sparge, and the electrochemical potential window of the ILs was recorded. Subsequently, O_2 was bubbled through the system for about 30 min to sufficiently saturate the medium and CV scans were acquired. Also, O_2 was bubbled briefly between successive CV runs to refresh the system with O_2 and to offset any concentration gradients arising. During the acquisition of CV data, both N_2 and O_2 sparging were discontinued.

3.2.4 Degradation of pharmaceutical compounds (APIs)

The ILs were dried overnight in a vacuum oven at 50 °C. Dried [BTEAmm$^+$][TFSI$^-$], [PTEAmm$^+$][TFSI$^-$], [OTEAmm$^+$][TFSI$^-$] and [EMIm$^+$][TFSI$^-$] were individually mixed with AcN as an aprotic solvent at different volume percentages (0, 5, 10, 20, 30, 50, 70, 80, 90 and 100 v/v %). All experiments for the oxidative degradation of ACTM, RLZ and CBM in the KO$_2$/IL/AcN system were performed in 40 mL EPA vials fitted with polytetrafluoroethylene (PTFE) lined caps as batch reactors. Unless otherwise mentioned, all reactions were carried out at room temperature (RT).

The pre-determined and calculated concentrations of APIs were successively introduced into the individual, labelled vials containing intended ratios of the IL-ApS mixtures. These were continuously stirred using Teflon-coated magnetic stir bars with a constant stirring speed of 650 r/min until complete dissolution of the drug compound in the binary medium took place. An aliquot of 1.0 mL sample was withdrawn from this mixture and analyzed using a high-performance liquid chromatography (HPLC) system, under the conditions and specifications mentioned in Table 3.4.

Table 3.4: HPLC instrument specifications and chromatographic operating conditions.

Analytical instruments	
Shimadzu HPLC systems	Liquid Chromatograph LC-10AD $_{VP}$
	System Controller SCL-10A $_{VP}$
	UV/Vis Detector SPD-10A $_{VP}$
	Auto injector SIL-10AD $_{VP}$
	Column oven CTO-10AS $_{VP}$
	Degasser DGU-14A
	Shimadzu LC solution software
Column	Size: 4.6 x 150 mm, 5µm
	Description: Eclipse PlusC18 Agilent
Guard column	Agilent Zorbax reliance cartridge
Separation conditions	
Mobile phase	AcN:Water (75:25%), HPLC grade
Flow rate	1 mL/min, low pressure gradient
Wavelength	254 nm
Column temperature	30 °C
Injection volume	10 µL

Subsequently, the reactions were initiated by gradually adding a desired amount of KO_2 to the mixture of IL/AcN/API and stirring for ca. 3.5 h. For the purpose of comparative evaluation, aliquots were collected for analyses prior to and after the addition of KO_2. All samples were taken out at a specified interval, using a 1 mL syringe and filtered into the 1.5 mL screw-necked auto-sampler vials, through a 0.22 µm Nylon microfiltration membrane syringe filter to remove any insolubilities before analyses. The oxidative degradation of APIs was carried out at a natural pH.

The change in concentrations of APIs was measured using HPLC. The entire procedure was replicated, but with an increased fraction of KO_2 each time, until the chromatographic peak of the drug under analysis either became constant in height or was no longer detected. Meanwhile, all experiments were independently repeated at least twice to avoid any

contingencies, and the data was plotted as mean values of duplicates. Error bars indicated the standard deviation from the mean.

Other than conducting the procedure at RT, the reactions were also carried out as a function of temperature. The higher temperatures at which the reactions were carried out ranged from 30, 40, 50, 60, and 70 °C. For two reasons this temperature range was selected; (i) the boiling point of acetonitrile (i.e., 82 °C) which was a component of the binary medium could not be exceeded, and (ii) the thermal instability of the drug being degraded at very high temperatures could affect the intended results.

All samples were stored at 4 °C and analyzed within 24–30 h of preparation.

3.2.5 IL recycling and reuse

Post-reaction, the mixture was extracted with water and centrifuged, each time for 15 min to separate the IL and aqueous phases. This process has been triplicated. From the resulting two-phase system, the water layer was extracted from the top with a needle and syringe, leaving behind the IL phase. The IL fraction after phase-separation was subsequently dried under vacuum at 60 °C for ca. 16 h to remove traces of water, generating a 98% recovery. After the recycling process, IL was reused for the next cycle of degradation reaction as described in Section 3.2.2. The purity of recovered ILs was analyzed using proton NMR and FTIR techniques. The recycling-reuse process was reiterated five times.

3.2.5.1 Fourier Transform IR (FTIR) Analysis

Both fresh and recycled ILs from each cycle were dried under a vacuum for 24 hours before analysis. FTIR spectra were obtained in the frequency range 4000−400 cm^{-1} using a PerkinElmer FTIR spectrometer with a built-in diamond-germanium ATR single reflection crystal. A drop of the liquid test sample was directly placed on the crystal and the IR spectra

were recorded via Attenuated Total Reflection (ATR) technique. A set of 16 scans was collected for each sample and all spectra were baseline corrected.

3.2.5.2 Proton NMR analysis

The structures of fresh and recycled ILs were determined and compared using proton NMR (^{1}H NMR) spectroscopy on FT-NMR AVN Bruker 400 spectrometer, at ambient temperature operating at 400 MHz. The samples were analyzed after the addition of deuterated methanol (Methanol-d4, CD$_3$OD) containing TMS (tetramethylsilane) as an internal reference.

3.2.6 Analysis of TOC

The removal of total organic carbon content (TOC) was determined by examining the organic contents of aqueous extracts of the reaction mixtures after separation from the hydrophobic ILs using a Shimadzu TOC-L analyzer. Potassium hydrogen phthalate was used to develop a calibration curve with an upper limit of 100 ppm. The relative standard deviation was below 2.0% in the range of the investigated concentrations.

3.2.7 LCMS-QToF (Liquid Chromatography Mass Spectrometry-Quadrupole Time of Flight)

The transformation products of ACTM were separated and identified using Agilent Technologies LCMS-QToF (quadrupole time of flight). A C18 Zorbax Eclipse Agilent column (4.6 mm × 100 mm, 3.5 μm) was used for the chromatographic separation. The elution was performed with a mobile phase consisting of AcN (75%) and HPLC-grade water (25%) at a flow rate of 0.3 mL/min for 30 min. The autosampler was used to perform 100 μL injections. The mass spectrometer was operated under the ion source of electrospray ionization (ESI) in the negative mode, ionization voltage of 175.0 V, ion accumulation time

of 30–50 ms, N$_2$ as nebulizing and drying gas, at a scan range of 50 to 800 m/z. Mass Hunter Data Acquisition software was used to verify the identification of ACTM and its by-products.

3.2.8   LC-MS-MS (Liquid Chromatography-Tandem Mass Spectrometry)

Liquid chromatography with tandem mass spectrometry (LC-MS-MS) was used as an analytical technique to identify the degradation products of carbamazepine (CBM) and riluzole (RLZ). A Linear Ion Trap Quadrupole LC/MS/MS Mass Spectrometer utilizing the separating power of liquid chromatography combined with highly selective and sensitive mass analysis capability of triple quadrupole mass spectrometry was employed with a Reverse Phase C18 column (2.0 x 100 mm, 4μm). The mobile phase used for the elution of products was a mixture of acetonitrile (0.1% formic acid) and ultra-pure water (0.1% formic acid). The autosampler used an injection volume of 30 μL. Enhanced MS (EMS) and Enhanced Product Ion (EPI) of the mass spectrometer were operated in the positive mode at a scan rate of 1000 Da/s and a scan range of 100 to 500 m/z. Software version Analyst 1.6.3 was used to hunt the products of the pharmaceutical compounds under investigation. The detailed specifications and operating conditions of LC-MS-MS are listed in Table 3.5.

Table 3.5: LC-MS-MS instrument specifications and chromatographic operating conditions.

Analytical instruments and Separation conditions	
Component name	Linear Ion Trap Quadrupole LC/MS/MS Mass Spectrometer
Component ID	4000 Q TRAP
Model	1004229-AI
Serial Number	U016130604
Ion Source Type	Turbo Spray
Source Temperature	500 °C
Software version	Analyst 1.6.3
Column description	Phenomenex Synergy RP C18
Column size	2.0 x 100 mm, 4μm
Scan type	Enhanced MS (EMS) and Enhanced Product Ion (EPI)
Scan rate	1000 Da/s
Polarity	Positive
Mobile phase	AcN (0.1% formic acid) : Ultra-pure water (0.1% formic acid)
Agilent LC Pump Model	Agilent 1260 Quaternary Pump
Maximum flow ramp	100.0 ml/min²
Maximum pressure ramp	290.0 psi/sec
Injection volume	30.00 μL

3.3 Safety and Precautions

During the experimentation, ascertaining several measures and precautions mentioned as follows are necessary to execute safe operative procedures in the laboratory:

3.3.1 General safety measures

1. It is essential that the laboratory personnel wear proper personal protective equipment (PPE) when working with potent oxidizers, such as KO_2.

2. Evaluate the entire guidelines thoroughly prior to the commencement of work with any form of chemical(s). Review the potential hazards that could arise from the

chemicals under use and ensure that you or anyone else working on the procedure fully understand the safe processes to follow, is using the proper PPE, and is familiar with the emergency equipment in the area.

3. Verify that the chemicals are stored and labelled properly with the tags to track the date any material was received and will expire.

4. Prior to handling, examine the chemicals for visual signs of contamination or crystallization. Visual inspection may help in determining if the substance has started to undergo contamination via some oxidation process. These signs primarily include:

- o Visible discoloration or appearance of cloudiness

- o White crystals under the rim of the cap

- o Precipitated crystal formation appearing as a solid mass, chips, or ice-like structures.

- o Clear liquid containing suspended wisp-like structures.

- o Gross contamination

5. Observe appropriate labelling procedures during any chemical waste collection and disposal.

3.3.2 Contamination

The uncontrolled decomposition of chemicals can be caused by some contaminants such as metal oxide salts, heavy metals, strong acids, alkaline materials (e.g., amines), and many sorts of dirt and dust. This condition can lead to the buildup of pressure, and in some cases may result in explosions and/or fire. In order to prevent such accidental contamination, it is

necessary to avoid returning a reagent to its original storage container once withdrawn for use.

3.3.3 Precautions

3.3.3.1 Preliminary

- Arrange for the availability of a written experimental protocol comprising safety information.

- Always read the handling and storage, and stability and reactivity sections in the Safety Data Sheet (SDS) before working with a specific chemical.

- Ensure familiarity with general University laboratory emergency procedures.

- Identify the location of the nearest eyewash and shower and verify that they are accessible. An appropriate fire extinguisher must be readily available in the work area.

- Prior to handling/opening the container, visually inspect for any crystallization therein.

3.3.3.2 Operative

- KO_2 is an air and moisture-sensitive reagent and must have limited to no exposure to the atmosphere. Thus, it should preferably be handled inside a glove box to reduce atmospheric contact. All combustible materials including paper products such as laboratory paper towels or Kimwipes should not be allowed to come in contact with KO_2 at any time. Beyond that, gloves must be worn when handling KO_2 (flame-retardant gloves should be used when handling this reagent in general laboratory settings).

- In case an inert glove box is not available or practical, handle KO_2 in a chemical lab hood in order to exhaust flammable vapors and reduce the possibility of fire.

- Dry soda lime or sand can be used to cover and extinguish small fires resulting from drips or small spills of such reagents.

- For routine handling of KO_2 outside of an inert atmosphere glove box, the proper chemical-resistant gloves (e.g., of nitrile material) are generally recommended where their use does not increase the risk owing to reduced dexterity or other factors.

- While removing air-sensitive chemicals (liquids) from the septum cap make certain that the syringe is completely depressed so as to not introduce any air into the bottle which might promote oxidation.

- Limit the quantity to a minimum possible for accomplishing the scientific goal. Do not return unused air-sensitive chemicals to the stock container.

- Conduct all procedures inside a fume hood or behind a protective shield.

- It is important to not use any metal-containing utensils as weighing boats while working with air or moisture-sensitive reagents.

3.3.3.3   Storage

- During prolonged storage the integrity of reagents like KO_2 can be compromised due to reaction with moisture or trace contaminants. The acquired quantities should be limited to amounts that would be used in planned experiments so as to avoid extended storage.

- It is best to store it in an inert atmosphere glove box, however, if that is not possible, store KO_2 in a sealed air-tight container placed in a drying cabinet. Do not store KO_2 near heat sources, flammable solvents, or water sources.

- Store the reagents and ILs in their original manufacturer container (e.g., Sure/Seal™ bottles) unless experimental work requires transfer to other vials. It is necessary to inspect the septum tops for probable leakage after perforation which could be replaced as needed.

- Do not return the chemicals from secondary containers to the original storage container, as small quantities of impurities can cause contamination of the entire stock.

- Reagents and samples that require refrigeration for storage must be kept in a dedicated refrigerator.

3.3.3.4 Disposal

- Never pour the peroxide-forming and other oxidizing waste down the drain. These chemicals must be disposed of as hazardous waste.

- Ensure to leave a label on the container with recent testing dates when disposing.

- Refer to the individual chemical hazard information sources or guidelines in case of specific disposal guidance.

3.3.4 Emergency procedures

3.3.4.1 Outside fume hood or ventilated enclosure

- Evacuate to a safe distance while alerting others and preventing entry into the lab.

- Contact the University emergency operations center and remain in a safe location until the response personnel arrive.

3.3.4.2   Inside fume hood or ventilated enclosure

- Using appropriate spill supplies and wearing PPE (such as face shields with throat protectors and heavy gloves), one may assist in the clean-up effort of small amounts if trained and confident:

    o Completely absorb the spilled chemicals on vermiculite as soon as possible. This is followed by sweeping up the material with a broom and dustpan located in the chemical spill kit.

    o Collect debris in an appropriate container labelled with a hazardous waste tag and move to your Satellite Accumulation Area (SAA) until a waste pickup is requested.

- If not trained, close the fume hood sash, and await assistance from technical support staff.

4.1 Generation of $O_2^{\bullet-}$ in various IL Systems

4.1.1 Generation of $O_2^{\bullet-}$ in Aprotic Solvent – The role of DMSO

The short lifespan of $O_2^{\bullet-}$ can be extended if the medium used for its generation is aprotic, for example, DMSO, DMF, or AcN (Hayyan et al., 2016). KO_2 salt was initially dissolved in an aprotic solvent, i.e., DMSO, to establish that there was no probability of the mass-controlling process during the investigation (Hayyan et al., 2012).

DMSO was preferred for this investigation because it has the potential to deactivate water (Sawyer, 1992b). The presence of water is important to avoid as it might cause $O_2^{\bullet-}$ to participate in other reactions (Eqs. 4.1 and 4.2), leading to rapid consumption.

$$2O_2^{\bullet-} + H_2O \rightarrow O_2 + HO_2^- + OH^- \tag{4.1}$$

$$HO_2^- + H^+ \rightarrow 2OH^- \tag{4.2}$$

In the spectrophotometric analysis, the absorbance band for $O_2^{\bullet-}$ generation was found to appear in the range of 250 nm to 270 nm (Hayyan et al., 2010). The results demonstrated that the generated $O_2^{\bullet-}$ was stable in DMSO. This is consistent with a preceding study that examined the reactivity of $O_2^{\bullet-}$ generated through electrochemical reduction of O_2 in DMSO (Sawyer & Roberts, 1966), and with the general regard of DMSO as a good medium for $O_2^{\bullet-}$ generation.

4.1.1.1   The role of water

Among the various reactions which $O_2^{\bullet-}$ may undergo, nucleophilic substitution, one-electron transfer, disproportionation and deprotonation are considered the most prominent ones (Islam et al., 2009b; Sawyer, 1992a; Weinberg et al., 2012). The reactivity of $O_2^{\bullet-}$ is determined by its chemical characteristics, e.g., free radical and redox properties, nucleophilicity and basicity. The tendency of $O_2^{\bullet-}$ to attack the positively charged constituents of any organic moiety in the absence of protons can be attributed to its strong nucleophilicity (Katayama et al., 2004a; Rogers et al., 2009). Moreover, it has been established via several studies (Belloni & Lecheheb, 1987; Gonçalves et al., 1999; Mohammad et al., 2001; Morrison et al., 1979) that in the presence of sources of proton, $O_2^{\bullet-}$ rapidly disproportionates to produce either H_2O and O_2, or forms hydroperoxide anion (HO_2^-) (Eq. 4.1) due to its predominant basicity.

Since $O_2^{\bullet-}$ possesses a very short lifetime in the presence of water (Dondoni et al., 1985), it was generated in aprotic media in a rather stable state via electrochemical reduction of oxygen in dimethyl sulfoxide (DMSO) (Sawyer & Roberts, 1966). This electrochemical reduction of O_2 in aprotic solvents generally occurs at E = +(−1.0) V vs. SCE (standard calomel electrode) in the absence of water or protonic species (Costentin et al., 2010; Hayyan, Mjalli, Al-Nashef, et al., 2012b; Sawyer, 1992a; Sawyer et al., 1995), however, the presence of water causes it to disproportionate according to Eq. 4.1 (Al-Nashef et al., 2001b; Chin et al., 1982; Sawyer et al., 1995).

A profound consideration of the hydration effects and various studies on the difference in the solvation enthalpies between aqueous and aprotic solutions was 2.5 kJ.mol^{-1} (Arshadi et al., 1970; Green et al., 1979; Michelson et al., 1977). It was demonstrated that the first, second and third gas-phase hydration enthalpies were 52.3, 40.6, and 29.3 kJ/mol, respectively,

hence proving a notable likeliness of the hydration degree to have a substantial effect on the properties, particularly on the redox (reduction-oxidation) potential and nucleophilicity of the ions (Michelson et al., 1977). Earlier investigations revealed that the $O_2^{\bullet-}$ is quite unstable in aqueous media ((NIST), 1973; Behar et al., 1970), and subsequently disproportionate with rapid second-order rate constants in the range of $10^7 - 10^{10}\ M^{-1}\,s^{-1}$.

4.1.2   Screening of ILs for $O_2^{\bullet-}$ generation

The stability of generated $O_2^{\bullet-}$ was tested in the presence of 25 ILs with different cation-anion combinations, which resulted in the selection of some IL systems for providing a stable media for $O_2^{\bullet-}$ generation, while others were screened out for acting as an unstable system after the kinetic studies. The specific outcomes of the spectrophotometric analysis leading to deductions which served as the basis of such screening process are presented and discussed in the following sections.

4.1.2.1   Stable systems for $O_2^{\bullet-}$ generation

The ammonium-based ILs, i.e., [EDMPAmm][TFSI], [TBAmm][TFSI], [N_{211},mom] [TFSI], and the morpholinium-based IL [MOEMMo][TFSI], were found to be greatly stable media for $O_2^{\bullet-}$ generation. These results are in agreement with literature reports concerning *N*-methoxyethyl-*N*-methylmorpholinium   [MOEMMo]$^+$ and   *N*-ethyl-*N*,*N*-dimethyl-2-methoxyethylammonium [N_{211},mom]$^+$ paired with [TFSI]$^-$ (Hayyan et al., 2012). In the present work, both [MOEMMo]$^+$ and [N_{211}, mom]$^+$ exhibited the ability to sustain $O_2^{\bullet-}$ for 2 h. Effectively, the absorbance values for ammonium-based ILs decreased gradually within the first hour, then remained fairly steady for the next 2 h, as illustrated in Figure 4.1 (a), (b), (c), and (d).
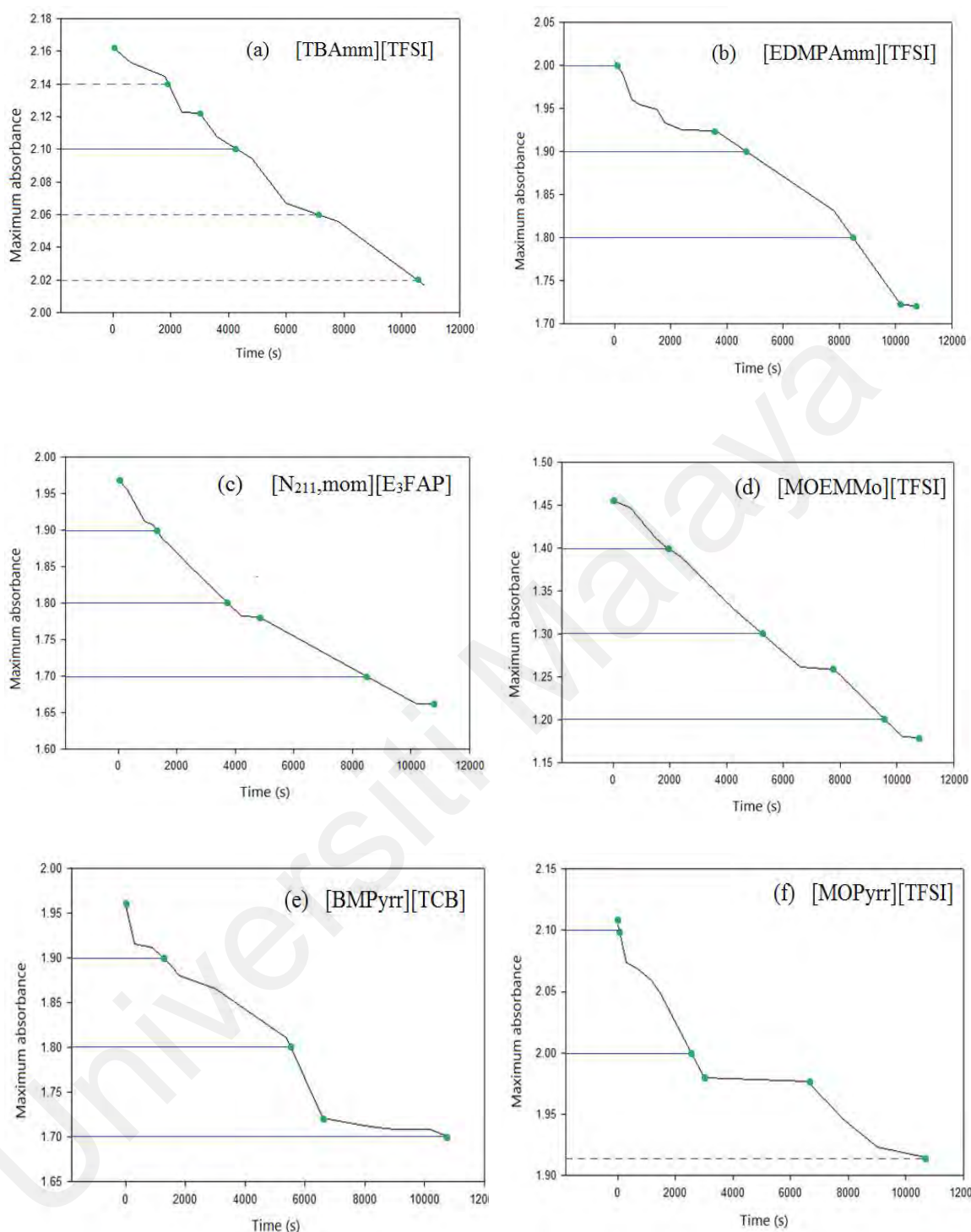
Figure 4.1: The consumption of $O_2^{\bullet-}$ over time as indicated by decreasing absorbance peaks in the wavelength range of 250 nm – 270 nm. The IL systems apparently generating stable or relatively stable $O_2^{\bullet-}$ include (a) [TBAmm][TFSI], (b) [EDMPAmm][TFSI], (c) [N$_{211}$,mom][E$_3$FAP], (d) [MOEMMo][TFSI], (e) [BMPyrr][TCB], (f) [MOPyrr][TFSI].
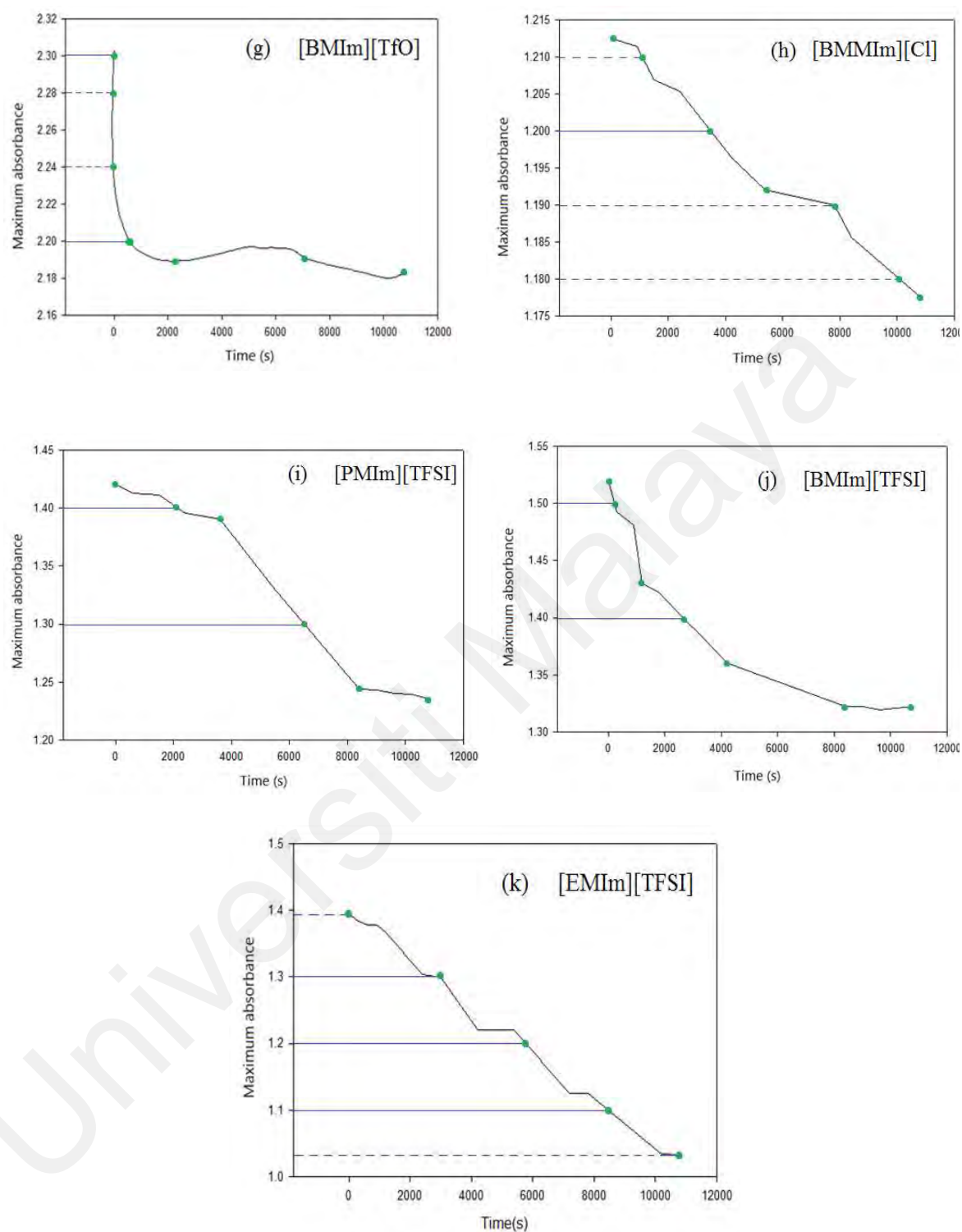
Figure 4.1, Continued, (g) [BMIm][TfO], (h) [BMMIm][Cl], (i) [PMIm][TFSI], (j) [BMIm][TFSI], and (k) [EMIm][TFSI].

Based on the kinetic analysis and consumption rate of the generated $O_2^{\bullet-}$, it was also evident that two pyrrolidinium-based ILs, i.e., [BMPyrr][TCB] and [MOPyrr][TFSI], and five imidazolium-based ILs, i.e., [BMIm][TfO], [BMMIm][Cl], [C_3MIm][TFSI], [BMIm] [TFSI], and [EMIm][TFSI], can be considered as media for stable generation of $O_2^{\bullet-}$. Figure 4.1 (e), (f), (g), (h), (i), (j), and (k) present the plots for the maximum absorbance of the generated $O_2^{\bullet-}$ over time in these ILs. These findings are congruent with previous studies reporting the reaction of $O_2^{\bullet-}$ with the C-atom at position 2 of imidazolium-based ILs (Hayyan et al., 2012). A work by Hayyan et al. also mentions that pyrrolidinium-based cations with [TFSI]$^-$ are potentially suitable as stable media for the generation of $O_2^{\bullet-}$.

Ultimately, it can be deduced from the observed absorbance values that the combinations of [EDMPAmm][TFSI], [TBAmm][TFSI], [$N_{211,mom}$][TFSI], [MOEMMo][TFSI], [BMPyrr][TCB], [MOPyrr][TFSI], [BMIm][TfO], [BMMIm][Cl], [C_3MIm][TFSI], [BMIm] [TFSI], and [EMIm][TFSI] are highly viable for stable $O_2^{\bullet-}$ generation. The slowly decreasing absorbance readings obtained for these ILs demonstrate relatively gradual consumption of $O_2^{\bullet-}$.

It can also be noted herein that the wavelength shift for the recorded maximum absorbance values depends on the medium, i.e., it changes from one IL to another which is related to the $O_2^{\bullet-}$ generation in that particular medium. However, the change in wavelength with varying IL medium is not very significant (differing only by a few nanometers), and largely falls within the range of 250 nm – 270 nm.

4.1.2.2 Unstable systems for $O_2^{\bullet-}$ generation

Al-Nashef et al. (Al-Nashef et al., 2001b) revealed that some imidazolium-based ILs resulted in high stability of the generated $O_2^{\bullet-}$, but many have also reported the unstable

generation of $O_2^{\bullet-}$ in other imidazolium-based ILs (Al-Nashef et al., 2010b; Islam et al., 2009a; Katayama et al., 2004a). This variable capability is ascribed to the crucial role of the cation and its association with charged substrates, especially with $O_2^{\bullet-}$ owing to its small size (Islam & Ohsaka, 2008b; Zigah et al., 2009). Furthermore, the mechanism of $O_2^{\bullet-}$ generation implicates the cation as the more dominating species in the reaction, rather than the anion (Laoire et al., 2009), i.e., there exists a high susceptibility of the system to reactions that might occur between $O_2^{\bullet-}$ and the IL cations (Marcinek et al., 2001). However, the probability of such reactions is significantly reliant on the structure of the cationic species. The nature of $O_2^{\bullet-}$ as a strongly nucleophilic agent suggests a high tendency for it to attack the aromatic cations in ILs, such as imidazolium cations (Katayama et al., 2004a). Indeed, many studies have reported that $O_2^{\bullet-}$ strongly interacts with imidazolium cations, leading to the production of $[\text{imidazolium}]^+\ldots O_2^{\bullet-}$ ion-pairs (Barnes et al., 2008a; Islam & Ohsaka, 2008b; Shkrob & Wishart, 2009). This ion pair complex is generated when $O_2^{\bullet-}$ attacks the imidazolium ring at the C-2 position, eventually resulting in a ring-opening reaction (Islam et al., 2009a). Thus, the primary determinant of stability when using imidazolium-based ILs is whether the generated $O_2^{\bullet-}$ could undergo a reaction with the cation to form 2-imidazolone (Katayama et al., 2004a) or H_2O_2 (Islam et al., 2009a).

Figure 4.2 displays a significant drop in the absorbance values over time for [BMIm][Cl], [BMIm][DCA], [MMMIm][I], [EMIm][SCN], [EMIm][EtSO$_4$], [C$_1$mim][DMP], [C$_4$DMIm][I], [MOPyr][FAP], and [BMPyr][Cl]. When generated in [BMIm][DCA] and [MMMIm][I], the absorbance bands of $O_2^{\bullet-}$ became steady within the range of 262 nm to 270 nm after an average of 17 min, indicating instability of the $O_2^{\bullet-}$ in these ILs specifically during that time duration. Besides the structure of the IL cation, consumption of the generated $O_2^{\bullet-}$ by impurities existing in an IL might also contribute towards its apparent instability (Hayyan et

al., 2012); this may explain the time-limited observation in these two ILs. Meanwhile, the rapid decrease in absorbance values obtained for [SEt$_3$][TFSI], shown in Figure 4.2 (v), establishes that this IL is not able to serve as a good medium for $O_2^{\bullet-}$ generation. This was also in accord with a previous study involving triethylsulfonium bis(trifluoromethylsulfonyl)imide, which reported instability of $O_2^{\bullet-}$ as a result of a high consumption rate (Hayyan et al., 2012).
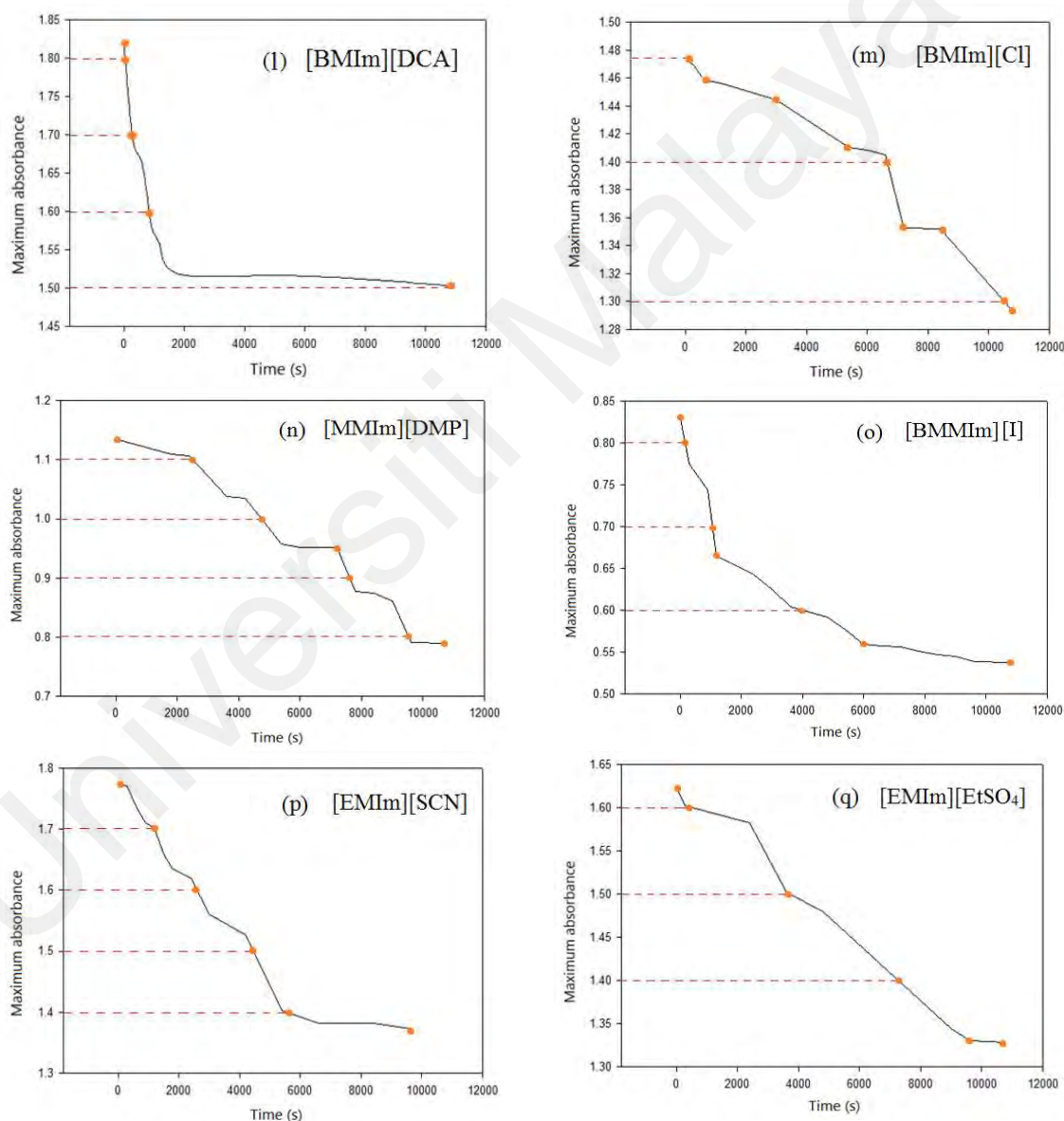
Figure 4.2: The consumption of $O_2^{\bullet-}$ over time as indicated by decreasing absorbance peaks in the wavelength range of 250 nm – 270 nm. The IL systems apparently generating unstable $O_2^{\bullet-}$ include (l) [BMIm][DCA], (m) [BMIm][Cl], (n) [MMIm][DMP], (o) [C$_4$DMIm][I], (p) [EMIm][SCN], (q) [EMIm][EtSO$_4$].
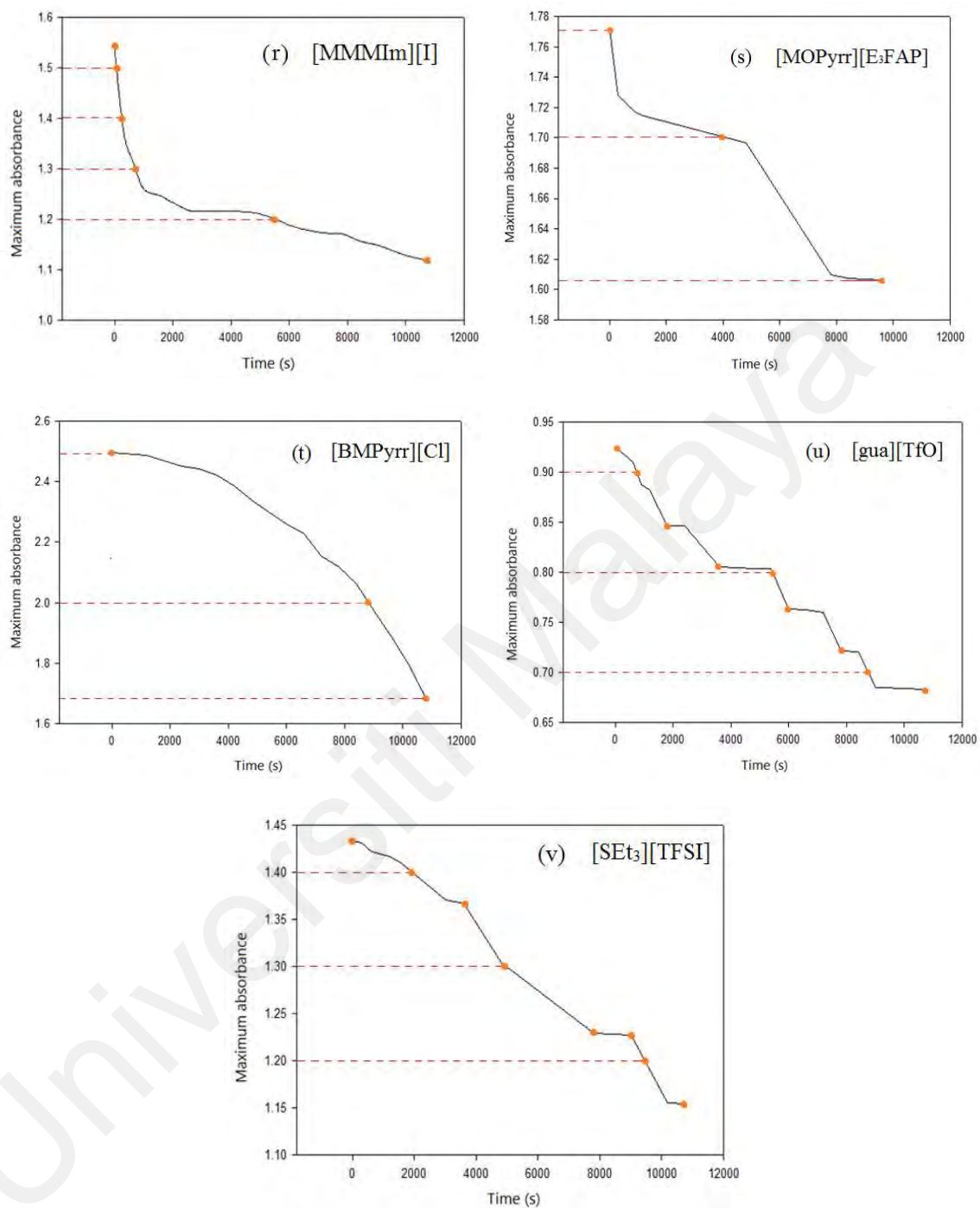
Figure 4.2, Continued, (r) [MMMIm][I], (s) [MOPyrr][E₃FAP], (t) [BMPyrr][Cl], (u) [gua][TfO], and (v) [SEt₃][TFSI].

In the case of guanidinium-based IL, while there was only a slight drop in observed absorbance values during the 180 min of monitoring, the consumption rate of 26.12% was considerably higher than those of the other ILs investigated accordingly, [gua][TfO] was categorized as an unsuitable medium for the stable generation of $O_2^{\bullet-}$. While no reports on $O_2^{\bullet-}$ generation in guanidinium-based ILs could be found in the literature, its consumption rate is comparable to that recorded for [BMPyrr][TfO], i.e., 17.88% (Hayyan et al., 2015a).

It is also noteworthy that the ranges for maximum absorbance curves as depicted in Figures 4.1 & 4.2 seemingly vary significantly while analyzing the consumption of $O_2^{\bullet-}$ in the presence of one IL in the medium to another. This observation refers to the effect originated by concentration of the stable $O_2^{\bullet-}$ being generated in that particular IL since concentration is directly proportional to the absorbance. Hence a slight difference in concentration of KO_2 salt used (calibrated and plotted as absorbance vs. concentration as a prerequisite) for the analysis appears as a different range for absorbance related to the $O_2^{\bullet-}$.

Figure 4.3 illustrates the UV-visible spectral curves for the absorbance (~258 nm) of $O_2^{\bullet-}$ generated in DMSO containing [BMPyrr][Cl] over a duration of 180 min, collected at a wavelength range of 200 nm – 400 nm. The maximum wavelength shift within the duration of the measurement visible in the case of [BMPyrr][Cl] can be in effect considered as a minor change since the variation over time was only a few nanometers, i.e., in the range of 255 nm – 260 nm. Although the shift in wavelength was not very substantial, it is supposed to have occurred due to slight variations in the interactions between the IL cation and $O_2^{\bullet-}$ over the time period during which it was being consumed in its medium. Moreover, the shifted values of wavelength with changing ILs or with time duration were still found to have fallen in the range which is demonstrative or typical of the $O_2^{\bullet-}$ for its detection.
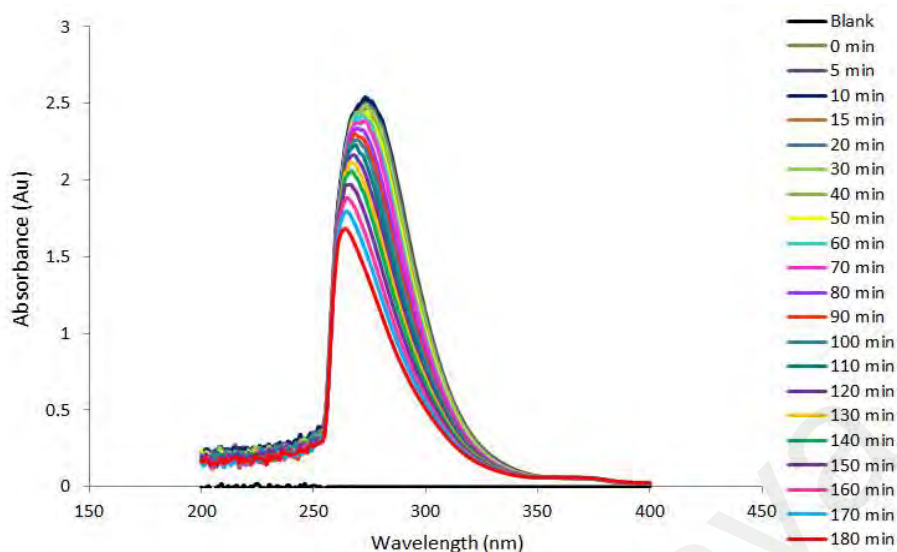
Figure 4.3: Absorbance spectra of $O_2^{\bullet-}$ generated in DMSO in the presence of [BMPyrr][Cl] (t), collected at a wavelength range of 200 nm − 400 nm over a duration of 180 min.

4.1.3 Rate constant, consumption rate, and the total consumption percentage of $O_2^{\bullet-}$

The rate constants, total consumption percentages after 180 min, and consumption rates of $O_2^{\bullet-}$ obtained for the investigated ILs are mentioned in Table 4.1. The rate constants were determined on the assumption that the reactions between IL cations and $O_2^{\bullet-}$ were either zero order, first order, or second order. The forms of these reactions are represented by Eqs. (4.3), (4.4) & (4.5), respectively.

$$r = k \tag{4.3}$$

$$r = k\,[O_2^{\bullet-}] \tag{4.4}$$

$$r = k\,[O_2^{\bullet-}]^2 \tag{4.5}$$

Indeed, the rate constants were found to follow the first-order reaction in some ILs, and the second-order reaction in others. Table 4.1 also provides the correlation coefficients of regression (R^2), which were low in some ILs; for example, an R^2 value of 0.278 was obtained for the second-order reaction in [BMIm][DCA]. This likely owes to the prompt reaction of $O_2^{\bullet-}$ with the IL after its addition to the DMSO/$O_2^{\bullet-}$ solution mixture (Hayyan et al., 2015).

A detailed calculation of kinetic analysis (rate constant, total consumption percentage and consumption rate) of $O_2^{\bullet-}$ in [BTEAmm$^+$][TFSI$^-$] has been demonstrated in Appendix D.

Table 4.1: Rate constant, total consumption percentage and consumption rate of $O_2^{\bullet-}$ in the investigated ILs.

ILs	0th order		1st order		2nd order		Total consumption %age after 180 min	Consumption rate of $O_2^{\bullet-}$ (mM/min)
	Rate constant (10^{-6})	R^2 of rate constant	Rate constant (10^{-6})	R^2 of rate constant	Rate constant (10^{-6})	R^2 of rate constant		
[BMIm][Cl]	79.18	0.943	27.79	0.927	9.79	0.908	32.51	8.554
[BMIm][DCA]	16.81	0.274	8.16	0.276	3.09	0.278	17.45	2.233
[BMIm][TfO]	14.62	0.926	5.16	0.927	1.82	0.928	5.19	0.841
[BMIm][TFSI]	22.72	0.905	12.72	0.908	7.13	0.910	12.98	1.386
[BMMIm][Cl]	6.00	0.905	4.00	0.906	2.00	0.907	2.87	0.245
[C$_4$DMIm][I]	30.00	0.949	40.00	0.958	50.00	0.965	35.25	2.056
[MMIm][DMP]	40.66	0.927	32.77	0.915	2.66	0.898	30.49	3.649
[MMMIm][I]	40.00	0.908	30.00	0.927	20.00	0.944	27.44	2.973
[EMIm][TFSI]	3.65	0.362	2.04	0.361	1.14	0.359	0.372	0.036
[EMIm][EtSO$_4$]	40.19	0.907	21.55	0.900	1.16	0.892	18.10	2.064
[EMIm][SCN]	58.09	0.909	29.77	0.915	15.32	0.918	21.43	2.675
[PMIm][TFSI]	20.00	0.933	10.00	0.929	9.00	0.924	12.98	1.943
[N$_{211}$,mom][E$_3$FAP]	33.79	0.912	14.73	0.911	6.43	0.908	15.59	2.159
[EDMPAmm][TFSI]	23.97	0.932	10.00	0.934	4.17	0.936	14.16	1.996
[TBAmm][TFSI]	19.59	0.943	7.42	0.941	2.81	0.939	6.74	1.024
[BMPyrr][Cl]	77.88	0.939	27.3	0.922	9.62	0.902	32.51	5.700
[BMPyrr][TCB]	33.13	0.949	14.43	0.949	6.29	0.947	15.20	1.817
[MOPyrr][TFSI]	20.00	0.912	8.00	0.914	3.00	0.916	9.04	1.338
[MOPyrr][E$_3$FAP]	81.03	0.951	28.68	0.941	10.21	0.929	32.51	5.702
[gua][TfO]	30.00	0.9611	29.62	0.964	29.38	0.963	26.12	1.695
[MOEMMo][TFSI]	0.87	0.181	0.47	0.180	0.25	0.180	0.04	0.004
[SEt$_3$][TFSI]	31.47	0.940	18.93	0.933	11.40	0.924	19.48	1.963

Notably, the rate constant values obtained for ILs containing [TFSI]⁻ in this study were much lower than that obtained for $O_2^{\bullet-}$ generated in DMSO in the presence of *N*-ethyl-*N*,*N*-dimethyl-2-methoxyethylammonium bis(trifluoromethylsulfonyl) imide [N$_{112,1O_2}$][TFSI], which was $0.143 \times 10^{-2}\,\mathrm{m}^{-1}\mathrm{s}^{-1}$ (Hayyan et al., 2015).

The total consumption of $O_2^{\bullet-}$ in the presence of ILs was calculated by comparing the initial concentration of $O_2^{\bullet-}$ with the concentration observed after 180 min, as indicated in Eq. (4.6). The consumption rate of $O_2^{\bullet-}$ was estimated by dividing the change in $O_2^{\bullet-}$ concentration over the duration of the measurement period, as expressed in Eq. (4.7).

$$\text{Total consumption percentage} \;=\; \frac{[O_2^{\bullet-}]_{\text{initial}} - [O_2^{\bullet-}]_{\text{final}}}{[O_2^{\bullet-}]_{\text{initial}}} \times 100\% \tag{4.6}$$

$$\text{Consumption rate} \;=\; \frac{-[O_2^{\bullet-}]_{\text{initial}} - [O_2^{\bullet-}]_{\text{final}}}{\Delta t} \times 1000 \tag{4.7}$$

After 180 min, the calculated total consumption of $O_2^{\bullet-}$ was very slight for [MOEMMo][TFSI], [EMIm][TFSI], [BMMIm][Cl], [BMIm][TfO], [TBAmm][TFSI] and [MOPyrr][TFSI], with respective values of 0.04%, 0.37%, 2.87%, 5.19%, 6.74%, and 9.04%. These results clearly establish that these ILs can potentially be utilized as media for the stable generation of $O_2^{\bullet-}$. Contrariwise, consumption rates as high as 32.51%, 30.49%, 35.25%, 27.44%, 32.51% and 26.12% were observed for [MOPyrr][FAP], [MMIm][DMP], [C₄DMIm][I], [MMMIm][I], [BMPyrr][Cl] and [gua][TfO]. These values are quite high in comparison with those obtained for the other studied ILs, and indicate these as unsuitable reaction media for the generation of $O_2^{\bullet-}$ in this specific system.

Therefore, this process of screening revealed that ILs consisting of morpholinium, ammonium, and pyrrolidinium cations are the most promising for the chemical generation of $O_2^{\bullet-}$. This inference is primarily proposed on the basis of low consumption rate and low total consumption percentage of $O_2^{\bullet-}$ as reflected in the kinetic analysis. In contrast, higher total consumption of $O_2^{\bullet-}$ was detected in the presence of ILs comprising imidazolium, guanidinium, and sulfonium-based cations; in particular, [BMIm][DCA], [BMIm][Cl], [MMIm][DMP], [C$_4$DMIm][I], [EMIm][SCN], [EMIm][EtSO$_4$], [MMMIm][I], [MOPyrr][E$_3$FAP], [BMPyrr][Cl], [gua][TfO], and [SEt$_3$][TFSI] did not yield stable $O_2^{\bullet-}$. This instability can be ascribed to reactions that might occur between the $O_2^{\bullet-}$ and the particular IL cationic species present in the system.

Several factors, such as the structures of the IL cation and anion and the substituent group(s) attached to the cation contribute towards stabilization of the generated $O_2^{\bullet-}$, particularly through impeding its reaction with the cation of the IL medium. [MOEMMo][TFSI], [EMIm][TFSI], [BMMIm][Cl], [BMIm][TfO], and [TBAmm][TFSI] were among the several ILs validated as the best media for the generation of highly stable $O_2^{\bullet-}$, as demonstrated by the low percentages of total $O_2^{\bullet-}$ consumption (0.04%, 0.372%, 2.87%, 5.19%, and 6.74%) and low consumption rates (0.004 mM/min, 0.036 mM/min, 0.245 mM/min, 0.841 mM/min, and 1.024 mM/min) observed in the presence of these ILs.

4.1.4 Influence of IL cation and anion on $O_2^{\bullet-}$ generation

The physical properties of ILs e.g., density, viscosity, and melting point vary with the structure of the cation, whereas the structure of the anion species affects the chemical behavior. Therefore, the specific combination of cations and anions that comprise an IL and their structures all together play a key role in determining the IL's physicochemical properties.

4.1.4.1 Influence of the cation

The cations of ILs are estimated to have strong ion associations with charged substrates like $O_2^{\bullet-}$ due to the substrate's small size (Islam & Ohsaka, 2008b). As is evident from Table 4.1 and Figures 4.1 & 4.2, the steady state and hence the amount of $O_2^{\bullet-}$ consumption was different for each of the tested ILs, indicating that cation structure has a substantial influence on the stability of the generated $O_2^{\bullet-}$ (Huang et al., 2009a). Moreover, $O_2^{\bullet-}$ stability is reported to be predominantly affected by the nature of the IL cation rather than the anion (Laoire et al., 2009). In this work, some [TFSI]-based ILs with varying cations were selected (Table 4.2) in order to elucidate the impact of the cation on $O_2^{\bullet-}$ stability.

A trend is noticeably evident amongst the ILs with different cations: namely, the best $O_2^{\bullet-}$ stability was observed in morpholinium, followed by ammonium, pyrrolidinium, imidazolium, and finally by sulfonium-based ILs, with corresponding consumption rates and total consumption percentages (in parentheses) of 0.004 mM/min (0.41%), 1.024 mM/min (6.74%), 1.338 mM/min (9.04%), 1.386 mM/min (12.98%), and 1.963 mM/min (19.48%). Listing the cations in decreasing order of total $O_2^{\bullet-}$ consumption gives [SEt$_3$] > [BMIm] > [MOPyrr] > [TBAmm] > [MOEMMo]. These outcomes are comparable to a prior study that also reported a similar ranking trend among cations, i.e., morpholinium, ammonium, pyrrolidinium, piperidinium, phosphonium, imidazolium, and finally sulfonium (Hayyan et al., 2015). The fact that the IL with morpholinium-based cation demonstrates the lowest total consumption compared to other cations corroborates that morpholinium may promote higher stability of $O_2^{\bullet-}$ during its generation. Moreover, the outcomes are also in agreement with earlier work on the tetraalkylammonium cation, which was found to be electrochemically more stable than an imidazolium-based cation (Buzzeo et al., 2003a; Sun et al., 1998).

Table 4.2: ILs used to investigate the effects of cations on $O_2^{\bullet-}$ stability.

Cations	Anion
[TBAmm]	
[MOPyrr]	
[BMIm]	[TFSI]
[MOEMMo]	
[SEt$_3$]	

Another study by Katayama and co-authors (Katayama et al., 2004a) investigated the electron distribution in organic cations of ILs comprising ammonium, pyrrolidinium, and imidazolium; they reported negative atomic charges at the carbon atoms in alicyclic and aliphatic cations such as 1-butyl-1-methylpyrrolidinium [BMPyrr]$^+$ and trimethyl-n-hexylammonium [TMHAmm]$^+$. This is highly indicative of the improbability of attack on these carbon atoms by nucleophilic reagents or species like $O_2^{\bullet-}$ or $^\bullet$OH. Conversely, in the case of heterocyclic cations, a positive charge is carried by the carbon atoms at positions 2, 4, and 5, with the carbon atom at position 2 harboring the maximum positive charge and consequently having the highest tendency to be attacked by a nucleophilic species. Moreover, the addition of a methyl group on the C-atom at position 2 leads to a high reactivity of nucleophilic reagents towards the imidazolium cations (Hayyan et al., 2016). Therefore, in ILs comprised of [BMIm]$^+$, [EMIm]$^+$, [BMMIm]$^+$, [C$_1$MIm]$^+$, and [C$_3$MIm]$^+$, the generated $O_2^{\bullet-}$ reacts with the C-atom at position 2, resulting in degradation of the IL (Katayama et al., 2004a).

Table 4.3: ILs used to investigate the effect of anions on $O_2^{\bullet-}$ stability.

Cation	Anions
[BMIm]	[DCA]
	[TFSI]
	[Cl]
[EMIm]	[SCN]
	[EtSO$_4$]
	[TFSI]
[MOPyrr]	[TFSI]
	[FAP]

The different behavior of various types of ILs is fundamentally due to the variations in nature and structures of the IL cations which can directly interact with oxygen radical species, such as $O_2^{\bullet-}$ in this study. In that matter, both the class of a cation and the substituents attached to it innately affect the interactions and hence the subsequent stability of the $O_2^{\bullet-}$. This phenomenon can also be put as the resultant overall stabilization of $O_2^{\bullet-}$ by a certain IL cationic species is attributable to the extent of its diminished electrophilicity, either primarily in the type (structure) of the cation or owing to the presence of attached substituents. The more distributed electron density via delocalization or induction by various functional groups causes a reduced polarity or electrophilicity on the positive atom of the cation. The lesser the electrophilic character of the cationic moieties through mesomeric effects, the more stabilized the positive charge would be, thus allowing the oxygen radical species to become more stable in turn by being prone to pair with the positively charged centre rather than attacking it.

As an example, morpholine having the chemical formula $O(CH_2CH_2)_2NH$, is a heterocyclic ring compound featuring both amine and ether functional groups. The presence of amine makes morpholine a base; its conjugate acid is called morpholinium. Morpholinium

cation-based ILs belong to a class of compounds with a morpholinium ring, which generally consists of two alkyl (R) groups on the nitrogen atom, and the alterations in these substituent groups can impart different functions and properties to the specific IL.

The ether group in the morpholinium ring is widely recognized as an electron-donating group due to its mesomeric effect. Moreover, the methoxy is also electron-donating from a resonance perspective. The lone pair on oxygen atom in the methoxy group of N-methoxyethyl-N-methylmorpholinium [MOEMMo] is well-positioned to cause delocalization and increase the electron density within the ring's conjugated system. This allows to better stabilize the positive charges through delocalization, and hence the generated $O_2^{\bullet-}$ also becomes more stable in such IL when used as a medium.

4.1.4.2   Influence of the anion

While the cationic species comprising an IL has a vital impact on $O_2^{\bullet-}$ generation and primarily affects its stability by altering the physical properties of the IL, the anion exerts an indirect effect by influencing the chemical properties of the IL (Stark & Seddon, 2007). For example, the thermal properties of ILs, such as heat capacity value, increase as the alkyl-side chain of the cation increases in size, which thus improves IL stability (Table 4.3). Notably, the heat capacities of ILs (that have the same cation) also increase with the increasing size of the anion (Gómez et al., 2013). For example, ILs comprised of the bis(trifluoromethylsulfonyl) imide [TFSI]$^-$ anion have higher heat capacity than their homologues with trifluoromethanesulfonate [TfO]$^-$ or dicyanamide [DCA]$^-$ as the anion. As reported by Huang et al (Huang et al., 2009a), variation in anionic species also tends to influence the hydrophilicity or hydrophobicity of an IL. In light of that finding, [TFSI]$^-$ and [TPTP]$^-$ have been proposed as the best among anions since they both tend to increase the hydrophobicity of ILs.

With the aim of comparing the influence of IL anions on the $O_2^{\bullet-}$ stability, we examined different anions combined with common cations, listed in Table 4.1. The table also records the consumption rates and total consumption percentages observed for the investigated ILs. The [BMIm]$^+$-based ILs demonstrated a clear ranking of [Cl]$^-$ > [DCA]$^-$ > [TFSI]$^-$ with respective consumption rate (percentage) values of 8.554 mM/min (32.51%), 2.233 mM/min (17.45%), and 1.386 mM/min (12.98%). The lower consumption rate obtained for the [TFSI]$^-$ anion shows that it is more able to support stable $O_2^{\bullet-}$ generation than other investigated anions. This is in agreement with a prior study on [C$_4$mim]$^+$-based ILs, which examined several anions and reported decreasing heat capacity values at 298 K in the order of [TFSI]$^-$ > [TfO]$^-$ > [PF$_6$]$^-$ > [DCA]$^-$ > [BF$_4$]$^-$ > [Cl]$^-$ > [Br]$^-$ (Fredlake et al., 2004).

Likewise, the investigated anions associated with [EMIm]$^+$ exhibited a trend of [TFSI]$^-$ > [EtSO$_4$]$^-$ > [SCN]$^-$ with respective consumption rate and total consumption percentage values of 0.0365 mM/min (0.372%), 2.064 mM/min (18.10%), and 2.675 mM/min (21.43%). A previous work examining the same anion-cation combinations also reported [TFSI]$^-$ as the most suitable anion (Huang et al., 2009a), with [EMIm][TFSI] demonstrating the lowest consumption rate. In the case of [MOPyrr]$^+$ cation combined with [TFSI]$^-$ and [FAP]$^-$, the values obtained were 1.388 mM/min (9.04%) and 5.702 mM/min (32.51%), respectively, which are in concordance with the study by Huang et al (Huang et al., 2009a).

4.1.4.3 Influence of the cationic substituents

The substituent groups attached to the IL cation also significantly impact the physical properties of the liquid. As a general tendency, increasing the alkyl chain length of these substituents leads to increased hydrophobicity of the IL (Freire et al., 2007; O'Mahony et al., 2008). Moreover, increasing alkyl chain length or fluorination on the cationic species tends

to increase IL viscosity owing to strengthening the van der Waal's interactions (Bonhôte et al., 1996). Table 4.4 lists the ILs selected in this study to govern the influence of cation substituents on the physical properties of ILs.

Table 4.4: ILs used to evaluate the effect of substituents attached to the cations.

IL
[BMIm][TFSI]
[EMIm][TFSI]
[BMIm][Cl]
[BMMIm][Cl]

The initial comparison considered the cations of [BMIm][TFSI] and [EMIm][TFSI], of which the former has a longer alkyl chain than the latter (structures presented in Scheme 3.1). [BMIm]$^+$ was found to have a lesser consumption rate of 1.386 mM/min and a consumption percentage of 12.98%, whereas the corresponding values for [EMIm]$^+$ were 2.537 mM/min and 25.88% (Table 4.1). This established that the generated $O_2^{\bullet-}$ was more stable when the medium was comprised of a cation with a substituent having a longer alkyl chain.

Scheme 3.1 also illustrates the structures of the cations comprising [BMIm][Cl] and [BMMIm][Cl]. As determined by the consumption rate of [BMMIm]$^+$ evidenced a consumption rate of 0.254 mM/min and total consumption percentage of 2.87%, which was less than the corresponding values observed for [BMIm]$^+$, at 8.554 mM/min and 32.51%. Hence, the introduction of a methyl group at the 2-position in [BMMIm][Cl] significantly enhanced the stability of $O_2^{\bullet-}$. However, this finding contrasts with the report of Al-Nashef and co-workers (Al-Nashef et al., 2001b), who claimed unstable electrochemical generation of $O_2^{\bullet-}$ when using [BMMIm][HFP] as a medium. Although a vivid account regarding the

existence of methyl group in the 2-position of imidazolium was not presented, it was supposed that the proton in [BMMIm][HFP] reacted with $O_2^{\bullet-}$.

4.2 Validation of $O_2^{\bullet-}$ as the Reactive Species in Degradation Media

4.2.1 Rationale for selection of specific ILs as components of the degradation media

The ILs selected further from those which were categorized as stable ones after the screening process were used for our application as degradation media. Since the generation and stability of the $O_2^{\bullet-}$ would be predominantly determined by the interaction with cationic part of the IL(s), 2 ILs ([BTEAmm$^+$][TFSI$^-$] and [EMIm$^+$][TFSI$^-$], enlisted in Table 4.5) were chosen with different cations but similar anions so as to ascertain the possibility of comparison among different cations and the effects produced by the same on degradation of pharmaceutical targets. Moreover, this selection also provided a means to compare the effects of an aliphatic cation against an aromatic cation of the ILs.

Since it was established that the IL with ammonium-based cation ([BTEAmm$^+$][TFSI$^-$]) was rendering a more stable environment for $O_2^{\bullet-}$ generation as compared to the other one, the second selection of ILs included chemically same ILs, i.e., possessing ammonium cationic parts with similar anions, differing only in the substituents attached to the cation (mentioned in Table 4.6). Such choice of ILs involved a comparison of the effect of different substituents (alkyl chains of varying lengths; butyl, pentyl, octyl) attached to the ammonium-based cation which could possibly be observed during the waste degradation.

Moreover, the degradation process for the APIs was pursued in such ILs which exhibited potentially high solubility for the drug substance used, which also functioned as a basis for selection of the reaction media utilized in the process. The study aimed at degradation of the

APIs into nonhazardous or biologically inactive substances, so as to gauge the process for its industrial scale viability.

4.2.2 Prediction of $O_2^{\bullet-}$ stability by UV-visible spectrophotometry in the screened ILs

In this work, the $O_2^{\bullet-}$ was chemically generated via dissolution of KO_2 in IL/aprotic solvent mixture systems. To study the long-term stability of $O_2^{\bullet-}$, ILs with different cations were introduced to DMSO with generated $O_2^{\bullet-}$. The decrease in $O_2^{\bullet-}$ concentration was then monitored for a duration of 2 h to study the long-term effect of ILs on the stability of $O_2^{\bullet-}$.

4.2.2.1 Long-term stability kinetics of $O_2^{\bullet-}$ in the presence of selected ILs

(a) *Comparison of aliphatic and aromatic media*

Figures 4.4(a) and 4.5(a) show the UV-visible spectra for the absorbance of $O_2^{\bullet-}$ in DMSO containing ILs [BTEAmm$^+$][TFSI$^-$] and [EMIm$^+$][TFSI$^-$]. The absorbance band of $O_2^{\bullet-}$ is generally in the range of 250 nm –270 nm, which is in accordance with previous studies (Hayyan et al., 2016; Islam et al., 2009b).
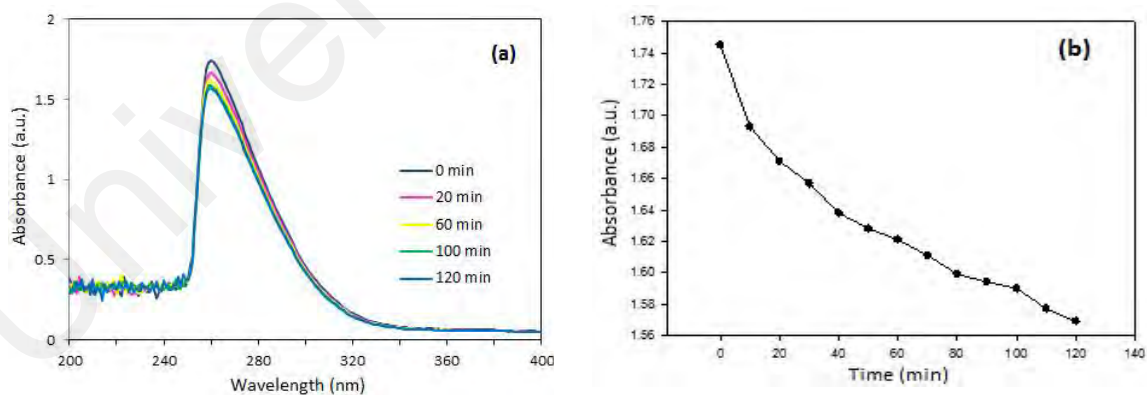
Figure 4.4: (a) Absorbance spectra of $O_2^{\bullet-}$ generated in DMSO in the presence of [BTEAmm$^+$][TFSI$^-$]; and (b) plot of absorbance ($O_2^{\bullet-}$) against time in DMSO containing [BTEAmm$^+$][TFSI$^-$], at a wavelength of 258 nm.
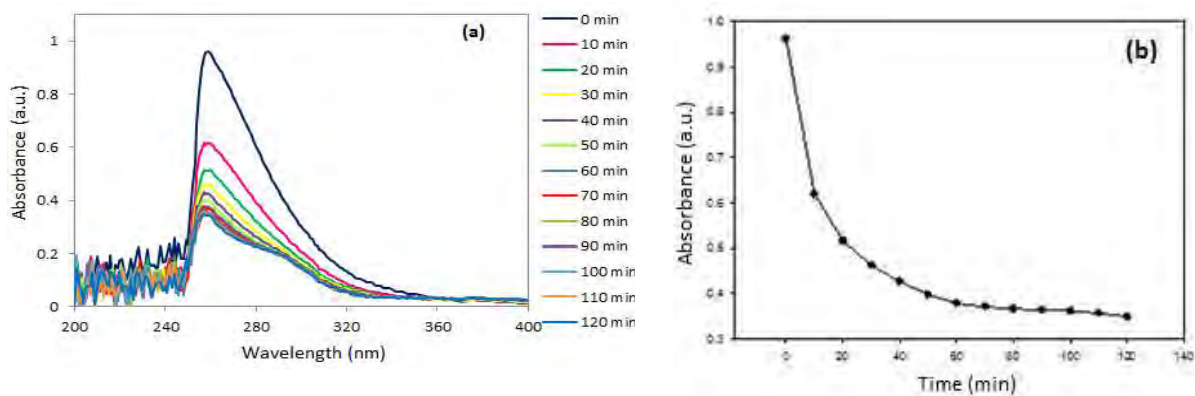
Figure 4.5: (a) Absorbance spectra of $O_2{}^{\bullet-}$ generated in DMSO in the presence of [EMIm$^+$][TFSI$^-$]; and (b) plot of absorbance ($O_2{}^{\bullet-}$) against time in DMSO containing [EMIm$^+$][TFSI$^-$], at a wavelength of 258 nm.

The decreasing absorbance of $O_2{}^{\bullet-}$ chemically generated in DMSO containing the corresponding IL for a duration of 2 h is displayed in Figures 4.4(b) and 4.5(b). The reaction kinetics was studied while supposing that the IL was added in excess to DMSO as compared to $O_2{}^{\bullet-}$. Hence, due to the negligible concentration of IL, there exists a possibility that such a reaction may follow the pseudo first-order kinetics represented in Eqs. (4.8) and (4.9).

$$r = k\,[O_2{}^{\bullet-}]^1 \tag{4.8}$$

$$[O_2{}^{\bullet-}] + [A] \rightarrow Z \tag{4.9}$$

where k is the rate constant, [A] is the concentration of the cation, and Z is either the $O_2{}^{\bullet-}$…cation ion-pair or the new product. The comparison of the initial concentration of $O_2{}^{\bullet-}$ with the concentration obtained after a time period of 2 h determined the total consumption of $O_2{}^{\bullet-}$. Furthermore, the consumption rate of $O_2{}^{\bullet-}$ was calculated by dividing the value for the concentration of $O_2{}^{\bullet-}$ consumed by the interval of time in which the measurement was obtained.

The rate constants for reaction, total consumption percentage and consumption rate of $O_2{}^{\bullet-}$ in the ILs under investigation are illustrated in Table 4.5. The value of the rate constant calculated and the more gradual slope for the absorbance of $O_2{}^{\bullet-}$ against time in DMSO containing ammonium-based IL evidently demonstrated a more stable generation of $O_2{}^{\bullet-}$, in comparison with the imidazolium-based IL. In the presence of [BTEAmm$^+$][TFSI$^-$] a consistent but very minor decrease in absorbance of $O_2{}^{\bullet-}$ with time can be depicted as compared to [EMIm$^+$][TFSI$^-$].

Table 4.5: Kinetic rate constants, total consumption percentage and consumption rate of $O_2{}^{\bullet-}$ in DMSO containing ILs.

ILs	Rate constant k_1 (s^{-1})	Total consumption % of $O_2{}^{\bullet-}$ after 120 min	Consumption rate of $O_2{}^{\bullet-}$ x 10^3 (mM/min)
[BTEAmm$^+$][TFSI$^-$]	2×10^{-5} $R^2 = 0.966$	36.78	1.423
[EMIm$^+$][TFSI$^-$]	3.5×10^{-5} $R^2 = 0.238$	46.11	11.359

These outcomes are in agreement with those attained in preceding studies on the long-term stability of $O_2{}^{\bullet-}$ in DMSO containing different ammonium and imidazolium-based ILs (Hayyan et al., 2015a; Hayyan et al., 2017). The first order rate constants for [BTEAmm$^+$][TFSI$^-$] and [EMIm$^+$][TFSI$^-$] were estimated to be 2×10^{-5} s^{-1} and 3.534×10^{-5} s^{-1}, respectively. These values are very close in order of magnitude to ILs *N*-ethyl-*N*,*N*-dimethyl-2-methoxyethylammonium bis(trifluoromethylsulfonyl)imide [N$_{112,1O_2}{}^+$][TFSI$^-$] and ethyl-dimethyl-propylammonium bis(trifluoromethylsulfonyl)imide [EDMPAmm$^+$] [TFSI$^-$], with values 2×10^{-5} s^{-1} and 1×10^{-5} s^{-1}, respectively (Hayyan et al., 2017), and for 1-ethyl-3-methylimidazolium methylsulfate [EMIm$^+$][MS$^-$] and 1-butyl-2,3-dimethylimidazolium trifluoromethylsulfonate [BDMIm$^+$][TfO$^-$] with values reported 7.9 $\times$

10^{-5} s^{-1} and 5.1×10^{-5} s^{-1}, respectively (Hayyan et al., 2015a). Also, the total consumption of $O_2^{\bullet-}$ after 2 h of analysis was calculated to be 36.78% for [BTEAmm$^+$][TFSI$^-$] and 46.11% for [EMIm$^+$][TFSI$^-$], which is comparable to the $O_2^{\bullet-}$ consumption evaluated in [N$_{112,1}$O$_2^+$][TFSI$^-$] and [BDMIm$^+$][TfO$^-$] specified as 10% and 45%, respectively. Correspondingly, the consumption rate of $O_2^{\bullet-}$ in DMSO containing [BTEAmm$^+$][TFSI$^-$] was 1.423 mM/min, while it was increased to 11.359 mM/min in DMSO containing [EMIm$^+$][TFSI$^-$]. This is in accordance with the values 2.30 mM/min and 11.43 mM/min obtained prior by Hayyan et al. for the consumption rate of $O_2^{\bullet-}$ in DMSO containing [N$_{112,1}$O$_2^+$][TFSI$^-$] and [BDMIm$^+$][TfO$^-$], respectively.

The amount of total consumption percentage after 2 h and consumption rate of $O_2^{\bullet-}$ indicated that this IL has a high capacity to function as a potent medium for stable $O_2^{\bullet-}$ generation. The results also substantiate the evidence which states that the reaction mechanism of $O_2^{\bullet-}$ varied depending on the medium, reaction time, as well as substrate.

The evasive process of stability of $O_2^{\bullet-}$ in an IL medium is a consequence of the high propensity of the reaction which might occur between cations in ILs and the $O_2^{\bullet-}$ (Marcinek et al., 2001). However, the plausibility of such a reaction is considerably dependent on the structure of the cationic species involved. It is determined from our previous understanding that the aliphatic organic cations for instance, trimethyl-n-hexylammonium, and alicyclic cations, for e.g., 1-butyl-1-methylpyrrolidinium have very little reactivity toward $O_2^{\bullet-}$, and hence holds a tendency to make it stable. On the other hand, the $O_2^{\bullet-}$ being a strong nucleophilic reagent possesses an inclination to attack ILs consisting of aromatic cations, such as imidazolium cations, like 1-ethyl-3-methylimidazolium or 1,2-dimethyl-3-propylimidazolium (Katayama et al., 2004a). Several studies revealed that the $O_2^{\bullet-}$ strongly interacts with imidazolium cations in ILs resulting in the formation of [imidazolium]$^+$…$O_2^{\bullet-}$

ion-pair. It has also been reported that the reaction of $O_2^{\bullet-}$ with imidazolium cations leads to the formation of hydrogen peroxide. The attack of $O_2^{\bullet-}$ on the C-2 position of the imidazolium ring generates an ion pair complex, which eventually experiences a ring-opening reaction (Islam et al., 2009b). Being among the most frequently studied ILs, imidazolium-based ILs have also been specified for their reaction with $O_2^{\bullet-}$ to yield the corresponding 2-imidazolones as a product generated at ambient conditions, using chemical and electrochemical methods (Al-Nashef et al., 2010b; Hayyan et al., 2013). The literature henceforth sufficiently substantiated that $O_2^{\bullet-}$ is unstable in ILs comprising imidazolium cations.

(b) Effect of increasing alkyl chain length in the aliphatic media

Subsequent to the screening of aliphatic ILs as a more stable medium for $O_2^{\bullet-}$ generation, the ammonium ion-based cations with varying alkyl chain lengths were selected to demonstrate the effects on the long-term stability of $O_2^{\bullet-}$ species. Figure 4.6 portrays the changing maximum absorbance against time for $O_2^{\bullet-}$ generated in DMSO in the presence of $[BTEAmm^+][TFSI^-]$, $[PTEAmm^+][TFSI^-]$ and $[OTEAmm^+][TFSI^-]$, in a wavelength range of 250 nm $-$270 nm.
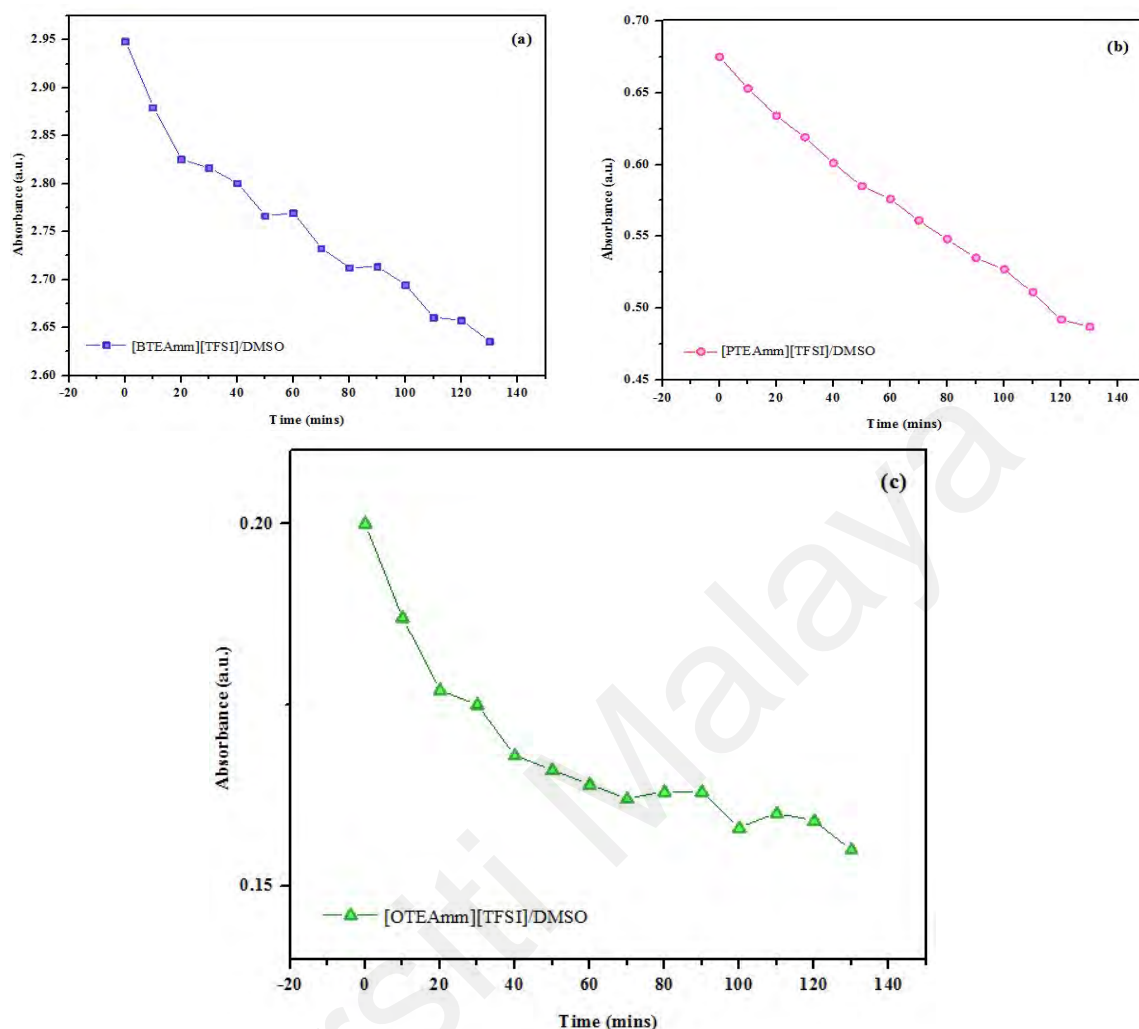
Figure 4.6: Plot of absorbance for $O_2^{\bullet-}$ generated in DMSO in the presence of (a) [BTEAmm$^+$][TFSI$^-$], (b) [PTEAmm$^+$][TFSI$^-$] and (c) [OTEAmm$^+$][TFSI$^-$] against time, at a wavelength of 258 nm.

The reaction kinetics of $O_2^{\bullet-}$ in the presence of these ILs was also investigated to assess its long-term stability in such reaction media. The total consumption of $O_2^{\bullet-}$ was determined by comparing the initial concentration of $O_2^{\bullet-}$ with the concentration obtained after a time period of 2 h. In addition, the rate constant for pseudo first-order kinetics of the reaction and the consumption rate of $O_2^{\bullet-}$ was also explored and presented in Table 4.6.

Table 4.6: Kinetic rate constants, total consumption percentage and consumption rate of $O_2^{\bullet-}$ in DMSO containing [BTEAmm$^+$][TFSI$^-$], [PTEAmm$^+$][TFSI$^-$] and [OTEAmm$^+$][TFSI$^-$].

ILs	Rate constant k_1 (s^{-1})	Total consumption % of $O_2^{\bullet-}$ after 120 min	Consumption rate of $O_2^{\bullet-}$ x 10^3 (mM/min)
[BTEAmm$^+$][TFSI$^-$]	2×10^{-5} $R^2 = 0.966$	36.78	1.423
[PTEAmm$^+$][TFSI$^-$]	2.8×10^{-5} $R^2 = 0.996$	27.11	0.470
[OTEAmm$^+$][TFSI$^-$]	0.6×10^{-5} $R^2 = 0.810$	20.50	0.105

It is rather evident from the scale ranges of maximum absorbance for $O_2^{\bullet-}$ showing the decreasing slopes against time that in the presence of an IL, the longer the alkyl chain attached to the ammonium cation the more gradual the decline in concentration of $O_2^{\bullet-}$ occurred. That is to say, in the presence of [BTEAmm$^+$][TFSI$^-$] having butyl chain as a substituent to ammonium cation, the maximum absorbance values for the $O_2^{\bullet-}$ decreased more rapidly than in the presence of [PTEAmm$^+$][TFSI$^-$] having pentyl chain attached, which is likewise more rapid in comparison to when $O_2^{\bullet-}$ was generated in the medium with [OTEAmm$^+$][TFSI$^-$], i.e., octyl chain substituent linked to the ammonium cation.

Table 4.6 illustrates the consumption percentage and consumption rate (mM/min) of $O_2^{\bullet-}$ in DMSO containing the ILs. The total percentage of $O_2^{\bullet-}$ that was consumed followed the order of [BTEAmm$^+$][TFSI$^-$] > [PTEAmm$^+$][TFSI$^-$] > [OTEAmm$^+$][TFSI$^-$], which was also in agreement with the values of the consumption rate that were determined. This identified that the $O_2^{\bullet-}$ was more stable in ammonium-based ILs with longer alkyl chain lengths attached as substituents. The rate constants, however, indicated slight differences in this order; such as, The rate constant however, for [PTEAmm$^+$][TFSI$^-$] was calculated to be

highest among the three ILs. This slight variation in the order for rate constants of ILs can be ascribed to the presence of residual moisture or impurities which were not amply removed during the preliminary measures.

4.2.3 Electrochemical proof on $O_2^{\bullet-}$ stability using Cyclic Voltammetry

4.2.3.1 Mechanism of $O_2/O_2^{\bullet-}$ reaction pathway

The direct electrochemical reduction of dissolved oxygen gas (O_2) in aprotic solvents to form $O_2^{\bullet-}$ typically occurs in the range of potential $\pm(-1.0)$ V vs. the standard calomel electrode (SCE) in the absence of protonic species or water (Costentin et al., 2010; Sawyer, 1992a), according to the reaction represented in Eq. (4.10). Sawyer et al. (Sawyer, 1995) determined that the reduction peak is due to the generation of $O_2^{\bullet-}$ and the oxidation peak is apparent as a consequence of the reverse of that reaction (Eq. (4.10)).

$$O_2 + e^- \leftrightarrows O_2^{\bullet-} \tag{4.10}$$

The electrochemistry of dissolved oxygen and of $O_2^{\bullet-}$ in DMSO solutions using voltammetric and chronopotentiometric techniques has been studied by Sawyer and Roberts (Sawyer & Roberts, 1966) as expressed in Eqs. (4.11 − 4.14):

$$O_2 + e^- \rightarrow O_2^{\bullet-}, \qquad E' = -0.75 \text{ V} \tag{4.11}$$

$$O_2^{\bullet-} + e^- \rightarrow O_2^{2-}, \qquad E' = -2.02 \text{ V} \tag{4.12}$$

$$O_2^{\bullet-} \rightarrow O_2 + e^-, \qquad E' = -0.73 \text{ V} \tag{4.13}$$

$$O_2^{2-} \rightarrow O_2 + 2e^-, \qquad E' = +0.75 \text{ V} \tag{4.14}$$

In the absence of protic solvents and electrolytes, oxygen is reduced in two one-electron steps; initially to $O_2^{\bullet-}$ at a potential of -0.75 V vs. SCE and then to peroxide ion at a potential of -2.02 V vs. SCE. The second step (Eq. (4.12)) was observed with gold and mercury electrodes, but not with a platinum electrode. $O_2^{\bullet-}$ is oxidized to oxygen at -0.73 V and is reduced to peroxide ion at -2.02 V. Peroxide ion is oxidized directly to oxygen at $+0.75$ V by a two-electron process.

However, in the presence of a proton source, a rapid disproportionation reaction occurs as represented by Eq. (4.15), and the $O_2^{\bullet-}$ promptly reacts with a proton to give a highly unstable protonated superoxide (Eq. (4.16)), which further disproportionates extremely rapidly to give hydrogen peroxide and oxygen, as depicted in Eq. (4.17), while the oxygen is reduced by the reaction in Eq. (4.11).

$$2O_2^{\bullet-} + 2H^+ \rightarrow H_2O_2 + O_2 \tag{4.15}$$

$$O_2^{\bullet-} + H^+ \rightarrow HO_2 \tag{4.16}$$

$$2HO_2 \rightarrow H_2O_2 + O_2 \tag{4.17}$$

Similarly, in the presence of a protic electrolyte (0.1 F NH$_4$ClO$_4$), oxygen is reduced directly to hydrogen peroxide (Eq. (4.18)) at -0.28 V (the potential of such reaction is dependent upon the proton concentration).

$$O_2 + 2H^+ + 2e^- \rightarrow H_2O_2 \tag{4.18}$$

The combination of Eqs. (4.11), (4.16) and (4.17) lead to the overall reduction process indicated by Eq. (4.18). Therefore, a plausible mechanism for oxygen reduction under all solvent conditions is a primary one-electron step to $O_2^{\bullet-}$ which, in the presence of protic solvents, disproportionates to oxygen and hydrogen peroxide.

4.2.3.2   Electrochemical generation of $O_2^{\bullet-}$

Cyclic voltammograms depicting evidence of the superoxide ion ($O_2^{\bullet-}$) obtained as a result of one-electron reduction of O_2 in (a) neat [BTEAmm$^+$][TFSI$^-$] and (b) 90% v/v [BTEAmm$^+$][TFSI$^-$] in AcN are illustrated in Figure 4.7 (reduction currents are positive). This was carried out in order to demonstrate the validity of the presence of $O_2^{\bullet-}$ in the binary mixture system comprising AcN and IL utilized, and also to compare it with the curves produced by $O_2^{\bullet-}$ generation in the corresponding neat IL.

Upon N_2 sparging, the negligible background currents are indicative of the media being electrochemically inert in this potential range, i.e., there is an absence of any intrinsic electrochemically active species in the two-reaction media. The sparging of O_2 in a binary system comprising 90% v/v [BTEAmm$^+$][TFSI$^-$] in AcN resulted in a faradaic reduction and oxidation peaks at −1.01 V and −0.74 V vs. Ag/AgCl, respectively (Fig. 4.7b). These potential values are much related to those acquired by Al-Nashef et al. (Al-Nashef et al., 2001a) while obtaining CV peaks for $O_2/O_2^{\bullet-}$ redox reaction using tetraethylammonium perchlorate (TEAP, 0.1 M) in AcN (reduction at −1.00 V and oxidation peak at −0.72 V vs. SCE), which has also been reported to be in consonance with the values attained by Sawyer et al (Sawyer, 1995). The generation of $O_2^{\bullet-}$ has also been identified in neat [BTEAmm$^+$][TFSI$^-$] at − 0.95 V vs. Ag/AgCl as an O_2 reduction peak, at a sweep rate of 9 mV.s^{-1} (Fig. 4.7a). This value of potential peak is in good agreement with a comparable ammonium-based IL i.e., ethyldimethyl-propylammonium bis(trifluoromethylsulfonyl) imide ([EDMPAmm$^+$][TFSI$^-$]), also used in pristine form for $O_2^{\bullet-}$ generation, as reported recently (Halilu et al., 2019). The reduction potential for $O_2/O_2^{\bullet-}$ couple shifts to more negative values as the solvating or charge transfer properties of the medium decrease. Hence,

the solvent and electrode materials can both influence the reversibility as well as the peak separation of the CVs (Sawyer, 1995).

Figure 4.7 (a and b) compares the ORR in neat [BTEAmm$^+$][TFSI$^-$] and 90% [BTEAmm$^+$][TFSI$^-$]/AcN. The cathode scans are verifying that $O_2^{\bullet-}$ can be generated in these media, and the reverse oxidation scans imply that the $O_2^{\bullet-}$ is stable. After the addition of AcN to [BTEAmm$^+$][TFSI$^-$] an enhancement of the voltammetric wave is clearly observed, caused by a change in the solvating properties of the medium. Although this variation results in a slight potential shift of reduction and oxidation peaks, the qualitative features of the CV are not considerably affected, that is, the oxygen reduction to $O_2^{\bullet-}$ produces a symmetric CV. In cases where these conditions are contrary, it is possible to simply distinguish from the profile of the experimental current-voltage curves.

As stated in the Nicholson model, a system which appears to be in an electrochemical equilibrium at low frequencies might be adapted to demonstrate kinetic behavior at higher frequencies, which is primarily indicated by increased separation of cathodic and anodic peak potentials. This theory implicates a fundamental yardstick of the reversibility of a CV reaction; if the cathodic/anodic potential peak separation is around 60 mV or lesser, the reaction appears to be reversible (Nicholson, 1965). In neat [BTEAmm$^+$][TFSI$^-$] and 90% [BTEAmm$^+$][TFSI$^-$]/AcN, the CV curves for their cathodic and anodic separations are higher than 60 mV, which is according to the criterion, suggestive of a quasi-reversible (or almost reversible) electrochemical process for the generation of $O_2^{\bullet-}$ therein (Fig. 4.7).
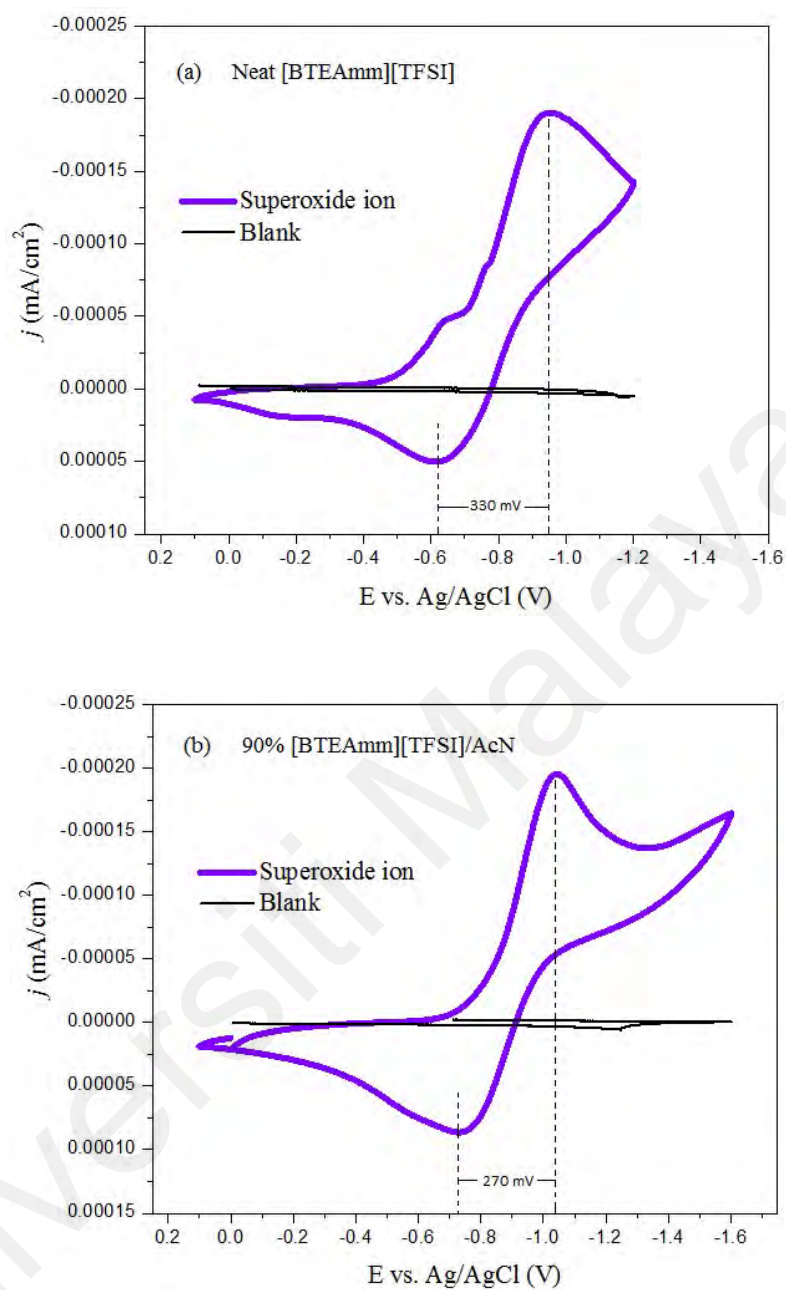
Figure 4.7: Cyclic voltammetry (CV) with nitrogen (black) and oxygen (blue) sparging in (a) neat [BTEAmm⁺][TFSI⁻] and (b) 90% v/v [BTEAmm⁺][TFSI⁻]/AcN at 9 mV.s⁻¹ scan rate. All scans used a glassy carbon working electrode (A = 0.07 cm²).

Furthermore, the separation in the peaks of $O_2/O_2^{\bullet-}$ potential in these media is adequately small, such that the difference represents the execution of the reaction in Eq. (4.10) in the two solvent systems. This quasi-reversible reaction can be principally inferred as the generation of $O_2^{\bullet-}$ such that it is available for further reaction. In pure $[BTEAmm^+][TFSI^-]$ the reduction/oxidation peak separation is larger (330 mV) while in 90% $[BTEAmm^+][TFSI^-]/AcN$ this separation is observed to be smaller (270 mV), representing greater availability of the generated $O_2^{\bullet-}$ for further reactions in the latter as compared to the former system.

However, the current densities for the $O_2/[BTEAmm^+][TFSI^-]$ and $O_2/[BTEAmm^+][TFSI^-]/AcN$ systems are approximately analogous at a sweep rate of 9 mV/s, as seen in Fig. 4.7. To quantify the difference in magnitude of the currents further, CVs were run in $[BTEAmm^+][TFSI^-]$ and 90% $[BTEAmm^+][TFSI^-]/AcN$ at several sweep rates (9, 36, 64, 81, 100, and 144 mV/s). CV curves for three of these scans in individual systems are illustrated in Figure 4.8 (a and b). The peak currents are proportional to the square root of the sweep rates in both media investigated which is pursuant to the electrochemistry of a quasi-reversible soluble redox couple (Bard, 2001). In addition, a linear relationship is evident while plotting the peak current density against the sweep rate (Figure 4.9 (a and b), which presumes that such an electrochemical process of oxygen reduction is a diffusion-controlled process hence governed in the bulk medium and that its occurrence on the surface of the electrode is implausible (Bard, 1980; J., 2006).
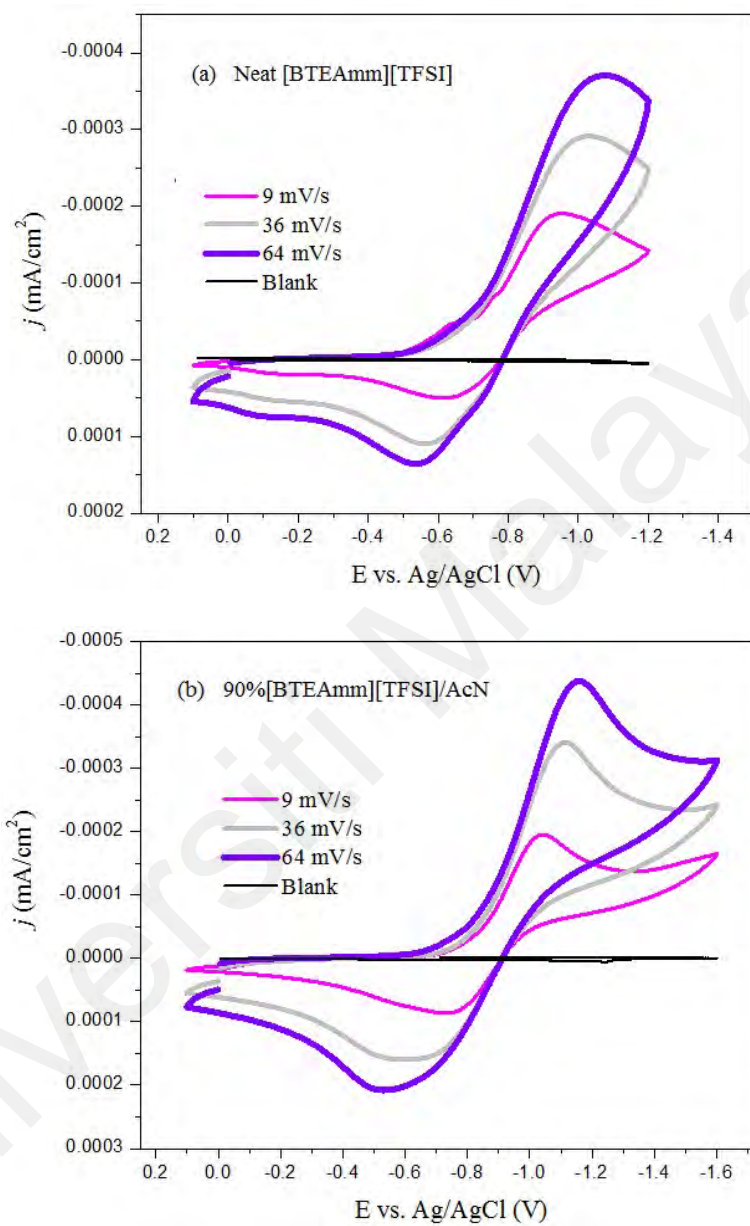
Figure 4.8: Cyclic voltammograms of $O_2^{\bullet-}$ generation at various scan rates (mV/s) in (a) neat [BTEAmm$^+$][TFSI$^-$] and (b) 90% v/v [BTEAmm$^+$][TFSI$^-$]/AcN.
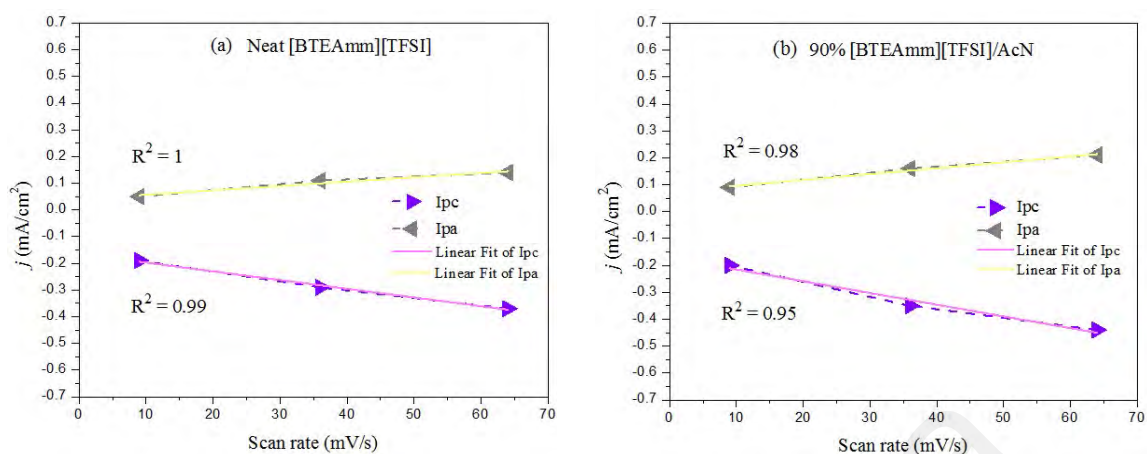
Figure 4.9: The relationship of current density (*j*) against scan rate in (a) neat [BTEAmm$^+$][TFSI$^-$] and (b) 90% v/v [BTEAmm$^+$][TFSI$^-$]/AcN.

A slight protrusion intervening in the cathodic curve at about $-$ 0.65 V is also of note, which is discernable in the CV scan acquired using neat [BTEAmm$^+$][TFSI$^-$] at 9 mV/s (Figure 4.7a). Nevertheless, it is not observable in CVs of the other medium or at higher sweep rates. A trace amount of impurity in the IL not removable after vacuum drying or argon purging, and being particularly dormant under nitrogen, but active in the presence of oxygen is often accountable for its appearance (Evans et al., 2004b; Randström et al., 2007a). Alternatively, this plateau-like bulge emerging during the reduction of O$_2$ has also been reported to occur due to the adsorption of IL cation on the surface of the working electrode, which might be able to instigate an extremely meagre electrochemical activity (Islam et al., 2005). A minor increase in current caused by electrical double-layer charging may also possibly contribute to the presence of such humps in the CV curves (Suarez et al., 2002).

4.3 Degradation of Pharmaceutical Substances

The process of degradation of pharmaceutical compounds (APIs) was carried out in the binary mixture systems comprising AcN as an aprotic solvent along with one of the best ILs which was screened for stable $O_2^{\bullet-}$ generation, i.e., $[BTEAmm^+][TFSI^-]$. Other than the ammonium cation-based IL, a relatively less effective IL was chosen to be utilized as a component of the binary medium, such as $[EMIm^+][TFSI^-]$. This imidazolium cation-based IL was investigated to demonstrate whether the aromaticity of an IL cation actually and to what extent affects the degradation of API, while it was screened out as one of the ILs producing less stable $O_2^{\bullet-}$ according to the kinetic studies. Therefore, an aliphatic and an aromatic cation of the ILs were chosen to compare together the influence observed on the degradation of the API as the first factor. As it was established via experimentation that the aliphatic cation based-IL was indeed more effective than the aromatic cation based-IL, we chose two more aliphatic ILs with the same cationic and anionic structural features but only differing in the length of the alkyl chain attached to the IL-cation, in order to determine the extent of their influences on API degradation.

In addition, the chemical generation of the $O_2^{\bullet-}$ was preferred for the degradation reactions over the electrochemical generation, since the former is more of a simpler process than the latter which is relatively a complicated and sensitive method. Since the chemical generation requires a solid oxidant, i.e., a superoxide salt, contrary to the electrochemical generation which occurs with high purity O_2, and hence more energy is required for such a process compared to the chemically generated $O_2^{\bullet-}$. There is a considerable reduction in the weight of dosage, reactor volume, storage, and transport/shipment controls for the superoxide salts (Chan et al., 2008), compared to the precautions and safety procedures needed to be followed for O_2 gas.

Role of acetonitrile as the aprotic solvent in degradation media

Acetonitrile (AcN) has been selected as an aprotic solvent since it is used in the laboratory as a medium-polarity solvent which would assist the solvation of APIs which are also polar to moderately polar in nature. Furthermore, AcN has a convenient liquid range and is miscible with water and a range of organic solvents as well (except saturated hydrocarbons), which improves its miscibility with the ILs under investigation. This is also because polar solvents tend to have a large dipole moment, possessing charge separation, and thus increasing the ability to solvate the ions, dissolved substances, and other polar materials.

4.3.1 Effect of cationic structure of ILs

4.3.1.1 Effect of aromaticity of the cation

Using neat [BTEAmm$^+$][TFSI$^-$] as a reaction medium, the degradation percentage of ACTM at RT increased markedly from 64.7% to 78.8% and finally to 84.9% with a KO$_2$/ACTM molar ratio of 10, 20, and 30, respectively. By contrast, the similar reactions (using KO$_2$/ACTM molar ratio of 10, 20 and 30) in neat [EMIm$^+$][TFSI$^-$] at RT showed a relatively minor increase in degradation percentages, i.e., 53.9%, 61.7%, and 62.6%, respectively. Eventually, the values using [BTEAmm$^+$][TFSI$^-$] reached as high as 94.1% while only 63.4% was accomplished in the case of [EMIm$^+$][TFSI$^-$], as the molar ratio of KO$_2$/ACTM was increased to 40 at RT. The effect of the structure of respective IL cations on the oxidative degradation of ACTM is illustrated in Figure 4.10. The change in the extent of degradation is demonstrable from the graph, implying its dependence on the structure of the cation being used.

Other than the difference in ACTM degradation observed using neat ILs, likewise, while using binary mixtures with [BTEAmm$^+$][TFSI$^-$] and [EMIm$^+$][TFSI$^-$] (90 vol.% IL/AcN), a

percentage degradation of 79% was achieved for the former system against 44% for the latter one, when a specific molar ratio of KO$_2$/ACTM (20) was used. Subsequently, by doubling the molar ratio of KO$_2$/ACTM (40), the degradation of ACTM attained with the binary mixture containing [EMIm$^+$][TFSI$^-$] is approximately half (51%) of what was achieved using [BTEAmm$^+$][TFSI$^-$] (96%), as presented in Figure 4.11. This perceivable difference in degradation percentage for the drug can be attributed to the fact that cations present in ILs directly influence the stability of generated O$_2$$^{\bullet-}$. This also supports the results attained for the prediction of O$_2$$^{\bullet-}$ stability by UV-visible spectrophotometry (Section 4.2.1), which describes the effect on O$_2$$^{\bullet-}$ stability in DMSO containing these ILs. Such influence of the nature of IL cations on the degradation of ACTM as well helps construe the catalytic activity role of ILs, in addition to acting as a medium for reaction.

Figure 4.10: Effect of structure of the cations in [BTEAmm$^+$][TFSI$^-$] and [EMIm$^+$][TFSI$^-$] on the percentage degradation of ACTM by O$_2$$^{\bullet-}$ in neat ILs (100 vol.%) at RT.
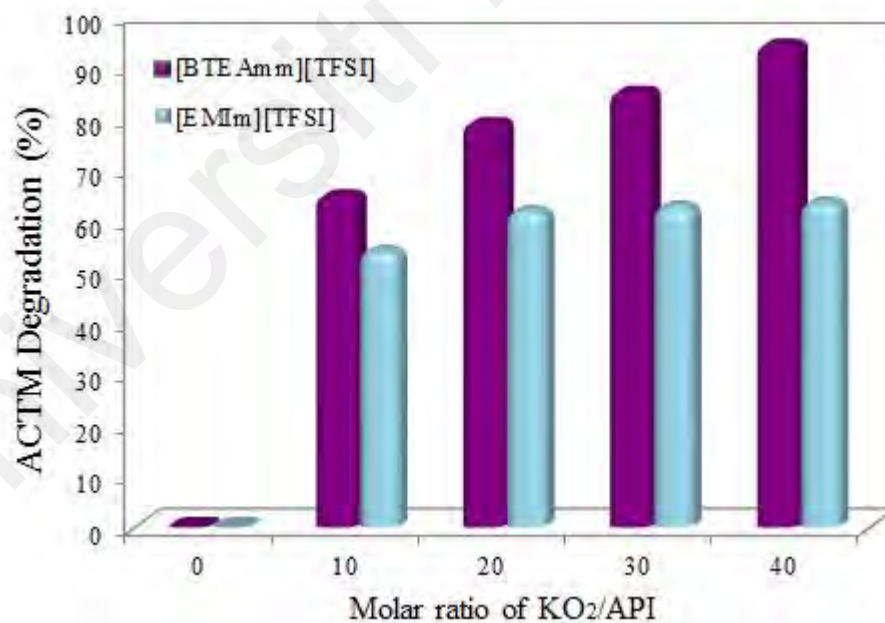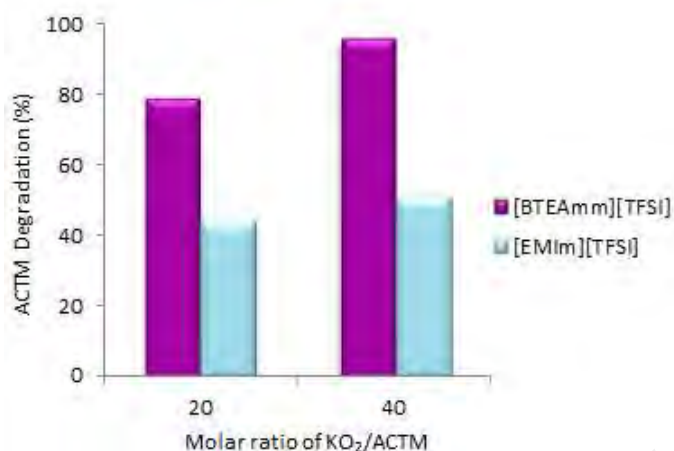
Figure 4.11: Effect of structure of the cations in the binary mixtures (90 vol.% IL/AcN) containing [BTEAmm⁺][TFSI⁻] and [EMIm⁺][TFSI⁻] on the percentage degradation of ACTM by $O_2^{\bullet-}$ at RT.

4.3.1.2 Effect of cation alkyl chain length

The investigation entails the effect of three ILs with [TFSI⁻] anion and ammonium-based cations differing only in their alkyl chain length, i.e., butyl triethylammonium bis(trifluoromethylsulfonyl)imide [BTEAmm⁺][TFSI⁻], triethylpentylammonium bis (trifluoromethylsulfonyl) imide [PTEAmm⁺][TFSI⁻] and octyltriethylammonium bis (trifluoromethylsulfonyl) imide [OTEAmm⁺][TFSI⁻], in order to explore the influence of varying length of IL cation alkyl chain on the API degradation efficiency.

This outcome is characteristically related to the stability of the $O_2^{\bullet-}$ in the presence of a particular IL medium. The long-term stability studies and kinetics of $O_2^{\bullet-}$ species in these reaction media have been demonstrated by means of UV-visible spectrophotometric analysis (Section 4.2.1). The analysis categorically demonstrated the reliance of the stable generation of $O_2^{\bullet-}$ on the structure of the IL cations present in the reaction media. This implies that using

the reaction mixture capable of generating more stable $O_2^{\bullet-}$ in situ as the contributive ROS would notionally lead to better degradation.

Figures 4.12, 4.13 and 4.14 show the increase in achieved degradation of ACTM, RLZ and CBM respectively, with time in IL/AcN binary reaction media with 90% and 10% volume ratios if ILs individually plotted to compare the efficiencies. In the case of ACTM (Figure 4.12), the results are empirically in agreement with the kinetics and stability studies which established that the presence of IL with octyl chain ($[OTEAmm^+][TFSI^-]$) in the reaction medium generates the most stable of $O_2^{\bullet-}$ species which contributes as a major ROS in the oxidative degradation of these target pharmaceuticals. It can also be observed from the plots of $[ACTM]/[ACTM]_0$ that using 10% $[OTEAmm^+][TFSI^-]$/AcN completed the degradation more rapidly as compared to when in the 90 vol.% IL in the reaction mixture (discussed in further sections).
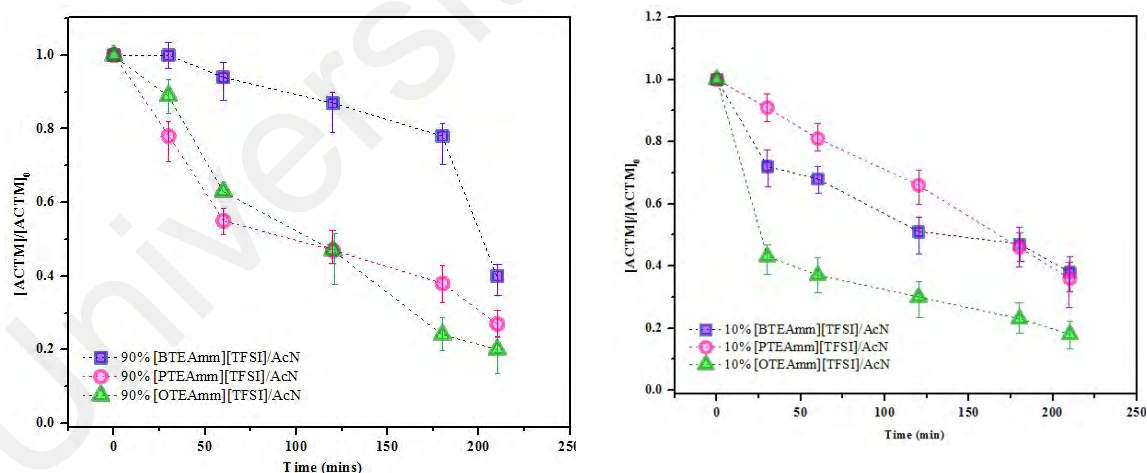
Figure 4.12: Effect of alkyl chain length of the cations in 90 vol.% IL/AcN containing [BTEAmm⁺][TFSI⁻], [PTEAmm⁺][TFSI⁻] and [OTEAmm⁺][TFSI⁻] (left) and 10 vol.% IL/AcN containing [BTEAmm⁺][TFSI⁻], [PTEAmm⁺][TFSI⁻] and [OTEAmm⁺][TFSI⁻] (right), on the degradation.
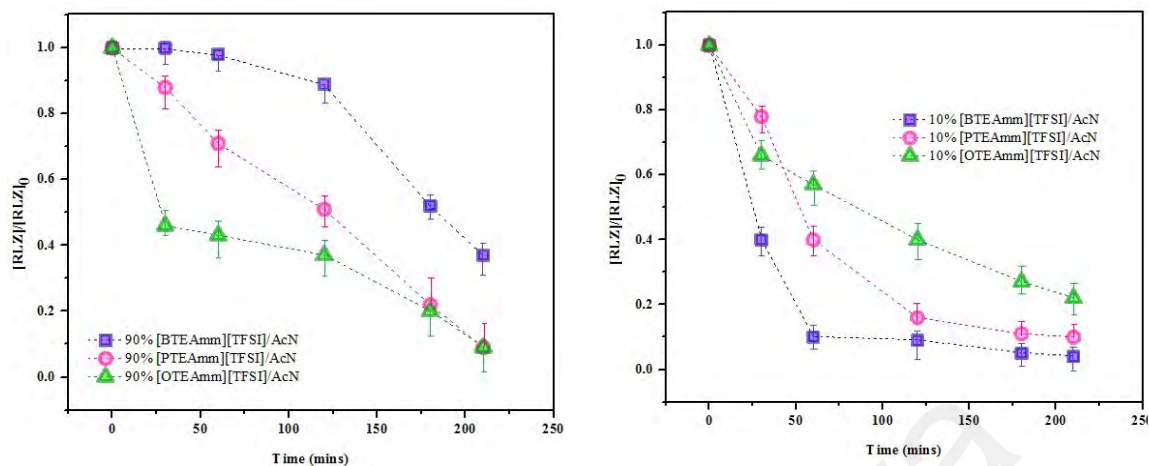
Figure 4.13: Effect of alkyl chain length of the cations in 90 vol.% IL/AcN containing [BTEAmm$^+$][TFSI$^-$], [PTEAmm$^+$][TFSI$^-$] and [OTEAmm$^+$][TFSI$^-$] (left), and 10 vol.% IL/AcN containing [BTEAmm$^+$][TFSI$^-$], [PTEAmm$^+$][TFSI$^-$] and [OTEAmm$^+$][TFSI$^-$] (right), on the degradation.
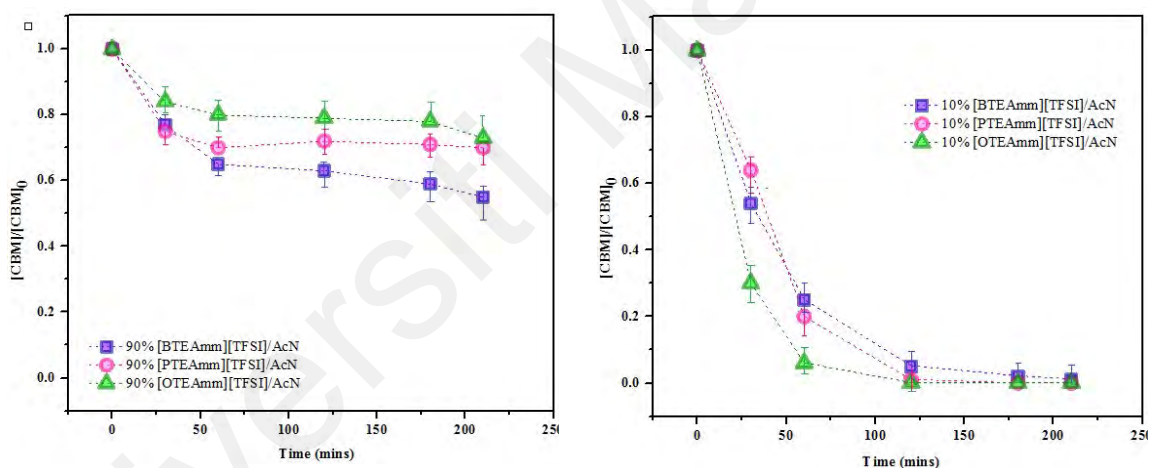
Figure 4.14: Effect of alkyl chain length of the cations in 90 vol.% IL/AcN containing [BTEAmm$^+$][TFSI$^-$], [PTEAmm$^+$][TFSI$^-$] and [OTEAmm$^+$][TFSI$^-$] (left), and 10 vol.% IL/AcN containing [BTEAmm$^+$][TFSI$^-$], [PTEAmm$^+$][TFSI$^-$] and [OTEAmm$^+$][TFSI$^-$] (right), on the degradation.

On the contrary, while investigating the degradation efficacy of RLZ in the three IL media with varying alkyl chain lengths, it was observed that using the 10 vol.% of IL/AcN mixtures, the extent of degradation achieved with time was greater in the presence of [BTEAmm$^+$][TFSI$^-$] rather than in [OTEAmm$^+$][TFSI$^-$]. This disagreement with the kinetic

study of the $O_2^{\bullet-}$ utilizing these ILs could be attributed to the altered concentrations of ILs used with acetonitrile as the aprotic solvent which contributes to the lowered viscosity and increased solubility of the target substance in the reaction mixture, hence enhancing the selectivity of the reaction even in presence of the ILs with shorter alkyl chain lengths. However, it can be seen in Figure 4.13 that in the case where 90 vol.% of IL/AcN mixtures were used, the degradation of RLZ is very well-coincided with the reaction kinetics of $O_2^{\bullet-}$ calculated in the presence of respective ILs, i.e., degradation is observed to be most rapid and efficient in the instance where $[OTEAmm^+][TFSI^-]$ was used in the binary mixture, since it is supposedly the most suitable component to generate stable $O_2^{\bullet-}$ according to the kinetic study.

The degradation efficacy of CBM as depicted in Figure 4.14 presents the effect of the alkyl chain length attached to the IL cations. The decreasing concentration of CBM with time in 90 vol.% IL/AcN containing $[BTEAmm^+][TFSI^-]$, $[PTEAmm^+][TFSI^-]$ and $[OTEAmm^+][TFSI^-]$ was not as significant. Nevertheless, a complete degradation was attained for the binary mixtures containing 10 vol.% IL/AcN in the presence of ILs with all 3 alkyl chain substituents, although $[OTEAmm^+][TFSI^-]$ was able to provide the fastest target degradation. This also supports the results attained for the prediction of $O_2^{\bullet-}$ stability by UV-visible spectrophotometry (Section 4.2.1).

These outcomes can also be related to the individual structure of each API investigated in this study, and the corresponding solubilities due to slightly different polarities in different binary solvent media. The results are more coinciding with the kinetic studies while utilizing 10 vol.% IL/AcN mixture systems in the case of all three ILs, along with a relatively rapid degradation observed in the same binary volume ratio as compared to that carried out in 90

vol.% IL/AcN mixtures which demonstrates a more gradual achievement and extent of API degradation.

4.3.2 Effect of oxidant dose (molar ratio of KO₂ to API)

The chromatograms of ACTM before and after the reaction with $O_2^{\bullet-}$ are displayed in Figure 4.15 and Figure 4.16. In the absence of KO_2, ACTM remained stable as verified by analysis of the blank samples containing the drug. However, ACTM concentration steadily decreased as the reaction proceeded after KO_2 was added to the reaction mixture, as indicated by an increase in percent degradation (Figure 4.17). The influence of varying molar ratios of KO_2 was evaluated at a constant volume percentage of ILs in the binary mixtures individually. The increasing ratio of KO_2 per mole of ACTM resulted in improved degradation percentages of ACTM in a binary system containing AcN with $[BTEAmm^+][TFSI^-]$ and $[EMIm^+][TFSI^-]$, from which the substantial efficiency of $O_2^{\bullet-}$ for oxidation of drug can be noticeably depicted (Figure 4.17 and Table 4.7). The highest percentage of the total amount of ACTM degraded in the process was more than 98% in both binary systems. Though while comparing the stoichiometry of the two reaction systems, 45 mol of KO_2 was required to oxidize one mole of ACTM in a system containing $[BTEAmm^+][TFSI^-]$ against 55 mol of KO_2 per mole of ACTM containing $[EMIm^+][TFSI^-]$. This implies that a lesser amount of KO_2 was required to achieve complete degradation using ammonium-based IL compared to imidazolium-based IL, owing to the aforementioned direct influence of stability of generated $O_2^{\bullet-}$ on the IL cations.
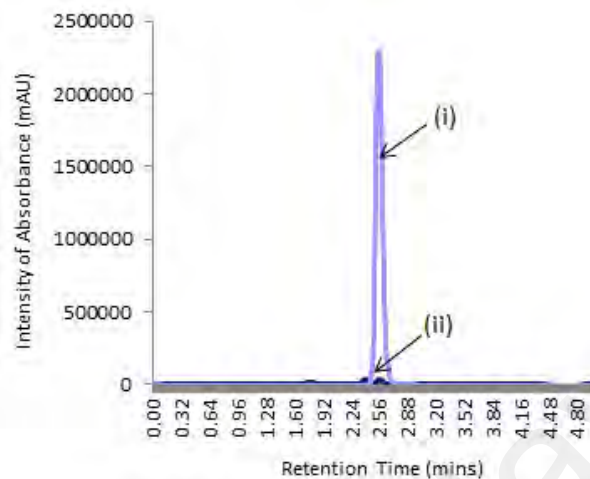
Figure 4.15: HPLC chromatograms of ACTM in binary mixture containing [BTEAmm⁺][TFSI⁻] (10 vol.%) (i) before and (ii) after addition of KO₂ (molar ratio 45), at RT.
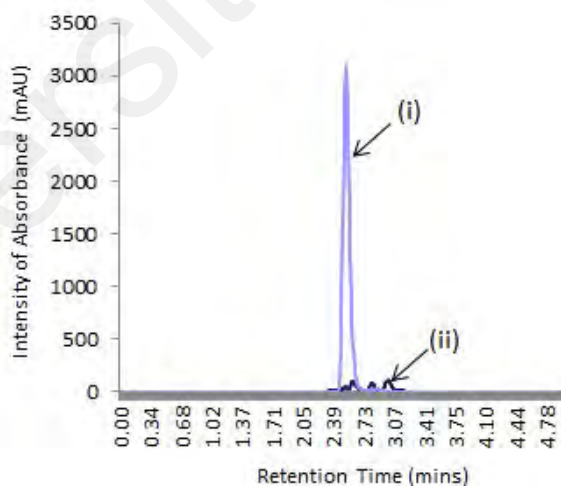
Figure 4.16: HPLC chromatograms of ACTM in binary mixture containing [EMIm⁺][TFSI⁻] (10 vol.%) (i) before, and (ii) after addition of KO₂ (molar ratio 55), at RT.

The initial KO_2 loading required to attain a complete degradation of ACTM at RT was estimated to be 21 mg per mg of ACTM when [BTEAmm$^+$][TFSI$^-$] was used as a component of the binary medium. This requisite amount of oxidant spent for ACTM removal is sizably lesser compared to several other studies (mentioned in Table 4.8) conducted in the last decade on oxidative removal of ACTM using different reactive oxygen species (ROS). The relatively minute amount of KO_2 employed for ACTM oxidation in this study defines the acclaimed efficacy of this reagent as an oxidant. Also, this draws attention toward the lucrative nature of $O_2^{\bullet-}$ for its usefulness as ROS in degradative oxidations of such complex organic compounds as pharmaceuticals, since no other study has attempted to exploit $O_2^{\bullet-}$ as ROS for direct oxidation of drugs.
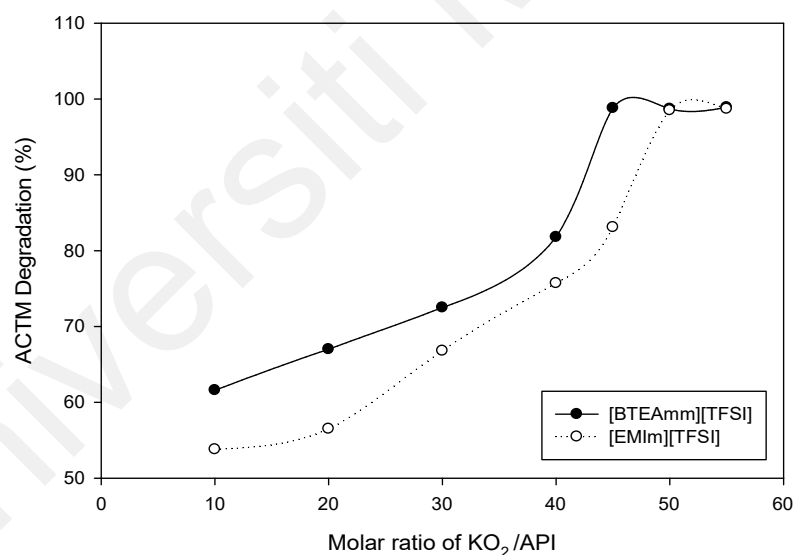
Figure 4.17: Effect of molar ratio of KO₂ in binary mixtures (5 vol.% IL/AcN) containing (a) [BTEAmm$^+$][TFSI$^-$] and (b) [EMIm$^+$][TFSI$^-$] on the degradation (%) of ACTM by O₂$^{\bullet-}$ at RT.

Table 4.7: The degradation (%) of ACTM at different molar ratios of KO$_2$ in binary mixtures (5 vol.%) containing [BTEAmm$^+$][TFSI$^-$] and [EMIm$^{+]}$[TFSI$^-$] at RT.

Molar ratio of KO$_2$/ACTM	Degradation of ACTM in AcN + 5 vol.% IL	
	[BTEAmm$^+$][TFSI$^-$]	[EMIm$^+$][TFSI$^-$]
10	61.6	53.8
20	67	56.5
30	72.5	66.8
40	81.8	75.7
45	98.8	83.1
50	98.7	98.5
55	98.9	98.7

The evaluation of work in the literature on ACTM removal via ROS (Table 4.8) also elaborates on other reaction conditions, such as time taken for maximum degradation, pH dependency, catalytic utility, percentage of drug removal achieved, and facility of the experimental mixture system used, etc. A basic factor which is economically contributive is the time of reaction (i.e., 2 h), which turns out to be either analogous or greatly reduced in the current setup when compared to other studies. Alongside, most oxidative reactions in the literature seem to be highly dependent on the specific pH values (mostly acidic conditions) in a way that variation in pH leads to ineffective reaction, whereas the present system is independent of this factor. This is mainly owing to the aprotic nature of media employed for the degradation of ACTM which benefits by posing no precondition to restore the consumed protons to make the reaction successful, unlike many other methods which require a continuous supply of hydrogen ions (H$^+$) for the reaction to move in the forward direction. Moreover, the ILs serving as green media for degradation were entirely recoverable. Relative to the studies on oxidative removal of ACTM, the remarkably simplistic experimental mixture system quite efficiently results in the acquirement of a much comparable degradation of ACTM (> 98%) against those reported in publications with similar objectives.

Table 4.8: Comparison of experimental conditions and reaction systems between this work and other studies in literature for oxidative degradation of ACTM.

System and Conditions	This work	(Zhang et al., 2012)	(Zhang et al., 2017)	(Jiang et al., 2017)	(Zhang et al., 2019b)
Oxidant dose	21 mg KO_2/mg ACTM	1000 mg Al/mg ACTM	100 mg ZVC*/mg ACTM	1800 mg PS*/mg ACTM	10 mg PS* + 300 mg oxygen deficient $CuFe_2O_4$/mg ACTM
Reaction time	2 h	16 h	4 h	8 h	1 h
pH	Independent of pH	1.5	3	8.3	3 - 4
Catalyst	-	Iron (Fe^{+2})	Copper (Cu^+)	$NaHCO_3$	oxygen deficient $CuFe_2O_4$
ACTM Degradation (%)	99 %	> 99 %	> 99 %	> 50 %	91 %
Experimental mixture system	ACTM + KO_2 /IL/AcN system	ACTM + Fe-fortified, ZVAl*/H^+/air system	ACTM + (zero-valent copper) ZVC/air system	ACTM + PS/bicarbonate system	ACTM + oxygen deficient $CuFe_2O_4$/ PS system
Main ROSs degrading ACTM	Superoxide anion radical ($O_2^{\bullet-}$)	Hydroxyl radical ($^{\bullet}OH$)	Hydroxyl radical ($^{\bullet}OH$)	Peroxymono-carbonate (HCO_4^-)	Sulfate radical ($SO_4^{\bullet-}$), hydroxyl radical ($^{\bullet}OH$)

*ZVAl: Zero-valent Aluminium; *ZVC: Zero-valent Copper; *PS: Persulfate

4.3.3 Effect of composition of binary system (IL/ApS)

Ionic liquids (ILs) are mixed with other solvents to make binary mixtures for several reasons, for example, to (i) lower the viscosity for improved processability, (ii) increase solubility of non-polar substances, (iii) achieve specific physical properties (e.g., boiling point, volatility), (iv) enhance the selectivity of chemical reactions, and (v) reduce the cost of using pure ILs, are a few to mention. By combining ILs with other solvents, the desired properties can be obtained while minimizing any undesirable characteristics of either component. A series of parallel reactions were conducted using [BTEAmm$^+$][TFSI$^-$]/AcN and [EMIm$^+$][TFSI$^-$]/AcN mixtures at different concentrations of these ILs, to comprehensively evaluate the degradation performance in binary system media. The effect

of increasing the volume ratio of ILs in a binary mixture system was estimated by keeping the molar ratio of KO_2 constant; in addition, to discern the effect with better certitude this influence was verified at two different (constant) molar ratios (Tables 4.9 and 4.10). While varying the amount (volume %) of ILs in such binary mixture systems with aprotic solvent, it is noticeable to observe a change in the degradation percentage of ACTM, as shown in Figure 4.18. As a general trend while altering the fractions of both ammonium and imidazolium-based ILs, a mutual pattern can be identified for the degradation of ACTM, such that initially the values for degradation percentage decreases as the percent volume of IL increases from 0 vol.% to 30 vol.% in the binary mixture, and then subsequently increases as the amount of IL further increases from 50 vol.% to 100 vol.% (Figure 4.18).

Table 4.9: The degradation (%) of ACTM by $O_2^{\bullet-}$ in binary mixtures containing AcN and ILs (AcN + x vol.% IL).

Constitution of binary mixtures of ILs in AcN (v/v% IL)	Degradation of ACTM in AcN + x vol.% [BTEAmm$^+$][TFSI$^-$] (%)		Degradation of ACTM in AcN + x vol.% [EMIm$^+$][TFSI$^-$] (%)	
	Molar ratio of KO_2/API		Molar ratio of KO_2/API	
	20	40	20	40
5	67.0	81.8	56.5	75.7
10	61.5	81.6	52.4	70.9
20	35.4	73.3	34.5	38.3
30	36.7	71.0	23.4	34.5
50	67.5	77.1	43.7	49.8
70	56.5	80.4	36.5	48.6
80	64.6	82.2	36.5	48.0
90	79.1	95.9	44.1	50.8
100 (Pure IL)	78.8	94.1	61.7	63.4

Table 4.10: The degradation (%) of ACTM by O₂•⁻ in pure AcN.

Constitution of reaction medium	Degradation percentage of ACTM in AcN	
	Molar ratio of KO₂/API	
	20	**40**
Pure AcN	81.4	86.7
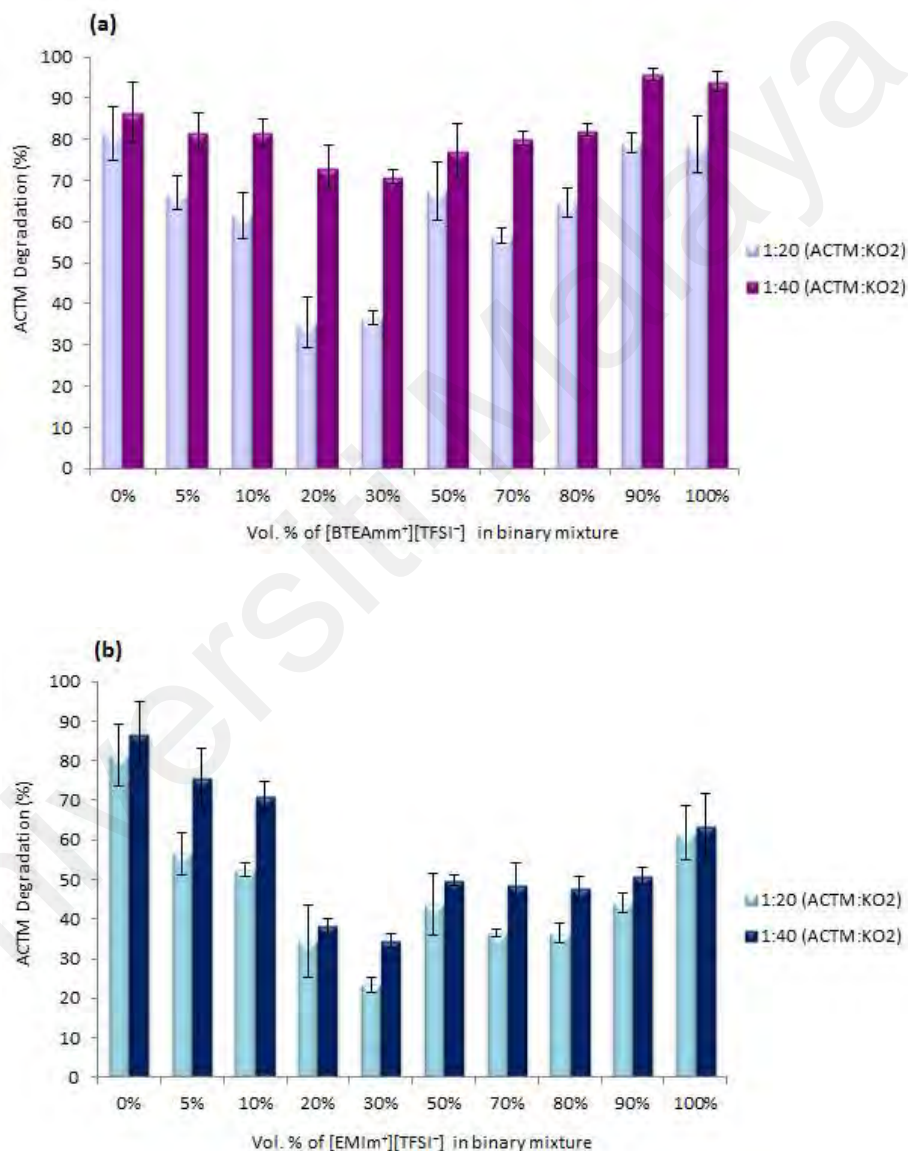
Figure 4.18: Effect of the amount (volume %) of ILs (a) [BTEAmm⁺][TFSI⁻] and (b) [EMIm⁺][TFSI⁻] in the binary mixture (IL/AcN) on degradation (%) of ACTM after reaction with the O₂•⁻ at two (constant) molar ratios of KO₂, at RT.

The gradual addition of IL (5 vol.% to 30 vol.%) in the binary mixture system gives rise to a considerably distinct decrease in the percentage degradation of the drug. It has been reported frequently that (i) neat ILs comprise strong ion pairs (Fraser et al., 2007; Tokuda et al., 2006; Yokozeki et al., 2007); (ii) aprotic, polar solvents, such as AcN when combined with an electrolyte, predominantly serve to solvate cations (rather than anions which have a lesser probability) (Fawcett et al., 2005; Hanke et al., 2002); and (iii) cations of the ILs play a significant role in stabilization of $O_2^{\bullet-}$, depending on the nature and amount of cations present (Hayyan et al., 2015a; Hayyan et al., 2012a; Hayyan et al., 2012b). Based on these facts, it is speculated that the addition of AcN to [BTEAmm$^+$][TFSI$^-$] and [EMIm$^+$][TFSI$^-$] would result in further dissociation of these ILs to produce more solvated [BTEAmm$^+$] and [EMIm$^+$] cations along with "free" [TFSI$^-$] anions. This view is also evidenced by Xu et al., where they demonstrated the preferential solvation of cations of the ILs by the aprotic solvents and applied it for the enhancement of cellulose dissolution (Xu et al., 2013).

The solvation of cations leading to high disposal of free anions in IL/AcN systems as compared to the respective pure ILs herein has been verified experimentally by measuring the conductivity values for [BTEAmm$^+$][TFSI$^-$], [EMIm$^+$][TFSI$^-$], and their respective binary mixtures with ApS (5 vol.% IL/AcN). The relative conductivity measurements (Table 4.11) have revealed that electrical conductivity of the ILs upon the addition of AcN has increased by more than 85% for ammonium-based IL, while for the imidazolium-based IL, the value for conductivity has improved by about 38%. This serves as evidence supporting the probable release of [TFSI$^-$] anions in the binary mixture system. These results are also coherent with recent work based on the effect of AcN as an additive on the ionic conductivity of imidazolium-based IL electrolyte (Rofika et al., 2019), and with the detailed simulation

studies conducted by Chaban et al. on conductivity enhancement of various imidazolium-based ILs when mixed with AcN as one of the binary components (Chaban et al., 2012).

Table 4.11: Conductivity measurements of pure [BTEAmm$^+$][TFSI$^-$], [EMIm$^+$][TFSI$^-$] and the respective binary mixtures (5 vol.% IL) with AcN.

Medium composition	Conductivity (mS cm^{-1})
[BTEAmm$^+$][TFSI$^-$]	0.14
5 vol.% [BTEAmm$^+$][TFSI$^-$]/AcN	0.95
[EMIm$^+$][TFSI$^-$]	0.78
5 vol.% [EMIm$^+$][TFSI$^-$]/AcN	1.27

The comparatively elevated degradation percentage in pure AcN (0 vol.% IL) strongly indicates estimable stability of $O_2^{\bullet-}$ in this aprotic solvent. This has also been explicitly reported by Gibian and co-workers that AcN is inert toward $O_2^{\bullet-}$, hence it effectively stabilizes the radical anion after its generation from KO_2 salt to make it well available for oxidation of ACTM. However, AcN is highly reactive toward the basic decomposition products of $O_2^{\bullet-}$ (Gibian et al., 1979). Although the nature of such decomposition products is vague, there is an ample probability of the rapid formation of HO_2^- (hydroperoxyl anion) species via Eq. (4.19). The proton (H^+) in this reaction to generate $HO_2^{\bullet}$ (hydroperoxyl radical) is derived either from the solvent (or electrolyte in case of electrochemical studies) or from the trace impurities. Typically proposed by small amounts of HO_2^- which sufficiently contributes to the slow rates that are perceived as $O_2^{\bullet-}$ disappearance, the disproportionation of $O_2^{\bullet-}$ species without acid catalysis is at large exceptionally slow (< 0.3 M^{-1} s^{-1}) (McClune & Fee, 1976).

$$O_2^{\bullet-} + HO_2^{\bullet} \rightarrow O_2 + HO_2^- \tag{4.19}$$

Nevertheless, presumably the decomposition of $O_2^{\bullet-}$ (Eq. (4.19)) generates a base (B^-) which is quite adequately basic to produce AcN anion (Eq. (4.20)). This species may further undergo condensation reaction with ACTM (Eq. (4.21)), followed by oxidation of the condensation product (or its anion) to a ketone, as represented in Eq. (4.22). However, such oxidation of organic compounds utilizing KO_2 is reported to be slow (Gibian et al., 1979).

$$B^- + CH_3CN \leftrightharpoons BH + {}^-CH_2CN \tag{4.20}$$

$$\underset{\displaystyle HOC_6H_4NHCH}{\overset{\displaystyle \overset{O}{\parallel}}{}} + {}^-CH_2CN \rightarrow \underset{\displaystyle HOC_6H_4NHCHCH_2CN}{\overset{\displaystyle \overset{O^-}{|}}{}} \tag{4.21}$$

$$\underset{\displaystyle HOC_6H_4NHCHCH_2CN}{\overset{\displaystyle \overset{O^-}{|}}{}} + O_2^{\bullet-} \rightarrow \underset{\displaystyle HOC_6H_4NHCCH_2CN}{\overset{\displaystyle \overset{O}{\parallel}}{}} \tag{4.22}$$
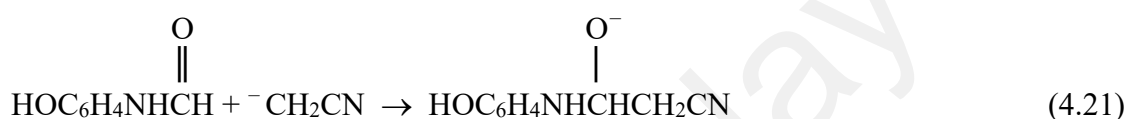
As a minor path, apparently, this referential route of AcN reaction in the presence of KO_2 is also partly contributing toward the possible slight increase of ACTM removal in the reaction mixture besides the main course of degradation of the drug caused by $O_2^{\bullet-}$, which alleviates the overall loss of ACTM in pure AcN. The ionic conductivity is primarily correlated with the composition of ionic clusters. Large volumes of AcN collapse the greater ionic clusters, hence resulting in the solvation of the ion pairs. With the aim of increasing the ionic motion in ILs, water or several organic solvents can be used as co-solvents (Tshibangu et al., 2011). The electrostatic forces such as intermolecular and ion-molecular interactions are likely to assist the ion pair dissociations, resulting in enhanced ionic mobility. Several pure ILs and their binary mixtures with water have been studied extensively for their

electrical conductivity (Castiglione et al., 2009; Ramírez et al., 2010; Takamuku et al., 2009; Zhou et al., 2008). The drastic increase in conductivity by the addition of AcN to ILs is reasoned by an accelerated ionic mobility in a way, such that the resultant conductivities have merely a slight dependence left on the shape, mass, and size of the cation (Borodin et al., 2010; Galiński et al., 2006). Given that, the decrease in the magnitude of degradation of ACTM appearing, as the amount of IL goes up from 5 vol.% to 30 vol.% can be attributed to the formation of ion-pairing of the respective cations of ILs which are solvated by AcN. The increasing volume of ILs results in more such cations pairing/associating with the $O_2^{\bullet-}$, leading to a lesser amount of this radical anion available for in-situ degradation of the drug which could take place in the reaction medium. In these cases, the unnecessary cationic consumption of $O_2^{\bullet-}$ induced the inhibitory effect on the mainstream oxidation process.

Conversely, amidst the pictorial illustration representing the variation in degradation percentage of ACTM (Figure 4.18), a gradual increase in the extent of degradation is evident while the volume of IL increases from 50 vol.% to 100 vol.%. This is highly suggestive of the estimated and much likely stability of the $O_2^{\bullet-}$ which is enhanced as the concentration of IL cations greatly increases. The equal or larger volumes of ILs in the binary systems have comparatively a greater number of cations available to play a role in sufficiently stabilizing the $O_2^{\bullet-}$, which in turn allows better degradation of ACTM in the respective reaction media.

Proclaiming more specifically however, the resultant degradation is all the more better in effect precisely for binary mixtures containing [BTEAmm$^+$][TFSI$^-$], since the stability of $O_2^{\bullet-}$ is reliant not just on quantity but also on the nature of cations comprising the ILs (see Section 4.2.1). [BTEAmm$^+$][TFSI$^-$] being an aliphatic IL, has lesser susceptibility to becoming confined with $O_2^{\bullet-}$, and thus serves to greatly improve its stability, more so, when present in high concentrations in the binary mixture. Thereupon, the values for degradation

percentage which are decreasing while going from 5 vol.% to 30 vol.% are marginally lower in magnitude when compared to the increasing values of ACTM degradation (%) while reaching from 50 vol.% till 100 vol.% on the other end of the graph, in the case of binary mixtures prepared with [BTEAmm$^+$][TFSI$^-$]. To be precise, the degradation values achieved at the extremities of the graphical illustration (Fig. 4.18a) i.e., for 5 vol.% and 10 vol.% ammonium-based IL are 81.8% and 81.6% respectively, while for 90 vol.% and 100 vol.% the degradation percentages are 95.9% and 94.1%, respectively. Hence, an overall percentage of ACTM degradation seemed to increase as the concentration of IL in binary mixtures comprising [BTEAmm$^+$][TFSI$^-$]/AcN increased, making the phenomenon directly proportional.

On the contrary, an inverse relationship between the concentration of IL and the degradation of ACTM is observed for the imidazolium-based IL. A general decrease in the extent of drug degradation is peculiarly apparent as the volume percent of IL in binary mixtures containing [EMIm$^+$][TFSI$^-$]/AcN is increased. Along the fringes of the bar chart (Fig. 4.18b), the specific values for degradation percentage for 5 vol.%, 10 vol.%, 90 vol.% and 100 vol.% imidazolium-based IL are 75.7%, 70.9%, 50.8%, and 63.4% respectively. Clearly, the former two values for percentage degradation are of higher magnitude than the latter ones, revealing that the increase in IL volume ratio leads to an overall decrease in ACTM loss. This inversely proportional development of pattern in the instance where the binary mixture system is comprised of [EMIm$^+$][TFSI$^-$] can be strongly ascribed to the nature of imidazolium cations in the IL. The aromatic cations in ILs are known to possess acidic characteristics and are consequently more prone to initiate proton-like effects, thus predisposing these to a reaction with $O_2^{\bullet-}$ leading to a production of imidazolones (Al-Nashef et al., 2010b; Hayyan et al., 2013). Wherefore, the more reactive imidazolium cations have

lesser involvement in maintaining the stability of $O_2^{\bullet-}$, compared to the ammonium cations which are non-reactive, and thus might play a part in supporting the $O_2^{\bullet-}$ stability. The data for the percentage of degradation in pure [BTEAmm$^+$][TFSI$^-$] (100 vol.%) indicated that $O_2^{\bullet-}$ did not undergo a fundamental reaction with the ammonium cations.

Notably, the spike which is discernable at 90 vol.% [BTEAmm$^+$][TFSI$^-$]/AcN system (Fig. 4.18a) is quite indicative of its association with the viscosity of binary mixtures. A slightly higher degree of ACTM degradation is seen in 90 vol.% [BTEAmm$^+$][TFSI$^-$]/AcN, i.e., 96%, as compared to 94% resulting from neat (100 vol.%) [BTEAmm$^+$][TFSI$^-$]. A plausible explanation for this result might be attributable to the fact that the addition of AcN to [BTEAmm$^+$][TFSI$^-$] caused a decrease in the viscosity of the reaction medium. Pure ILs are exceedingly viscous, typically having a viscosity of more than 50 mPa s at ambient temperature. As a result, these demonstrate very low self-diffusion, ca. 0.1×10^{-9} m^2/s (Noda et al., 2001). Ammonium-based ILs are documented to have rather high values of viscosity, for example, the viscosities of butyltrimethylammonium bis(trifluoromethylsulfonyl)imide and tributylmethylammonium bis(trifluoromethylsulfonyl)imide are 105.2 and 538.9 mPa s respectively, at 25 °C (Bhattacharjee et al., 2014). In that context, AcN is an appropriate aprotic solvent as it has a low shear viscosity, i.e., 0.34 mPa s and a fairly high diffusion coefficient of 4.3×10^{-9} m^2/s. Hence, AcN profoundly improves diffusion and reduces the viscosity of ILs/AcN binary mixture systems (Chaban et al., 2012). Subsequently with polar ILs, the dipole-dipole interactions in pure AcN tend to drive its structure and dynamics which is a predicting factor for adequate miscibility. Therefore, the use of AcN in conjunction with [BTEAmm$^+$][TFSI$^-$] is likely to reduce the viscosity of the binary system altogether, which assists in accelerating the dissolution rate of superoxide salt. The more facilitated diffusion and dissolution of the reactants thereby leads to better degradation of ACTM. Essentially,

the interrelation of various physical properties helps comprehend and alter the targeted performance of materials. Such practice of exploiting the advantages of a mixture of IL with another solvent is also in agreement with a recent work where the relatively high viscosity of IL was reduced manifold by adding some amount of organic solvents, like ethylene carbonate and propylene carbonate, for "thinning" purpose (Quan et al., 2019). The resultant IL-based electrolytes proved to be useful in improving the safety problems related to Li/Na ion batteries.

The degradation of three different APIs, i.e., acetaminophen (ACTM), riluzole (RLZ) and carbamazepine (CBM) was monitored in parallel reactions conducted in three identically structured ammonium-based ILs ([BTEAmm$^+$][TFSI$^-$], [PTEAmm$^+$][TFSI$^-$] and [OTEAmm$^+$][TFSI$^-$]), differing only in the length of the attached alkyl chain. The ILs were used in varying concentrations in a binary mixture with acetonitrile. The preceding experiments using various IL/ApS volume ratios in the binary system demonstrated that either the highest IL ratio (90%) or those on the rather lower side, e.g., 10 volumes % in the mixture served as the most effective or optimal percentages for improved API degradation efficiencies. Therefore, the subsequent in situ degradation was carried out in these volume ratios of ILs, with the performance compared to the neat ILs. Figures 4.19, 4.20 and 4.21 illustrate the change in degradation of ACTM, RLZ and CBM, respectively, using different volume ratios of the three ILs for each API.
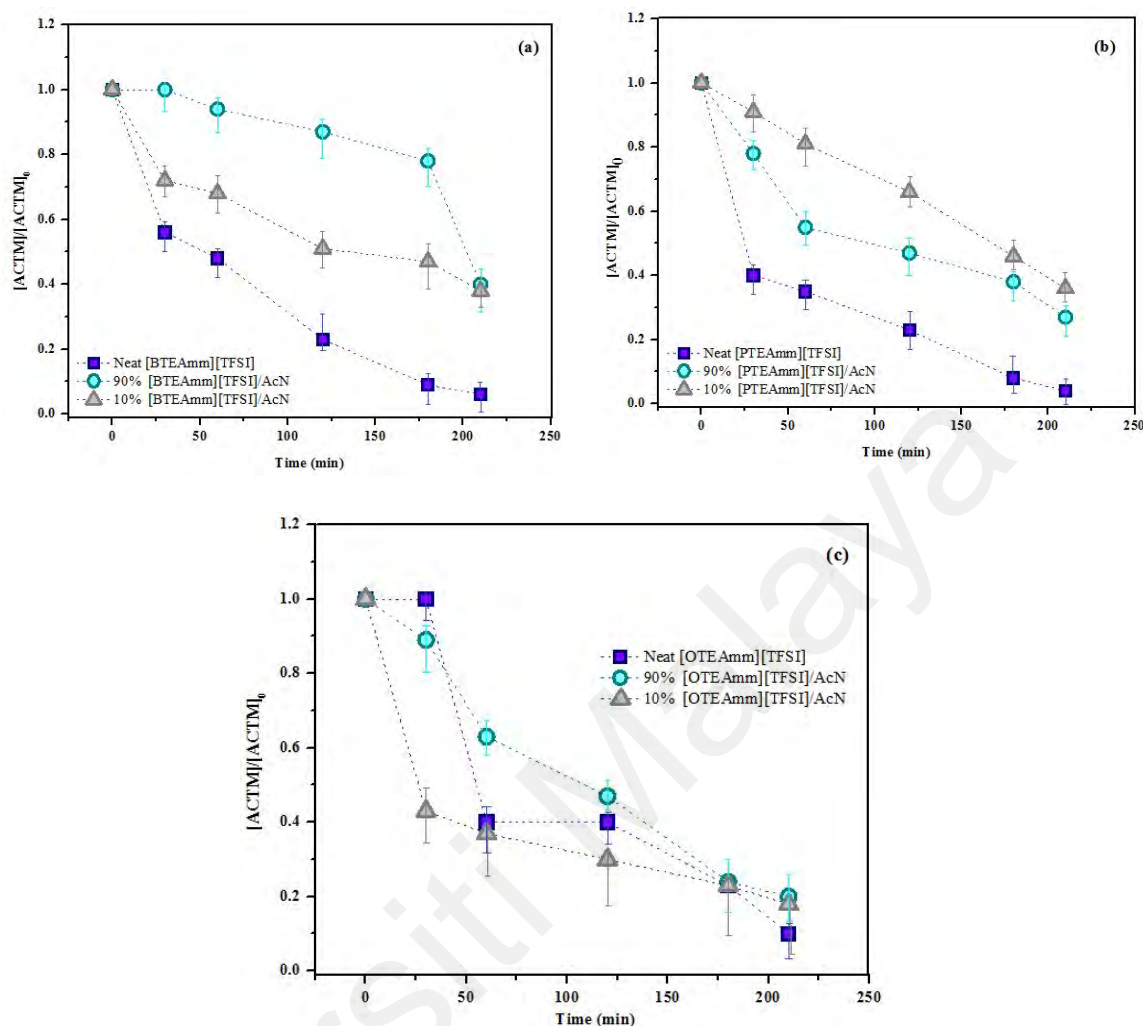
Figure 4.19: Effect of the amount (volume%) of ILs (a) [BTEAmm⁺][TFSI⁻], (b) [PTEAmm⁺][TFSI⁻] and (c) [OTEAmm⁺][TFSI⁻] in the binary mixture (IL/AcN) on the degradation of ACTM after reaction with the $O_2^{\bullet-}$, at RT.

Since the degradation of an API is exclusively dependent on its structure, each of the investigated drug substances exhibited an effective degradation pattern in different ratios of ILs present in the binary mixture system with acetonitrile as the aprotic solvent. Fig. 4.19 shows the highest ACTM degradation was acquired in the neat ILs in the case of all three ILs with varying alkyl chain lengths. In the instance where the target compound was RLZ, the IL volume ratio attaining the highest degradation varies with the modifying alkyl chain length.

For example, in the event of butyl side-chain present on the IL cation, the degradation of RLZ was almost comparable both in neat and 10 vol.% [BTEAmm$^+$][TFSI$^-$] (Fig. 4.20a). This extent of RLZ degradation went slightly lower with IL having pentyl side-chain, but still the highest magnitude was observed in neat [PTEAmm$^+$][TFSI$^-$] (Fig. 4.20b), while on the other hand the IL cation with an 8C-alkyl chain demonstrated the lowest degradation of all the three ILs, with the highest degradation achieved in 90% [OTEAmm$^+$][TFSI$^-$]/AcN binary mixture, as depicted in Figure 4.20c.
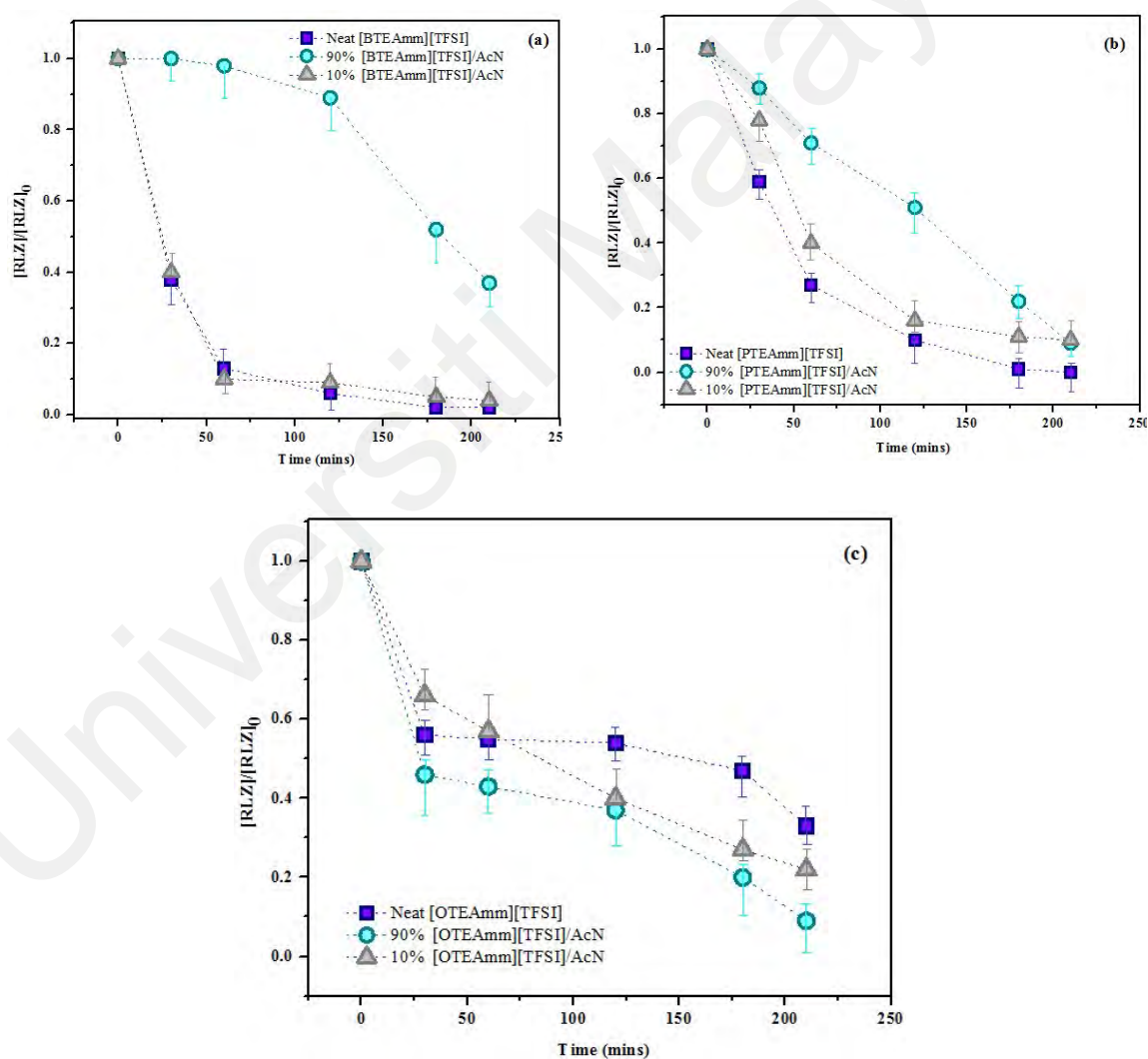
Figure 4.20: Effect of the amount (volume%) of ILs (a) [BTEAmm$^+$][TFSI$^-$], (b) [PTEAmm$^+$][TFSI$^-$] and (c) [OTEAmm$^+$][TFSI$^-$] in the binary mixture (IL/AcN) on the degradation of RLZ after reaction with the O$_2$$^{\bullet-}$, at RT.

Figure 4.21: Effect of the amount (volume%) of ILs (a) [BTEAmm$^+$][TFSI$^-$], (b) [PTEAmm$^+$][TFSI$^-$] and (c) [OTEAmm$^+$][TFSI$^-$] in the binary mixture (IL/AcN) on the degradation of CBM after reaction with the O$_2$$^{\bullet-}$, at RT.
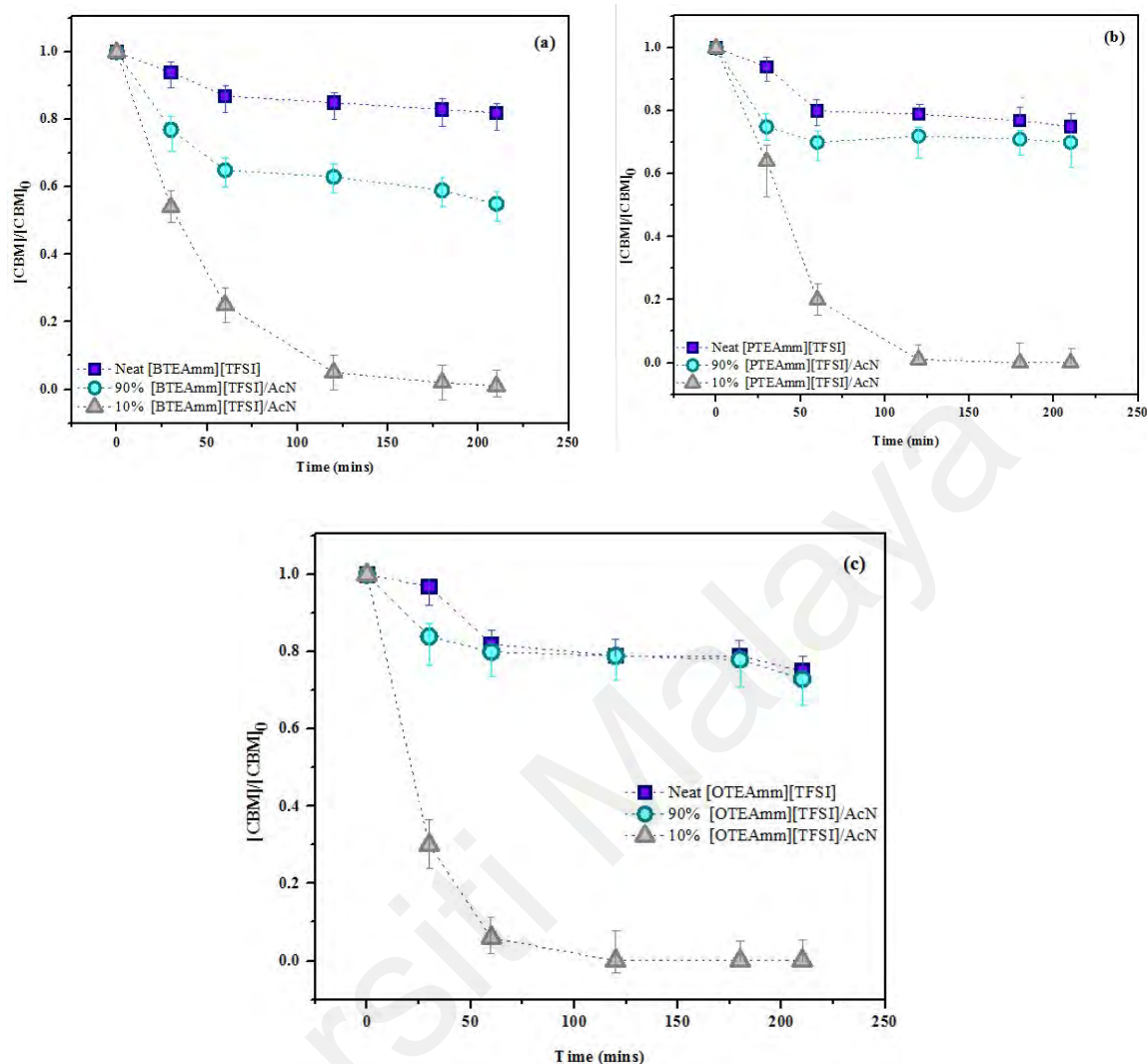
In the case where CBM was subject to the oxidative degradation with O$_2$$^{\bullet-}$ in the binary mixtures as stabilizing media for its generation, the influence of the ratio of ILs is presented in Figure 4.21. It was established that the highest degradation efficiency was exhibited using the 10 vol.% of ILs in binary systems with ILs consisting of all three alkyl (butyl, pentyl and octyl) side chain lengths on the cation. Moreover, the neat ILs and even the 90 vol.% of ILs were not observed to deliver a complete degradation of CBM. This phenomenon was

149

markedly a consequence of increased solubility of the large-sized drug molecule in the lesser IL concentrations contained in the binary reaction media. Table 4.12 presents a comparative evaluation of this work with several studies in the literature on CBM degradation in terms of the efficiency of the process, contributive ROS, experimental systems, and reaction conditions utilized. It can be observed that in comparison with some recent reports, complete degradation can be achieved using rather simpler conditions and experimental setups, utilizing economical and sustainable materials which further elaborates on the effectiveness of the superoxide salt /IL/AcN process.

Table 4.12: Comparison of experimental conditions, reaction systems and degradation efficiencies between this work and other studies in literature for oxidative degradation of CBM.

System and Conditions	This work	(Liu et al., 2016a)	(Ghasemian et al., 2017)	(Zhao et al., 2023)	(Martínez et al., 2011)
Oxidant/ catalyst/ radiation/ CBM dosage	15.05 mg KO_2/mg API, IL/AcN mixture, [CBM] = 100 mg/L	50 mmol H_2O_2/ 2.63 kGy^{-1}, [CBM] = 75 mg/L	UV irradiation, Sb-doped Sn80%-W20%-oxide coated anode, Applied current density = 6 mA/cm^2, [CBM] = 0.2 mg/L	Visible light radiation, MOF/Bi4O7 S-scheme heterojunction (MIL-68(In)-NH_2/Bi4O7 S-scheme system), photocatalyst dosage: 1.0 g/L [CBM] = 50 mg/L	UV irradiation, TiO_2 P25 = 0.5 g/L, composites of 10-MWCNT:anatase, and ZnO, 5 mmol H_2O_2 or 50% v/v O_2, [CBM] = 8 mg/L
Reaction time	2 h	-	1 h	2 h	1 h
Catalyst	-	H_2O_2	Sb-doped Sn80%-W20%-oxide coated electrodes	Photocatalyst	ZnO suspensions
CBM degradation	100%	95%	100%	92.7%	100%
Experimental system	Superoxide salt /IL/AcN system	Ionizing radiolysis/ H_2O_2 system	Photo-electrocatalytic system	Photoelectrochemical system	Photocatalytic system
Contributive ROS	$O_2^{\bullet-}$	$^{\bullet}OH$, e_{aq}^{-} and $H^{\bullet}$	$^{\bullet}OH$	$^{\bullet}OH$, $O_2^{\bullet-}$ and h^+	$^{\bullet}OH$ and h^+

4.3.4   Effect of initial concentration of the APIs

To investigate the influence of initial concentrations of the APIs employed for degradation, a varying amount of 0.5 mg, 1.0 mg, and 2.0 mg, each of ACTM, CBM and RLZ were used in analogous reactions. These experiments were conducted in otherwise identical operating conditions, i.e., using 10% v/v [BTEAmm$^+$][TFSI$^-$]/AcN composition of the binary medium, by means of ~15 mg of KO_2 at room temperature. Figure 4.22

demonstrates the effect of initial concentrations (0.5 mg, 1.0 mg, and 2.0 mg) used on the degradation of these APIs after reaction with the $O_2^{\bullet-}$.
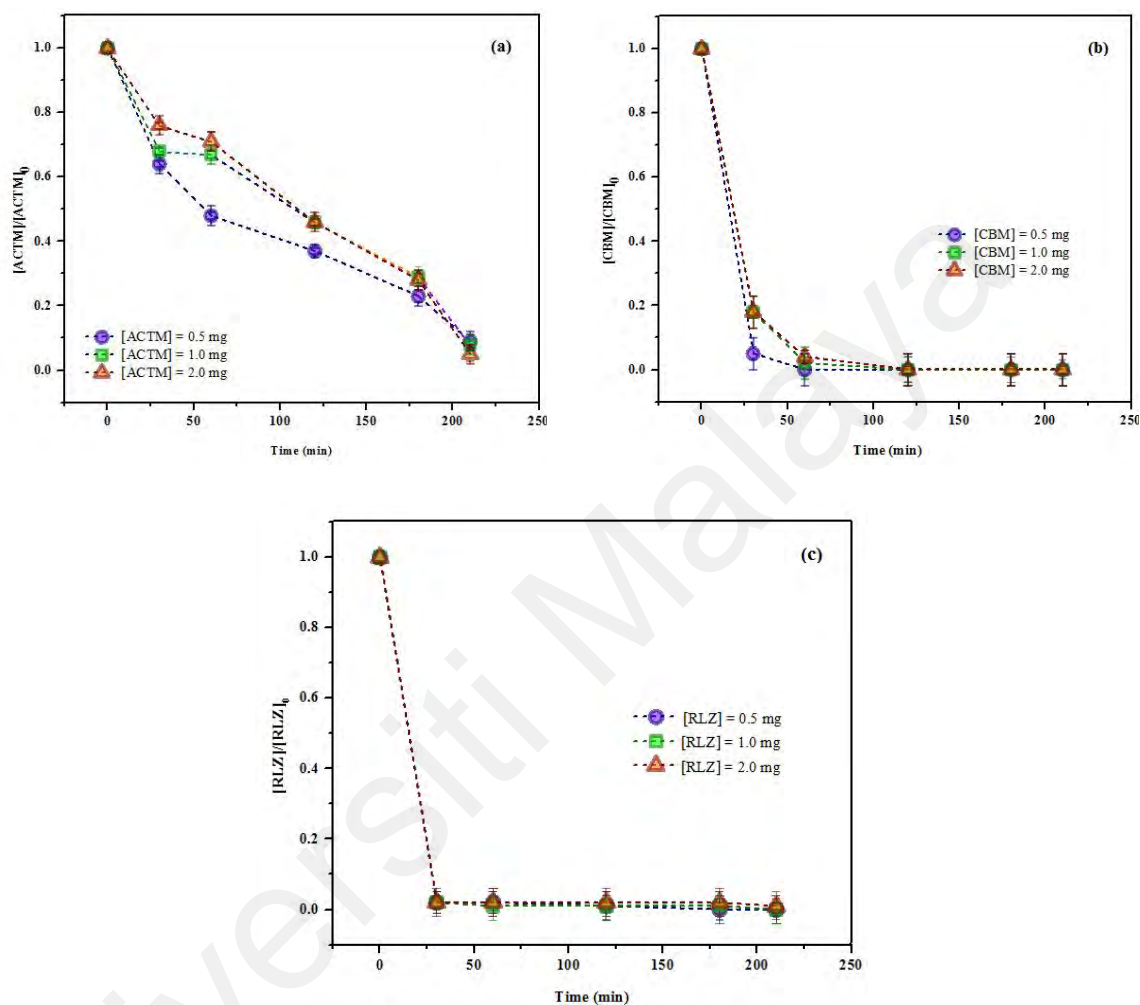
Figure 4.22: Effect of initial concentrations (0.5 mg, 1.0 mg, and 2.0 mg) of the APIs used on the degradation of (a) ACTM, (b) CBM and (c) RLZ after reaction with the $O_2^{\bullet-}$ (Experimental conditions: 10% [BTEAmm$^+$][TFSI$^-$]/AcN binary mixture composition, [KO$_2$] = 15 mg.

Quite interestingly, the increase in the amount of each drug compound used initially in the successive experiments under comparable conditions exhibited a distinct pattern. In the case of ACTM, as the concentration is increased from 0.5 mg to 1.0 mg and 2.0 mg, the degradation took place more gradually with the higher amounts of API as compared to that

observed with 0.5 mg. However, the extent of degradation eventually achieved after 210 mins was highest while using 2.0 mg concentration of ACTM.

While monitoring the same trend for degradation of CBM, it was simultaneously observed that its complete degradation was attained more abruptly, i.e., within 120 min. In comparison to that, RLZ reflected the most rapid decline in its concentration as compared to ACTM and CBM and demonstrated a complete degradation within 60 mins of reaction time with each amount of API used initially.

This difference in the time taken for the complete degradation to occur among these drugs can be ascribed to the extent of stability which accompanies each of these compounds. ACTM among these possess a more stable structure as compared to the other two, and hence the degradation of ACTM was observed to be gradual and took more time. In comparison with that the 7-membered ring of CBM is less stable and is thus more vulnerable to attack by the reactive oxidant species. Therefore, as soon as the middle ring in the structure of CBM is oxidized it quickly gets converted into its transformation products and a more rapid degradation is seen to occur in that case. Whereas in the instance of RLZ also, the structure comprises several susceptible sites like benzothiazole moiety, amine and trifluoromethoxy ($-OCF_3$) groups which are readily available and multiple positions for the attack by $O_2^{\bullet-}$, subsequently resulting in a comparatively abrupt decline in the concentration of RLZ because of a quick transformation of the parent compound into degradation products.

Table 4.13 lists the experimental systems, reaction conditions and process efficiencies with the study carried out by Bensalah and coworkers (Bensalah et al., 2023) since not many investigations have reported the degradation of RLZ. The major advantage of the KO_2

/IL/AcN system over the heterogeneous Fenton oxidation is the simplicity and sustainability of the process, along with the increased efficiency in the approach.

Table 4.13: Comparison of experimental conditions, reaction systems and degradation efficiencies between this work and other studies in literature for oxidative degradation of RLZ.

System and Conditions	This work	(Bensalah et al., 2023)
Oxidant/catalyst/RLZ dosage	15.2 mg KO_2/mg API, IL/AcN mixture, [RLZ] = 100 mg/L	Heterogeneous natural Fe-based catalyst = 200 mg/L/ Fe^{2+} = 140 mg/L / H_2O_2 = 1000 mg/L / pH = 3.0 / UV irradiation / [RLZ] = 23.4 mg/L
Reaction time	120 min	360 min
pH	-	pH range 3 –12
Catalyst	-	Hematite-rich (α-Fe_2O_3) and magnetite (Fe_3O_4)
RLZ degradation	100 %	100 %
Experimental system	Superoxide salt /IL/AcN system	Heterogeneous Fenton oxidation system
Contributive ROS	$O_2^{\bullet -}$	$^{\bullet}OH$ and $HO_2^{\bullet}$

4.3.5　Effect of temperature

The effect of temperature on the degradation of ACTM is demonstrated in Table 4.14. It can be observed that the percentage degradation for the drug in binary mixtures with both ILs, [BTEAmm$^+$][TFSI$^-$]/AcN and [EMIm$^+$][TFSI$^-$]/AcN was considerably improved. This can be ascribed to the increased solubility of KO_2 in the reaction media, which in turn results in greater $O_2^{\bullet -}$ availability for the reaction causing degradation of drug molecules.

Table 4.14: The degradation (%) of ACTM by $O_2^{\bullet-}$ (KO₂/ACTM molar ratio 20) in binary mixture system.

Temperature (°C)	Degradation of ACTM (%)	
	[BTEAmm⁺][TFSI⁻]/AcN	[EMIm⁺][TFSI⁻]/AcN
RT	67.0	56.5
40	67.8	57.9
50	69.2	60.5
60	77.9	65.7
70	86.6	74.2

The degradation of ACTM in the binary mixture with [BTEAmm⁺][TFSI⁻]/AcN was only 67% at RT, most likely due to the lower solubility of KO₂. However, the degradation process was boosted and the percentage was increased to 86.6% degradation after the temperature was increased to 70 °C. Likewise at 70 °C, 74.2% of ACTM degradation was accomplished using the binary mixture with [EMIm⁺][TFSI⁻]/AcN, while only 56.5% was achieved by the same binary system at RT. The gradual rise in this percentage degradation with the increase in temperature markedly determines that temperature is a significant factor influencing the oxidation process. These outcomes are also in compliance with the work directed by Hayyan et al. comprising oxidative desulfurization of thiophene and 2-methylthiophene using $O_2^{\bullet-}$ chemically generated in neat ILs. It has been reported in the study that elevated temperatures affect the conversion of sulfur compounds, and an increased temperature improves the conversion percentage against the value obtained at room temperature; the extent of conversion being dependent on the nature of IL utilized (Hayyan et al., 2015a). At higher temperatures the degradation process is evidently assisted as it is expected to effectively accelerate the dissolution rate of superoxide salts, subsequently resulting in higher amounts

of the dissolved oxidant. The increased temperature also alleviates the degradation reaction to take place by causing a greater number of molecular collisions between $O_2^{\bullet-}$ and the API. In due course, at 70 °C the degradation of ACTM improved to 86.6% and 74.2% in 10 vol.% of [BTEAmm$^+$][TFSI$^-$]/AcN and 10 vol.% [EMIm$^+$][TFSI$^-$]/AcN, respectively, at a ratio of 1:20 ACTM:KO$_2$.

At a similar molar ratio of KO$_2$ with CBM and RLZ, the change in percentage degradation of these drug compounds was also investigated in a binary system consisting of 10% [BTEAmm$^+$][TFSI$^-$]/AcN (Table 4.15). The obtained values also depict that a slight increase in the temperature of the media would lead to a lesser amount of oxidant that is required for the degradation of APIs. Table 4.15 accrues the calculated degradation percentages for ACTM, CBM and RLZ via the KO$_2$/IL/AcN system under different operational parameters.

Table 4.15: Calculated degradation percentages for ACTM, CBM and RLZ via KO$_2$/IL/AcN system under different operational parameters.

Factors	Variations	Conditions (Constant)	% Degradation		
			ACTM	CBM	RLZ
KO$_2$ molar ratio/API	10	10% [BTEAmm$^+$][TFSI$^-$]/AcN [API] = 100 mg/L Temperature = 25 °C	61.6	64.6	62
	20		67	65.2	63.5
	30		72.5	77.9	72.9
	40		81.8	83.7	84
	45		98.8	98.9	95.8
	50		98.7	99.1	96.3
	55		98.9	99.7	96.9
IL(cation): AcN ratio	100 % [BTEAmm$^+$][TFSI$^-$]	KO$_2$ molar ratio/API = 50 [API] = 100 mg/L Temperature = 25 °C	94.2	18.7	98.3
	100 % [PTEAmm$^+$][TFSI$^-$]		96.5	25.2	99.9
	100 % [OTEAmm$^+$][TFSI$^-$]		90.9	25.9	67.7
	90% [BTEAmm$^+$][TFSI$^-$]		60.1	45.4	63.9
	90% [PTEAmm$^+$][TFSI$^-$]		73.8	30.1	91.8
	90% [OTEAmm$^+$][TFSI$^-$]		80.2	27.5	91.9
	10% [BTEAmm$^+$][TFSI$^-$]		62.5	99.1	96.3
	10% [PTEAmm$^+$][TFSI$^-$]		64.2	99.8	90.4
	10% [OTEAmm$^+$][TFSI$^-$]		82.7	99.9	78.9
Initial API concentration	50 mg/L	10% [BTEAmm$^+$][TFSI$^-$]/AcN KO$_2$ molar ratio/API = 50 Temperature = 25 °C	91.9	99.8	100
	100 mg/L		92.1	99.9	100
	200 mg/L		95.6	100	99.9
Temperature	RT	KO$_2$ molar ratio/API = 20 [API] = 100 mg/L 10% [BTEAmm$^+$][TFSI$^-$]/AcN	67	72.1	70.9
	40		67.8	77.6	82.1
	50		69.2	79.8	86.4
	60		77.9	87.9	88.2
	70		86.6	90.1	95.6

4.4 Recycling and Reuse of ILs

The physical appearances and water content of both the ammonium and imidazolium-based recycled ILs obtained from the first and the fifth cycles were compared. As presented in Table 4.16 with the first and fifth recycled ionic liquids (RILs), the appearance of the RIL recycled five times (5th RIL) was similar to that of the fresh ones. However, the water content of the RILs slightly increased as the number of cycles increased. As the ILs used were hydrophobic in nature, it was possible to regenerate these by washing them with water. This

aspect further contemplates the sustainability of the process, as no volatile organic solvents are needed for the extraction/recycling step. [BTEAmm$^+$][TFSI$^-$] and [EMIm$^+$][TFSI$^-$] utilized herein were effectively recycled and reused five times for ACTM degradation, demonstrating that these ILs have exceptional reusability.

Table 4.16: The physical appearances and water content of RILs.

IL Samples		Appearance	Content %	
			IL	H$_2$O
[BTEAmm$^+$][TFSI$^-$]	Fresh IL	Colorless/transparent	99.99	0.01
	1st RIL	Colorless/transparent	99.95	0.05
	5th RIL	Colorless/transparent	99.94	0.06
[EMIm$^+$][TFSI$^-$]	Fresh IL	Colorless/transparent	99.98	0.02
	1st RIL	Colorless/transparent	99.93	0.07
	5th RIL	Colorless/transparent	99.92	0.08
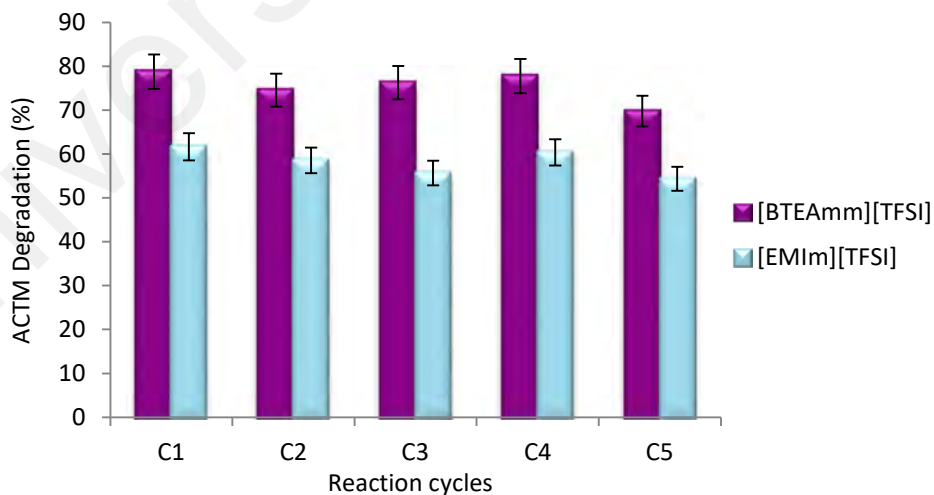
Figure 4.23: Degradation percentages of ACTM obtained after reaction in fresh (C1) and recycled ILs (C2, C3, C3 and C4).

The purity of the recycled ILs was confirmed using FTIR and ^{1}H NMR spectroscopic techniques. The FTIR and ^{1}H NMR analyses of the recycled ILs indicated no variations in their spectra when compared to the fresh ones (Figures 4.24, 4.25, 4.26, and 4.27), hence signifying that the recovered versions can be potentially reused as a medium for the degradation of ACTM. The RILs from the reaction mixture were then used for the next cycle of degradation exhibiting comparable results to that of the fresh ones (Figure 4.23).

4.4.1 FTIR Spectra of RILs

The IR spectra of the fresh ILs (FILs) and RILs from the first and fifth cycles were characterized and compared (Figures 4.24 and 4.25). All the absorbance peaks of the RILs were consistent with the respective FILs. As no new peaks were observed, it could be inferred that no byproducts were generated. The comparison of spectra indicates high purity as the structure of the RILs remained unchanged. The main IR absorption frequencies for [BTEAmm$^+$][TFSI$^-$] and [EMIm$^+$][TFSI$^-$] are presented in Tables 4.17 and 4.18.

In the spectra of [BTEAmm$^+$][TFSI$^-$], the strong bands at the frequency range $1410-1380$ cm^{-1} and $1100-1000$ cm^{-1} can be ascribed to S=O and C$-$F stretching vibrations, respectively. The medium intensity peak at $1250-1020$ cm^{-1} indicates the presence of C$-$N bond of the ammonium cation. The stretching and bending motions of the C$-$H bonds of alkyl chains are observed in the ranges $3000-2840$ cm^{-1} and $1390-1380$ cm^{-1}. A medium peak at 1460 cm^{-1} is characteristic of the C$-$H bending of the methyl groups.

Table 4.17: Characteristic Infrared absorption frequencies for [BTEAmm⁺][TFSI⁻].

Bond/Functional group	Vibrational motion	Observed frequency for [BTEAmm⁺][TFSI⁻] (cm⁻¹)
C−H (alkane)	stretching	2969
C−H (methyl group)	bending	1460
C−H (alkane)	bending	1397
S=O (sulfonyl group)	stretching	1346, 1329
C−N (amine)	stretching	1175, 1133
C−F (fluoro group)	stretching	1051

Figure 4.24: FTIR spectra of [BTEAmm⁺][TFSI⁻] (FIL and RILs) used for degradation of ACTM. (1- FIL; 2- 1st RIL; 3- 5th RIL).

The distinct absorbance peaks of [EMIm⁺][TFSI⁻] were observed at 1574 cm⁻¹ for C=C stretching of cyclic alkene, and at 3124 cm⁻¹ for C−H stretching of alkene, which is perceived in the range 3100 − 3000 cm⁻¹. A weak absorption band exhibited in the range 3000 − 2840 cm⁻¹ can be assigned to C−H bond stretching, while a peak at 1455 cm⁻¹ to C-H bending of

160

the methyl groups. The prominent peaks in the range $1250 - 1020 \text{ cm}^{-1}$ are characteristic of C−N bond stretching in the ammonium group. The [TFSI⁻] anion was characterized mainly by the presence of strong peaks in the regions $1410 - 1380 \text{ cm}^{-1}$ and $1100 - 1000 \text{ cm}^{-1}$, attributed to S=O and C−F vibrations respectively.

Table 4.18: Characteristic Infrared absorption frequencies for [EMIm⁺][TFSI⁻] (cm⁻¹).

Bond/Functional group	Vibrational motion	Observed frequency for [EMIm⁺][TFSI⁻] (cm⁻¹)
C−H (alkene)	stretching	3124
C−H (alkane)	stretching	2988
C=C (cyclic alkene)	stretching	1574
C−H (methyl group)	bending	1455
S=O (sulfonyl group)	stretching	1346, 1328
C−N (amine)	stretching	1167, 1132
C−F (fluoro group)	stretching	1051

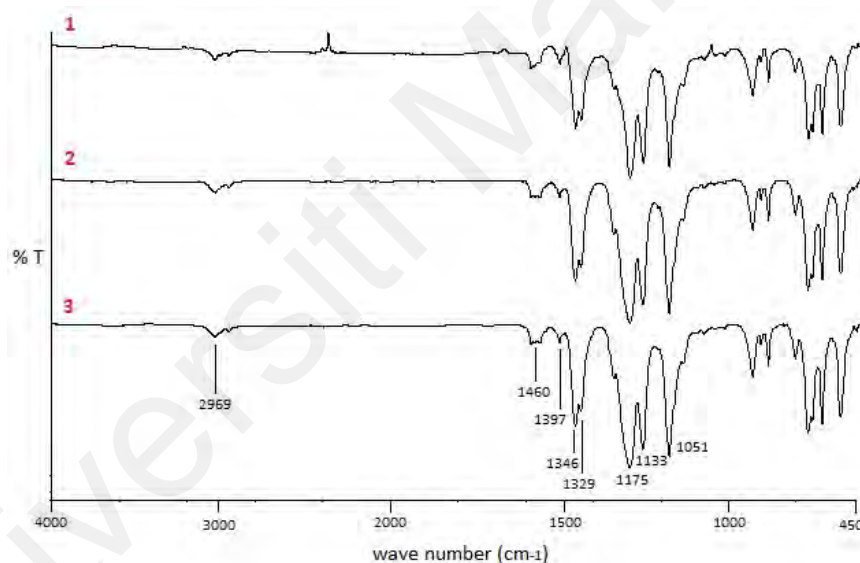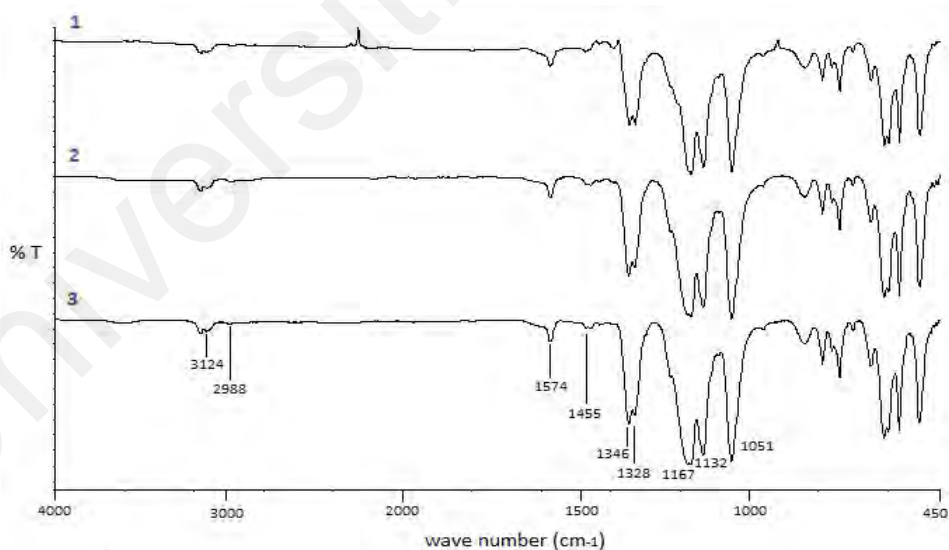**Figure 4.25: FTIR spectra of [EMIm⁺][TFSI⁻] (FIL and RILs) used for degradation of ACTM. (1- FIL; 2- 1st RIL; 3- 5th RIL).**

4.4.2 Proton NMR Spectra of RILs

The purity of the RILs was also confirmed via ^{1}H NMR spectroscopy while comparing with the spectra of fresh ones (Figure 4.26 and 4.27). The ^{1}H NMR spectra of the RILs from the first and fifth cycles (Spectra 2 and 3) were consistent with the ones obtained from fresh ILs. Since no new peaks were generated due to any byproducts in the ^{1}H NMR spectra of RILs, it was established that these can be recovered with purity equivalent to the fresh ones. Figure 4.28 shows the peaks assigned to the protons in each cation molecule of the ILs. The ^{1}H NMR data for [BTEAmm$^+$][TFSI$^-$] is presented in Table 4.19. The assigned chemical shifts well correspond to the structure of the cation which is indicative of good purity. The spectra have multiplets in the upfield region for methyl protons (primary) in the range 1 − 1.35 ppm. The signals for secondary methyl protons are observed as multiplets which are relatively downfield in the range 1.38 − 1.72 ppm, and even more downfield in the range 3.14 − 3.36 ppm are the protons of methyl groups adjacent to the ammonium cation center. The singlet observed at 4.78 ppm corresponds to the presence of deuterated methanol (MeOD).

Table 4.19: ^{1}H NMR spectral data for [BTEAmm$^+$][TFSI$^-$].

Chemical shifts assignments	
Type of protons	δ (ppm)
CH$_3$	1.00-1.06 (3H)
CH$_3$	1.26-1.32 (9H)
CH$_2$	1.38-1.48 (2H)
CH$_2$	1.62-1.72 (6H)
CH$_2$	3.14-3.20 (2H)
CH$_2$	3.28-3.36 (2H)
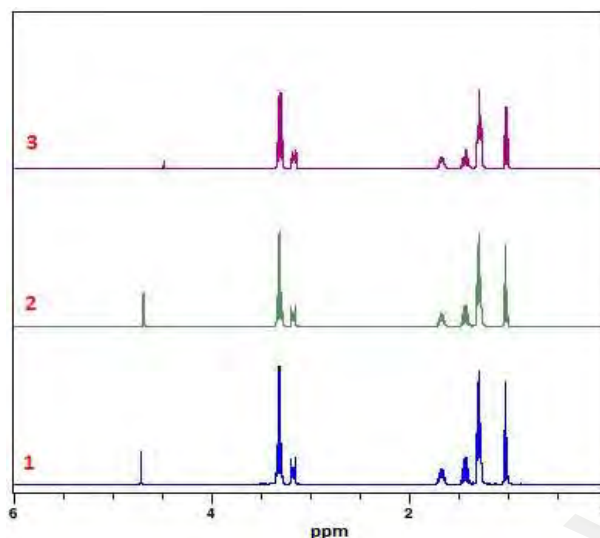
Figure 4.26: ^{1}H NMR spectra of [BTEAmm$^+$][TFSI$^-$] (FIL and RILs) used for the degradation of ACTM. (1- FIL; 2- 1st RIL; 3- 5th RIL).

The ^{1}H NMR data for [EMIm$^+$][TFSI$^-$] is presented in Table 4.20. The structure of imidazolium cation can be precisely resolved from the chemical shift signals in the spectrum. A triplet for primary methyl group protons is observed upfield at 1.5 ppm. Due to being adjacent to the nitrogen atom of ammonium, the methyl (primary) protons show a downfield signal in the form of a singlet at 3.9 ppm. A quartet of secondary methyl protons is present at 4.3 ppm, while the protons on three tertiary carbon atoms in the imidazolium ring are observed downfield at 7.4, 7.6 and 8.8 ppm. The deuterated methanol (MeOD) shows a singlet at 4.78 ppm.

Table 4.20: ^{1}H NMR spectral data for [EMIm$^+$][TFSI$^-$].

| Chemical shifts assignments	
Type of protons	δ (ppm)
CH$_3$	1.5 (3H)
CH$_3$	3.9 (3H)
CH$_2$	4.3 (2H)
CH	7.4 (1H)
CH	7.6 (1H)
CH	8.8 (1H)
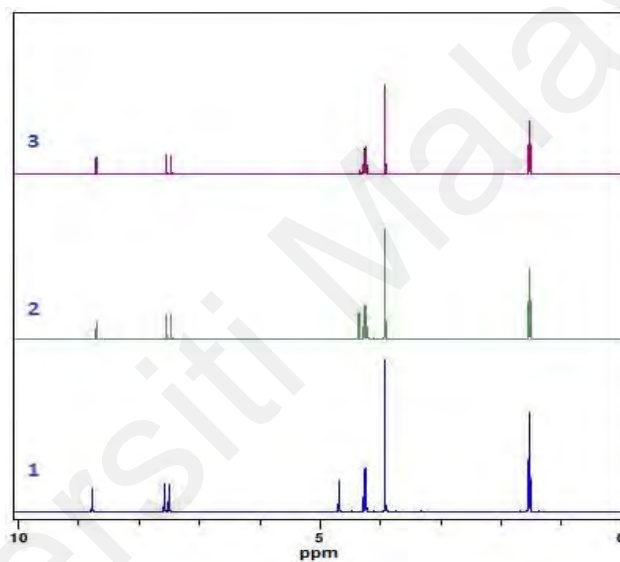
Figure 4.27: ^{1}H NMR spectra of [EMIm$^+$][TFSI$^-$] (FIL and RILs) used for the degradation of ACTM (1- FIL; 2- 1st RIL; 3- 5th RIL).
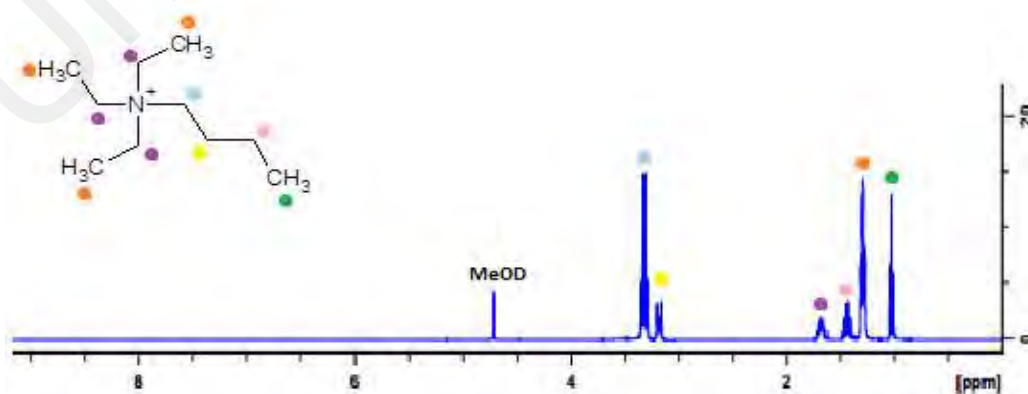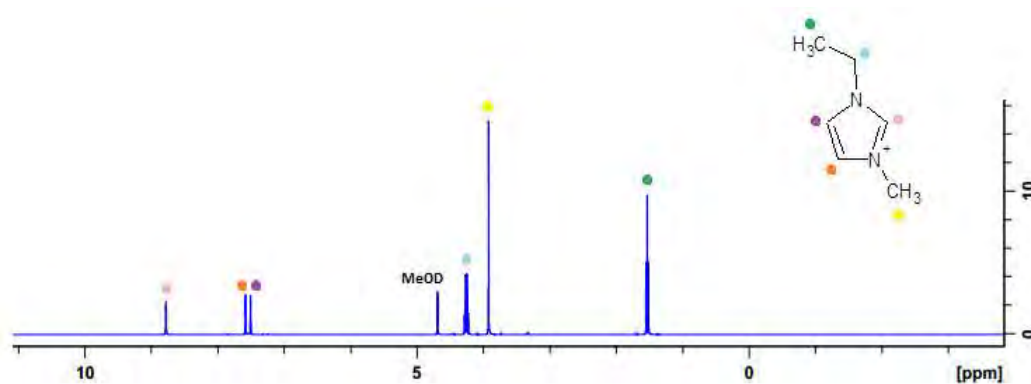
Figure 4.28: ¹H NMR of [BTEAmm⁺][TFSI⁻] (top) and [EMIm⁺][TFSI⁻] (bottom).

4.5   TOC Removal Efficiency

The TOC removal efficiency was evaluated and compared in different reaction media used for ACTM degradation. Figure 4.29 shows the extent of total mineralization of ACTM after treatment under the same (optimum) conditions using various compositions of the IL/AcN mixtures at RT. Although some mineralization did take place in the reaction set up in pure AcN (without any IL), it is evident from the TOC values obtained that the more the amount of IL was used in the binary mixture, the more mineralization was achieved. Moreover, the type of IL used also affected the removal of TOC attained; [BTEAmm⁺][TFSI⁻] allows more mineralization as compared to [EMIm⁺][TFSI⁻]. The graph also indicates that a small addition (5%) of [EMIm⁺][TFSI⁻] in effect gives a higher value of TOC as compared to the medium with no IL (pure AcN). This is also in accordance with the results acquired for the long-term stability of $O_2^{\bullet-}$ in the presence of these ILs and the influence of the nature of ILs on the degradation of ACTM, as discussed in prior sections.
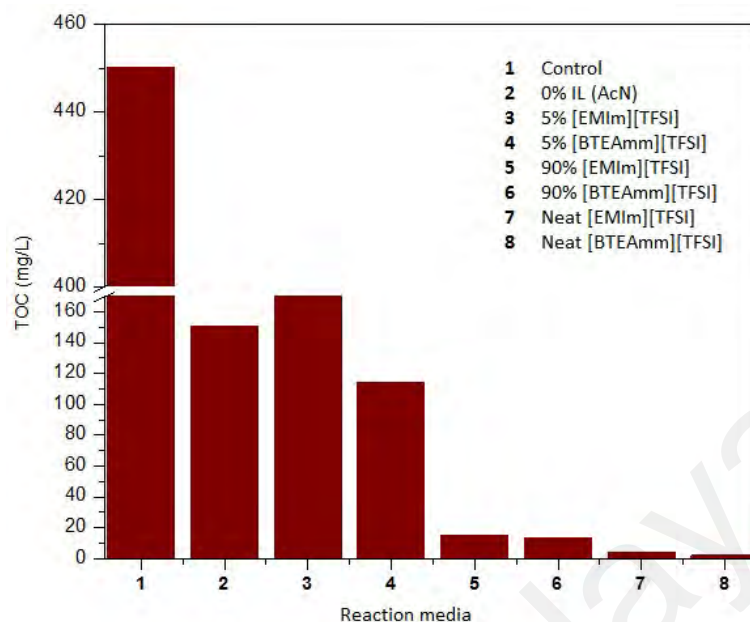
Figure 4.29: Total mineralization of ACTM after treatment using different reaction media (KO₂/ACTM molar ratio 50 at RT).

The percentage of TOC removal is highlighted in Table 4.21 which seems to be greatly dependent on the amount of IL utilized. As the volume percent ratio of $[BTEAmm^+][TFSI^-]$ increases from 5% to 90% and 100%, the TOC decay as well increases by the same extent i.e., 74.6%, 97%, and 99.5%, respectively. Likewise, an increase in the concentration of $[EMIm^+][TFSI^-]$ tends to increase the TOC removal percentage although lesser in extent compared to values achieved with the former IL. These outcomes infer that the degradation process of employing $O_2^{\bullet-}$ stably generated in IL media is effectively mineralizing ACTM to innocuous substances. Skoumal et al. (Skoumal et al., 2006) also demonstrated the comparative TOC removal with direct ozonation and for the O_3/UVA system. The former system yielded a slow and progressive mineralization reaching up to 39% in 4 h, while using the latter resulted in more rapid pollutant degradation and a final TOC reduction of 96% was reported. Similarly, the catalytic activity of a mesoporous composite ($CoFe_2O_4/mpg-C_3N_4$, CF/MCN) for mineralization of ACTM evaluated by peroxymonosulfate (PMS) activation through the generation of $SO_4^{\bullet-}$ revealed a removal efficiency of 92.6%, which was superior

166

when compared to other conventional metal oxides (Co_3O_4, Fe_3O_4, and CuO) (Hassani et al., 2020).

Table 4.21: Percentage removal of TOC in different compositions of reaction media after treatment of ACTM under optimum conditions.

Reaction media	v/v ratio of IL in AcN	TOC removal (%)
[BTEAmm$^+$][TFSI$^-$]	5%	74.6
	90%	97
	100% (neat)	99.5
[EMIm$^+$][TFSI$^-$]	5%	61.4
	90%	96.6
	100% (neat)	99
Pure AcN	0%	66.5

The evaluation of TOC removal efficiency of ACTM, RLZ and CBM in pure [BTEAmm$^+$][TFSI$^-$], [PTEAmm$^+$][TFSI$^-$] and [OTEAmm$^+$][TFSI$^-$] and in binary mixtures of these with AcN has been illustrated in Appendix A. For the sake of vivid comparison of the extent of total mineralization of the target pharmaceuticals, TOC values (mg/L) after treatment in different reaction media used for the in-situ degradation were plotted against neat ILs, and their 90% and 10% volume ratios in acetonitrile as binary mixtures. The total mineralization of ACTM was found to be highest in the 10% volume ratio in all three ILs utilized, i.e., in [BTEAmm$^+$][TFSI$^-$], [PTEAmm$^+$][TFSI$^-$] and [OTEAmm$^+$][TFSI$^-$], and the least while using neat ILs in each case. This can be rearticulated as the TOC removal after treatment of ACTM in 10% IL/AcN > 90% IL/AcN > neat IL. However, the oxidative degradation reactions of RLZ led to the maximum extent of TOC removal in 90% IL/AcN binary mixtures using [BTEAmm$^+$][TFSI$^-$], [PTEAmm$^+$][TFSI$^-$], as well as in [OTEAmm$^+$][TFSI$^-$]. The observed TOC was almost negligible after the treatment in these media, which proves it to be the most effective for RLZ removal. The volume ratio of 10%

IL/AcN media was also capable of reducing a good amount of TOC (dropping to ~20 mg/L compared to 400 mg/L in control). In neat ILs on the other hand, the total mineralization of this drug was not observed to be very significant (Appendix A2).

Contrariwise, the TOC removal after treating CBM was perceived as the highest in neat ILs with a maximum in [BTEAmm$^+$][TFSI$^-$] (Appendix A3). The order of total mineralization of CBM achieved in neat ILs was [BTEAmm$^+$][TFSI$^-$] > [PTEAmm$^+$][TFSI$^-$] > [OTEAmm$^+$][TFSI$^-$]. 10% [BTEAmm$^+$][TFSI$^-$]/AcN was also effective enough to reduce the amount of TOC significantly (~97.8% removal), although this removal percentage was much less in [PTEAmm$^+$][TFSI$^-$] and [OTEAmm$^+$][TFSI$^-$]. The outcomes of this analysis indicate that the catalytic role of IL in the media and also the effectiveness of its ratio in the binary mixture are highly dependent on the structure and polarities of the pharmaceutical compounds undergoing the degradation reactions.

4.6   Identification of Degradation Products of APIs
4.6.1   LC/MS analysis
4.6.1.1 Acetaminophen

The intermediates and byproducts detected by LCMS during the treatment of ACTM using different molar ratios of KO$_2$ in IL/AcN systems are summarized in Table 4.22.

Table 4.22: Transformation products and intermediates detected during degradation process of ACTM.

Compound	Chemical Formula
N-(2,4-dihydroxyphenyl)acetamide	$C_8H_9NO_3$
N-(formylmethyl)acetamide	$C_4H_7NO_2$
N-methylacetamide	C_3H_7NO
Butan-2-ol	$C_4H_{10}O$
Hydroquinone	$C_6H_6O_2$
4-aminophenol	C_6H_7NO
Butan-2-amine	$C_4H_{11}N$
Ethenamine	C_2H_5N
Acetamide	C_2H_5NO
Ethylamine	C_2H_7N
Propan-2-one	C_3H_6O
Acetic acid	$C_2H_4O_2$
Acetaldehyde	C_2H_4O

The aromatic intermediates such as hydroquinone and 4-aminophenol were detected at very short reaction times; moreover, under these conditions, the release of acetamide and acetaldehyde was also observed with the formation of hydroquinone and 4-aminophenol, respectively (Andreozzi et al., 2003). Similar oxidation products have been previously reported for ACTM degradation with various advanced oxidation systems (Andreozzi et al., 2003; Vogna et al., 2002). However, the aromatic intermediates were found to be converted to short carboxylic acids, aldehydes, and ketones, as expected from the oxidative destruction of the aryl moiety of the aromatic products. Figure 4.30 shows the MS spectra of oxidation products identified, such as propan-2-one, acetaldehyde, and acetic acid. These eventually convert to propane and CO_2 respectively, also supporting the results of TOC decay in optimum reaction media indicating complete mineralization of ACTM, which was also

accompanied by the conversion of its initial nitrogen to inorganic ions, such as NH_4^+ and NO_3^- (Skoumal et al., 2006). Such oxidation products have also been obtained as indicated in the current literature on ACTM degradation (Zhang et al., 2019a).
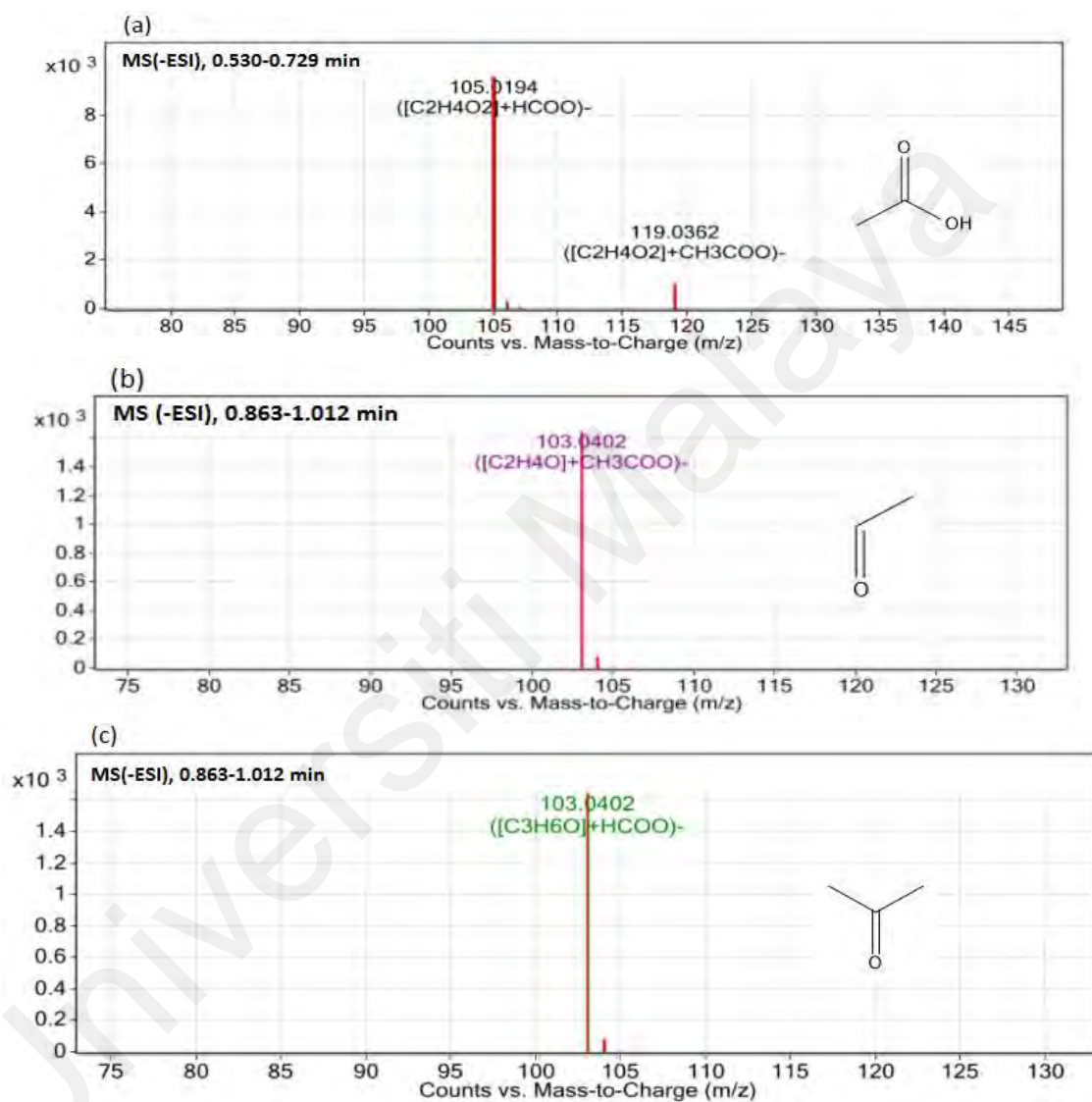
Figure 4.30: MS Spectra and the proposed structures of by-products identified in this study; (a) ([C2H4O2]+HCOO)− = 105 m/z, (b) ([C2H4O]+CH3COO)− = 103 m/z, and (c) ([C3H6O]+HCOO)− = 103 m/z.

4.6.1.2 Carbamazepine

The chemical formulae, structures, and molar masses (m/z) for the intermediate compounds and transformation products identified via LCMS upon treatment of CBM using the KO₂/IL/AcN system are listed in Table 4.23.

Table 4.23: Transformation products and intermediates detected during degradation process of CBM.
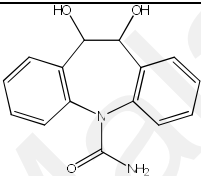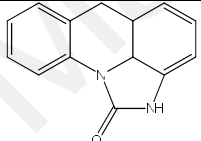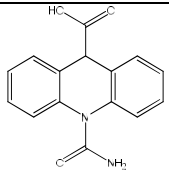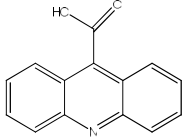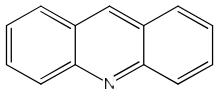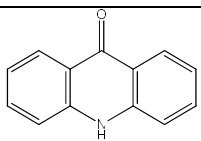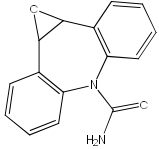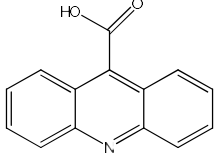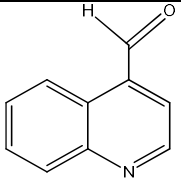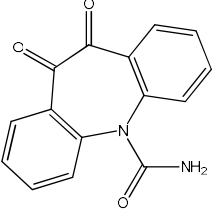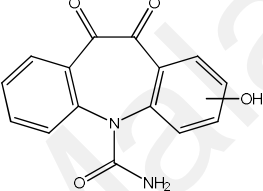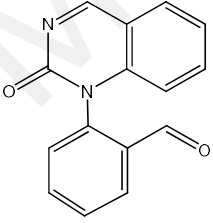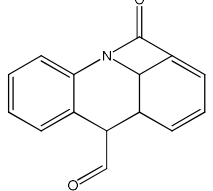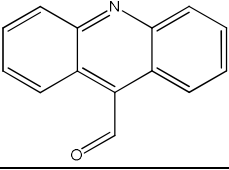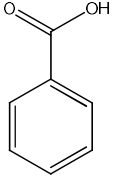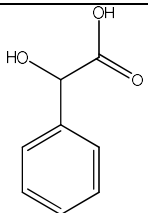
Product code	Chemical formula	Structure	m/z [M + H]⁺
P1	$C_{15}H_{14}N_2O_3$		271.04
P2	$C_{14}H_{12}N_2O$		223.76
P3	$C_{15}H_{12}N_2O_2$		251.04
P4	$C_{14}H_9NO_2$		200.13
P5	$C_{13}H_9N$		180.00
P6	$C_{13}H_9NO$		195.92
P7	$C_{15}H_{12}N_2O_2$		251.04
P8	$C_{14}H_9NO_2$		223.76

Table 4.23, Continued.

Product code	Chemical formula	Structure	m/z [M + H]$^+$
P9	$C_{10}H_7NO$		174.00
P10	$C_{15}H_{10}N_2O_3$		267.04
P11	$C_{16}H_{14}N_2O_4$		284.16
P12	$C_{15}H_{10}N_2O_2$		250.88
P13	$C_{15}H_{11}NO_2$		236.96
P14	$C_{14}H_9NO$		207.92
P15	$C_7H_6O_2$		120.88
P16	$C_8H_8O_3$		150.96

4.6.1.3   Riluzole

Several transformation products and intermediates enlisted in Table 4.24 were found to be generated and detected via LCMS-MS analysis for the first time after the degradation treatment of RLZ. The chemical formulae, structures and molar masses (m/z) of the identified compounds are also tabulated.

Table 4.24: Transformation products and intermediates detected during degradation process of RLZ.
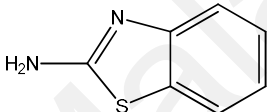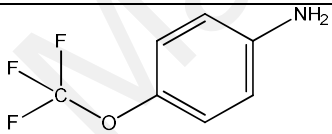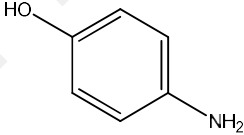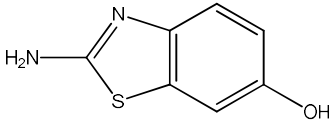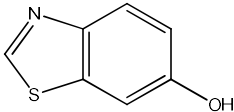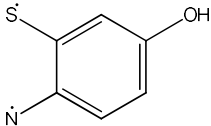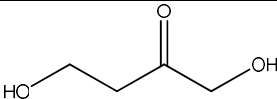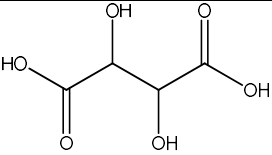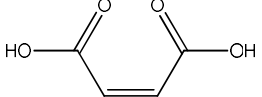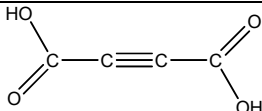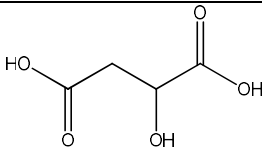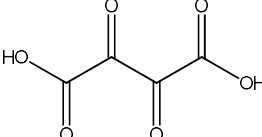
Product code	Chemical formula	Structure	m/z [M + H]$^+$
P1	$C_7H_6N_2S$		165.84
P2	$C_7H_6F_3NO$		178.88
P3	C_6H_7NO		112.64
P4	$C_7H_6N_2OS$		165.84
P5	C_7H_5NOS		151.92
P6	$C_6H_4NOS_2{}^\bullet$		138.88
P7	$C_4H_8O_3$		104.88
P8	$C_4H_6O_6$		151.92
P9	$C_4H_4O_4$		117.76

P10	C$_4$H$_2$O$_4$		114.08
P11	C$_4$H$_6$O$_5$		114.08
P12	C$_4$H$_2$O$_6$		133.95

4.6.2 Proposed reaction pathways for degradation reactions of APIs

4.6.3 Acetaminophen

A general reaction pathway for the degradation of ACTM by O$_2^{\bullet-}$ was proposed as presented in Scheme 4.1. The tentative pathway involves all intermediates which were detected via LCMS during degradation of ACTM. The process is initiated by the parallel attack of oxidant radicals either on the C(3)-position of ACTM yielding *N*-(2,4-dihydroxyphenyl) acetamide as a first proposed pathway (I), or on its C(4)-position producing hydroquinone with release of acetamide (Skoumal et al., 2006) as visible in pathway II (Scheme 4.1). As a consequence of the ring-opening of hydroquinone, 2-propanone and propane were released, while acetamide further degraded into ethylamine, subsequently mineralizing into ammonium (NH$_4^+$) and nitrate (NO$_3^-$) ions. Further, the attack of O$_2^{\bullet-}$ on the aromatic ring resulted in the transformation of *N*-(2,4-dihydroxyphenyl)acetamide to ring-opening products such as *N*-(formylmethyl)acetamide and butan-2-ol. *N*-(formylmethyl) acetamide further undergoes conversion into *N*-methylacetamide, which eventually transforms into simpler molecules, such as acetic acid and acetaldehyde. The aromatics which were identified, being the basic structures of ACTM,

suggested that its degradation was primarily caused by the attack of radicals on aromatic rings at the ortho and para positions. The progression of ring cleavage of aromatic oxidation products such as 4-aminophenol leads to the formation of butan-2-amine, ethenamine, acetaldehyde, acetic acid, and other small organics. The detected intermediates and degradation products were comparable to those determined in other studies on ACTM mineralization (Andreozzi et al., 2003; Vogna et al., 2002; Zhang et al., 2019a).
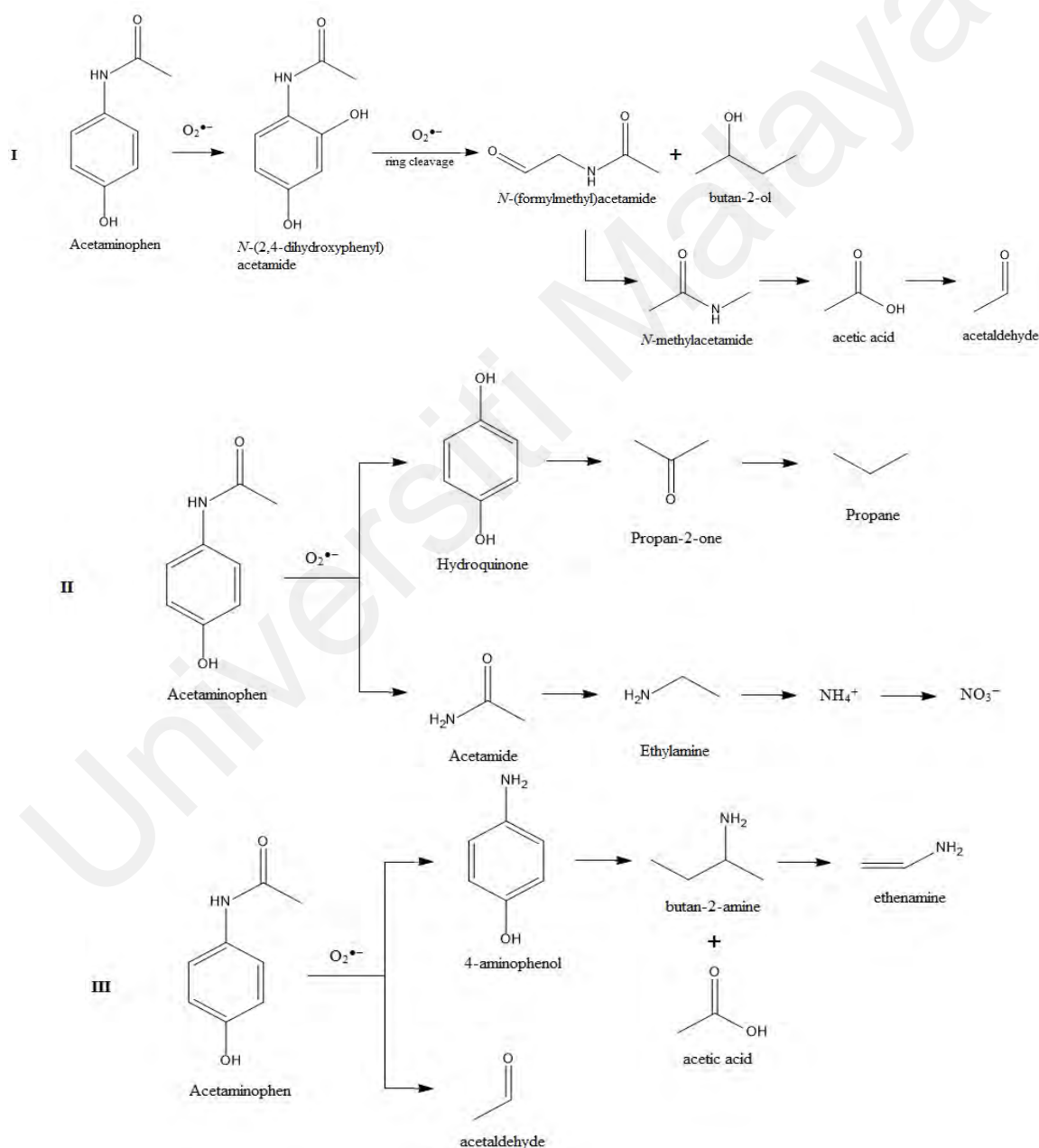
Scheme 4.1: Proposed reaction pathways for the degradation of ACTM by $O_2^{\bullet-}$.

4.6.3.1   Carbamazepine

Portraying upon the aforementioned experimental outcomes, some plausible mechanistic pathways for the degradation of carbamazepine are expounded in Scheme 4.2.
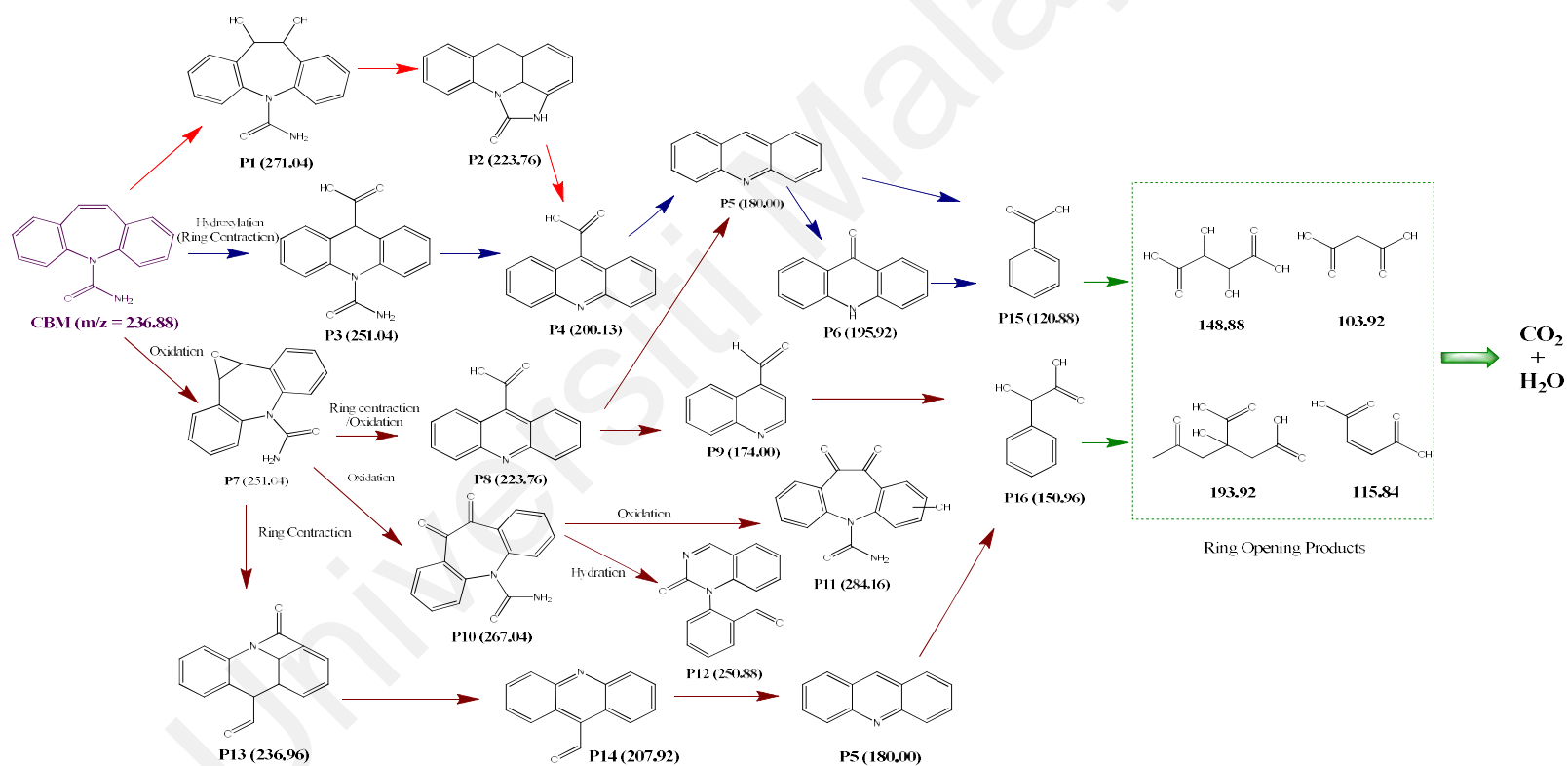
Scheme 4.2: Proposed reaction pathways for the degradation of CBM by $O_2^{\bullet-}$.

Based on LC-MS-MS analysis results, both CBM and its transformation products were detected, and possible mechanisms were proposed in Scheme 4.2. Firstly, the generated $O_2^{\bullet-}$ species converted CBM to P1 (m/z = 271.04 g/mol) and P2 (m/z = 223.76 g/mol) by attacking the olefinic double bond and the nitrogen respectively, present in the heterocyclic ring. These two compounds have also been identified by Ghasemian et al. (Ghasemian et al., 2017) and Calza et al. (Calza et al., 2012) respectively.

In addition, CBM could also be transformed to produce P3 (m/z = 251.04 g/mol) (Calza et al., 2012), P4 (m/z = 200.13 g/mol), P5 (m/z = 180.00 g/mol) (Ghasemian et al., 2017; Liu et al., 2016b; Martínez et al., 2011; Murgolo et al., 2019) and P6 (m/z = 195.92 g/mol) (Bessa et al., 2019; Ghasemian et al., 2017; Liu et al., 2016b) via hydroxylation leading to ring contraction products. Moreover, CBM could also undergo epoxidation to generate P7 (m/z = 251.04 g/mol), which has been reported by various recent studies on CBM degradation (Bessa et al., 2019; Ghasemian et al., 2017; Liu et al., 2016a; Martínez et al., 2011; Murgolo et al., 2019). P7 undergoes azepine heterocyclic ring contraction and cleavage of the amino group in further steps to yield P13 (m/z = 236.96 and P14 (m/z = 207.92 g/mol) and eventually transforms into P5 again. Simultaneously, ring contraction takes place as a result of cleavage and carboxylation of the amide group of P7 to produce P8 (m/z = 223.76 g/mol) (Liu et al., 2016b; Murgolo et al., 2019), which is further oxidized to P9 (m/z = 174.00 g/mol) (Franz et al., 2020) and P5.

In yet another pathway, P7 is subsequently converted to P10 (m/z = 267.04 g/mol) (Bessa et al., 2019; Ghasemian et al., 2017; Murgolo et al., 2019) and P11 (m/z = 284.16 g/mol) (Bessa et al., 2019) via oxidation and also yielded an intermediate product P12 (m/z = 250.88 g/mol) (Ghasemian et al., 2017; Murgolo et al., 2019) through hydration and intramolecular cyclization of P10. P5 was produced by the deketonization of P14 and also by the

177

decarboxylation of P8. Further, P5 was also found to be able to oxidize into P6. An eventual heterocyclic ring opening process resulted in the generation of P15 (m/z = 120.88 g/mol) and P16 (m/z = 150.96 g/mol) which are lower molecular mass carboxylic acids, such as benzoic acid and mandelic acid. Further degradation of these carboxylic acids and intermediates into smaller ring-opening compounds leads to an ultimate mineralization into CO_2, H_2O and NH_4^+.

4.6.3.2   Riluzole

A mechanistic reaction pathway based on the transformation products and intermediates yielded and identified after degradation of RLZ has been proposed for the first time, as illustrated in Scheme 4.3. The LCMS analysis reveals the formation of product P1 (m/z = 165.84) after the elimination of the −OCF$_3$ group, which is further converted to intermediate 4-(trifluoromethoxy) aniline (m/z = 178.88; P2) after the opening of the triazole ring. P2 is oxidized to another aromatic derivative, 4-aminophenol (m/z = 112.64; P3) as a result of the release of organic sulfur, fluorine, and nitrogen in the form of sulfate, fluoride and nitrate ions, respectively. The loss of fluorine also leads to the formation of P4 (m/z = 165.84) in a parallel pathway, and a further loss of an amine group yields P5 (m/z = 151.92). This is followed by the loss of a carbon atom opening the 5-membered ring moiety, thus producing P6 (m/z = 138.88).

Oxidation of these organics led to the formation of C4-carboxylic acids, e.g., hydroxybutanoic acid (P7; m/z = 104.88), tartaric acid (P8; m/z = 151.92), maleic acid (P9; m/z = 117.76), acetylenedicarboxylic acid (P10; m/z = 114.08), malic acid (P11; m/z = 114.08), and oxaloacetic acid (P12; m/z = 133.95) by means of oxidative opening of the benzene ring. The successive fragmentation of C4 carboxylic acids into C2 carboxylic acids leads to their eventual mineralization to CO_2 and H_2O. A few of these transformation

178

products, though not all, have been recently reported by Bensalah and coworkers (Bensalah et al., 2023); however, their detection was not via direct mass spectrometry.
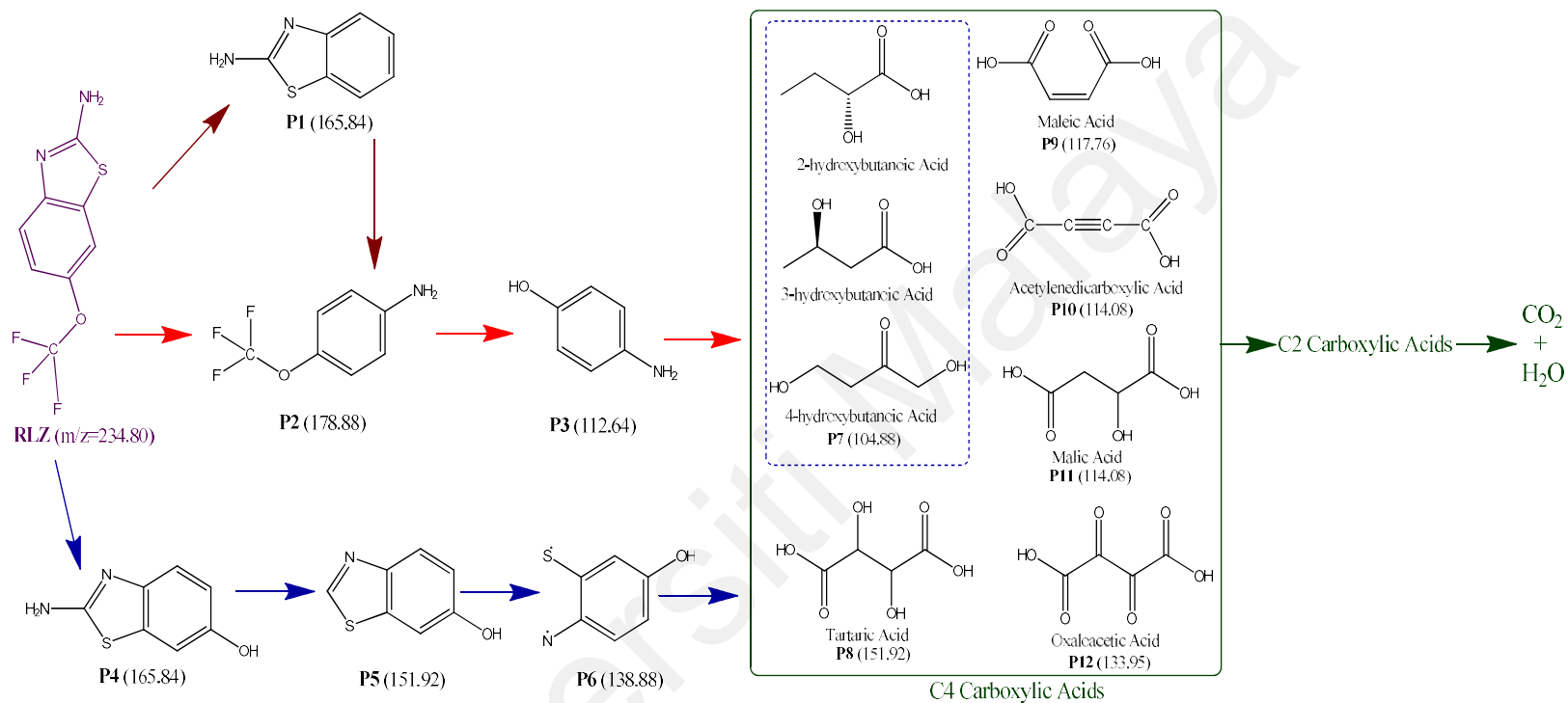
Scheme 4.3: Proposed reaction pathways for the degradation of RLZ by O₂•⁻.

The in-situ degradation of active pharmaceutical ingredients (APIs) was carried out using $O_2^{\bullet-}$, generated in binary IL/AcN mixture media using various ILs comprising different cations, i.e., [BTEAmm$^+$], [PTEAmm$^+$], [OTEAmm$^+$] and [EMIm$^+$] paired with [TFSI$^-$]. The results demonstrated that the KO$_2$/IL/AcN system was very effective for the oxidative degradation of pharmaceutical pollutants such as acetaminophen (ACTM), riluzole (RLZ) and carbamazepine (CBM) under mild conditions. When compared, the degradation percentage using the ammonium-based IL was greater than the imidazolium-based IL, owing to the more stable generation of $O_2^{\bullet-}$ in the former one which was ascertained by UV-visible spectrophotometric analysis. Moreover, the presence of $O_2^{\bullet-}$ in the utilized media was validated by electrochemical evidence using the cyclic voltammetry (CV) technique, which proved that $O_2^{\bullet-}$ was the principal radical species contributing towards degradation.

A simplistic and efficient method for degradation of pharmaceutical waste was devised using $O_2^{\bullet-}$ as an oxidant by investigating the influence of different factors such as the amount of oxidant, nature of cations in ILs, the ratio of IL:AcN (constituency of binary mixture), and the reaction temperature. The utilized ILs were recycled and reused in five cycles for degradation of ACTM with a potency comparable to the fresh ones. The purity of recovered ILs was also found to be analogous to the fresh ILs which was verified via FTIR and ^{1}H NMR spectroscopy; hence, establishing the green aspect of the formulated procedure. The results of TOC demonstrated the extent of mineralization in varied combinations of reaction media. LCMS-QToF as an eventual analysis identified 12 intermediates suggesting that after the aromatic ring cleavage reaction ACTM was converted to small molecule organics which could be further oxidized to CO_2, H_2O, propane, and inorganic ions such as NH_4^+ and NO_3^-. This finding anticipates opening up further prospects in the design of combinative solvent media for stable generation of $O_2^{\bullet-}$ as a promising agent for diverse implications. Stimulating

parallel studies, this investigation also proposes to set off further research while extending a new scenario for practical use of $O_2^{\bullet-}$ in the degradation of compounds belonging to varied therapeutic groups and classified as pharmaceutical waste in the environment. The provided results in this work offer a proof of concept for the use of $O_2^{\bullet-}$ as a potent oxidant in pharmaceutical waste degradation.

CHAPTER 5: CONCLUSION

5.1 Conclusion of the Work

5.1.1 Introduction

The generation and stability of $O_2^{\bullet-}$ in 25 different ILs with varying cations and anions have been investigated. The ILs comprised of cations mainly based on morpholinium, ammonium, piperidinium, imidazolium, pyrrolidinium, guanidinium and sulfonium, paired with several anions, such as bis(trifluoromethylsulfonyl)imide [TFSI], trifluoromethane sulfonate [TfO], tetracyanoborate [TCB], ethylsulfate [EtSO$_4$], chloride [Cl], thiocyanate [SCN], iodide [I], dicyanamide [DCA], tricyanomethane [TCM], dimethyl phosphate [DMP], and tri(pentafluoroethyl)trifluorophosphate [E$_3$FAP]. UV-visible spectrophotometric analysis was conducted to predict the stability of $O_2^{\bullet-}$ over a longer time period (*viz.* 2 – 3 h). Moreover, the presence of $O_2^{\bullet-}$ in the selected media was validated by means of electrochemical evidence using the cyclic voltammetry (CV) technique, which proved that $O_2^{\bullet-}$ was the principal radical species being generated in the reaction mixtures.

After the stability tests, 4 ILs were selected for further investigation and utilized as components of the binary mixture systems with acetonitrile (AcN) as an aprotic solvent, for the in-situ oxidative degradation of active pharmaceutical ingredients (APIs) using $O_2^{\bullet-}$ as the oxidant. The ILs utilized were composed of different cations, i.e., [BTEAmm$^+$], [PTEAmm$^+$], [OTEAmm$^+$] and [EMIm$^+$] paired with the same anion, i.e., [TFSI$^-$], in order to study the effect of IL cations on the degradation process. By comparing the [BTEAmm$^+$] and [EMIm$^+$] as cations in ILs, the influence of the aliphatic and aromatic cations was demonstrated. Comparing [BTEAmm$^+$], [PTEAmm$^+$], and [OTEAmm$^+$] cations resulted in determining the effects of varying lengths of the alkyl chain attached to the IL. Furthermore,

these ILs were used in various volume/volume ratios with AcN as binary reaction mixture systems. The target pharmaceutical contaminants used for this study were acetaminophen (ACTM), riluzole (RLZ) and carbamazepine (CBM).

5.1.2 Significant outcomes

The long-term stability kinetic studies deduced that ILs consisting of morpholinium, ammonium, and pyrrolidinium cations are the most promising for the chemical generation of $O_2^{\bullet-}$. This conclusion was primarily proposed on the basis of low consumption rate and low total consumption percentage of $O_2^{\bullet-}$ as reflected by the kinetic analysis. In contrast, higher total consumption of $O_2^{\bullet-}$ was detected in the presence of ILs comprising imidazolium, guanidinium, and sulfonium-based cations; in particular, [BMIm][DCA], [BMIm][Cl], [MMIm][DMP], [C₄DMIm][I], [EMIm][SCN], [EMIm][EtSO₄], [MMMIm][I], [MOPyrr] [E₃FAP], [BMPyrr][Cl], [gua][TfO], and [SEt₃][TFSI] did not yield stable $O_2^{\bullet-}$. This instability can be ascribed to reactions that might occur between the $O_2^{\bullet-}$ and the particular IL cationic species present in the system. Several factors, such as the structures of the IL cation and anion and the substituent group(s) attached to the cation contribute towards stabilization of the generated $O_2^{\bullet-}$, particularly through impeding its reaction with the cation of the IL medium. [MOEMMo][TFSI], [EMIm][TFSI], [BMMIm][Cl], [BMIm][TfO], and [TBAmm][TFSI] were among the several ILs validated as the best media for the generation of highly stable $O_2^{\bullet-}$, as demonstrated by the low percentages of total $O_2^{\bullet-}$ consumption (0.04%, 0.372%, 2.87%, 5.19%, and 6.74%) and low consumption rates (0.004 mM/min, 0.036 mM/min, 0.245 mM/min, 0.841 mM/min, and 1.024 mM/min) observed in the presence of these ILs. Moreover, the stability of $O_2^{\bullet-}$ decreased following the addition of IL in the following order: morpholinium > ammonium > piperidinium ~ pyrrolidinium >> imidazolium >> sulfonium.

The stable generation of superoxide ion ($O_2^{\bullet-}$) in various binary media was utilized for the simultaneous in-situ degradation of three solid APIs, namely, acetaminophen (ACTM), riluzole (RLZ) and carbamazepine (CBM). Initially, the degradation of ACTM was carried out using $O_2^{\bullet-}$ generated in binary IL/AcN media using two ILs comprising different cations, i.e., [BTEAmm$^+$] and [EMIm$^+$], paired with [TFSI$^-$]. The results demonstrated that the KO$_2$/IL/AcN system was very effective for the oxidative degradation of the model pharmaceutical pollutant, i.e., ACTM under mild conditions. When compared, the degradation percentage using the ammonium-based IL was greater than in the imidazolium-based IL, owing to the more stable generation of $O_2^{\bullet-}$ in the former one which was also in accordance with the stability studies and kinetic calculations via UV-visible spectrophotometric analysis. It is noteworthy that the extent of degradation for all drug compounds was dependent on the structure of the IL used, which indicated that the IL not only served as a medium for the dissolution of reaction components but also had catalytic activity to accelerate the reaction rate between $O_2^{\bullet-}$ and the substrate being oxidized. Moreover, the presence of $O_2^{\bullet-}$ in the utilized media was validated by electrochemical evidence using the cyclic voltammetry (CV) technique, which proved that $O_2^{\bullet-}$ was the principal radical species contributing towards degradation.

The binary mixture system of ILs with AcN serves as a technique to lower the viscosity, increase the diffusion rate, and a higher solubility of KO$_2$ salt resulting in more $O_2^{\bullet-}$ species being available for reaction. This leads to the reaction being more efficient at moderate temperatures and with lesser reaction times. The optimum value for ACTM degradation occurred using 10% [BTEAmm$^+$][TFSI$^-$]/AcN as the reaction medium with KO$_2$/API molar ratio 50 at RT within 210 min. Similarly, the most efficient and complete degradation of CBM was observed to occur utilizing 10% [OTEAmm$^+$][TFSI$^-$]/AcN with KO$_2$/API molar

ratio 50 at RT within 120 min. RLZ exhibited the most rapid degradation in 10% [BTEAmm$^+$][TFSI$^-$]/AcN under the same conditions, but with the least reaction time of 60 min. The difference in the time taken for the complete degradation to occur among these drugs can be ascribed to the extent of stability which each of these compounds possesses. ACTM among these have a more stable structure as compared to the other two, and hence the degradation of ACTM was observed to be gradual and took more time. In comparison with that the 7-membered ring of CBM is less stable and is thus more vulnerable to attack by the reactive oxidant species. Therefore, as soon as the middle ring in the structure of CBM is oxidized it quickly gets converted into its transformation products and a more rapid degradation is seen to occur in that case. Whereas in the instance of RLZ also, the structure comprises several susceptible sites like benzothiazole moiety, amine and trifluoromethoxy ($-OCF_3$) groups which are readily available and multiple positions for the attack by $O_2{}^{\bullet-}$, subsequently resulting in a comparatively abrupt decline in the concentration of RLZ because of a quick transformation of the parent compound into degradation products.

The study also demonstrated that the temperature does not have a very considerable effect on the degradation of APIs. However, increasing the temperature slightly to about 70 °C substantially reduced the viscosity of the IL and hence increased diffusion and interaction of the reaction components. Furthermore, the dissolution of KO_2 salt was also found to improve with an increase in the temperature of the media which was the reason for slightly increased degradation percentage observed.

The ILs used in this work for degradation were hydrophobic and thus could be easily recycled by aqueous extraction. The recycled ILs were found to be reusable for up to five consecutive replica cycles without significant changes in the degradation efficiencies, depicting the high efficacy of the environmentally benign regenerated media. The aqueous

extract was analyzed for TOC removal extent which established complete mineralization of the drug compounds under optimum conditions. Based on LCMS-QToF as well as LCMS-MS analyses, the degradation products of the investigated APIs were identified, and possible reaction pathways for transformation were proposed. A pathway for RLZ was found to be speculated for the first time, as very few studies were dedicated to exploring the oxidative degradation of RLZ.

This finding anticipates opening further prospects in the design of combinative solvent media for stable generation of $O_2^{\bullet-}$ as a promising agent for diverse implications. Stimulating parallel studies, this investigation also proposes to set off further research while extending a new scenario for practical use of $O_2^{\bullet-}$ in the degradation of compounds belonging to varied therapeutic groups and classified as pharmaceutical waste in the environment. The provided results in this work offer a proof of concept for the use of $O_2^{\bullet-}$ as a potent oxidant in pharmaceutical waste degradation.

The conclusions of this study can be outlined in the following abridgement:

1. A simplistic and efficient method for the degradation of pharmaceutical waste was devised using $O_2^{\bullet-}$ as an oxidant generated and stabilized in binary mixture systems.

2. Investigating the influence of different parameters, such as the amount of oxidant and initial concentration of API, nature of cations in ILs, the ratio of IL:AcN (constituency of binary mixture), and reaction temperature, revealed the optimum operating conditions for the process.

3. The utilized ILs were recycled and reused in five successive cycles for degradation of APIs with a potency comparable to the fresh ones, hence establishing the green aspect of the formulated procedure.

4. The results of TOC demonstrated the extent of mineralization in varied combinations of reaction media.

5. LCMS analysis eventually identified intermediates and transformation products (TPs) suggesting that after aromatic ring cleavage the APIs were converted to small molecule organics which could be further oxidized to CO_2, H_2O, and inorganic ions such as NH_4^+ and NO_3^-.

5.2 Limitations

The limitations encountered during this work are indicated as follows:

- The generation of $O_2^{\bullet-}$ in aprotic mixture media was still exposed to atmospheric moisture while setting up the reactions, and taking out the aliquots which could affect the results of the study. More inert setups would be useful in that concern but could also alter the economic feasibility of the process.

- Impurity and moisture levels of the commercial ILs also served as contributing factors to influence the degradation percentage achieved in each case, getting rid of which in the real-time process could also lead to a highly sophisticated and less viable setup.

- Detection and quantification of $O_2^{\bullet-}$ contributing toward the API degradation using quenching experiments was not possible in the $KO_2/IL/AcN$ system, unlike other experiments using aqueous reaction media.

5.3 Recommendations and Future Work

The study investigating the in-situ generation of reactive oxidants and simultaneous degradation of pharmaceutical contaminants demands additional exploration which is underway. Moreover, the transformation products could be evaluated for any alterations in

toxicity of the reaction solution that may offset the advantages of utilizing the KO_2/IL/AcN system for the degradation of solid APIs.

This research work studied ACTM, CBM and RLZ as pharmaceutical waste models and demonstrated that the degradation efficiency considerably improved even with changing (increasing) initial concentrations of APIs that were used, for all three drug compounds despite the differences in chemical structures and polarities. Nevertheless, this may not be the case for other pharmaceutical contaminants, therefore, further investigation is required to monitor the degradation patterns of other drug pollutant compounds and the resultant transformation products to validate such phenomenon.

Also, conducting DFT (Density Functional Theory) studies to calculate the differences in energies would be valuable for extrapolating the transformation of pollutant substances with various chemical structures in the investigated oxidation process.

REFERENCES

(NIST), N. I. S. T. (1973). *Reactivity of the hydroxyl radical in aqueous solutions.* Retrieved from https://www.govinfo.gov/app/details/GOVPUB-C13-bad243eb813a372 fe3f3f361f7 939ac1.

(PSI), P. S. I. (2023). *Pharms & Sharps Stewardship: Building capacity for EPR - Product Stewardship Institute (PSI).* Hanz Atia. https://productstewardship.us/w ebinar/pharms-sharps-stewardship-building-capacity-for- epr/

A.J. Bard, L. R. F. (2001). *Electrochemical methods. Fundamentals and applications* (2nd ed. ed.). John Wiley & Sons, Inc.

Abramov, V., Abramova, A., Bayazitov, V., Kameneva, S., Veselova, V., Kozlov, D., & Cravotto, G. (2022). Fast degradation of tetracycline and ciprofloxacin in municipal water under hydrodynamic cavitation/plasma with CeO_2 nanocatalyst. *Processes*, *10*(10), 2063-2078.

Ahmed, O. U., Mjalli, F. S., Al-Wahaibi, T., Al-Wahaibi, Y., & AlNashef, I. M. (2015). Stability of superoxide ion in phosphonium-based ionic liquids. *Industrial & Engineering Chemistry Research*, *54*(7), 2074-2080.

Ahrens, S., Peritz, A., & Strassner, T. (2009). Tunable aryl alkyl ionic liquids (TAAILs): The next generation of ionic liquids. *Angewandte Chemie International Edition*, *48*(42), 7908-7910.

Al-Quliti, K. W. (2015). Update on neuropathic pain treatment for trigeminal neuralgia. The pharmacological and surgical options. *Neurosciences (Riyadh)*, *20*(2), 107-114.

Ali, A. Z., Wu, Y., Bennani, Y.-D., Spanjers, H., & Hoek, J. P. v. d. (2023). Photo-electrocatalytic based removal of acetaminophen: Application of visible light driven heterojunction based $BiVO_4$/BiOI photoanode. *Chemosphere*, *324*, Article#138322.

Alnashef, I., Leonard, M., Kittle, M., Matthews, M., & Weidner, J. (2001a). Electrochemical generation of superoxide in room-temperature ionic liquids. *Electrochemical and Solid State Letters - Electrochem Solid State Lett*, *4*, Article# D16.

Al-Nashef, I. M., Hashim, M. A., Mjalli, F. S., Ali, M. Q., & Hayyan, M. (2010a). A novel method for the synthesis of 2-imidazolones. *Tetrahedron Lett.*, *51*(15), 1976–1978.

Al-Nashef, I. M., Hashim, M. A., Mjalli, F. S., Ali, M. Q. A.-h., & Hayyan, M. (2010b). A novel method for the synthesis of 2-imidazolones. *Tetrahedron Letters*, *51*(15), 1976-1978.

Al-Nashef, I. M., & Hayyan, M. (2012). Kinetics of homogeneous reactions in ionic liquids. *International Journal of Electrochemical Science*, *7*(9), 8236-8254.

Al-Nashef, I. M., Leonard, M. L., Kittle, M. C., Matthews, M. A., & Weidner, J. W. (2001b). Electrochemical generation of superoxide in room-temperature ionic liquids. *Electrochem. Solid State Lett.*, *4*(11), D16 -D18.

Al-Nashef, I. M., Leonard, M. L., Matthews, M. A., & Weidner, J. W. (2002a). Superoxide electrochemistry in an ionic liquid. *Industrial & Engineering Chemistry Research*, *41*(18), 4475-4478.

Al-Nashef, I. M., Leonard, M. L., Matthews, M. A., & Weidner, J. W. (2002b). Superoxide electrochemistry in an ionic liquid. *Industrial and Engineering Chemistry Research*, *41*(18), 4475-4478.

Al-Saleem, S. S., Zahid, W. M., Alnashef, I. M., & Haider, H. (2019). Destruction of environmentally hazardous halogenated hydrocarbons in stable ionic liquids with superoxide ion radical. *Separation and Purification Technology*, *215*, 134-142.

Anastas, P. T. W. J. C. (1998). *Green chemistry : Theory and practice*. Oxford University Press.

Andreozzi, R., Caprio, V., Marotta, R., & Vogna, D. (2003). Paracetamol oxidation from aqueous solutions by means of ozonation and H_2O_2/UV system. *Water Research*, *37*(5), 993-1004.

Angell, C. A., Byrne, N., & Belieres, J.-P. (2007). Parallel developments in aprotic and protic ionic liquids: Physical chemistry and applications. *Accounts of Chemical Research*, *40*(11), 1228-1236.

Archer, E., Petrie, B., Kasprzyk-Hordern, B., & Wolfaardt, G. M. (2017). The fate of pharmaceuticals and personal care products (PPCPs), endocrine disrupting contaminants (EDCs), metabolites and illicit drugs in a WWTW and environmental waters. *Chemosphere*, *174*, 437-446.

Arshadi, M., Yamdagni, R., & Kebarle, P. (1970). Hydration of the halide negative ions in the gas phase. II. Comparison of hydration energies for the alkali positive and halide negative ions. *The Journal of Physical Chemistry*, *74*(7), 1475-1482.

Ashton, D., Hilton, M., & Thomas, K. V. (2004). Investigating the environmental transport of human pharmaceuticals to streams in the United Kingdom. *Science of The Total Environment*, *333*(1), 167-184.

Asif, A. H., Rafique, N., Hirani, R. A. K., Shi, L., Zhang, S., Wang, S., & Sun, H. (2023). Graphitic carbon nitride engineered α-Fe_2O_3/rGO heterostructure for visible-light-driven photochemical oxidation of sulfamethoxazole. *Chemical Engineering Journal*, *451*, Article#138630.

aus der Beek, T., Weber, F.-A., Bergmann, A., Grüttner, G., & Carius, A. (2016). *Pharmaceuticals in the environment: Global occurrence and potential cooperative*

action under the Strategic Approach to International Chemicals Management (SAICM).

Ballou, D., Palmer, G., & Massey, V. (1969). Direct demonstration of superoxide anion production during the oxidation of reduced flavin and of its catalytic decomposition by erythrocuprein. *Biochemical and Biophysical Research Communications*, *36*(6), 898-904.

Baltes, N., Beyle, F., Freiner, S., Geier, F., Joos, M., Pinkwart, K., & Rabenecker, P. (2013). Trace detection of oxygen – Ionic liquids in gas sensor design. *Talanta*, *116*(0), 474-481.

Bao, Q., Qiao, K., Tomida, D., & Yokoyama, C. (2008). Preparation of 5-hydroymethylfurfural by dehydration of fructose in the presence of acidic ionic liquid. *Catalysis Communications*, *9*(6), 1383-1388.

Bard, A. J. F., L. R.; Leddy, J.; Zoski, C. G. (1980). *Electrochemical Methods: Fundamentals and Applications* (Vol. 2). Wiley: New York.

Barnes, A. S., Rogers, E. I., Streeter, I., Aldous, L., Hardacre, C., Wildgoose, G. G., & Compton, R. G. (2008). Unusual voltammetry of the reduction of O_2 in [C4dmim][N (Tf) 2] reveals a strong interaction of $O_2^{\bullet-}$ with the [C4dmim]+ cation. *The Journal of Physical Chemistry C*, *112*(35), 13709-13715.

Behar, D., Czapski, G., Rabani, J., Dorfman, L. M., & Schwarz, H. A. (1970). Acid dissociation constant and decay kinetics of the perhydroxyl radical. *The Journal of Physical Chemistry*, *74*(17), 3209-3213.

Belieres, J. P., & Angell, C. A. (2007). Protic ionic liquids: preparation, characterization, and proton free energy level representation. *J Phys Chem B*, *111*(18), 4926-4937.

Belloni, J., & Lecheheb, A. (1987). Heterogeneous catalysis of superoxide anion dismutation. *International Journal of Radiation Applications and Instrumentation. Part C. Radiation Physics and Chemistry*, *29*(2), 89-92. h

Bensalah, N., Neily, E., Bedoui, A., & Ahmad, M. I. (2023). Mineralization of Riluzole by heterogeneous Fenton oxidation using natural iron catalysts. *Catalysts*, *13*(1), Article#68.

Bernot, R. J., Kennedy, E. E., & Lamberti, G. A. (2005). Effects of ionic liquids on the survival, movement, and feeding behavior of the freshwater snail, Physa acuta. *Environ Toxicol Chem*, *24*(7), 1759-1765.

Bessa, V. S., Moreira, I. S., Murgolo, S., Mascolo, G., & Castro, P. M. L. (2019). Carbamazepine is degraded by the bacterial strain Labrys portucalensis F11. *Science of The Total Environment*, *690*, 739-747.

Beyersdorff, T., Schubert, T. J. S., Welz-Biermann, U., Pitner, W., Abbott, A. P., McKenzie, K. J., & Ryder, K. S. (2008). Synthesis of ionic liquids. In *Electrodeposition from Ionic Liquids*, 15-46.

Bhattacharjee, A., Luís, A., Santos, J. H., Lopes-da-Silva, J. A., Freire, M. G., Carvalho, P. J., & Coutinho, J. A. P. (2014). Thermophysical properties of sulfonium- and ammonium-based ionic liquids. *Fluid Phase Equilibria*, *381*, 36-45.

Bonhôte, P., Dias, A.-P., Papageorgiou, N., Kalyanasundaram, K., & Grätzel, M. (1996). Hydrophobic, highly conductive ambient-temperature molten salts. *Inorganic Chemistry*, *35*(5), 1168-1178.

Borah, P., Chandra Boro, S., & Kalita, M. P. C. (2023). Effective photodegradation of acetaminophen by V_2O_5 nanocrystals under simulated solar radiation. *Materials Letters*, *342*, 134317.

Borodin, O., Gorecki, W., Smith, G. D., & Armand, M. (2010). Molecular dynamics simulation and pulsed-field gradient NMR Studies of bis(fluorosulfonyl)imide (FSI) and bis[(trifluoromethyl)sulfonyl]imide (TFSI)-based ionic liquids. *The Journal of Physical Chemistry B*, *114*(20), 6786-6798.

Bovard, R. M. (1960). Oxygen sources for space flights. *Aerosp Med*, *31*, 407-412.

Buzzeo, M. C., Hardacre, C., & Compton, R. G. (2004). Use of room temperature ionic liquids in gas sensor design. *Analytical Chemistry*, *76*(15), 4583-4588.

Buzzeo, M. C., Klymenko, O. V., Wadhawan, J. D., Hardacre, C., Seddon, K. R., & Compton, R. G. (2003). Voltammetry of oxygen in the room-temperature ionic liquids 1-ethyl-3-methylimidazolium bis ((trifluoromethyl) sulfonyl) imide and hexyltriethylammonium bis ((trifluoromethyl) sulfonyl) imide: One-electron reduction to form superoxide. Steady-state and transient behavior in the same cyclic voltammogram resulting from widely different diffusion coefficients of oxygen and superoxide. *The Journal of Physical Chemistry A*, *107*(42), 8872-8878.

Buzzeo, M. C., Klymenko, O. V., Wadhawan, J. D., Hardacre, C., Seddon, K. R., & Compton, R. G. (2004). Kinetic analysis of the reaction between electrogenerated superoxide and carbon dioxide in the room temperature ionic liquids 1-ethyl-3-methylimidazolium bis (trifluoromethylsulfonyl) imide and hexyltriethylammonium bis (trifluoromethylsulfonyl) imide. *The Journal of Physical Chemistry B*, *108*(12), 3947-3954.

Cako, E., Dudziak, S., Głuchowski, P., Trykowski, G., Pisarek, M., Fiszka Borzyszkowska, A., & Zielińska-Jurek, A. (2023). Heterojunction of (P, S) co-doped g-C3N4 and 2D TiO_2 for improved carbamazepine and acetaminophen photocatalytic degradation. *Separation and Purification Technology*, *311*, Article#123320.

Calza, P., Medana, C., Padovano, E., Giancotti, V., & Baiocchi, C. (2012). Identification of the unknown transformation products derived from clarithromycin and

carbamazepine using liquid chromatography/high-resolution mass spectrometry. *Rapid Communications in Mass Spectrometry*, *26*(15), 1687-1704.

Carlin, R. T., Truelove, P. C., & Osteryoung, R. A. (1992). Electrochemical and spectroscopic study of anthracene in a mixed Lewis—Brønsted acid ambient temperature molten salt system. *Electrochimica Acta*, *37*(14), 2615-2628.

Carter, M. T., Hussey, C. L., Strubinger, S. K. D., & Osteryoung, R. A. (1991a). Electrochemical reduction of dioxygen in room-temperature imidazolium chloride-aluminum chloride molten salts. *Inorganic Chemistry*, *30*(5), 1149-1151.

Castiglione, F., Moreno, M., Raos, G., Famulari, A., Mele, A., Appetecchi, G. B., & Passerini, S. (2009). Structural Organization and Transport Properties of Novel Pyrrolidinium-Based Ionic Liquids with Perfluoroalkyl Sulfonylimide Anions. *The Journal of Physical Chemistry B*, *113*(31), 10750-10759.

Chaban, V. V., Voroshylova, I. V., Kalugin, O. N., & Prezhdo, O. V. (2012). Acetonitrile Boosts Conductivity of Imidazolium Ionic Liquids. *The Journal of Physical Chemistry B*, *116*(26), 7719-7727.

Chan, N. Y. (2010). *Superoxide radical and UV irradiation in ultrasound assisted oxidative desulfurization (UAOD): A potential alternative for greener fuels* [Ph.D., University of Southern California]. ProQuest Dissertations & Theses Global. Ann Arbor. https://www.proquest.com/dissertations-theses/superoxide-radical-uv-irradiation-ultrasound/docview/365445013/se-2?accountid=41453

Chan, N. Y., Lin, T.-Y., & Yen, T. F. (2008). Superoxides: Alternative oxidants for the oxidative desulfurization process. *Energy & Fuels*, *22*(5), 3326-3328.

Chaskar, A., Bhandari, S., Patil, A., Sharma, O., & Mayeker, S. (2009). Solvent-free oxidation of alcohols with potassium persulphate in the presence of Brönsted acidic ionic liquids. *Synthetic Communications®*, *39*, 366-370. https://doi.org/10.1080/00397910802374117

Cheah, B. C., Vucic, S., Krishnan, A. V., & Kiernan, M. C. (2010). Riluzole, Neuroprotection and Amyotrophic Lateral Sclerosis. *Current Medicinal Chemistry*, *17*(18), 1942-1959.

CheeMei, L., Aiin, B. A. A. N., Palaniandy, P., & Amr, S. S. A. (2017). Performance of natural sunlight on paracetamol removal from synthetic pharmaceutical wastewater using heterogeneous TiO2 photocatalyst. *Desalination and Water Treatment*, *78*, 341-349.

Chen, H., Lin, T., Wang, P., Zhang, X., Jiang, F., & Wang, Y. (2023). Novel solar/sulfite advanced oxidation process for carbamazepine degradation: Radical chemistry, transformation pathways, influence on disinfection byproducts and toxic changes. *Chemical Engineering Journal*, *451*, Article# 138634.

Chen, L., Mullen, G. E., Le Roch, M., Cassity, C. G., Gouault, N., Fadamiro, H. Y., Barletta, & Davis, J. H., Jr. (2014). On the formation of a protic ionic liquid in nature. *Angew Chem Int Ed Engl*, *53*(44), 11762-11765.

Chen, P.-Y., & Hussey, C. L. (2005). Electrochemistry of ionophore-coordinated Cs and Sr ions in the tri-1-butylmethylammonium bis((trifluoromethyl)sulfonyl)imide ionic liquid. *Electrochimica Acta*, *50*(12), 2533-2540.

Chen, Y., Bai, X., Ji, Y., & Chen, D. (2023). Enhanced activation of peroxymonosulfate using ternary MOFs-derived MnCoFeO for sulfamethoxazole degradation: Role of oxygen vacancies. *Journal of Hazardous Materials*, *441*, Article#129912.

Chen, Y., Kang, J., Li, Z., Zhu, M., & Yin, R. (2023a). Activation of peroxymonosulfate by Co_2P via interfacial radical pathway for the degradation and mineralization of carbamazepine. *Surfaces and Interfaces*, *40*, Article# 103045.

Chijioke-Okere, M., Abdullah, A. H., Mohd Hir, Z. A., Alinnor, J. I., & Oguzie, E. E. (2023). Efficient photodegradation of paracetamol by integrated PES-ZnO photocatalyst sheets. *Inorganic Chemistry Communications*, *148*, Article# 110377.

Chin, D. H., Chiericato, G., Jr., Nanni, E. J., Jr., & Sawyer, D. T. (1982). Proton-induced disproportionation of superoxide ion in aprotic media. *J Am Chem Soc*, *104*(5), 1296-1299.

Chin, L. S., Patel, S., Mattingly, T., & Kwok, Y. (2008). Trigeminal Neuralgia. In L. S. Chin & W. F. Regine (Eds.), *Principles and Practice of Stereotactic Radiosurgery,* 519-526. Springer New York.

Cho, C.-W., Jeon, Y.-C., Pham, T. P. T., Vijayaraghavan, K., & Yun, Y.-S. (2008). The ecotoxicity of ionic liquids and traditional organic solvents on microalga Selenastrum capricornutum. *Ecotoxicol Environ Saf*, *71*(1), 166-171.

Cocalia, V. A., Holbrey, J. D., Gutowski, K. E., Bridges, N. J., & Roqers, R. D. (2006). Separations of metal ions using ionic liquids: The challenges of multiple mechanisms. *Tsinghua Science and Technology*, *11*(2), 188-193.

Commission, E. (2008). *Priority Substances Daughter Directive-directive 2008/105/EC of the European Parliament and of the Council of 16 December 2008 on Environmental Quality Standards in the Field of Water Policy.*

Commission, E. (2012). *Proposal for a Directive of the European Parliament and of the Council Amending Directives 2000/60/EC and 2008/105/EC as Regards Priority Substances in the Field of Water Policy.*

Conaghan, P. G., Arden, N., Avouac, B., Migliore, A., & Rizzoli, R. (2019). Safety of Paracetamol in Osteoarthritis: What Does the Literature Say? *Drugs Aging*, *36*(Suppl 1), 7-14.

Costentin, C., Robert, M., & Savéant, J.-M. (2010). Concerted Proton−Electron Transfers: Electrochemical and Related Approaches. *Accounts of Chemical Research*, *43*(7), 1019-1029.

Cui, S., Lu, B., Cai, Q., Cai, X., Li, X., Xiao, X., Hou, L., & Han, Y. (2006). Highly selective synthesis of diphenylmethane with acidic ionic liquids. *Industrial & Engineering Chemistry Research*, *45*(5), 1571-1574.

D. T. Sawyer, A. S., and J. L. Roberts. (1995). *Electrochemistry for Chemists*. In (2nd ed. ed.). Wiley Interscience.

Daescu, M., Chivu, M., Matei, E., Negrila, C., Cramariuc, O., & Baibarac, M. (2023). Photocatalytic activity of the blends based on TiO_2 nanoparticles and reduced graphene oxide for degradation of acetaminophen. *Molecules*, *28*(11), Article# 4546.

Daniels, S. L. (2002). "On the ionization of air for removal of noxious effluvia" (Air ionization of indoor environments for control of volatile and particulate contaminants with nonthermal plasmas generated by dielectric-barrier discharge). *IEEE Transactions on Plasma Science*, *30*(4), 1471-1481.

Ding, J., & Armstrong, D. W. (2005). Chiral ionic liquids: Synthesis and applications. *Chirality*, *17*(5), 281-292.

Ding, K. (2009). The electrocatalysis of multi-walled carbon nanotubes (MWCNTs) for oxygen reduction reaction (ORR) in room temperature ionic liquids (RTILs). *Port. Electrochim. Acta*, *27*(2), 165-175.

Dondoni, A., Galliani, G., Mastellari, A., & Medici, A. (1985). Reaction of n-alkylthiazolium halides, including thiamine, with superoxide ion. Chemistry and biological implications. *Tetrahedron Letters*, *26*(24), 2917-2920.

Earle, M. J., & Seddon, K. R. (2000). Ionic liquids. Green solvents for the future. *Pure and Applied Chemistry*, *72*(7), 1391-1398.

Estager, J., Holbrey, J. D., & Swadźba-Kwaśny, M. (2014). Halometallate ionic liquids – revisited [10.1039/C3CS60310E]. *Chemical Society Reviews*, *43*(3), 847-886.

Evans, R. G., Klymenko, O. V., Saddoughi, S. A., Hardacre, C., & Compton, R. G. (2004b). Electroreduction of oxygen in a series of room temperature ionic liquids composed of group 15-centered cations and anions. *The Journal of Physical Chemistry B*, *108*(23), 7878-7886.

Fang, D., Zhou, X.-L., Ye, Z.-W., & Liu, Z.-L. (2006). Brønsted acidic ionic liquids and their use as dual solvent−Catalysts for Fischer esterifications. *Industrial & Engineering Chemistry Research*, *45*(24), 7982-7984.

Fang, Z., Liu, Y., Qi, J., Xu, Z.-F., Qi, T., & Wang, L. (2023). Establishing a high-speed electron transfer channel via CuS/MIL-Fe heterojunction catalyst for photo-Fenton

degradation of acetaminophen. *Applied Catalysis B: Environmental*, *320*, Article#121979.

Fatta-Kassinos, D., Meric, S., & Nikolaou, A. (2011). Pharmaceutical residues in environmental waters and wastewater: current state of knowledge and future research. *Anal Bioanal Chem*, *399*(1), 251-275.

Fawcett, W. R., Brooksby, P., Verbovy, D., Bakó, I., & Pálinkás, G. (2005). Studies of anion solvation in polar aprotic solvents. *Journal of Molecular Liquids*, *118*(1), 171-178.

Fischer, T., Sethi, A., Welton, T., & Woolf, J. (1999). Diels-Alder reactions in room-temperature ionic liquids. *Tetrahedron Letters*, *40*(4), 793-796.

Fraga-Dubreuil, J., Bourahla, K., Rahmouni, M., Bazureau, J. P., & Hamelin, J. (2002). Catalysed esterifications in room temperature ionic liquids with acidic counteranion as recyclable reaction media. *Catalysis Communications*, *3*(5), 185-190.

Franz, S., Falletta, E., Arab, H., Murgolo, S., Bestetti, M., & Mascolo, G. (2020). Degradation of carbamazepine by photo(electro)catalysis on nanostructured TiO_2 meshes: Transformation products and reaction pathways. *Catalysts*, *10*(2), Article#169.

Fraser, K. J., Izgorodina, E. I., Forsyth, M., Scott, J. L., & MacFarlane, D. R. (2007). Liquids intermediate between "molecular" and "ionic" liquids: Liquid Ion Pairs?. *Chemical Communications*, (37), 3817-3819.

Fredlake, C. P., Crosthwaite, J. M., Hert, D. G., Aki, S. N. V. K., & Brennecke, J. F. (2004). Thermophysical properties of imidazolium-based ionic liquids. *Journal of Chemical & Engineering Data*, *49*(4), 954-964.

Freire, M., Santos, L., Fernandes, A., & Marrucho, I. (2007). An Overview of the mutual solubilities of water-imidazolium-based ionic liquids systems. *Fluid Phase Equilibria*, *261*, 449-454.

Fridovich, I., & Handler, P. (1961). Detection of free radicals generated during enzymic oxidations by the initiation of sulfite oxidation. *Journal of Biological Chemistry*, *236*(6), 1836-1840.

Frimer, A. A. (1983). *The Chemistry of Functional Groups, Peroxides*. John Wiley & Sons Ltd.

Gabet, A., Guy, C., Fazli, A., Métivier, H., de Brauer, C., Brigante, M., & Mailhot, G. (2023). The ability of recycled magnetite nanoparticles to degrade carbamazepine in water through photo-Fenton oxidation at neutral pH. *Separation and Purification Technology*, *317*, 123877.

Galiński, M., Lewandowski, A., & Stępniak, I. (2006). Ionic liquids as electrolytes. *Electrochimica Acta*, *51*(26), 5567-5580.

Gathergood, N., & Scammells, P. J. (2002). Design and preparation of room-temperature ionic liquids containing biodegradable side chains. *Australian Journal of Chemistry*, *55*(9), 557-560.

Ghasemian, S., Nasuhoglu, D., Omanovic, S., & Yargeau, V. (2017). Photoelectrocatalytic degradation of pharmaceutical carbamazepine using Sb-doped Sn80%-W20%-oxide electrodes. *Separation and Purification Technology*, *188*, 52-59.

Ghilane, J., Lagrost, C., & Hapiot, P. (2007). Scanning electrochemical microscopy in nonusual solvents: inequality of diffusion coefficients problem. *Analytical chemistry*, *79*(19), 7383-7391.

Gibian, M. J., Sawyer, D. T., Ungermann, T., Tangpoonpholvivat, R., & Morrison, M. M. (1979). Reactivity of superoxide ion with carbonyl compounds in aprotic solvents. *Journal of the American Chemical Society*, *101*(3), 640-644.

Gladysz, J. A., Curran, D. P., & Horváth, I. T. (2006). *Handbook of fluorous chemistry*. John Wiley & Sons.

Glaze, W. H., Kang, J.-W., & Chapin, D. H. (1987). The chemistry of water treatment processes involving ozone, hydrogen peroxide and ultraviolet radiation. *Ozone: Science & Engineering*, *9*(4), 335-352.

Gómez, E., Calvar, N., Domínguez, Á., & A. Macedo, E. (2013). Thermal analysis and heat capacities of 1-alkyl-3-methylimidazolium Ionic Liquids with NTf_2^-, TFO^-, and DCA^- anions. *Industrial & Engineering Chemistry Research*, *52*(5), 2103-2110.

Gonçalves, A. M., Mathieu, C., Herlem, M., & Etcheberry, A. (1999). Oxygen reduction mechanisms at p-InP and p-GaAs electrodes in liquid ammonia in neutral buffered medium and acidic media. *Journal of Electroanalytical Chemistry*, *462*(1), 88-96.

Gong, K., Wang, H.-L., Fang, D., & Liu, Z.-L. (2008). Basic ionic liquid as catalyst for the rapid and green synthesis of substituted 2-amino-2-chromenes in aqueous media. *Catalysis Communications*, *9*, 650-653.

Gracia-Lor, E., Sancho, J. V., & Hernández, F. (2011). Multi-class determination of around 50 pharmaceuticals, including 26 antibiotics, in environmental and wastewater samples by ultra-high performance liquid chromatography–tandem mass spectrometry. *Journal of Chromatography A*, *1218*(16), 2264-2275.

Greaves, T. L., & Drummond, C. J. (2008). Protic ionic liquids: Properties and applications. *Chemical Reviews*, *108*(1), 206-237.

Green, M. R., Allen, H., Hill, O., & Turner, D. R. (1979). The nature of the superoxide ion in dipolar aprotic solvents: The electron paramagnetic resonance spectra of the superoxide ion in N, N-dimethylformamide—evidence for hydrated forms. *Febs Letters*, *103*(1), 176-180.

Grzegórska, A., Gajewicz-Skretna, A., Trykowski, G., Sikora, K., & Zielińska-Jurek, A. (2023). Design and synthesis of TiO_2/Ti_3C_2 composites for highly efficient photocatalytic removal of acetaminophen: The relationships between synthesis parameters, physicochemical properties, and photocatalytic activity. *Catalysis Today*, *413-415*, Article# 113980.

Gülçin, İ., Huyut, Z., Elmastaş, M., & Aboul-Enein, H. Y. (2010). Radical scavenging and antioxidant activity of tannic acid. *Arabian Journal of Chemistry*, *3*(1), 43-53.

Haag, G., Diener, H. C., May, A., Meyer, C., Morck, H., Straube, A., & Evers, S. (2011). Self-medication of migraine and tension-type headache: summary of the evidence-based recommendations of the Deutsche Migräne und Kopfschmerzgesellschaft (DMKG), the Deutsche Gesellschaft für Neurologie (DGN), the Österreichische Kopfschmerzgesellschaft (ÖKSG) and the Schweizerische Kopfwehgesellschaft (SKG). *The journal of headache and pain, 12*(2), 201-217.

Hajipour, A. R., & Rafiee, F. (2009). Basic ionic liquids. A short review. *Journal of the Iranian Chemical Society*, *6*(4), 647-678. https://doi.org/10.1007/BF03246155

Hajipour, A. R., Rafiee, F., & Ruoho, A. E. (2006). Oxidation of benzylic alcohols to their corresponding carbonyl compounds using KIO_4 in ionic liquid by microwave irradiation. *Synthetic Communications*, *36*(17), 2563-2568.

Hajipour, A. R., Rafiee, F., & Ruoho, A. E. (2007). Facile and selective oxidation of benzylic alcohols to their corresponding carbonyl compounds with sodium nitrate in the presence of Brønsted acidic ionic liquids. *Synlett*, *2007*(07), 1118-1120.

Halilu, A., Hayyan, M., Aroua, M. K., Yusoff, R., & Hizaddin, H. F. (2019). In situ electrosynthesis of peroxydicarbonate anion in ionic liquid media using carbon dioxide/superoxide system. *ACS Applied Materials & Interfaces*, *11*(29), 25928-25939.

Halilu, A., Hayyan, M., Aroua, M. K., Yusoff, R., & Hizaddin, H. F. (2021). Mechanistic insights into carbon dioxide utilization by superoxide ion generated electrochemically in ionic liquid electrolyte [10.1039/D0CP04903D]. *Physical Chemistry Chemical Physics*, *23*(2), 1114-1126.

Halilu, A., Hayyan, M., Aroua, M. K., Yusoff, R., Hizaddin, H. F., & Basirun, W. J. (2021). Hybridized Fe/Ru-SiMWCNT-ionic liquid nanofluid for CO_2 conversion into carbamate using superoxide ion. *Journal of Environmental Chemical Engineering*, *9*(4), Article#105285.

Hamaguchi, H., & Ozawa, R. (2005). Structure of ionic liquids and ionic liquid compounds: are ionic liquids genuine liquids in the conventional sense. *Advances in Chemical Physics, 131*, 85-104.

Hanke, C., Atamas, N., & Lynden-Bell, R. (2002). Solvation of small molecules in imidazolium ionic liquids: A simulation study. *Green Chemistry - Green Chem*, *4*, 107-111.

Hassani, A., Eghbali, P., Kakavandi, B., Lin, K.-Y. A., & Ghanbari, F. (2020). Acetaminophen removal from aqueous solutions through peroxymonosulfate activation by $CoFe_2O_4/mpg-C_3N_4$ nanocomposite: Insight into the performance and degradation kinetics. *Environmental Technology & Innovation*, *20*, Article#101127.

Hayes, R., Warr, G. G., & Atkin, R. (2015). Structure and nanostructure in ionic liquids. *Chemical Reviews*, *115*(13), 6357-6426.

Hayyan, M., Alakrach, A. M., Hayyan, A., Hashim, M. A., & Hizaddin, H. F. (2017). Superoxide ion as oxidative desulfurizing agent for aromatic sulfur compounds in ionic liquid media. *ACS Sustainable Chemistry & Engineering*, *5*(2), 1854-1863. https://doi.org/10.1021/acssuschemeng.6b02573

Hayyan, M., Hashim, M., & Alnashef, I. (2015a). Kinetics of superoxide ion in dimethyl sulfoxide containing ionic liquids. *Ionics*, *21*, 719-728.

Hayyan, M., Hashim, M. A., & AlNashef, I. M. (2016). Superoxide ion: Generation and chemical implications. *Chemical Reviews*, *116*(5), 3029-3085. https://doi.org/10.1021/acs.chemrev.5b00407

Hayyan, M., Ibrahim, M., Hayyan, A., & Hashim, M. (2017a). Investigating the long-term stability and kinetics of superoxide ion in dimethyl sulfoxide containing ionic liquids and the application of thiophene destruction. *Brazilian Journal of Chemical Engineering*, *34*, 227-239.

Hayyan, M., Ibrahim, M. H., Hayyan, A., AlNashef, I. M., Alakrach, A. M., & Hashim, M. A. (2015). Facile route for fuel desulfurization using generated superoxide ion in ionic liquids. *Industrial & Engineering Chemistry Research*, *54*(49), 12263-12269.

Hayyan, M., Mjalli, F., Alnashef, I., & Hashim, M. (2012a). Stability and kinetics of generated superoxide ion in trifluoromethanesulfonate anion-based ionic liquids. *International Journal of Electrochemical Science*, *7*, 9658-9667.

Hayyan, M., Mjalli, F., Hashim, M., & Alnashef, I. (2011a). Utilizing of 1-hexyl-1-methyl-pyrrolidinium bis (trifluoromethyl-sulfonyl) imide as medium for electrochemical generation of superoxide ion-radical. *International Islamic University Malaysia Engineering Journal*, *12*, 37-41.

Hayyan, M., Mjalli, F. S., AlNashef, I. M., & Hashim, M. A. (2012b). Chemical and electrochemical generation of superoxide ion in 1-butyl-1-methylpyrrolidinium bis (trifluoromethylsulfonyl) imide. *International Journal of Electrochemical Science*, *7*(9), 8116-8127.

Hayyan, M., Mjalli, F. S., AlNashef, I. M., & Hashim, M. A. (2012c). Generation and stability of superoxide ion in tris (pentafluoroethyl) trifluorophosphate anion-based ionic liquids. *Journal of Fluorine Chemistry*, *142*, 83-89.

Hayyan, M., Mjalli, F. S., AlNashef, I. M., & Hashim, M. A. (2012d). Generation and stability of superoxide ion in tris(pentafluoroethyl)trifluorophosphate anion-based ionic liquids. *Journal of Fluorine Chemistry*, *142*, 83-89.

Hayyan, M., Mjalli, F. S., AlNashef, I. M., & Hashim, M. A. (2012e). Stability and kinetics of generated superoxide ion in trifluoromethanesulfonate anion-based ionic liquids. *International Journal of Electrochemical Science*, *7*(10), 9658-9667.

Hayyan, M., Mjalli, F. S., Hashim, M. A., & AlNashef, I. M. (2010). A novel technique for separating glycerine from palm oil-based biodiesel using ionic liquids. *Fuel Processing Technology*, *91*(1), 116-120. https://doi.org/https://doi.org/10.1016/j.fuproc.2009.09.002

Hayyan, M., Mjalli, F. S., Hashim, M. A., & AlNashef, I. M. (2011b). Electrochemical generation of superoxide ion in ionic liquid 1-(3-Methoxypropyl)-1-methylpiperidinium bis (trifluoromethylsulfonyl) imide. In *IOP Conference Series: Materials Science and Engineering, 17* (1), 1-4.

Hayyan, M., Mjalli, F. S., Hashim, M. A., & AlNashef, I. M. (2012). Generation of superoxide ion in pyridinium, morpholinium, ammonium, and sulfonium-based ionic liquids and the application in the destruction of toxic chlorinated phenols. *Industrial & Engineering Chemistry Research*, *51*(32), 10546-10556.

Hayyan, M., Mjalli, F. S., Hashim, M. A., & AlNashef, I. M. (2013). An investigation of the reaction between 1-butyl-3-methylimidazolium trifluoromethanesulfonate and superoxide ion. *Journal of Molecular Liquids*, *181*, 44-50.

Hayyan, M., Mjalli, F. S., Hashim, M. A., AlNashef, I. M., Al-Zahrani, S. M., & Chooi, K. L. (2012a). Generation of superoxide ion in 1-butyl-1-methylpyrrolidinium trifluoroacetate and its application in the destruction of chloroethanes. *Journal of Molecular Liquids*, *167*, 28-33.

Hayyan, M., Mjalli, F. S., Hashim, M. A., AlNashef, I. M., Al-Zahrani, S. M., & Chooi, K. L. (2012b). Long term stability of superoxide ion in piperidinium, pyrrolidinium and phosphonium cations-based ionic liquids and its utilization in the destruction of chlorobenzenes. *Journal of Electroanalytical Chemistry*, *664*, 26-32.

Hayyan, M., Mjalli, F. S., Hashim, M. A., AlNashef, I. M., & Tan, X. M. (2011a). Electrochemical reduction of dioxygen in Bis (trifluoromethylsulfonyl) imide based ionic liquids. *Journal of Electroanalytical Chemistry*, *657*(1), 150-157.

Hayyan, M., Mjalli, F. S., Hashim, M. A., AlNashef, I. M., Tan, X. M., & Chooi, K. L. (2010). Generation of superoxide ion in trihexyl (tetradecyl) phosphonium bis (trifluoromethylsulfonyl) imide room temperature ionic liquid. *Journal of Applied Sciences*, *10*(12), 1176-1180.

He, D., Wang, D., Luo, H., Zeng, Y., Zeng, G., Li, J., & Pan, X. (2023). Tungsten disulfide (WS$_2$) is a highly active co-catalyst in Fe(III)/H$_2$O$_2$ Fenton-like reactions for efficient acetaminophen degradation. *Science of The Total Environment*, *871*, Article#162151.

Henze, G. (2001). Analytical voltammetry and polarography. In *Handbook of Analytical Techniques*, 785-825.

Hochberg, M. C., Altman, R. D., April, K. T., Benkhalti, M., Guyatt, G., McGowan, J., ... & Tugwell, P. (2012). American College of Rheumatology 2012 recommendations for the use of nonpharmacologic and pharmacologic therapies in osteoarthritis of the hand, hip, and knee. *Arthritis Care & Research*, *64*(4), 465-474.

Holm, C., & Weis, J. J. (2005). The structure of ferrofluids: A status report. *Current Opinion in Colloid & Interface Science*, *10*(3), 133-140. https://doi.org/https://doi.org/10.1016/j .cocis.2005.07.005

Hu, R., Yang, S.-Q., Li, J.-Y., Sun, F., Liu, Z.-Q., Yang, J., Cui, Y.-H., & Zhang, B. (2023). Insight into micropollutant abatement during ultraviolet light-emitting diode combined electrochemical process: Reaction mechanism, contributions of reactive species and degradation routes. *Science of The Total Environment*, *876*, 162798.

Hu, Y., Chen, J., Le, Z. G., & Zheng, Q. (2005). Organic reactions in ionic liquids: Ionic liquids ethylammonium nitrate promoted Knoevenagel condensation of aromatic aldehydes with active methylene compounds. *Synthetic Communications*, *35*, 739-744. https://doi.org/10.1081/SCC-200050380

Huang, C., Yang, T., Li, M., Mai, J., Wu, S., Li, J., & Ma, J. (2023). Generation of hydroxyl radicals via activation of Cr(VI) by UVA-LED for rapid decontamination: The important role of Cr(V). *Journal of Hazardous Materials*, *442*, Article#129913.

Huang, X. J., Aldous, L., O'Mahony, A. M., Del Campo, F. J., & Compton, R. G. (2010). Toward membrane-free amperometric gas sensors: A microelectrode array approach. *Analytical Chemistry*, *82*(12), 5238-5245.

Huang, X. J., Rogers, E. I., Hardacre, C., & Compton, R. G. (2009b). The reduction of oxygen in various room temperature ionic liquids in the temperature range 293- 318 K: Exploring the applicability of the Stokes- Einstein relationship in room temperature ionic liquids. *Journal of Physical Chemistry B*, *113*(26), 8953-8959.

Huddleston, J. G., Willauer, H. D., Swatloski, R. P., Visser, A. E., & Rogers, R. D. (1998). Room temperature ionic liquids as novel media for 'clean' liquid–liquid extraction [10.1039/A803999B]. *Chemical Communications*(16), 1765-1766.

Humayun, S., Hayyan, M., Alias, Y., & Hayyan, A. (2021). Oxidative degradation of acetaminophen using superoxide ion generated in ionic liquid/aprotic solvent binary system. *Separation and Purification Technology*, *270*, Article#118730.

Ionic Liquids-Properties and Preparation. (2005). *Metal Catalysed Reactions in Ionic Liquids.* In P. Dyson & G. Tilmann (Eds.), (pp. 15-40). Springer Netherlands. https://doi.org/10.1007/1-4020-3915-8_2

Islam, M. M., Ferdousi, B. N., Okajima, T., & Ohsaka, T. (2005). A catalytic activity of a mercury electrode towards dioxygen reduction in room-temperature ionic liquids. *Electrochemistry Communications*, *7*(7), 789-795.

Islam, M. M., Imase, T., Okajima, T., Takahashi, M., Niikura, Y., Kawashima, N., & Ohsaka, T. (2009a). Stability of superoxide ion in imidazolium cation-based room-temperature ionic liquids. *The Journal of Physical Chemistry A*, *113*(5), 912-916.

Islam, M. M., Imase, T., Okajima, T., Takahashi, M., Niikura, Y., Kawashima, N., ... & Ohsaka, T. (2009). Stability of superoxide ion in imidazolium cation-based room-temperature ionic liquids. *The Journal of Physical Chemistry A*, *113*(5), 912-916.

Islam, M. M., & Ohsaka, T. (2008a). Roles of ion pairing on electroreduction of dioxygen in imidazolium-cation-based room-temperature ionic liquid. *Journal of Physical Chemistry C*, *112*(4), 1269-1275.

Islam, M. M., Saha, M. S., Okajima, T., & Ohsaka, T. (2005). Current oscillatory phenomena based on electrogenerated superoxide ion at the HMDE in dimethylsulfoxide. *Journal of Electroanalytical Chemistry*, *577*(1), 145-154.

J., W. (2006). In *Analytical Electrochemistry* (Third ed., pp. 243). John Wiley & Sons. https://doi.org/https://doi.org/10.1002/0471790303.ch1

Jain, N., Wang, Y., Jones, S. K., Hawkett, B. S., & Warr, G. G. (2010). Optimized steric stabilization of aqueous ferrofluids and magnetic nanoparticles. *Langmuir*, *26*(6), 4465-4472.

Jallouli, N., Pastrana Martinez, L., Ribeiro, A. R. L., Moreira, N., Faria, J., Hentati, O., & Ksibi, M. (2017). Heterogeneous photocatalytic degradation of ibuprofen in ultrapure water, municipal and pharmaceutical industry wastewaters using a TiO_2 /UV-LED system. *Chemical Engineering Journal*, *334*, 976–984.

Janus, E., Goc-Maciejewska, I., Lozynski, M., & Pernak, J. (2006). Diels-Alder reaction in ionic liquids. *Tetrahedron Letters*, *47*, 4079-4083. https://doi.org/10.1016/j.tetlet.2006.03.172

Jastorff, B., Störmann, R., Ranke, J., Mölter, K., Stock, F., Oberheitmann, B., & Filser, J. (2003). How hazardous are ionic liquids? Structure–activity relationships and biological testing as important elements for sustainability evaluation [10.1039/B211971D]. *Green Chemistry*, *5*(2), 136-142.

Jiang, M., Lu, J., Ji, Y., & Kong, D. (2017). Bicarbonate-activated persulfate oxidation of acetaminophen. *Water Research*, *116*, 324-331. https://doi.org/10.1016/j.watres.2017.03.043

Jiang, T., Gao, H., Han, B., Zhao, G., Chang, Y., Wu, W., & Yang, G. (2004). Ionic liquid catalyzed Henry reactions. *Tetrahedron Letters*, *45*(12), 2699-2701.

Jusys, Z., Schnaidt, J., & Behm, R. J. (2019). O_2 reduction on a Au film electrode in an ionic liquid in the absence and presence of Mg^{2+} ions: Product formation and adlayer dynamics. *The Journal of Chemical Physics*, *150*(4), 041724.

Katayama, Y., Onodera, H., Yamagata, M., & Miura, T. (2004a). Electrochemical reduction of oxygen in some hydrophobic room-temperature molten salt systems. *Journal of The Electrochemical Society*, *151*(1), Article#A59.

Katayama, Y., Onodera, H., Yamagata, M., & Miura, T. (2004b). Electrochemical reduction of oxygen in some hydrophobic room-temperature molten salt systems. *Journal of the Electrochemical Society*, *151*(1), A59-A63.

Katayama, Y., Sekiguchi, K., Yamagata, M., & Miura, T. (2005). Electrochemical behavior of oxygen/superoxide ion couple in 1-butyl-1-methylpyrrolidinium bis (trifluoromethylsulfonyl) imide room-temperature molten salt. *Journal of the Electrochemical Society*, *152*(8), E247-E250.

Khan, A., & Zhao, C. (2014). Enhanced performance in mixture DMSO/ionic liquid electrolytes: Toward rechargeable Li–O2 batteries. *Electrochemistry Communications*, *49*, 1–4.

Khan, A., & Zhao, C. (2016). Oxygen reduction reactions in aprotic ionic liquids based mixed electrolytes for high performance of Li–O_2 batteries. *ACS Sustainable Chemistry & Engineering*, *4*(2), 506-513.

Knowles, P. F., Gibson, J. F., Pick, F. M., & Bray, R. C. (1969). Electron-spin-resonance evidence for enzymic reduction of oxygen to a free radical, the superoxide ion. *Biochem J*, *111*(1), 53-58.

Kram, M. L., Stang, P. M., & Seligman, P. F. (1989). Adsorption and desorption of tributyltin in sediments of San Diego Bay and Pearl Harbor. *Applied Organometallic Chemistry*, *3*(6), 523-536.

Krawietz, T. R., Murray, D. K., & Haw, J. F. (1998). Alkali metal oxides, peroxides, and superoxides: A multinuclear MAS NMR study. *The Journal of Physical Chemistry A*, *102*(45), 8779-8785.

Kremer, K., & Grest, G. S. (1990). Dynamics of entangled linear polymer melts: A molecular-dynamics simulation. *The Journal of Chemical Physics*, *92*(8), 5057-5086.

Kummerer, K. (2009a). Antibiotics in the aquatic environment--a review--part I. *Chemosphere*, *75*(4), 417-434.

Kummerer, K. (2009b). The presence of pharmaceuticals in the environment due to human use--present knowledge and future challenges. *J Environ Manage*, *90*(8), 2354-2366.

Laoire, C. O., Mukerjee, S., Abraham, K. M., Plichta, E. J., & Hendrickson, M. A. (2009). Elucidating the mechanism of oxygen reduction for lithium-air battery applications. *Journal of Physical Chemistry C*, *113*(46), 20127-20134.

Lee, J., Murugappan, K., Arrigan, D. W. M., & Silvester, D. S. (2013). Oxygen reduction voltammetry on platinum macrodisk and screen-printed electrodes in ionic liquids: Reaction of the electrogenerated superoxide species with compounds used in the paste of Pt screen-printed electrodes? *Electrochimica Acta*, *101*(0), 158-168.

Li, S., Lin, Y., Xie, H., Zhang, S., & Xu, J. (2006). Brønsted guanidine acid-base ionic liquids: novel reaction media for the palladium-catalyzed Heck reaction. *Org Lett*, *8*(3), 391-394.

Li, X., Yao, Y., & Wang, B. (2022). Incorporating Fe-O cluster in multivariate (MTV) metal–organic frameworks for promoting visible-light photo-Fenton degradation of micropollutants from water. *Chemical Engineering Journal*, *446*, Article#137446.

Liang, J., Fu, L., Gao, K., & Duan, X. (2022). Accelerating radical generation from peroxymonosulfate by confined variable Co species toward ciprofloxacin mineralization: ROS quantification and mechanisms elucidation. *Applied Catalysis B: Environmental*, *315*, Article#121542.

Lin, J.-H., Zhang, C.-P., Zhu, Z.-Q., Chen, Q.-Y., & Xiao, J.-C. (2009). A novel pyrrolidinium ionic liquid with 1,1,2,2-tetrafluoro-2-(1,1,2,2-tetrafluoroethoxy)ethanesulfonate anion as a recyclable reaction medium and efficient catalyst for Friedel–Crafts alkylations of indoles with nitroalkenes. *Journal of Fluorine Chemistry*, *130*(4), 394-398.

Liu, B., Mullen, L., Payne, E. M., & Linden, K. G. (2023). Accelerated ultraviolet treatment of carbamazepine and NDMA in water under 222 nm irradiation. *Environmental Science & Technology,* 57(47), 18909–18917.

Liu, N., Lei, Z.-D., Wang, T., Wang, J.-J., Zhang, X.-D., Xu, G., & Tang, L. (2016a). Radiolysis of carbamazepine aqueous solution using electron beam irradiation combining with hydrogen peroxide: Efficiency and mechanism. *Chemical Engineering Journal*, *295*, 484-493.

Liu, N., Lei, Z. D., Wang, T., Wang, J. J., Zhang, X. D., Xu, G., & Tang, L. (2016b). Radiolysis of carbamazepine aqueous solution using electron beam irradiation combining with hydrogen peroxide: Efficiency and mechanism. *Chemical Engineering Journal*, *295*, 484-493.

Liu, T., Xie, Z., Zhou, P., Xiong, Z., Zhang, H., Pan, Z., & Lai, B. (2022). Enhanced degradation of carbamazepine by iron/S(IV) system using a novel S(IV) source. *Chemical Engineering Journal*, *431*, 133464.

Liu, X., Xu, P., Zhu, P., Yang, Z., Wu, R., & Baolin, H. (2023). Rapid oxidation of acetaminophen with zero-valent copper induced hydrogen peroxide process in

presence of ferric ion and chloride ion. *Chemical Engineering Journal*, *470*, Article#144202.

Maciorowski, A., Sims, J., Little, L., & Gerrard, E. (1981). Bioassays: Procedures and results. *Journal (Water Pollution Control Federation)*, 974-993.

Mamantov, G. P. A. I. (1994). *Chemistry of nonaqueous solutions : current progress*. VCH.

Mann, J. P., McCluskey, A., & Atkin, R. (2009). Activity and thermal stability of lysozyme in alkylammonium formate ionic liquids—influence of cation modification. *Green Chemistry*, *11*(6), 785-792.

Marcinek, A., Zielonka, J., Gębicki, J., Gordon, C. M., & Dunkin, I. R. (2001). Ionic Liquids: novel media for characterization of radical ions. *The Journal of Physical Chemistry A*, *105*(40), 9305-9309.

Marti, E., Variatza, E., & Balcazar, J. L. (2014). The role of aquatic ecosystems as reservoirs of antibiotic resistance. *Trends Microbiol*, *22*(1), 36-41. https://doi.org/10.1016/j.tim.2013.11.001

Martínez, C., Canle L, M., Fernández, M. I., Santaballa, J. A., & Faria, J. (2011). Kinetics and mechanism of aqueous degradation of carbamazepine by heterogeneous photocatalysis using nanocrystalline TiO2, ZnO and multi-walled carbon nanotubes–anatase composites. *Applied Catalysis B: Environmental*, *102*(3), 563-571.

Martiz, B., Keyrouz, R., Gmouh, S., Vaultier, M., & Jouikov, V. (2004). Superoxide-stable ionic liquids: New and efficient media for electrosynthesis of functional siloxanes. *Chemical Communications*, *2004*(6), 674-675.

McClune, G. J., & Fee, J. A. (1976). Stopped flow spectrophotometric observation of superoxide dismutation in aqueous solution. *FEBS Lett*, *67*(3), 294-298.

McCord, J. M., & Fridovich, I. (1969). Superoxide dismutase: an enzymic function for erythrocuprein (hemocuprein). *Journal of Biological Chemistry*, *244*(22), 6049-6055.

Mecerreyes, D. (2011). Polymeric ionic liquids: Broadening the properties and applications of polyelectrolytes. *Progress in Polymer Science*, *36*(12), 1629-1648.

Merritt, M. V., & Sawyer, D. T. (1970). Electrochemical studies of the reactivity of superoxide ion with several alkyl halides in dimethyl sulfoxide. *The Journal of Organic Chemistry*, *35*(7), 2157-2159.

Michelson, A. M., McCord, J. M., & Fridovich, I. (1977). *Superoxide and superoxide dismutases*. Academic Press.

206

Miran, M. S., Yasuda, T., Susan, M. A. B. H., Dokko, K., & Watanabe, M. (2014). Binary protic ionic liquid mixtures as a proton conductor: High fuel cell reaction activity and facile proton transport. *The Journal of Physical Chemistry C*, *118*(48), 27631-27639.

Mirjafari, A., Pham, L. N., McCabe, J. R., Mobarrez, N., Salter, E. A., Wierzbicki, A., & Davis, J. H. (2013). Building a bridge between aprotic and protic ionic liquids [10.1039/C2RA22752E]. *RSC Advances*, *3*(2), 337-340.

Mohammad, M., Khan, A. Y., Subhani, M. S., Bibi, N., Ahmad, S., & Saleemi, S. (2001). Kinetics and electrochemical studies on superoxide. *Research on Chemical Intermediates*, *27*(3), 259-267.

Mohtasham, H., Rostami, M., Gholipour, B., Sorouri, A. M., Ehrlich, H., Ganjali, M. R., & Luque, R. (2023). Nano-architecture of MOF (ZIF-67)-based Co3O4 NPs@N-doped porous carbon polyhedral nanocomposites for oxidative degradation of antibiotic sulfamethoxazole from wastewater. *Chemosphere*, *310*, Article#136625.

Monaco, S., Arangio, A. M., Soavi, F., Mastragostino, M., Paillard, E., & Passerini, S. (2012). An electrochemical study of oxygen reduction in pyrrolidinium-based ionic liquids for lithium/oxygen batteries. *Electrochimica Acta*, *83*(0), 94-104.

Monteil, H., Péchaud, Y., Oturan, N., & Oturan, M. A. (2019). A review on efficiency and cost effectiveness of electro- and bio-electro-Fenton processes: Application to the treatment of pharmaceutical pollutants in water. *Chemical Engineering Journal*, *376*, Article#119577. https://doi.org/https://doi.org/10.1016/j.cej.2018.07.179

Moore, R. A., & Moore, N. (2016). Paracetamol and pain: the kiloton problem. *Eur J Hosp Pharm*, *23*(4), 187-188.

Morrison, M. M., Roberts, J. L., Jr., & Sawyer, D. T. (1979). Oxidation-reduction chemistry of hydrogen peroxide in aprotic and aqueous solutions. *Inorganic Chemistry*, *18*(7), 1971-1973.

Münstedt, H. (2011). Rheological properties and molecular structure of polymer melts. *Soft Matter*, *7*(6), 2273-2283.

Murgolo, S., Franz, S., Arab, H., Bestetti, M., Falletta, E., & Mascolo, G. (2019). Degradation of emerging organic pollutants in wastewater effluents by electrochemical photocatalysis on nanostructured TiO2 meshes. *Water Research*, *164*, Article#114920. https://doi.org/https://doi.org/10.1016/j.watres.2019.114920

Murray, S. M., O'Brien, R. A., Mattson, K. M., Ceccarelli, C., Sykora, R. E., West, K. N., & Davis Jr, J. H. (2010). The fluid-mosaic model, homeoviscous adaptation, and ionic liquids: dramatic lowering of the melting point by side-chain unsaturation. *Angewandte Chemie International Edition*, *49*(15), 2755-2758.

Nagoshi, N., Nakashima, H., & Fehlings, M. G. (2015). Riluzole as a neuroprotective drug for spinal cord injury: From bench to bedside. *Molecules*, *20*(5), 7775-7789.

Neale, A. R., Li, P., Jacquemin, J., Goodrich, P., Ball, S. C., Compton, R. G., & Hardacre, C. (2016). Effect of cation structure on the oxygen solubility and diffusivity in a range of bis{(trifluoromethyl)sulfonyl}imide anion based ionic liquids for lithium–air battery electrolytes [10.1039/C5CP07160G]. *Physical Chemistry Chemical Physics*, *18*(16), 11251-11262.

Nentwig, G. (2008). Another example of effects of pharmaceuticals on aquatic invertebrates: Fluoxetine and ciprofloxacin. In K. Kümmerer (Ed.), *Pharmaceuticals in the Environment: Sources, Fate, Effects and Risks* (pp. 205-222). Springer Berlin Heidelberg.

Nghia, T. H., Khanh, V. T., Vu, C. T., Oanh, N. T. K., Van Anh, N. T., Luyen, L. H., & Van Hoi, B. (2023). Removal of carbamazepine in aqueous solution by TiO_2 ceramic photo-catalyst under simulated solar light: kinetics, effects of environmental Factors and degradation pathways. *Water*, *15*(8), 1583. https://www.mdpi.com/2073-4441/15/8/1583

Nicholson, R. S. (1965). Theory and application of cyclic voltammetry for measurement of electrode reaction kinetics. *Analytical Chemistry*, *37*(11), 1351-1355.

Noda, A., Hayamizu, K., & Watanabe, M. (2001). Pulsed-gradient spin−Echo 1H and 19F NMR ionic diffusion coefficient, viscosity, and ionic conductivity of non-chloroaluminate room-temperature ionic liquids. *The Journal of Physical Chemistry B*, *105*(20), 4603-4610.

Noda, A., Susan, M. A. B. H., Kudo, K., Mitsushima, S., Hayamizu, K., & Watanabe, M. (2003). Brønsted acid−base ionic liquids as proton-conducting nonaqueous electrolytes. *The Journal of Physical Chemistry B*, *107*(17), 4024-4033.

Nolte, T., & Peijnenburg, W. (2018). Use of quantum-chemical descriptors to analyze reaction rate constants between organic chemicals and superoxide/hydroperoxyl ($O_2^{\cdot-}$/$HO_2\cdot$). *Free Radical Research*, *52*, 1-411.

O'Mahony, A. M., Silvester, D. S., Aldous, L., Hardacre, C., & Compton, R. G. (2008). Effect of water on the electrochemical window and potential limits of room-temperature ionic liquids. *Journal of Chemical & Engineering Data*, *53*(12), 2884-2891.

Oae, S., Takata, T., & Kim, Y. H. (1981). Reaction of organic sulfur compounds with superoxide anion—III: Oxidation of organic sulfur compounds to sulf1nic and sulfonic acids. *Tetrahedron*, *37*(1), 37-44.

Ogoshi, T., Onodera, T., Yamagishi, T.-a., & Nakamoto, Y. (2008). Green polymerization of phenol in ionic liquids. *Macromolecules*, *41*(22), 8533-8536.

Ohno, H. (2005). *Electrochemical Aspects of Ionic Liquids*. Wiley. https://books.google.com.my/books?id=sSEpAAAAYAAJ

Ohno, H., & Fukumoto, K. (2007). Amino acid ionic liquids. *Accounts of Chemical Research*, *40*(11), 1122-1129. https://doi.org/10.1021/ar700053z

P., K. S. (August 5, 2023). *The Top 300 of 2020, ClinCalc DrugStats Database* Version 2022.08). https://clincalc.com/DrugStats/Top300Drugs.aspx

Parker, A. J. (1962). The effects of solvation on the properties of anions in dipolar aprotic solvents. *Quarterly Reviews, Chemical Society*, *16*(2), 163-187.

Peric, B., Sierra, J., Martí, E., Cruañas, R., Garau, M. A., Arning, J., ... & Stolte, S. (2013). (Eco) toxicity and biodegradability of selected protic and aprotic ionic liquids. *Journal of Hazardous Materials*, *261*, 99-105.

Perrott, D. A., Piira, T., Goodenough, B., & Champion, G. D. (2004). Efficacy and safety of acetaminophen vs ibuprofen for treating children's pain or fever: a meta-analysis. *Archives of Pediatrics & Adolescent Medicine*, *158*(6), 521-526.

Posselt, M., Jaeger, A., Schaper, J. L., Radke, M., & Benskin, J. P. (2018). Determination of polar organic micropollutants in surface and pore water by high-resolution sampling-direct injection-ultra high performance liquid chromatography-tandem mass spectrometry [10.1039/C8EM00390D]. *Environmental Science: Processes & Impacts*, *20*(12), 1716-1727.

Pozo-Gonzalo, C., Howlett, P. C., Hodgson, J. L., Madsen, L. A., MacFarlane, D. R., & Forsyth, M. (2014). Insights into the reversible oxygen reduction reaction in a series of phosphonium-based ionic liquids . *Physical Chemistry Chemical Physics*, *16*(45), 25062-25070.

Pozo-Gonzalo, C., Torriero, A. A., Forsyth, M., MacFarlane, D. R., & Howlett, P. C. (2013). Redox chemistry of the superoxide ion in a phosphonium-based ionic liquid in the presence of water. *The Journal of Physical Chemistry Letters*, *4*(11), 1834-1837.

Prasanna.V, L., & Avisar, D. (2022). Investigation of the degradation behavior of cyclophosphamide by catalytic ozonation based on $Mg(OH)_2$. *Energies*, *15*(6), Article#2274.

Prosser, R. S., & Sibley, P. K. (2015). Human health risk assessment of pharmaceuticals and personal care products in plant tissue due to biosolids and manure amendments, and wastewater irrigation. *Environment International*, *75*, 223-233.

Qiang, L., Cheng, J., Yi, J., Rotchell, J. M., Zhu, X., & Zhou, J. (2016). Environmental concentration of carbamazepine accelerates fish embryonic development and disturbs larvae behavior. *Ecotoxicology*, *25*(7), 1426-1437. https://doi.org/10.1007/s10646-016-1694-y

Qiao, K., & Chiaki, Y. (2006). Koch carbonylation of tertiary alcohols in the presence of acidic ionic liquids. *Catalysis Communications*, *7*, 450-453.

Quan, P., le, P., Tran, V., nguyen van, H., Vo, T., & Nguyen, Q. (2019). Carbonate solvents and ionic liquid mixtures as an electrolyte to improve cell safety in sodium-ion batteries. *Journal of Chemistry*, *2019*.

Ramírez, R. E., Torres-González, L. C., Hernández, A., García, A., & Sánchez, E. M. (2010). Conductivity and viscosity behavior of asymmetric phosphonium iodides. *The Journal of Physical Chemistry B*, *114*(12), 4271-4275.

Randström, S., Appetecchi, G., Lagergren, C., Moreno, A., & Passerini, S. (2007a). The influence of air and its components on the cathodic stability of N-butyl-N-methylpyffolidinium bis(trifluoromethanesulfonyl)imide. *Electrochimica Acta*, *53*, 1837-1842.

Ranke, J., Mölter, K., Stock, F., Bottin-Weber, U., Poczobutt, J., Hoffmann, J., & Jastorff, B. (2004). Biological effects of imidazolium ionic liquids with varying chain lengths in acute Vibrio fischeri and WST-1 cell viability assays. *Ecotoxicol Environ Saf*, *58*(3), 396-404. https://doi.org/10.1016/s0147-6513(03)00105-2

Reichardt, C. (2007). Solvents and solvent effects: An introduction. *Organic Process Research & Development*, *11*(1), 105-113. https://doi.org/10.1021/op0680082

René, A., Hauchard, D., Lagrost, C., & Hapiot, P. (2009). Superoxide protonation by weak acids in imidazolium based ionic liquids. *The Journal of Physical Chemistry B*, *113*(9), 2826-2831.

Rivera-Utrilla, J., Gómez-Pacheco, C. V., Sánchez-Polo, M., López-Peñalver, J. J., & Ocampo-Pérez, R. (2013). Tetracycline removal from water by adsorption/bioadsorption on activated carbons and sludge-derived adsorbents. *J Environ Manage*, *131*, 16-24.

Rivera-Utrilla, J., Sanchez-Polo, M., Ferro-Garcia, M. A., Prados-Joya, G., & Ocampo-Perez, R. (2013). Pharmaceuticals as emerging contaminants and their removal from water. A review. *Chemosphere*, *93*(7), 1268-1287. 9

Rofika, R. N. S., Honggowiranto, W., Jodi, H., Sudaryanto, S., Kartini, E., & Hidayat, R. (2019). The effect of acetonitrile as an additive on the ionic conductivity of imidazolium-based ionic liquid electrolyte and charge-discharge capacity of its Li-ion battery. *Ionics*, *25*, 3661-3671.

Rogers, E. I., Huang, X. J., Dickinson, E. J., Hardacre, C., & Compton, R. G. (2009). Investigating the mechanism and electrode kinetics of the oxygen| superoxide (O_2| $O_2^{\bullet-}$) couple in various room-temperature ionic liquids at gold and platinum electrodes in the temperature range $298-318$ K. *The Journal of Physical Chemistry C*, *113*(41), 17811-17823.

Rogers, R. D. (2007). Reflections on ionic liquids. *Nature*, *447*(7147), 917-918.

Rogers, R. D., & Seddon, K. R. (2003). Ionic liquids--solvents of the future? *Science*, *302*(5646), 792-793.

Rogers, R. D., Seddon, K. R., & Volkov, S. (2012). *Green industrial applications of ionic liquids* (Vol. 92). Springer Science & Business Media.

S.P., K. (2023). *The Top 300 of 2020* Version 2022.08.). ClinCalc: https://clincalc.com/DrugStats/Top300Drugs.aspx.

Sahoo, S., Joseph, T., & Halligudi, S. B. (2006). Mannich reaction in Brönsted acidic ionic liquid: A facile synthesis of β-amino carbonyl compounds. *Journal of Molecular Catalysis A: Chemical*, *244*(1), 179-182.

Sanganyado, E., Lu, Z., Fu, Q., Schlenk, D., & Gan, J. (2017). Chiral pharmaceuticals: A review on their environmental occurrence and fate processes. *Water Research*, *124*, 527-542.

Santos, E., Albo, J., & Irabien, A. (2014). Magnetic ionic liquids: synthesis, properties and applications [10.1039/C4RA05156D]. *RSC Advances*, *4*(75), 40008-40018.

Sawyer, D. T. (1992a). *Oxygen Chemistry*.

Sawyer, D. T. (2020, 2021/9/20/). *Superoxide chemistry*. McGraw-Hill Education. https://www.accessscience.com/content/superoxide-chemistry/669650

Sawyer, D. T., & Roberts, J. L. (1966). Electrochemistry of oxygen and superoxide ion in dimethylsulfoxide at platinum, gold and mercury electrodes. *Journal of Electroanalytical Chemistry (1959)*, *12*(2), 90-101.

Sawyer, D. T., & Roberts, J. L. (1988). Hydroxide ion: an effective one-electron reducing agent? *Accounts of Chemical Research*, *21*(12), 469-476.

Sawyer, D. T., S. Jeon, and P.K. Tsang (1992b). *Methods for producing superoxide ion in situ*. G. Patents.

Sawyer, D. T., Sobkowiak, A., & Roberts, J. L. (1995). *Electrochemistry for chemists* (2nd ed ed.). Wiley. https://cir.nii.ac.jp/crid/1130000798045572224

Sawyer, D. T., & Valentine, J. S. (1981). How super is superoxide? *Accounts of Chemical Research*, *14*(12), 393-400.

Shen, M., Zhang, X., Zhao, S., Cai, Y., & Wang, S. (2023). A novel photocatalytic system coupling metal-free Carbon/g-C3N4 catalyst with persulfate for highly efficient degradation of organic pollutants. *Chemosphere*, *314*, 137728.

Shen, Y., Kennedy, D. F., Greaves, T. L., Weerawardena, A., Mulder, R. J., Kirby, N., Song, G., & Drummond, C. J. (2012). Protic ionic liquids with fluorous anions:

physicochemical properties and self-assembly nanostructure [10.1039/C2CP40463J]. *Physical Chemistry Chemical Physics*, *14*(22), 7981-7992.

Shkrob, I. A., & Wishart, J. F. (2009). Charge trapping in imidazolium ionic liquids. *The Journal of Physical Chemistry B*, *113*(16), 5582-5592. https://doi.org/10.1021/jp811495e

Siddiqui, S. A., Narkhede, U. C., Palimkar, S. S., Daniel, T., Lahoti, R. J., & Srinivasan, K. V. (2005). Room temperature ionic liquid promoted improved and rapid synthesis of 2,4,5-triaryl imidazoles from aryl aldehydes and 1,2-diketones or α-hydroxyketone. *Tetrahedron*, *61*(14), 3539-3546.

Silvester, D. S., Rogers, E. I., Barrosse-Antle, L. E., Broder, T. L., & Compton, R. G. (2008). The electrochemistry of simple inorganic molecules in room temperature ionic liquids. *Journal of the Brazilian Chemical Society*, *19*, 611-620.

Silvester, D. S., Ward, K. R., Aldous, L., Hardacre, C., & Compton, R. G. (2008). The electrochemical oxidation of hydrogen at activated platinum electrodes in room temperature ionic liquids as solvents. *Journal of Electroanalytical Chemistry*, *618*(1), 53-60.

Sinensky, M. (1974). Homeoviscous Adaptation—A Homeostatic process that regulates the viscosity of membrane lipids in Escherichia coli. *Proceedings of the National Academy of Sciences*, *71*(2), Article#522.

Sisodiya, S. M., & Goldstein, D. B. (2007). Drug resistance in epilepsy: more twists in the tale. *Epilepsia*, *48*(12), 2369-2370.

Składanowski, A. C., Stepnowski, P., Kleszczyński, K., & Dmochowska, B. (2005). AMP deaminase in vitro inhibition by xenobiotics A potential molecular method for risk assessment of synthetic nitro- and polycyclic musks, imidazolium ionic liquids and N-glucopyranosyl ammonium salts. *Environ Toxicol Pharmacol*, *19*(2), 291-296.

Skoumal, M., Cabot, P.-L., Centellas, F., Arias, C., Rodríguez, R. M., Garrido, J. A., & Brillas, E. (2006). Mineralization of paracetamol by ozonation catalyzed with Fe^{2+}, Cu^{2+} and UVA light. *Applied Catalysis B: Environmental*, *66*(3), 228-240.

Sole, M., Shaw, J. P., Frickers, P. E., Readman, J. W., & Hutchinson, T. H. (2010). Effects on feeding rate and biomarker responses of marine mussels experimentally exposed to propranolol and acetaminophen. *Anal Bioanal Chem*, *396*(2), 649-656.

Song, C., & Zhang, J. (2008). Electrocatalytic oxygen reduction reaction. In J. Zhang (Ed.), *PEM Fuel Cell Electrocatalysts and Catalyst Layers: Fundamentals and Applications*, 89-134. Springer London.

Staemmler, V. (1979). Book Review: The donor-acceptor approach to molecular interactions. By V. Gutmann. *Angewandte Chemie International Edition in English*, *18*(7), 560-560.

Staines, A. G., Coughtrie, M. W., & Burchell, B. (2004). N-glucuronidation of carbamazepine in human tissues is mediated by UGT2B7. *Journal of Pharmacology and Experimental Therapeutics*, *311*(3), 1131-1137.

Stark, A., & Seddon, K. R. (2007). Ionic Liquids. In *Kirk-Othmer Encyclopedia of Chemical Technology*. https://doi.org/https://doi.org/10.1002/0471238961.ionisedd.a01

Stepnowski, P., Składanowski, A., Ludwiczak, A., & Laczyńska, E. (2004). Evaluating the cytotoxicity of ionic liquids using human cell line Hela. *Human & experimental toxicology*, *23*, 513-517.

Stepnowski, P., & Zaleska, A. (2005). Comparison of different advanced oxidation processes for the degradation of room temperature ionic liquids. *Journal of Photochemistry and Photobiology A: Chemistry*, *170*(1), 45-50.

Stock, F., Hoffmann, J., Ranke, J., Störmann, R., Ondruschka, B., & Jastorff, B. (2004). Effects of ionic liquids on the acetylcholinesterase – a structure–activity relationship consideration [10.1039/B402348J]. *Green Chemistry*, *6*(6), 286-290.

Suarez, P. A. Z., Consorti, C. S., Souza, R. F. d., Dupont, J., & Gonçalves, R. S. (2002). Electrochemical behavior of vitreous glass carbon and platinum electrodes in the ionic liquid 1-n-butyl-3-methylimidazolium trifluoroacetate. *Journal of the Brazilian Chemical Society*, *13*, 106-109.

Sugimoto, H., Matsumoto, S., & Sawyer, D. T. (1988). Degradation and dehalogenation of polychlorobiphenyls and halogenated aromatic molecules by superoxide ion and by electrolytic reduction. *Environmental Science & Technology*, *22*(10), 1182-1186.

Sun, J., Forsyth, M., & MacFarlane, D. R. (1998). Room-temperature molten salts based on the quaternary ammonium ion. *The Journal of Physical Chemistry B*, *102*(44), 8858-8864.

Sun, Q., Wang, X., Liu, Y., Xia, S., & Zhao, J. (2022). Activation of peroxymonosulfate by a floating oxygen vacancies - CuFe2O4 photocatalyst under visible light for efficient degradation of sulfamethazine. *Science of The Total Environment*, *824*, Article#153630.

Takamuku, T., Kyoshoin, Y., Shimomura, T., Kittaka, S., & Yamaguchi, T. (2009). Effect of water on structure of hydrophilic imidazolium-based ionic liquid. *The Journal of Physical Chemistry B*, *113*(31), 10817-10824.

Tan, S. H. S., Hong, C. C., Saha, S., Murphy, D., & Hui, J. H. (2020). Medications in COVID-19 patients: summarizing the current literature from an orthopaedic perspective. *Int Orthop*, *44*(8), 1599-1603.

Tang, M. C. Y., Wong, K. Y., & Chan, T. H. (2005). Electrosynthesis of hydrogen peroxide in room temperature ionic liquids and in situ epoxidation of alkenes. *Chemical Communications*, *2005*(10), 1345-1347.

Taylor, D., & Senac, T. (2014). Human pharmaceutical products in the environment−the "Problem" in perspective. *Chemosphere*(115), 95-99.

Tian, S., Yin, Y., Liu, M., Shi, L., Zhang, S., Asif, A. H., & Sun, H. (2023). Atomically dispersed Cu-N$_3$ on hollow spherical carbon nitride for acetaminophen degradation: Generation of ^{1}O$_2$ from H$_2$O$_2$. *Separation and Purification Technology*, *318*, Article#124016.

Tokuda, H., Ishii, K., Susan, M. A. B. H., Tsuzuki, S., Hayamizu, K., & Watanabe, M. (2006). Physicochemical properties and structures of room-temperature ionic liquids. 3. Variation of cationic structures. *The Journal of Physical Chemistry B*, *110*(6), 2833-2839.

Tsaplev, Y. B., & Trofimov, A. V. (2021). Potassium superoxide as an intricate source of superoxide anion. Elucidating the composition of its samples in dimethyl sulfoxide by reactions with (5,10,15,20-tetraphenylporphinato)manganese(III) chloride and curcumin. *Spectrochimica Acta Part A: Molecular and Biomolecular Spectroscopy*, *251*, Article#119425.

Tshibangu, P. N., Ndwandwe, S. N., & Dikio, E. (2011). Density, viscosity and conductivity study of 1-butyl-3-methylimidazolium bromide. *International Journal of Electrochemical Science*, *6*, 2201-2213.

Vasudevan, D., & Wendt, H. (1995). Electroreduction of oxygen in aprotic media. *Journal of Electroanalytical Chemistry*, *392*(1), 69-74.

Vayssière, P., Chaumont, A., & Wipff, G. (2005). Cation extraction by 18-crown-6 to a room-temperature ionic liquid: The effect of solvent humidity investigated by molecular dynamics simulations [10.1039/B412794C]. *Physical Chemistry Chemical Physics*, *7*(1), 124-135.

Ventura, S. P. M., Marques, C. S., Rosatella, A. A., Afonso, C. A. M., Gonçalves, F., & Coutinho, J. A. P. (2012). Toxicity assessment of various ionic liquid families towards Vibrio fischeri marine bacteria. *Ecotoxicol Environ Saf*, *76*, 162-168.

Villagrán, C., Aldous, L., Lagunas, M. C., Compton, R. G., & Hardacre, C. (2006). Electrochemistry of phenol in bis {(trifluoromethyl) sulfonyl} amide ([NTf$_2$]$^-$) based ionic liquids. *Journal of Electroanalytical Chemistry*, *588*(1), 27-31.

Visser, A. E., Swatloski, R. P., Reichert, W. M., Griffin, S. T., & Rogers, R. D. (2000). Traditional extractants in nontraditional solvents: Groups 1 and 2 extraction by crown ethers in room-temperature ionic liquids. *Industrial & Engineering Chemistry Research*, *39*(10), 3596-3604.

Visser, A. E., Swatloski, R. P., Reichert, W. M., Mayton, R., Sheff, S., Wierzbicki, A., & Rogers, R. D. (2002). Task-specific ionic liquids incorporating novel cations for the coordination and extraction of Hg2+ and Cd2+: synthesis, characterization, and extraction studies. *Environ Sci Technol*, *36*(11), 2523-2529.

Vogna, D., Marotta, R., Napolitano, A., & d'Ischia, M. (2002). Advanced oxidation chemistry of paracetamol. UV/H$_2$O$_2$-induced hydroxylation/degradation pathways and 15N-aided inventory of nitrogenous breakdown products. *The Journal of Organic Chemistry*, *67*(17), 6143-6151.

Wang, H., Liu, S., Liu, Y., Tang, Y., Dai, M., Chen, Q., & Deng, Y. (2022). Fe$_3$N nanoparticles embedded in N-doped porous magnetic graphene for peroxymonosulfate activation: Radical and nonradical mechanism. *Chemosphere*, *305*, Article#135317.

Wang, H., Xu, W., Su, L., Yang, Q., Shen, C., Chen, X., & Lu, Z. (2022). Ultra-adsorption enhancing peroxymonosulfate activation by ultrathin NiAl-layered double hydroxides for efficient degradation of sulfonamide antibiotics. *Journal of Cleaner Production*, *369*, Article# 133277.

Wang, J., & Zhuan, R. (2020). Degradation of antibiotics by advanced oxidation processes: An overview. *Science of The Total Environment*, *701*, Article#135023.

Wang, L., Liu, S. Y., Jiang, H. M., Chen, Y. Y., Wang, L. N., Duan, G. Y., & Wan, P. Y. (2018). Electrochemical generation of ROS in ionic liquid for the degradation of lignin model compound. *Journal of The Electrochemical Society*, *165*(11), H705-H710.

Wang, X., Zhou, Y., Ndayiragije, S., Wang, N., Tang, H., & Zhu, L. (2023). Advanced oxidative degradation of sulfamethoxazole by using bowl-like FeCuS@Cu2S@Fe0 catalyst to efficiently activate peroxymonosulfate. *Journal of Environmental Sciences*, *126*, 348-364.

Wang, Y.-Y., Li, W., & Dai, L.-Y. (2008). Brønsted acidic ionic liquids as efficient reaction medium for cyclodehydration of diethylene glycol. *Chinese Journal of Chemistry,26*, 1390-1394.

Wang, Y., & Dong, X. (2023). PMS activation by natural pyrite for APAP degradation: Underlying mechanism and long-term removal of APAP. *Catalysis Communications*, *177*, Article#106661.

Wang, Z., Liu, F., Gao, Y., Zhuang, W., Xu, L., Han, B., & Zhang, G. (2005). Hexagonal liquid crystalline phases formed in ternary systems of Brij 97−water−ionic liquids. *Langmuir*, *21*(11), 4931-4937.

Wang, Z., Meng, C. C., Zhang, W., Zhang, S. Z., Yang, B., & Zhang, Z. H. (2022). Honeycomb-like holey Co$_3$O$_4$ membrane triggered peroxymonosulfate activation for rapid degradation of organic contaminants. *Science of The Total Environment*, *814*, Article 152698.

Wasserscheid, P., & Welton, T. (2008). *Ionic liquids in synthesis* (Vol. 1). Wiley Online Library.

Weinberg, D. R., Gagliardi, C. J., Hull, J. F., Murphy, C. F., Kent, C. A., Westlake, B. C., & Meyer, T. J. (2012). Proton-coupled electron transfer. *Chemical Reviews*, *112*(7), 4016-4093.

Weisler, R. H. (2006). Carbamazepine extended-release capsules in bipolar disorder. *Neuropsychiatr Dis Treat*, *2*(1), 3-11.

Welton, T. (1999). Room-temperature ionic liquids. Solvents for synthesis and catalysis. *Chemical Reviews*, *99*(8), 2071-2084.

Wen, Y., Huang, C.-H., Ashley, D. C., Meyerstein, D., Dionysiou, D. D., Sharma, V. K., & Ma, X. (2022). Visible light-induced catalyst-free activation of peroxydisulfate: pollutant-dependent production of reactive species. *Environmental Science & Technology*, *56*(4), 2626-2636.

White, M. G., & Paris, D. (1982). *Engineering analysis--control of breathing atmospheres using alkali metal superoxides.* Demetrius Theodore, Paris.

Wilkes, J. S. (2002). A short history of ionic liquids—from molten salts to neoteric solvents. *Green Chemistry*, *4*(2), 73-80.

World Health, O. (2019). *World Health Organization model list of essential medicines: 21st list 2019* CC BY-NC-SA 3.0 IGO).

Wu, S., Zhang, L., & Chen, J. (2012). Paracetamol in the environment and its degradation by microorganisms. *Appl Microbiol Biotechnol*, *96*(4), Article# 875-884.

Xiao, C., & Zeng, X. (2013). In situ EQCM evaluation of the reaction between carbon dioxide and electrogenerated superoxide in ionic liquids. *Journal of The Electrochemical Society*, *160*(10), H749-H756.

Xu, A., Zhang, Y., Zhao, Y., & Wang, J. (2013). Cellulose dissolution at ambient temperature: Role of preferential solvation of cations of ionic liquids by a cosolvent. *Carbohydrate Polymers*, *92*(1), 540-544.

Xu, W., & Angell, C. A. (2003). Solvent-free electrolytes with aqueous solution-like conductivities. *Science*, *302*(5644), 422-425.

Yang, P., Li, S., Xiaofu, L., Xiaojing, A., Liu, D., & Huang, W. (2022). Singlet oxygen-dominated activation of peroxymonosulfate by CuO/MXene nanocomposites for efficient decontamination of carbamazepine under high salinity conditions: Performance and singlet oxygen evolution mechanism. *Separation and Purification Technology*, *285*, Article# 120288.

Yang, S.-R., He, C.-S., Xie, Z.-H., Li, L.-L., Xiong, Z.-K., Zhang, H., & Lai, B. (2022). Efficient activation of PAA by FeS for fast removal of pharmaceuticals: The dual role of sulfur species in regulating the reactive oxidized species. *Water Res*, *217*, Article# 118402.

Yang, Y.-l., Huang, Z., Liu, Y.-y., Guo, D., Zhang, Q., & Hong, J.-m. (2023). Mechanism exploration of highly conductive Ni-metal organic frameworks/reduced graphene oxide heterostructure for electrocatalytic degradation of paracetamol: Functions of metal sites, organic ligands, and rGO basement. *Journal of Colloid and Interface Science*, *629*, 667-682.

Yavari, I., & Kowsari, E. (2007). Ionic liquids as novel and recyclable reaction media for N-alkylation of amino-9,10-anthraquinones by trialkyl phosphites. *Tetrahedron Letters*, *48*, 3753-3756.

Ye, Y., Hu, X., Pu, C., Ren, G., Lu, G., & Zhu, M. (2023). Efficient carbamazepine degradation with Fe^{3+} doped 1T/2H hybrid molybdenum disulfide as peroxymonosulfate activator under high salinity wastewater. *Chemosphere*, *336*, Article#139245.

Yokozeki, A., Kasprzak, D., & Shiflett, M. (2007). Thermal effect on C-H stretching vibrations of the imidazolium ring in ionic liquids. *Physical Chemistry Chemical Physics, PCCP*, *9*, 5018-5026.

Yoshizawa, M., Xu, W., & Angell, C. A. (2003). Ionic liquids by proton transfer: Vapor pressure, conductivity, and the relevance of Δp K a from aqueous solutions. *Journal of the American Chemical Society*, *125*(50), 15411-15419.

Yu, M., Liu, C., Zhao, H., Yang, Y., & Sun, J. (2020). The effects of 1-hexyl-3-methylimidazolium bromide on embryonic development and reproduction in Daphnia magna. *Ecotoxicol Environ Saf*, *190*, Article# 110137.

Yu, S., Zhang, R., Dang, Y., Zhou, Y., & Zhu, J.-J. (2022). Electrochemical activation of peroxymonosulfate at $Ti/La_2O_3-PbO_2$ anode to enhance the degradation of typical antibiotic wastewater. *Separation and Purification Technology*, *294*, Article# 121164.

Yu, Y., Xiong, Z., Huang, B., Wang, X., Du, Y., He, C., & Lai, B. (2022a). Synchronous removal of pharmaceutical contaminants and inactivation of pathogenic microorganisms in real hospital wastewater by electro-peroxone process. *Environment International*, *168*, Article# 107453.

Yuan, X.-Z., Alzate, V., Xie, Z., Ivey, D. G., Dy, E., & Qu, W. (2014). Effect of water and dimethyl sulfoxide on oxygen reduction reaction in bis(trifluoromethanesulfonyl)imide-based ionic liquids. *Journal of The Electrochemical Society*, *161*(4), A458-A466.

Zech, O., Kellermeier, M., Thomaier, S., Maurer, E., Klein, R., Schreiner, C., & Kunz, W. (2009). Alkali metal oligoether carboxylates—A new class of ionic liquids. *Chemistry – A European Journal*, *15*(6), 1341-1345.

Zhang, C., Zhang, S., Zhu, L., Wang, J., Wang, J., & Zhou, T. (2017). The acute toxic effects of 1-alkyl-3-methylimidazolium nitrate ionic liquids on Chlorella vulgaris and Daphnia magna. *Environ Pollut*, *229*, 887-895.

Zhang, D., Okajima, T., Matsumoto, F., & Ohsaka, T. (2004). Electroreduction of dioxygen in 1-n-alkyl-3-methylimidazolium Tetrafluoroborate Room-Temperature Ionic Liquids. *Journal of the Electrochemical Society*, *151*, D31-D37.

Zhang, H., Cao, B., Liu, W., Lin, K., & Feng, J. (2012). Oxidative removal of acetaminophen using zero valent aluminum-acid system: Efficacy, influencing factors, and reaction mechanism. *Journal of Environmental Sciences*, *24*(2), 314-319.

Zhang, J., Jiang, T., Han, B., Zhu, A., & Ma, X. (2006). Knoevenagel condensation catalyzed by 1,1,3,3-tetramethylguanidium lactate. *Synthetic Communications*, *36*(22), 3305-3317.

Zhang, S., Zhi, S., Wang, H., Guo, J., Sun, W., Zhang, L., & Wu, D. (2023). Laser-assisted rapid synthesis of anatase/rutile TiO_2 heterojunction with function-specified micro-zones for the effective photo-oxidation of sulfamethoxazole. *Chemical Engineering Journal*, *453*, Article#139702.

Zhang, X., Wu, F., Wu, X., Chen, P., & Deng, N. (2008). Photodegradation of acetaminophen in TiO(2) suspended solution. *J Hazard Mater*, *157*(2-3), 300-307.

Zhang, Y., Fan, J., Yang, B., Huang, W., & Ma, L. (2017). Copper–catalyzed activation of molecular oxygen for oxidative destruction of acetaminophen: The mechanism and superoxide-mediated cycling of copper species. *Chemosphere*, *166*, 89-95.

Zhang, Y., Zhang, Q., Dong, Z., Wu, L., & Hong, J. (2019a). Structurally modified $CuFe_2O_4$/persulfate process for acetaminophen scavenging: high efficiency with low catalyst addition. *Journal of Chemical Technology & Biotechnology*, *94*(3), 785-794.

Zhang, Y. C., Zhang, Q., Dong, Z. Y., Wu, L. Y., & Hong, J. M. (2019b). Structurally modified $CuFe_2O_4$/persulfate process for acetaminophen scavenging: high efficiency with low catalyst addition. *Journal of Chemical Technology and Biotechnology*, *94*(3), 785-794.

Zhao, C., Bond, A. M., Compton, R. G., O'Mahony, A. M., & Rogers, E. I. (2010). Modification and implications of changes in electrochemical responses encountered when undertaking deoxygenation in ionic liquids. *Analytical chemistry*, *82*(9), 3856-3861.

Zhao, G., Jiang, T., Gao, H., Han, B., Huang, J., & Sun, D. (2004). Mannich reaction using acidic ionic liquids as catalysts and solvents. *Green Chemistry*, *6*(2), 75-77.

Zhao, W., Yan, M., Chen, Y., Shen, J., Hong, X., Mu, F., & Sun, C. (2023). Rational design of novel metal-organic framework/Bi_4O_7 S-scheme heterojunction photocatalyst for boosting carbamazepine degradation. *Applied Surface Science*, *622*, Article#156876.

Zheng, J., Lin, Q., Liu, Y., Fan, X., Xu, K., Ma, Y., & Fu, H. (2023). Peroxymonosulfate activation by Mg-introduced Fe-N carbon nanotubes to accelerate sulfamethoxazole

degradation: Singlet oxygen-dominated nonradical pathway. *Chemical Engineering Journal*, *452*, Article#139233.

Zheng, M., Gao, B., Zhang, J., El-Din, M. G., Snyder, S. A., Wu, M., & Tang, L. (2022). In-situ chemical attenuation of pharmaceutically active compounds using CaO_2: Influencing factors, mechanistic modeling, and cooperative inactivation of water-borne microbial pathogens. *Environmental Research*, *212*, Article#113531.

Zhi, J., Moore, R., Kanitra, L., & Mulligan, T. E. (2003). Effects of orlistat, a lipase inhibitor, on the pharmacokinetics of three highly lipophilic drugs (amiodarone, fluoxetine, and simvastatin) in healthy volunteers. *The Journal of Clinical Pharmacology*, *43*(4), 428-435.

Zhou, Q., Henderson, W. A., Appetecchi, G. B., Montanino, M., & Passerini, S. (2008). Physical and electrochemical properties of N-alkyl-N-methylpyrrolidinium bis (fluorosulfonyl) imide ionic liquids: PY13FSI and PY14FSI. *The Journal of Physical Chemistry B*, *112*(43), 13577-13580.

Zhu, A., Jiang, T., Wang, D., Han, B., Liu, L., Huang, J., & Sun, D. (2005). Direct aldol reactions catalyzed by 1,1,3,3-tetramethylguanidine lactate without solvent [10.1039/B501925G]. *Green Chemistry*, *7*(7), 514-517.

Zhu, K., Xia, W., He, D., Huang, J., He, H., Lei, L., & Liu, X. (2022). Facile fabrication of Fe/Fe_3C embedded in N-doped carbon nanofiber for efficient degradation of tetracycline via peroxymonosulfate activation: Role of superoxide radical and singlet oxygen. *Journal of Colloid and Interface Science*, *609*, 86-101.

Zigah, D., Wang, A., Lagrost, C., & Hapiot, P. (2009). Diffusion of molecules in ionic liquids/organic solvent mixtures. Example of the reversible reduction of O_2 to superoxide. *The Journal of Physical Chemistry B*, *113*(7), 2019-2023.